STATIC AND DYNAMIC ASSESSMENT OF THE INFLUENCE OF ASPHALT LAYERS ON THE STRUCTURAL RESPONSE OF STEEL GUARDRAIL POSTS

A Dissertation
Presented to
The Academic Faculty

by

Seo-Hun Lee

In Partial Fulfillment
Of the Requirements for the Degree
Doctor of Philosophy in the
School of Civil and Environmental Engineering

Georgia Institute of Technology
December 2017

STATIC AND DYNAMIC ASSESSMENT OF THE INFLUENCE OF ASPHALT LAYERS ON THE STRUCTURAL RESPONSE OF STEEL GUARDRAIL POSTS

Approved by:

Dr. David W. Scott, Advisor
School of Civil and Environmental Engineering
Georgia Institute of Technology

Dr. Donald W. White
School of Civil and Environmental Engineering
Georgia Institute of Technology

Dr. Lauren K. Stewart
School of Civil and Environmental Engineering
Georgia Institute of Technology

Dr. Yang Wang
School of Civil and Environmental Engineering
Georgia Institute of Technology

Dr. Min Zhou
School of Mechanical Engineering
Georgia Institute of Technology

Date Approved: 10/20/2017

To my father and mother

ACKNOWLEDGEMENTS

The author would like to gratefully acknowledge his advisor Dr. David W. Scott for his support, guidance, consideration, and patience, which enables the author to complete the thesis and finally to have a chance of writing this section.

Additional acknowledgement must be given to the thesis committee members, Dr. Donald W. White, Dr. Lauren K. Stewart, Dr. Yang Wang, Dr. Min Zhou, plus their time and valuable comments on the dissertation.

This study was sponsored by the Georgia Department of Transportation (GDOT) under two research projects: 13-21 and 15-08. The author wishes to thank GDOT officials for their full assistance on these projects. Additional thanks to Wildcat Striping, Dykes Paving, and GTRI for their service and support.

Due to the size and physical demand of the research program, this research was helped by many Georgia Tech students and facility staffs. Thanks to Blake Baklini, Billy Plum, and Andrew Udell for their laboratory assistance, and more greatly to Jeremy Mitchell for his incredible support. The author is also grateful to Clifford Tribble, Tyler Young, Ryan Vazquez, Jamie Ghitelman, Lawrence Wolffis, Zachary Wilson, Caleb Brown, Alesa Stallman, and other undergraduate assistants.

In addition to their graduate study, Javaid Anwar, Genevieve Pezzola, Nan Gao, and Kathryn Sanborn substantially offered their time for this research. Special thanks to

Marc Sanborn, who made the biggest effort on the dynamic impact tests. Additional thanks to Giovanni Loretto, Alvaro Paul, Longde Jin, Xinjun Dong, and Xi Liu for their help and information. The author wants to give a special acknowledgement to Esmaeel Bakhtiary, who has been always the first person to come and assist the research tasks.

The author would like to acknowledge his Korean colleagues, Jiuk Shin, Youngho Jin, Gun Kim, Hyun Woong Cho, Chunhee Cho, and Hyun-Joong Kim, for their advice. Sincere appreciation to Austin Wright, Jungmin Lee, Xin Zhang, Jerome Sin, Collen Leng and other Journey Church of Atlanta members for their support and prayer.

Also, there should be a space for his uncle Byungtag Kim, aunt Pyunghwa Gwak, and their daughters: Jihae, Jisun, and Mirhee Kim. The author cannot imagine any academic accomplishment nor thesis completion without their endless love, support, and prayer. Thanks to Dr. Geum Joon Cho for being a great mentor.

To his family in Korea, the author is grateful for his parents and brother Changhoon. They have always been the greatest supporters on this Ph.D. study. Thanks to God for their everlasting love, patience, and sacrifice. The author strongly believes they are proud of the author, and wishing the author's future to be happier than ever.

Finally and without exception, the author would like to thank his beloved fiancée and best friend, Sanghee Kang. She has been the greatest helper, mentor, and endless source of energy to the author more than anybody else in the world. The author cannot emphasize more that this dissertation would not be finished without her emotional love, encouragement, and support.

TABLE OF CONTENTS

LIST OF TABLES

LIST OF FIGURES

LIST OF SYMBOLS

$a(t)$	Acceleration
b_f	Flange width
c_1, c_2, c_3	Coefficients of soil properties as a function of the internal friction angle
e	Eccentricity of loading (loading height)
f	Spring force
f_{max}	Maximum (peak) force in the asphalt layer
$f_{max,eff}$	Adjusted maximum (peak) force in the asphalt layer
$f_c{}'$	Asphalt compressive strength
$f_t{}'$	Asphalt tensile strength
h	Section height (depth of post cross section)
k	Initial modulus of subgrade reaction of soil as a function of the internal friction angle
k_a	Lateral resistance/stiffness of the asphalt
k_s	lateral resistance/stiffness of the soil
m	Mass
n	Number of guardrail posts in a test section
p	Lateral load
p_u	Ultimate lateral bearing capacity for sand
r	Rear distance of asphalt mow strip
t	- Age of the asphalt material (Chapter 4) - Time (Chapter 5)
t_f	Flange thickness

t_k	Asphalt mow strip thickness
t_w	Web thickness
v	Velocity
y	Lateral displacement at the loading height
z	Depth
A	Dimensionless factor for the static loading conditions
C	Asphalt cohesion (stress)
D	Size factor of post/pile
E	Young's modulus of steel
$E_{D,avg}$	Average dissipated energy on each guardrail post
E_K	Kinetic energy contributing the lateral displacement of the guardrail system
$E_{K,avg}$	Average kinetic energy input on single guardrail post
$F(t)$	Dynamic force
F_{eff}	Effective dynamic force
G	Shear modulus of asphalt
H	Total depth of post/pile
I	Section moment of inertia
M	Bending moment in the beam
M_P	Plastic moment of steel section
M_y	Yield moment of steel section
N	Number of springs in the analysis model (Chapter 6)
P	Applied static load
T	Temperature

W	Work done by the applied load
α	Plastic amplification factor
$\beta(v)$	Modification factor of the programmer, primarily a function of velocity
γ	Effective soil unit weight
δ	Spring deflection/displacement
δ_1	Asphalt layer displacement at which the peak force occurs
$\delta_{1,eff}$	Adjusted asphalt layer displacement at which the peak force occurs
δ_2	Asphalt layer displacement at which the layer no longer provides any lateral resistance
θ	Impact angle in AASHTO MASH full-scale crash tests
θ_P	Plastic rotation of the steel post
θ_y	Yield rotation of the steel post
κ	Curvature of the beam
λ_f	Asphalt peak force correction factor
λ_δ	Asphalt peak displacement correction factor
ρ	Density of soil
σ_y	Yield stress of steel
σ	Normal stress in Mohr-Coulomb model
$\sigma_1, \sigma_2, \sigma_3$	Principal stresses
τ	Yield (failure) shear stress in Mohr-Coulomb model
ϕ	Internal friction angle
ϕ_a	Internal friction angle of asphalt
ϕ_s	Internal friction angle of soil
$\Delta(t)$	Displacement

Δ_p	Displacement at the elevation of the load *P*
Δ_g	Displacement at ground or asphalt level

LIST OF ABBREVIATIONS

AASHTO	American Association of State Highway and Transportation Officials
API	American Petroleum Institute
ASTM	American Society for Testing and Materials
CFC	Channel Frequency Class
CMA	Cold Mix Asphalt
DOT	Department of Transportation
FEA	Finite Element Analysis
FHWA	Federal Highway Administration
GL	Ground-level
HMA	Hot Mix Asphalt
LO	Leave-out
MASH	Manual for Assessing Safety Hardware
MGS	Midwest Guardrail System
MwRSF	Midwest Roadside Safety Facility
M-C	Mohr-Coulomb
NCHRP	National Cooperative Highway Research Program
PG	Performance Grade
RD	Rear Distance
RDG	Roadside Design Guide
SAE	Society of Automotive Engineers
SYP	Southern Yellow Pine
TTI	Texas Transportation Institute

SUMMARY

The practice of installing asphalt layers (usually called “mow strips”) around guardrail posts is common in many states where vegetation growth around and adjacent to the guardrail system is problematic. Recent studies have indicated that these layers can produce excessive ground-level restraint on the post, which may result in unsatisfactory performance of the guardrail system. However, the influence of critical design parameters related to the asphalt mow strip on the structural behavior of guardrail posts has not been evaluated. This study presents the results of a comprehensive structural performance assessment on a guardrail subcomponent system including a standard steel post installed through an asphalt mow strip. A total of 19 static tests were conducted to provide a first-stage evaluation of mow strip design alternatives, and a total of 14 dynamic tests were performed to provide a more comprehensive evaluation of the dynamic behavior of these design alternatives. Specifically, a dynamic test protocol using a high-speed hydraulic actuator was developed and proposed as an alternative test method. The reduction of the thickness/width of the asphalt behind the post (rear distance) as well as the installation of pre-cuts resulted in less ground-level restraint than a mow strip with a conventional leave-out. The variability in asphalt strength as a function of temperature and age was evaluated by uniaxial compression tests on asphalt cylindrical specimens. A simplified semi-empirical analysis model was constructed and calibrated using experimental data to predict the expected structural performance of posts installed with a specific mow strip design condition. Design guidance for mow strips was

developed based on the analysis results and the service conditions including the critical design temperature and the target asphalt age.

CHAPTER 1
INTRODUCTION

1.1 Problem statement

1.1.1 W-beam guardrail system

Guardrail systems, often referred to as "longitudinal barriers," are one of the most common roadside safety hardware systems found on U.S. roadways [1]. The main design purpose of guardrail systems is to redirect the errant vehicle into a controlled stop by absorbing its kinetic energy as well as securing the structural integrity of system itself.

Even though there are several different types of guardrail systems currently in use (e.g., cable, W-beam with weak-post, W-beam with strong-post, Thrie-beam, etc.), one of the most frequently used guardrail systems installed along high-speed expressways (e.g., interstate highways) is the W-beam with strong-post guardrail system [2]. When properly-designed and installed, this system has shown satisfactory crash performance over the last few decades as validated by numerous full-scale crash tests [3]. In the rest of the thesis, the W-beam with strong post guardrail system is referred to as the "W-beam guardrail system". Figure 1.1 shows the W-beam guardrail system consisting of three main structural elements: guardrail posts, W-beam rails, and blockouts (offset blocks).

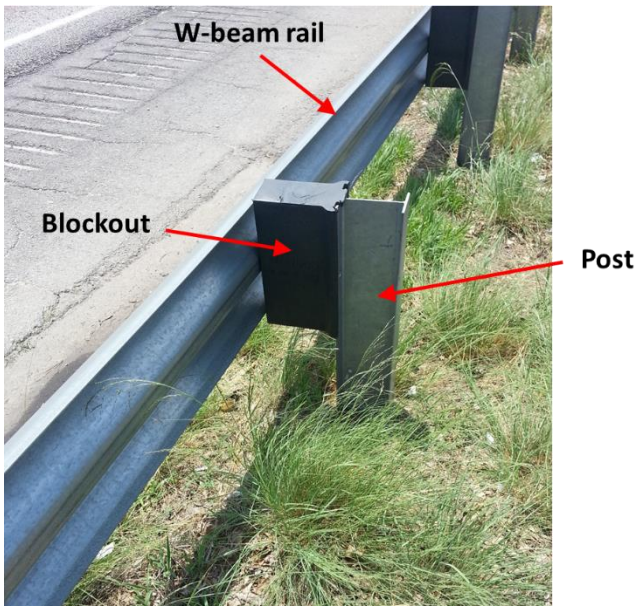

Figure 1.1 Structural elements in W-beam guardrail system

While either wide flange steel beams or wood beams can be installed as guardrail posts, there are advantages in using steel posts in many field installations. Firstly, wood is a less ductile material and can exhibit a more brittle failure of during a vehicle collision, while steel posts are more ductile and better handle the large deformations caused by the collision. Secondly, the underground part of wood posts can degrade over time from a variety of causes including moisture and/or insects; the corrosion of steel posts is significantly reduced by using galvanized materials. Steel posts typically have a longer service life in a service environment which would encourage active deterioration of organic materials like wood. Finally, installation methods utilizing a hydraulic driving machine (Figure 1.2) become highly efficient with steel guardrail posts. The standard steel guardrail posts (W6x9 or W6x8.5) are capable of penetrating the asphalt layer and compacted soil foundation without significant damage. This method has been historically

used due to its efficiency in construction cost and time - a single post typically only takes a few minutes to be installed.

Figure 1.2 Steel guardrail post installation using hydraulic driving machine

The W-beam guardrail system is designed to provide enough load-bearing capacity when the guardrail is subjected to vehicle impact. The guardrail posts must carry the required dynamic load perpendicular to the direction of traffic. At the same time, these posts should be designed to dissipate the kinetic energy from the vehicle to the system.

Unfortunately, these two requirements for guardrail posts are generally in conflict with each other. Increasing the lateral stiffness of guardrail posts and surrounding

materials (e.g., posts installed in concrete base) would decrease the after-impact displacement of the posts and colliding vehicle. The energy dissipation capacity of the guardrail system, the crashworthiness of the impacting vehicle, and the risk of occupant injury during an impact could reach an unsatisfactory level even though the lateral load-bearing capacity is sufficient [4, 5]. In contrast, a large amount of energy dissipation can be achieved by reducing the lateral load-bearing capacity of the post (e.g., a weak soil condition around the post) which leads to large translation and rotation of the whole guardrail system. However, this type of guardrail system may neither redirect an impacting vehicle to stop nor prevent the vehicle from riding over the guardrail [6, 7].

Therefore, a guardrail post and surrounding materials should be designed based on a comprehensive understanding on their structural behavior and interaction. To satisfy the design purposes of the guardrail system, the structural behavior of the subcomponent system, which can be defined as one guardrail post and the surrounding installation, must be fully identified.

1.1.2 Asphalt mow strip

Asphalt mow strips (also known as "extended pavement shoulders") are a pavement layer installed around guardrail posts as a vegetation barrier as shown in Figure 1.2 and Figure 1.3. Without the mow strip, regular vegetation around the guardrail is required because overgrown vegetation can obstruct the vision of motorists and trigger roadside crashes. The installation of mow strips can reduce expenses related to roadside

maintenance such as mowing and herbicide application, and improve safety for workers associated with these tasks.

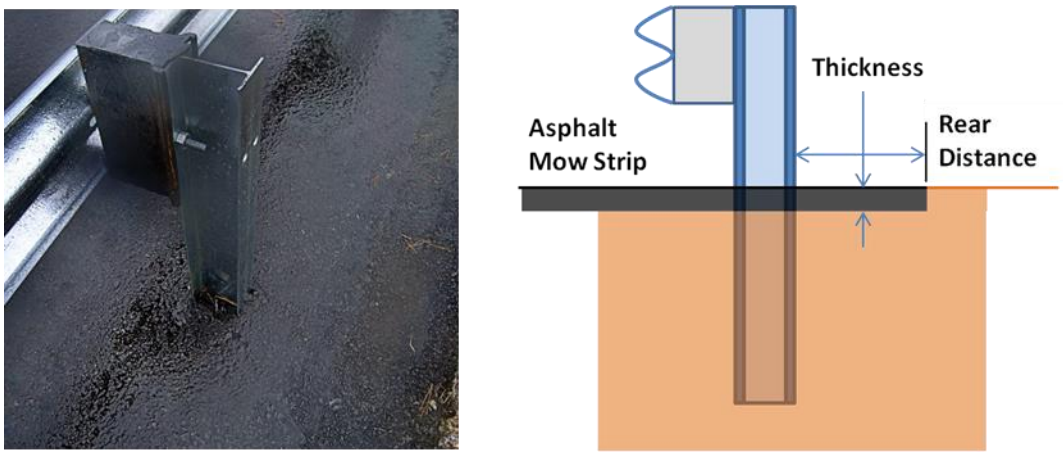

Figure 1.3 Typical post installation detail with asphalt mow strip

Nevertheless, installing mow strips around the guardrail posts has caused concerns related to excessive ground-level restraint which can lead to an unsatisfactory performance of the guardrail system. A study performed by the Texas Transportation Institute (TTI) in 2004 [4] concluded that asphalt mow strips increase the ground-level restraint of guardrail posts significantly. The TTI 2004 study asserted that steel guardrail posts confined in asphalt would result in the sudden development of a plastic hinge during a vehicle impact, which is not desirable in guardrail systems. Based on this study, the fourth edition of the *Roadside Design Guide* (RDG) [1] published by the American Association of State Highway and Transportation Officials (AASHTO) classifies mow strips as "rigid" foundations and states that guardrail posts in mow strips are not able to rotate/translate under impact.

The TTI 2004 study formed the basis of the guardrail post installation details incorporating a leave-out where the portion of the mow strip around the post is removed and replaced by a relatively weak material such as a low-strength cementitious grout. This leave-out detail, as shown in Figure 1.4, was adopted by the *RDG* as a recommended method of reducing ground-level restraint on the post/mow strip system.

However, considering the number of guardrail posts to be installed along a newly constructed highway, it is evident that leave-out installation requires more construction time and cost compared to an installation method where posts are driven through the asphalt. This can be attributed to the additional construction processes needed such as the removal of mow strip around the posts as well as the preparation and placement of leave-out materials for guardrail system maintenance.

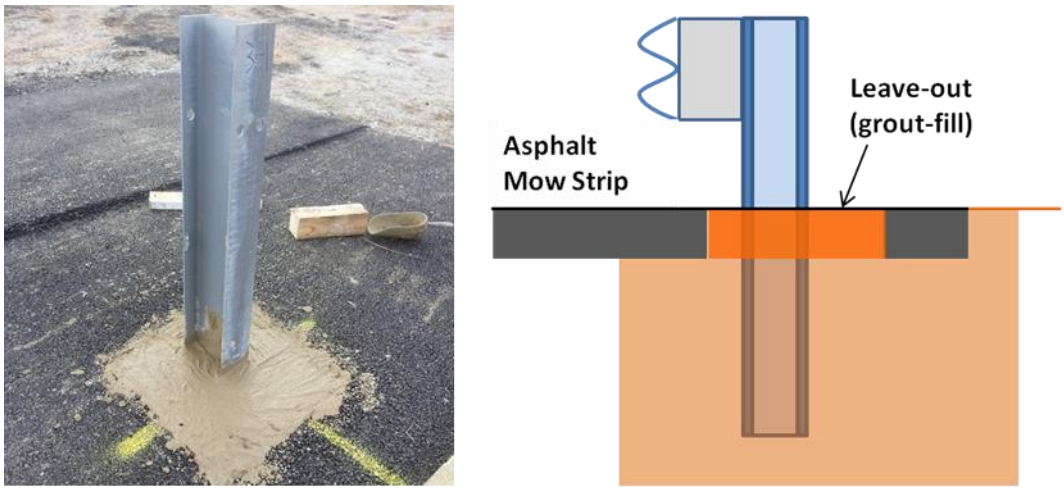

Figure 1.4 Typical post installation detail with leave-out application in asphalt mow strip

Furthermore, the TTI 2004 study focused on enhancing the performance of guardrail post systems by incorporating leave-outs and as such did not consider other possible alternative methods to reduce ground-level restraint. Consideration of alternative methods may include designs such as reducing geometric parameters of the mow strip such as thickness and rear distance (as shown in Figure 1.3). Since it is well known [8-11] that asphalt strength and other material properties of the mow strip are sensitive to temperature and age, asphalt mow strips installed on roadsides can be considered as a deformable material under a range of ambient conditions rather than a "rigid" material as defined in previous investigations.

These considerations imply that the performance assessment of steel guardrail post installation methods should rely on a comprehensive understanding of the effect of mow strip dimensions and asphalt/soil properties on ground-level restraint, which has not yet been investigated in a quantitative manner. Therefore, this research addresses a portion of this deficiency by assessing the influence of asphalt mow strip design parameters on the static and dynamic structural behavior of guardrail posts.

1.2 Research objectives

The main objective of this research is to determine the influence of asphalt mow strip layers on the structural response of steel guardrail posts. Two subcomponent test protocols (static and dynamic test methods) are developed and then used for testing standard steel posts installed in asphalt mow strip layers. In particular, the high-speed hydraulic actuator located at the Georgia Institute of Technology is calibrated to generate

a dynamic impact load similar to a vehicle impact on the posts. In conjunction with the static and dynamic test results, a simplified empirical analysis model is developed to estimate the performance of the guardrail post system with an asphalt mow strip. To assess ground-level restraint imparted to the post by the asphalt layer, a series of performance assessment criteria are developed and compared with the experimental results. Additionally, the variability in asphalt strength as a function of temperature and age is evaluated by uniaxial compression tests on asphalt cylindrical specimens. The specimen test results are integrated with the analysis model to predict the structural response of a guardrail post installed with a specific mow strip design condition. Ultimately, asphalt mow strip design guidelines considering possible design variables and environmental factors are proposed.

The work presented in this dissertation is part of a larger research effort sponsored by the Georgia Department of Transportation focusing on the performance evaluation of steel guardrail systems with posts encased in various types of asphalt mow strip through experimental investigation and numerical simulation. The first phase of the project included static subcomponent testing with relevant finite element simulation, while the second phase covered dynamic subcomponent testing and finite element simulation. Static and dynamic experimental data from this dissertation were used to calibrate finite element models for both subcomponent elements and full sections of guardrails. The same performance assessment criteria were utilized in both studies. The results of the finite element simulations performed in the overall research project have been reported separately [12].

1.3 Dissertation organization

The remainder of the dissertation consists of the following chapters, followed by a list of references and appendices.

Chapter 2 contains a literature review of background information on guardrail systems and experimental studies on the behavior of steel guardrail posts. The studies with subcomponent testing on steel posts are featured and a critical appraisal of previous studies on mow strips is made.

Chapter 3 describes a comprehensive program of static experimental performance assessment of guardrail posts. This chapter includes the static test program and the performance assessment of asphalt mow strips based on test results and relevant quantitative criteria.

Chapter 4 presents the material characterization of asphalt used in the static and dynamic subcomponent testing programs. This chapter presents the results of the asphalt compression test program and the estimation of the strength variability by roadway conditions.

Chapter 5 illustrates a newly-developed dynamic impact test program using a high-speed hydraulic actuator and a moveable test bed. The test program includes the development of a dynamic test protocol and the test bed construction. The structural performance of the guardrail post under dynamic loading was evaluated through relevant quantitative criteria.

Chapter 6 describes a semi-empirical analysis model developed from findings in Chapter 3 through 5. A parametric study on design variables of the asphalt mow strip with a broader range is performed through the analysis model. A performance evaluation method for various mow strip designs under a specific design condition is proposed.

Chapter 7 summarizes the major contributions of this study and makes suggestions for future research investigations related to the use of asphalt layers in highway safety hardware systems.

CHAPTER 2
LITERATURE REVIEW

2.1 Full-scale crash testing on guardrail systems

Full-scale crash testing using an actual vehicle has been used as a primary tool for assessing and validating the structural performance of roadside safety hardware including the W-beam guardrail system with steel posts. In order to design and specify crash testing methods and their evaluation criteria, the "worst practical case/scenario" with an actual vehicle has been regarded as a key philosophy. Based on this, crash testing methods and supporting guidelines have evolved continuously since 1962 [13]. Existing W-beam guardrail systems and other safety hardware were tested under approved guidelines which define satisfactory structural performance.

2.1.1 NCHRP Report 350 and relevant research studies

In 1993, *NCHRP Report 350* [14] was released to provide uniform guidelines for the crash testing of highway safety hardware and to recommend evaluation criteria for assessing the test results. *NCHRP 350* specifies the following: (1) "service levels of roadway" which determine the initial selection of safety hardware, (2) "test levels" which are defined by impact severity conditions of target safety hardware, (3) "test vehicles" which represent common types of vehicles on the roadway, (4) "performance characteristics" which are determined by overall structural purpose and expected performance, and (5) "recommended evaluation criteria" which are given as a series of

pass/fail criteria and determine whether a test hardware exhibits satisfactory performances or not.

After the publication of *NCHRP 350*, W-beam guardrail systems with various types of alternative components, materials, design dimensions, and roadside conditions were tested and evaluated under these test guidelines and evaluation criteria. Mak et al. [6] classified the most frequently used guardrail systems into six categories (Cable, W-beam weak post, W-beam strong post, Box-beam, Thrie-beam, and Modified Thrie-beam) and performed eight full-scale crash tests in accordance with *NCHRP 350* guidelines. The purpose of this experimental study was to evaluate the crash performance of all existing guardrail systems and to determine if the devices in the systems need to be redesigned for improving their crash performance. Five of the guardrail systems showed satisfactory performance, whereas three of them showed unsatisfactory performance under *NCHRP 350* criteria. One of the systems which failed to meet the criteria was the W-beam strong post guardrail system with wide flange steel posts. During the test, the test vehicle (4410 lb. pickup truck) was successfully redirected by the guardrail but was rolled over by 90 degrees after exiting from the contact with the guardrail.

For the guardrail systems with unsatisfactory performance, numerous experimental studies on design modifications of the guardrail system have been performed by previous researchers. Bullard et al. [15] tested a modified W-beam guardrail system replacing the W6x9) steel flange blockouts (also known as “rail spacer” or “offset block”) with nominal 6” x 8” timber blockouts. The guardrail system showed a satisfactory crash performance under the same test condition of the previous crash test [6]. A different type of design modification was made by Bligh et al [16]. The research team successfully

tested a combination of shorter (5’-6”) steel posts with less embedment depth (38”) and reduced size (6” x 6”) timber blockout compared to those (6’-0”, 44”, and 6” x 8”, respectively) of the previous study by Bullard et al. [15]. Bligh and Menges [17] tested the combination of standard posts with recycled polyethylene blockouts; the authors concluded these blockouts were suitable for use in both steel and wood post guardrail systems. Rohde and Herr [18] investigated the performance of guardrail systems when steel posts were installed in a rock foundation. Based on computer simulations and physical testing of posts with various embedment conditions, the researchers developed a post installation method and modification details. A full-scale crash test with a 4410-lb. pickup truck was conducted, and the test results were determined to be acceptable.

Alternative steel sections were also tested and evaluated under *NCHRP 350* criteria. Compared to the conventional wide flange section beams for the steel guardrail posts, Alberson et al. [19] tested steel guardrail posts of a section labeled X-44 as shown in Figure 2.1; a full-scale crash test with the alternative steel post section was successful. Kennedy et al. [20] evaluated a guardrail system with X-48 steel posts, an updated version of the X-44, using both experimental full-scale crash tests and computational analysis. The researchers conducted a series of finite element simulations using LS-DYNA® software to identify design deficiencies and a full-scale crash test was subsequently performed after favorable results from the computational analysis. The updated guardrail system successfully passed *NCHRP 350* safety requirements.

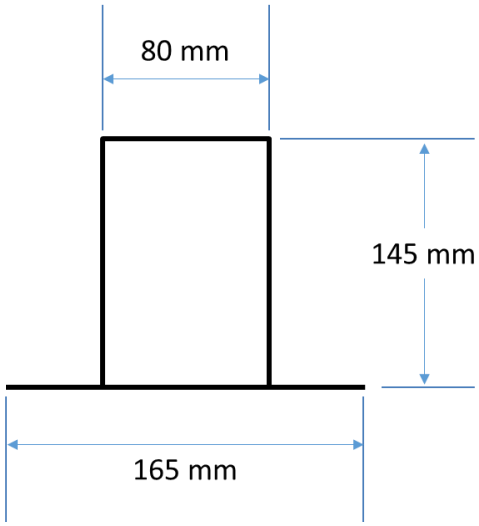

Figure 2.1 Alternative steel guardrail post section investigated by Kennedy et al. [20]

There have been several experimental studies on the W-beam guardrail system constructed with guardrail posts using materials other than steel. In particular, wood posts have been used frequently in the United States. A round-shaped wood post has been regarded as a standard wood post type because of its lower manufacturing cost [21]. Bligh and Bullard [22] confirmed the satisfactory performance of standard round-shaped wood posts using full-scale crash tests in accordance with *NCHRP 350*. Alberson et al [23] performed a full-scale crash test for a guardrail system consisting of recycled rectangular plastic posts with wood blockouts. The same researchers also tested a guardrail system consisting of Glu-Laminated rectangular wood posts and blockouts [24]. Both guardrail systems satisfied *NCHRP 350* evaluation criteria.

The Midwest Guardrail System (MGS) [25], tested and evaluated under *NCHRP 350*, is a non-proprietary guardrail system developed by the Midwest Roadside Safety Facility (MwRSF). The MGS modifes previous systems by (1) raising the rail height for

improved performance for light truck vehicles of high center-of-gravity, (2) moving rail splices from near the post to the midspan between posts, and (3) increasing the size of the bolt slots on the steel posts. These three design modifications were shown to improve the crash performance of the system through several full-scale crash tests [26-28]. In addition, a series of design updates on the MGS were made based on full-scale crash tests in compliance with *NCHRP 350*.

Polivka et al. [29] performed a total of six full-scale crash test to investigate the alternative design of the guardrail system with reduced post spacing (half and quarter) and a design configured with 6 inch tall concrete curbs under the rail. Prior to the full-scale crash tests, computer simulation modeling with LS-DYNA® and BARRIER VII was conducted to study guardrail design parameters and predict the dynamic performance of various guardrail systems. Hascall et al. [30] tested a modified version of the MGS using round-shaped softwood posts including three different species of lumber: Douglas Fir, Ponderosa Pine, and Southern Yellow Pine. In conjunction with computer simulation and dynamic subcomponent testing, two full-scale tests showed that wood posts with diameters ranging between 7-1/4" and 8" can substitute for standard steel posts (W6x9) in the MGS. Lechtenberg et al. [31] investigated the use of the MGS installed on a sloped terrain. From two full-scale tests using a pickup truck and a small passenger car, a guardrail installation on an 8:1 slope was identified as the critical (steepest) slope to apply the MGS design to. The research team also investigated the application of MGS in stiffer slope conditions by performing two full-scale tests [32]. For installation with a 2:1 slope, design recommendations using longer posts (9'-0") with an increased embedment depth (76") were made to ensure the safe and economical application of the MGS.

Bielenberg et al. [33] performed two full-scale crash tests to investigate the application of the MGS with long span culverts. The modified design met all safety requirements of *NCHRP 350* and performed functionally without the need for less economical design practices such as (1) large lateral offsets between the rail and the culvert, and (2) a nested rail system.

2.1.2 MASH and relevant research studies

In 2009, the American Association of State Highway Transportation and Officials (AASHTO) published the *Manual for Assessing Safety Hardware* (MASH) [13], which supersedes *NCHRP 350*. This manual revised certain test conditions including the test vehicle and impact conditions, reflecting newer manufactured vehicles and their crash features such as mass and height of mass center. In addition, test matrices were consolidated by removing ambiguous concepts. Evaluation criteria and reporting procedures were more strongly specified than *NCHRP 350*. The Federal Highway Administration (FHWA) requires any modification in approved safety hardware later than January 1, 2011 to be tested under *MASH* [34]. The fourth edition of the *AASHTO Roadside Design Guide (RDG)* [1] incorporates the guardrail systems approved by the relevant crash testing criteria. One can select an appropriate design from the *RDG* or develop a new/modified design. In general, once the roadway condition and the type of guardrail system are determined, corresponding test levels, type of test vehicles, and full-scale test configurations can be chosen in accordance with *MASH*. Any new/modified design of a guardrail system must be successfully crash tested; the design is then submitted for approval by the FHWA for official use in the United States. As a result, a series of *MASH* full-scale tests on the W-beam guardrail systems have been performed

for two main reasons since 2010: (1) the reevaluation of existing design specifications/practices and (2) the adoption of new design features and installation methods.

Wiebelhaus et al. [35] tested the performance of the MGS (Midwest Guardrail System) placed adjacent to steep roadside slopes in accordance with *MASH* guidelines. The system, incorporating 9-ft long steel posts with a standard post spacing of 75-in., showed satisfactory performance under the *MASH* full-scale crash test criteria as well as under *NCHRP 350* criteria [32]. Bligh et al. [36] reviewed the W-beam guardrail standards and installation methods of the Texas Department of Transportation (TxDOT) using *MASH*. The research group evaluated a 31-in. tall W-beam guardrail system incorporating conventional 8-in. deep offset blocks and the system met all required *MASH* performance criteria. Williams and Menges [37] performed a research study testing the W-beam guardrail on a low-fill box culvert in accordance with *MASH*. This study incorporated the use of standard W6x9 steel posts with welded base plate details and an epoxy anchoring system for a simplified installation. The guardrail system was tested under *MASH* Test 3-11 (which involves a 5000-lb. pickup truck) and performed acceptably.

Stolle et al. [38] investigated the MGS with white pine wood posts in lieu of southern yellow pine (SYP) posts, which had been successfully tested under *NCHRP 350* in the former MwRSF study [30]. Based on an interest by a number of State Departments of Transportation to use various species of wood such as white pine and red pine, the researchers evaluated the crash performance of the MGS utilizing the white pine wood posts with the same cross-sectional dimensions as standard SYP posts. While satisfying

MASH performance criteria, the alternative system showed successful redirection of the testing vehicle (5000-lb. pickup truck) and the system was determined to be acceptable. Stolle et al. [39] also evaluated the MGS with two different mounting height and embedment depth combinations and then established the maximum mounting height of the system under *MASH*. While there had been a recommended minimum top rail mounting height of 27-3/4 in. according to the full-scale tests in compliance with *NCHRP 350*, no maximum height recommendation existed. The research group performed two full-scale crash tests on the different MGS setups: (1) 34 in. height and 37 in. depth, and (2) 36 in. height and 35 in. depth. Both system heights/depths were found to meet the *MASH* evaluation criteria.

Schrum et al. [40] evaluated the MGS without offset blocks. Since a narrow roadside condition hinders the use of standard 12-in. offset blocks in the W-beam guardrail system, several State Departments of Transportation requested the development of a non-proprietary, non-blocked MGS which can be a comparable option to the proprietary guardrail systems with higher costs. Accordingly, the non-blocked MGS was modified to have additional rail components and the modified MGS was successfully tested using a small passenger car (*MASH* Test 3-10) and a pickup truck (*MASH* Test 3-11). The research proposed an alternative for W-beam guardrail installation when roadside width is restricted. Weiland et al. [41] investigated the minimum effective guardrail length for the MGS. The research group showed a reduced 75-ft long MGS performed satisfactorily under the *MASH* full-scale test using a pickup truck (Test 3-11) compared to the recommended standard minimum length of 175-ft based on crash testing in accordance with *NCHRP 350* and *MASH*. The researchers also suggested the possible use of shorter

lengths of 50-ft and 62.5-ft. MGS configurations based on computer simulation results, but no actual crash tests were performed on those configurations.

2.2 Subcomponent tests for performance evaluation of guardrail posts

Even a single full-scale crash test requires significant resources; as such, performing iterative full-scale crash tests is not a very cost-effective way to make design modifications. Due to the limited amount of quantitative measures specified in the *MASH* guidelines, one cannot easily gather enough information from a "failed" full-scale test to answer the following questions: (1) how influential is one design variable in a specific failure mode of guardrail system, (2) what level of change is needed to enhance a design to satisfactory levels, and (3) how consistent will test results be in different environmental conditions. Therefore, it is more cost-efficient to perform a series of subcomponent tests for design parametric evaluation of guardrail components. By assessing the difference in structural performance in a quantitative manner, an implemented subcomponent system can be developed to potentially satisfy the performance evaluation criteria of *MASH*. As such, guardrail posts and the surrounding asphalt mow strips can be separately examined using dynamic subcomponent tests in conjunction with empirical analysis or finite element simulation.

There have been a number of prior research studies incorporating subcomponent tests on steel and wood guardrail posts [4, 5, 42-53]. In 1970, in one of the earliest approaches to subcomponent testing, the Southwest Research Institute (SwRI) performed an experimental study [43] to assess the structural behavior of guardrail post-soil interaction.

A total of 72 guardrail posts were tested with static and dynamic loading to evaluate the effect of three factors: soil type, embedment depth, and width of the posts. The load-bearing capacity of the post and the kinetic energy absorbed by the soil (which is equivalent to the dissipated energy) were used as primary measures of the performance evaluation. The study concluded that (1) the performance of the guardrail post (the post-soil interaction characteristics) is influenced by all three factors, and (2) the dynamic resistance force and the absorbed kinetic energy are greater than those of the static.

In 1983, the Texas Transportation Institute (TTI) performed a research study [44] on the soil-structure interaction behavior of wood and steel guardrail posts, including six static load tests and four dynamic load tests with different test configurations. The study proposed static and dynamic subcomponent testing methods for guardrail posts. As shown in Figure 2.2, the static loading system consisted of a hydraulic cylinder and a concrete anchor, while the dynamic loading system consisted of a cart guided and accelerated by a truck with concrete barriers, a cable, and a cable release mechanism. The research showed that (1) steel posts performed similar to wood posts of the same embedment depth and (2) there was no significant difference but a slight correlation in maximum lateral load and dissipated energy (calculated from the load-displacement response curve) among the different test conditions.

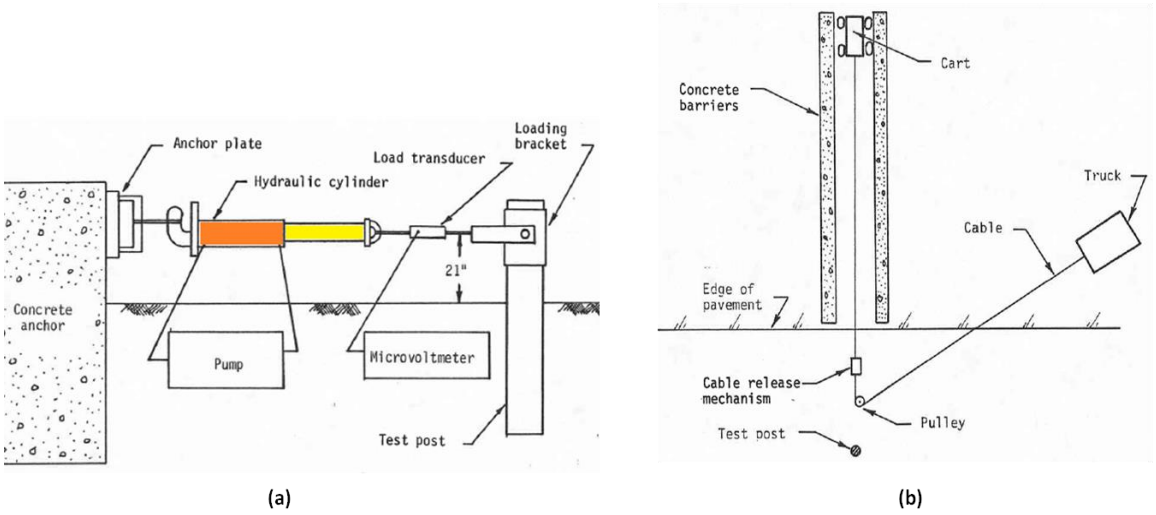

Figure 2.2 Schematic of (a) static and (b) dynamic loading systems by Dewey et al. [44]

In 1999, after the release of *NCHRP 350*, a study was performed by the Midwest Roadside Safety Facility (MwRSF) to provide data on the post-soil interaction of steel/wood guardrail posts rotating in the soil base [47]. This study included a detailed instrumentation plan and data collection methods including accelerometers, load/displacement transducers and strain gages attached on the posts. Dynamic impact tests using a bogie vehicle were conducted at three different test speeds. Nine wide-flange steel posts (which had been used a standard steel post) and six wood posts were tested and showed significantly different failure modes from one another even though the number of tests were too few for thorough statistical analysis. All steel posts exhibited ductile-plastic deformations with failure (dilation) of the soil, while half of the wood posts failed in a brittle manner by the impacting bogie.

In 2007, MwRSF investigated the dynamic structural performance of standard steel guardrail posts installed on a 2:1 slope using a bogie vehicle [48]. A total of 21 dynamic

impact tests were performed with varying post lengths (from 6- to 9-ft) and embedment depths (from 40- to 76-in.) since it was necessary to determine the required embedment depth of the post installed in sloped terrains. Using acceleration data from the bogie vehicle, the force-displacement and dissipated energy-displacement responses were computed. From the comparison of average forces to that of the level terrain (reference) as shown in Table 2.1, a recommended configuration for length and embedment depth on a 2:1 slope was found. This research study determined that the standard post length and embedment depth (6-ft. and 40-in.) was not adequate for steep slope conditions, and also contributed to follow-up studies incorporating full-scale tests on the recommended configuration performed by Polivka et al. [32] and Wiebelhaus et al. [35].

Table 2.1 Summary of bogie test results reproduced from Dey et al. [48]

Test description	Corresponding test numbers	Post length (ft.)	Embedment depth (in.)	Average force (kip)
2:1 sloped terrain	1,10	6.0	40	2.022
	2,9	6.5	46	3.774
	3,8	7.0	52	5.338
	4,11	7.5	58	6.318
	5,12,15	8.0	64	5.752
	6,13	8.5	70	6.248
	7,14,16,17	9.0	76	6.916
Level terrain (reference)	18,19,20,21	6.0	40	6.464

In 2010, Gabauer et al. [49] conducted a series of subcomponent tests using a pendulum mass system as shown in Figure 2.3 to investigate the structural performance of W-beam guardrails with minor damage. Since guardrail systems had generally been

tested in an undamaged condition, the research study focused on the lack of knowledge regarding the performance of guardrails that have experienced minor damage in service conditions. Two categories of minor damage were investigated: (1) vertical/horizontal tears and splice damage in rail component, and (2) twisted/missing blockouts. Based on pendulum impact test results with these damage conditions, vertical tears were determined to be the most significant risk to the structural adequacy of the guardrail system, while missing blockouts were found to be the second most significant risk.

Figure 2.3 Pendulum mass and impactor face by Gabauer et al. [49]

Hampton and Gabler [50] investigated W-beam guardrail systems with missing offset blocks, which they identified to be one of the most common damage conditions for roadside guardrails. Results from three pendulum tests and finite element simulation using LS-DYNA® indicated a missing blockout can decrease the ability of guardrail system to contain and redirect a colliding vehicle.

In 2012, Schmidt et al. [51] evaluated the energy dissipation characteristics of W6x8.5 steel guardrail posts with a reduced embedment depth of 36 in. compared to those of the standard embedment depth of 40 in. A total of eight dynamic subcomponent tests were performed using a bogie vehicle. Two different soil conditions (moderately and highly compacted) and load heights (24-7/8 and 28-7/8 in.) were included as test design variables. The force-displacement and dissipated energy-displacement relationships were computed from acceleration data for the bogie vehicle. It is concluded that a W6x8.5 post with a 36-in. embedment depth can provide enough lateral resistance force to be used with the existing MGS designs.

2.3 Mow strip with guardrail posts

Relatively few research studies have been performed to address the effect of mow strips on the overall behavior of guardrail posts [4, 5, 52-54]. In addition, the dimensions and material properties of the mow strip have not been evaluated for their impact on the ground-level restraint of guardrail posts.

Research performed by the Texas Transportation Institute (TTI) to investigate the impact of mow strips on the performance of guardrail systems [4] formed the basis for the adoption of the guardrail post installation detail incorporating grout leave-outs into the *AASHTO Roadside Design Guide*. The researchers examined the performance of guardrail and mow strip systems using experimental evaluation and numerical simulation. A concrete mow strip of 5-in. thickness and an asphalt mow strip of 8-in. thickness were considered in addition to the presence of "leave-out" sections around posts. Seventeen

configurations of wood and steel guardrail posts embedded in various confinement conditions were subjected to dynamic impact testing with a bogie vehicle (Figure 2.4). The dynamic impact tests were numerically simulated, and full-scale mow strip system models were assembled using the subcomponent models. Based on predictive numerical simulations, a concrete mow strip with grout-filled leave-outs was selected for full-scale crash testing in accordance with *NCHRP 350* criteria. Crash tests of a steel post guardrail system and wood post guardrail system encased in the selected mow strip configuration were deemed successful.

Figure 2.4 Typical setup for asphalt mow strip test cases by Bligh et al. [4]

Further research on the performance of guardrail systems with concrete mow strips was presented in 2009 [52]. This work focused primarily on alternative materials used in the post leave-outs: a urethane foam, two types of molded rubber mat, and a precast concrete wedge. All posts were placed with a concrete mow strip of 5-in. thickness but with different leave-out materials. These alternative configurations were evaluated using the bogie vehicle employed in the previous study. The authors asserted that three of the four alternative leave-out materials demonstrated satisfactory performance in comparison with a post with no mow strip installed.

In 2011, an experimental study incorporating a low-strength concrete mow strip was conducted by California Department of Transportation (CALTRANS) to solve the problem of weed growth beneath a metal beam guardrail system [54]. In this study, two guardrail systems installed with low-strength concrete mow strips with expanded polystyrene foam around steel guardrail posts were tested according to *NCHRP 350* as shown in Figure 2.5. The installation of relatively weak foam material around the posts was an alternative to the leave-out method proposed by the TTI studies. From the two full-scale crash tests, the researchers recommended the depth (thickness) of the low-strength concrete mow strip should be two inches or less to achieve the desired performance of their guardrail system.

Figure 2.5 Installation of concrete mow strip with alternative leave-out by Whitesel et al. [54]

In 2012, Jowza et al. [53] conducted a series of dynamic tests using a bogie vehicle to investigate the effect of asphalt mow strips located on a sloped terrain. In most of the tests conducted, the impacted wood posts could break the asphalt mow strips and rotate backward (Figure 2.6) when 2-in. asphalt mow strips were used. However, the researchers recommended the wood posts not be completely surrounded by asphalt since the post-soil resistance observed from the mow strip-incorporated tests was higher than the resistance of tests without a mow strip.

Figure 2.6 Test pictures of wood post with asphalt mow strip by Jowza et al. [53]

In 2015, a series of dynamic impact tests on weak steel posts (S3x5.7) embedded in three different surrounding soil conditions (weak soil, strong soil, and strong soil covered by an asphalt mow strip) were conducted by Rosenbaugh et al. [5]. A total of ten bogie vehicle tests were run, and one of the tests included the asphalt mow strip of 4-in. thickness and 24-in. rear distance. As shown in Figure 2.7, the test with a mow strip showed excessive ground-level restraint which prevented the rotation of the post and caused the formation of a plastic hinge at ground-level.

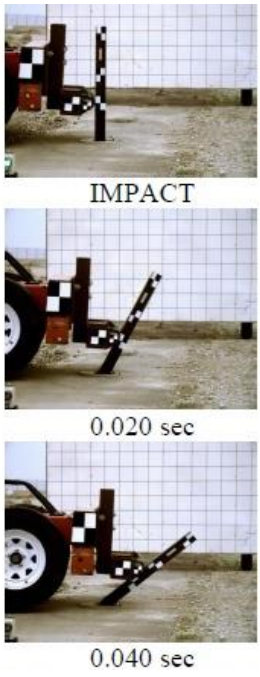

Figure 2.7 Test pictures of socketed steel post with asphalt mow strip by Rosenbaugh et al. [5]

CHAPTER 3
STATIC TESTS FOR PERFORMANCE ASSESSMENT OF GUARDRAIL POSTS

This chapter details the development of a static loading test setup and protocol for evaluating the effect of asphalt mow strips on the structural behavior of steel guardrail posts. A static loading test can be considered as an economical evaluation method to provide an initial assessment of critical design variables prior to costly full-scale dynamic testing. A total of 19 guardrail posts were tested with various mow strip designs to evaluate a range of mow strip design variables in terms of satisfactory performance. Experimental results – force, displacement, and strain data measured during the static tests – were analyzed under quantitative performance assessment criteria related to ground-level restraint. Based on the performance assessment, two pertinent geometric parameters of the mow strip – thickness and rear distance – were determined to effectively reduce the restraint to a desired level.

3.1 Static test protocol

3.1.1 Use of static test methodology

In certain loading situations, the static performance of a structural system can be a general indicator of dynamic performance. If a structural system fails to show satisfactory performance by a considerable margin under static loading, it can be inferred that the system would be unlikely to exhibit satisfactory performance under a similar

dynamic loading situation. Even though static tests cannot be used to describe the dynamic response of the structural system, it is not unreasonable to find a correlation between the static and dynamic structural responses (e.g., deformation). Based on this correlation, static testing methodologies have been utilized in the automotive industry to predict the structural performance of test vehicles under dynamic loading [55, 56]. In several early experimental studies on guardrail systems, static tests were also conducted to evaluate the performance of guardrail posts in various embedment conditions [43, 44]. Hence, a series of static tests on steel guardrail posts encased in various types of asphalt mow strip can be used as a first-stage assessment of the effect of geometric and material parameters of the asphalt mow strip, which will allow subsequent dynamic testing programs to be more focused and therefore cost-effective.

3.1.2 Test description

Test dimensions of the static test program were determined from the design of the Midwest Guardrail System (MGS) [57] which is one of the most widely-used guardrail systems in the United States, and also specified as a standard roadside barrier in the *AASHTO RDG* [1]. Figure 3.1 shows the test dimensions for the standard wide flange steel guardrail post (W6x9) used in this static test program.

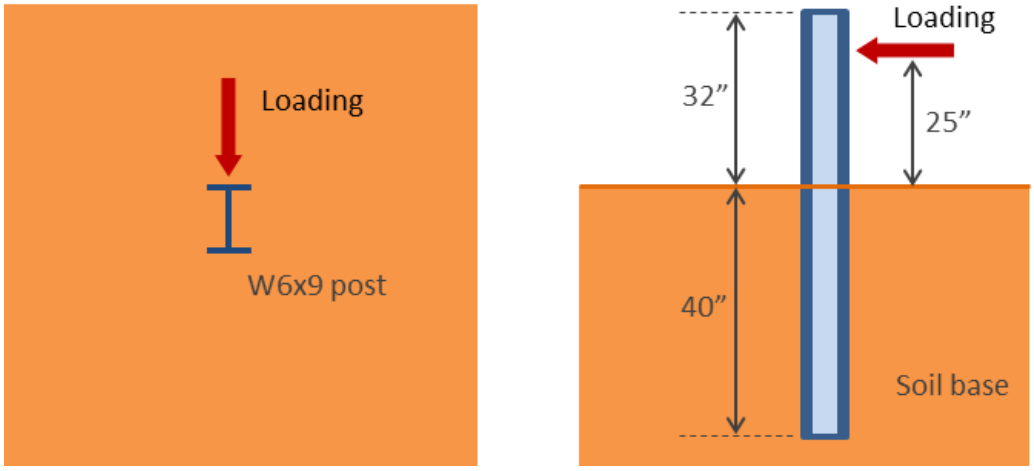

Figure 3.1 Static test dimensions for standard steel post after [1]

Figure 3.2 illustrates the static test setup including the soil base, asphalt mow strip, steel guardrail post, loading fixture, and instrumentation. A lateral load on the guardrail post was applied by a hydraulic cylinder with a controlled quasi-static rate of approximately 2.0 in./min. Each test was mainly controlled by manual retraction of the hydraulic cylinder on the loading fixture.

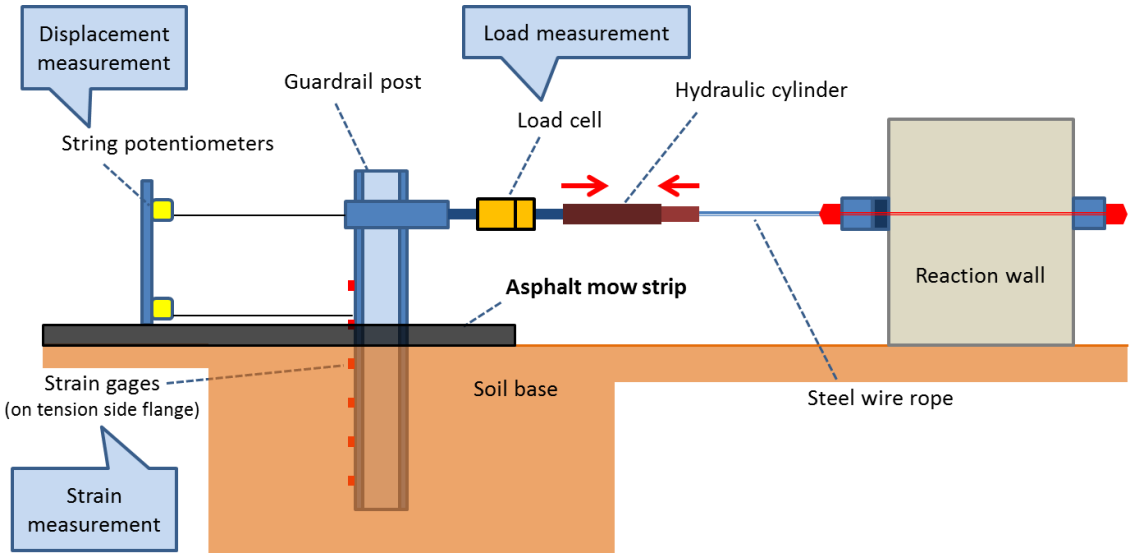

(a)

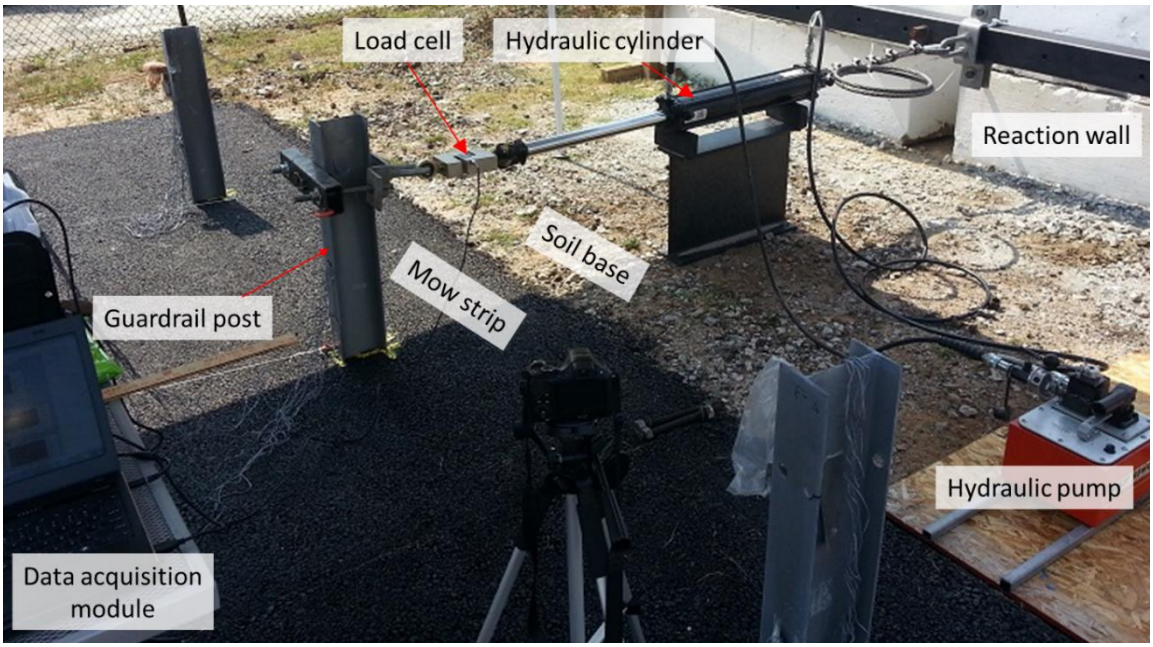

(b)

Figure 3.2 Static test setup: (a) schematic, and (b) site picture with description

3.1.3 Test site preparation

The outdoor test site for the static test program shown in Figure 3.2 is located at the Structural Engineering, Mechanics, and Materials Laboratory of the Georgia Institute of Technology, Atlanta, GA. Standardizing soil conditions throughout the test program is one of the essential processes for performing experiments on guardrail posts in a repeatable manner. Since there is no directly relevant guideline for static testing of guardrail posts, the *MASH* guidelines offered for static soil strength tests [13] were used to determine a standard soil condition and grading/compaction requirements. According to the *MASH* guideline, the test soil should meet *AASHTO M147* [58] grading A or B requirements and should be compacted in accordance with *AASHTO's Construction Manual for Highway Construction* [59]. The in-situ dry density of the compacted soil, determined by a sand cone test as given in *AASHTO T191* [60] or other specified methods, should exceed 95% of the maximum dry density of soil, determined by a Modified Proctor test (*AASHTO T180*) [61] or other specified methods.

Based on these requirements, the native soil was replaced with a graded aggregate base soil which satisfies the *AASHTO M147* Grading B requirement with a maximum dry density of 144 lb/ft^3. Prior to each test, the soil was compacted to exceed 95 percent of the maximum dry density of soil (Figure 3.3). A plate vibratory compactor was used to compact the imported soil and sand cone tests were performed to determine whether the soil was adequately compacted or not. The in-situ dry density was 145 lb/ft^3 and as such the *MASH* compaction requirement was met. Further details on the laboratory soil test results are given in Appendix A.

Figure 3.3 Soil replacement and compaction at static test site

For asphalt mow strips, a standard type of hot mixed asphalt (HMA), classified as PG 76-22 binder with a 3/4-inch aggregate size, was installed by local asphalt contractors in Atlanta, GA. Approximately one week after the asphalt installation, the standard steel guardrail posts (W6x9) were driven through the asphalt layer and into the ground by blows from a hydraulic post driver provided by the Georgia Department of Transportation as shown in Figure 1.2. The time duration of each post installation was less than two minutes.

3.1.4 Test instrumentation

Lateral load on the post, displacement of the post, and longitudinal strains along the post flange were measured and recorded through a data acquisition system. As shown in Figure 3.4, an S-shaped load cell was linked with the retracting arm of the hydraulic cylinder and with a bracket transmitting the lateral load to the post. Threaded bearing

rods were attached on both sides of the load cell to prevent bending and torsion along the load axis. This also allowed the lateral load to be applied perpendicular to the flanges of the post - normal to the edge of mow strip. Two string potentiometers were mounted on a reference pole with a stand-off distance approximately 6 ft. from the post. One string potentiometer measured the lateral displacement at the level of the loading (25 in. from the ground level) and one measured the displacement at ground level.

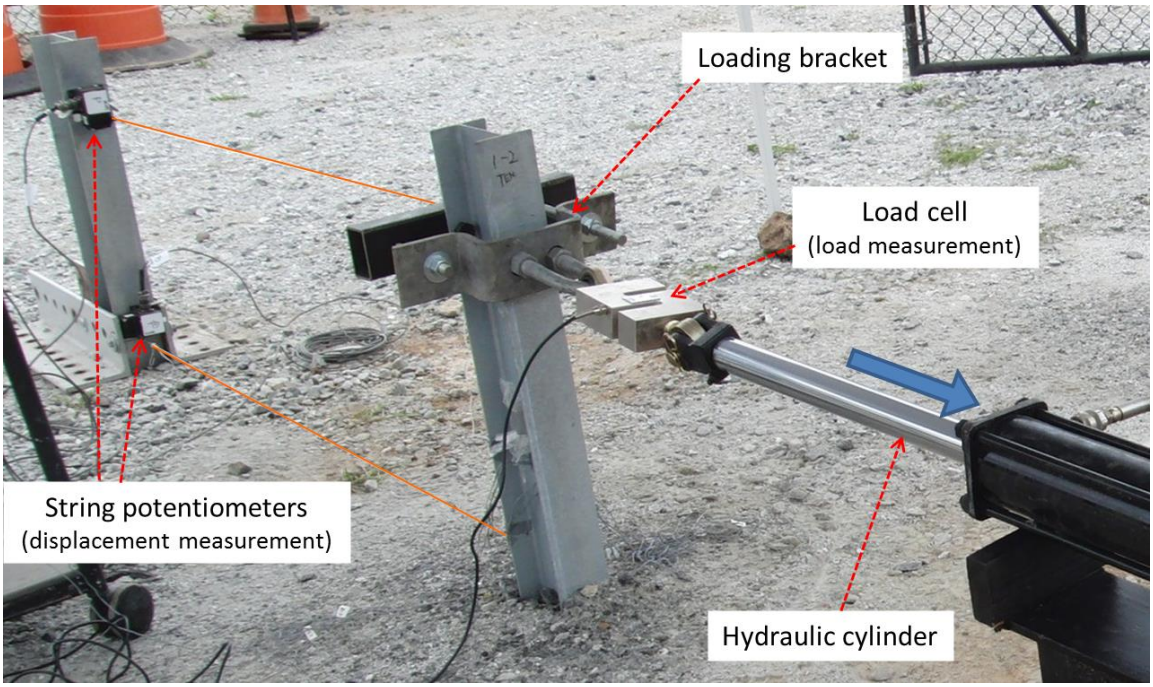

Figure 3.4 Loading fixture and instrumentation details for static test program

As shown in Figure 3.5, a total of nine strain gauges were attached to the tension side flange of each guardrail post and measured the longitudinal strain from 30 in. below the ground level to 10 in. above the ground level. A metal shim was attached at the bottom of the flange and covered all gages and wires under the ground level to prevent the

damage from post-driving. Detailed information on the instrumentation used in this test program is specified in Appendix B.

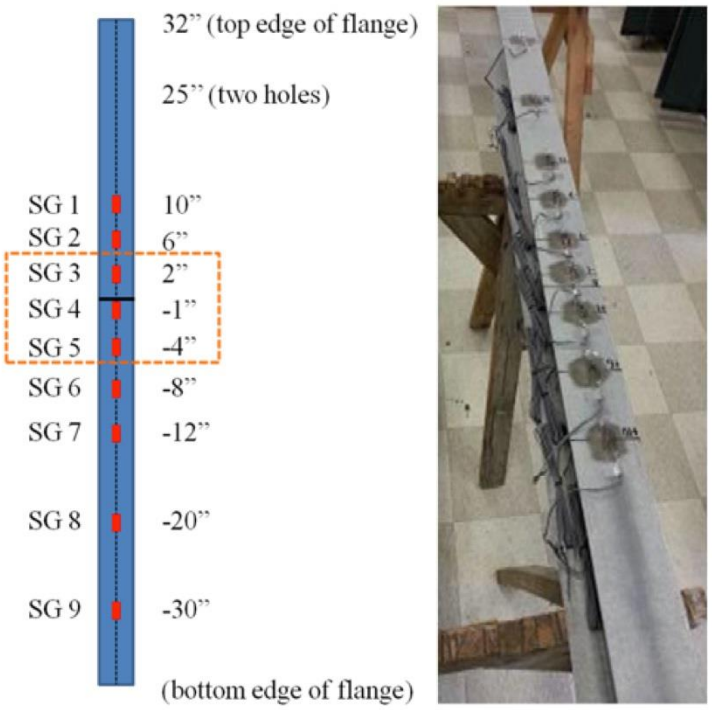

Figure 3.5 Post strain gage installation details for static test program

3.2 Static test matrix

3.2.1 Asphalt mow strip state-of-the-art

The previous studies described in the Chapter 2 did not consider alternative methods to reduce ground-level restraint from asphalt mow strips without resorting to the installation of a leave-out as given in *AASHTO Roadside Design Guide* [1]. Consideration of other methods may provide designs that can sufficiently reduce ground-

level restraint with better constructability. Specifically, less ground-level restraint can be achieved by reducing two geometric parameters of the mow strip: thickness and rear distance. In this study, the mow strip thickness refers to the average thickness of mow strip installed around and behind the post, and the rear distance refers to the minimum distance from the guardrail post to the edge of the mow strip (Figure 1.3). The mow strip thickness and rear distance were not considered as a design parameter in roadside design; there is no common standard or specification regulating the upper limit of the mow strip geometric parameters based on the performance of guardrail posts.

Thus, it was first necessary to study the current state of practice related to the use of asphalt mow strips (also called as vegetation barriers or shoulders) in the United States. The first identification of current practice on asphalt mow strip installation in the United States was made by researchers at the Georgia Institute of Technology [62]. The researchers conducted a two-part survey. They performed phone solicitations and investigated publicly accessible websites for all 50 State Departments of Transportation (DOT). The electronic documents accessed through the websites included relevant roadside construction standards, specification, and drawings for each state.

The survey resulted in the identification of a range of geometric parameters employed in asphalt mow strip designs. Figure 3.6 shows a summary of maximum thickness and rear distance used in asphalt mow strips in the United States. For the 25 states where the thickness of a mow strip is specified, the maximum thickness of the asphalt layer ranges from 1.5 to 8 inches, while for the 17 states where the rear distance of mow strip is specified, the maximum rear distance ranges from 6 to 48 inches. The most common

mow strip geometry is a combination of 2 inches in thickness and 24 inches in rear distance.

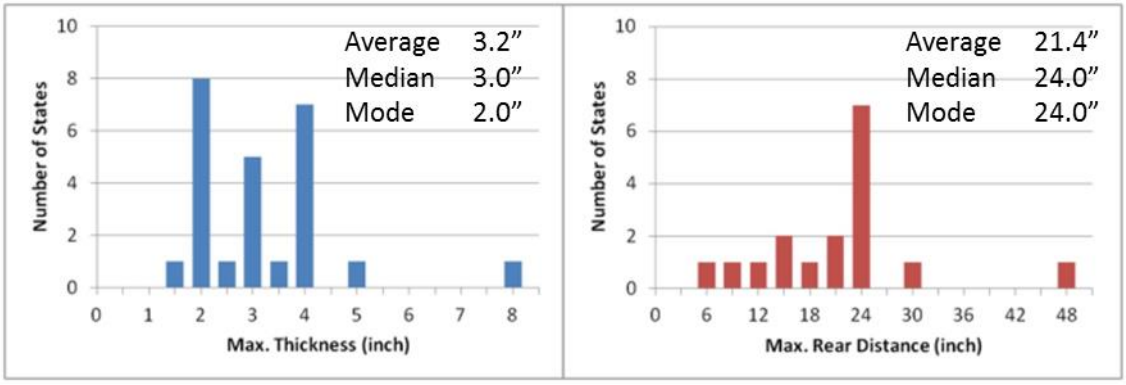

(a) (b)

Figure 3.6 Asphalt mow strip geometric parameters found in state DOT databases: (a) maximum thickness, and (b) maximum rear distance

3.2.2 Application of pre-cutting

Pre-cutting is a possible mow strip modification technique which can be defined as using a saw or other tools to cut slots in the rear (behind the post) side of the mow strip to induce failure planes when a guardrail post is hit by a vehicle. Properly applied pre-cuts may expedite the failure of the mow strip as part of the mow strip will detach from the main body with relatively low lateral force applied on the post. As such, pre-cutting may be an efficient and economical retrofit technique for mitigating the ground-level restraint induced by mow strips similar to the reduction of rear distance. It is obvious that new mow strip installation requiring demolition of existing pavement would cost significantly more than the installation of pre-cuts.

As illustrated in Figure 3.7, an efficient pre-cutting pattern can be chosen by observing cracks and their propagation in the rear side of mow strips where the posts are loaded to rupture the asphalt layer. Practical considerations on the constructability are required for choosing the pattern so that pre-cutting can be conducted safely and not damage existing guardrail structural components.

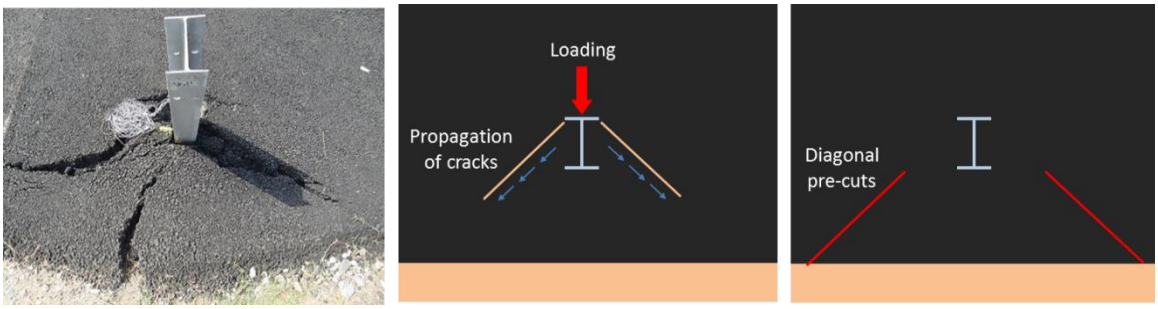

(a) (b) (c)

Figure 3.7 Pre-cutting of mow strip: (a) observation on cracks, (b) schematic of crack propagation, and (c) example of pre-cutting pattern

3.2.3 Determination of test matrix

Table 3.1 outlines the test matrix for the static experimental program for 19 guardrail posts: the mow strip geometry, test condition, and related figures for further details. The static test matrix consists of five test groups: B, T, L, R, and P. The capital letter in the test numbering designates the test group – B for baseline, T for typical mow strip, L for leave-out, R for reduced rear distance, and P for pre-cut.

Table 3.1 Static test matrix

Test number	Test group description	Mow strip geometry		Test condition		Related figures for details
		Thickness (inch)	Rear distance (inch)	Test temperature (°F)	Asphalt age (day)	
B1,2,3	Baseline	0	0	80	-	Figure 3.8
T1,2 T3 T4 T5,6 T7	Typical mow strip	2 2 2 3.5 3.5	24 24 24 24 24	90 50 75 90 50	18 118 40 18 118	Figure 3.9
L1,2 L3	Leave-out application	3.5 3.5	24 24	50 70	118 32	Figure 3.10
R1 R2 R3	Reduced rear distance	2 2 3.5	6 12 12	75 75 70	40 40 32	Figure 3.11
P1 P2 P3	Pre-cut application	2 3.5 3.5	24 24 24	75 70 70	40 32 32	Figure 3.12

Initially, two test groups were identified to provide a useful frame of reference to compare to the alternative post installation methods evaluated in this research. The first three tests (B1-3) were designated as the baseline configuration, which were used to calibrate computer models without an asphalt mow strip (Figure 3.8). The baseline tests represent the lower bound of the ground-level restraint among all test configurations. The next seven tests (T1-7) were designated as typical mow strip configurations, which were identified from the state-of-the-art survey described in Section 3.2.1. These tests were performed to calibrate computer models including a mow strip (Figure 3.9). The typical configuration represents current practice of asphalt mow strip installation with no attempt on reducing the ground-level restraint by the mow strip.

(a)

(b)

Figure 3.8 Static test on baseline configuration with no mow strip: (a) details, and (b) test setup

(a)

(b)

Figure 3.9 Static test on typical mow strip configuration: (a) details, and (b) test setup

Other test groups represent alternative mow strip installation methods to mitigate ground-level restraint induced by the mow strip. They include a total of nine tests; three tests where leave-outs are installed (L1-3), three tests with reduced rear distances (R1-3), and three tests on mow strips with pre-cuts (P1-3). Figure 3.10 shows the leave-out configuration used in this study where an 18-in. by 18-in. square portion of the asphalt layer around the post was removed and replaced by a low-strength cementitious grout. The 28-day compressive strengths of the grout materials used as the leave-out were always less than 120 psi. Both dimensions and material strength satisfied the recommendation in the *AASHTO Roadside Design Guide* [1]. Figure 3.11 shows the details for the reduced rear distance configuration – two different rear distances (6- and 12-in.) were tested. Figure 3.12 shows the details for the pre-cut-applied configurations. Two effective pre-cut patterns (parallel and diagonal cut) were selected out of six different pre-cut patterns by finite element simulations in the previous research [62]. The parallel pre-cut was applied in the P1 test and the diagonal pre-cut was used in the P2 and P3 tests.

(a)

(b)

Figure 3.10 Static test on leave-out configuration: (a) details, and (b) test setup

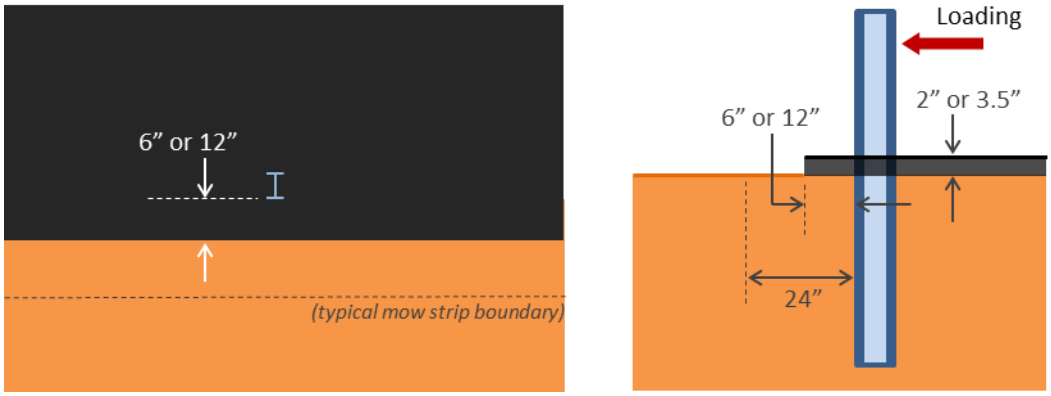

(a)

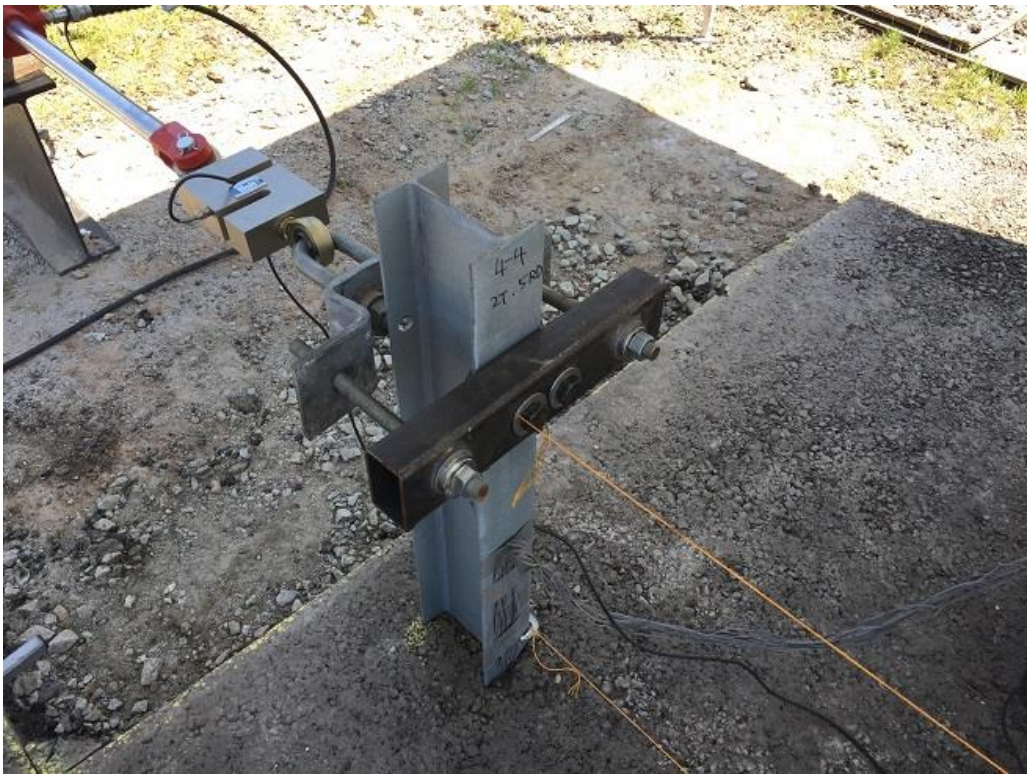

(b)

Figure 3.11 Static test on reduced rear distance configuration: (a) details, and (b) test setup

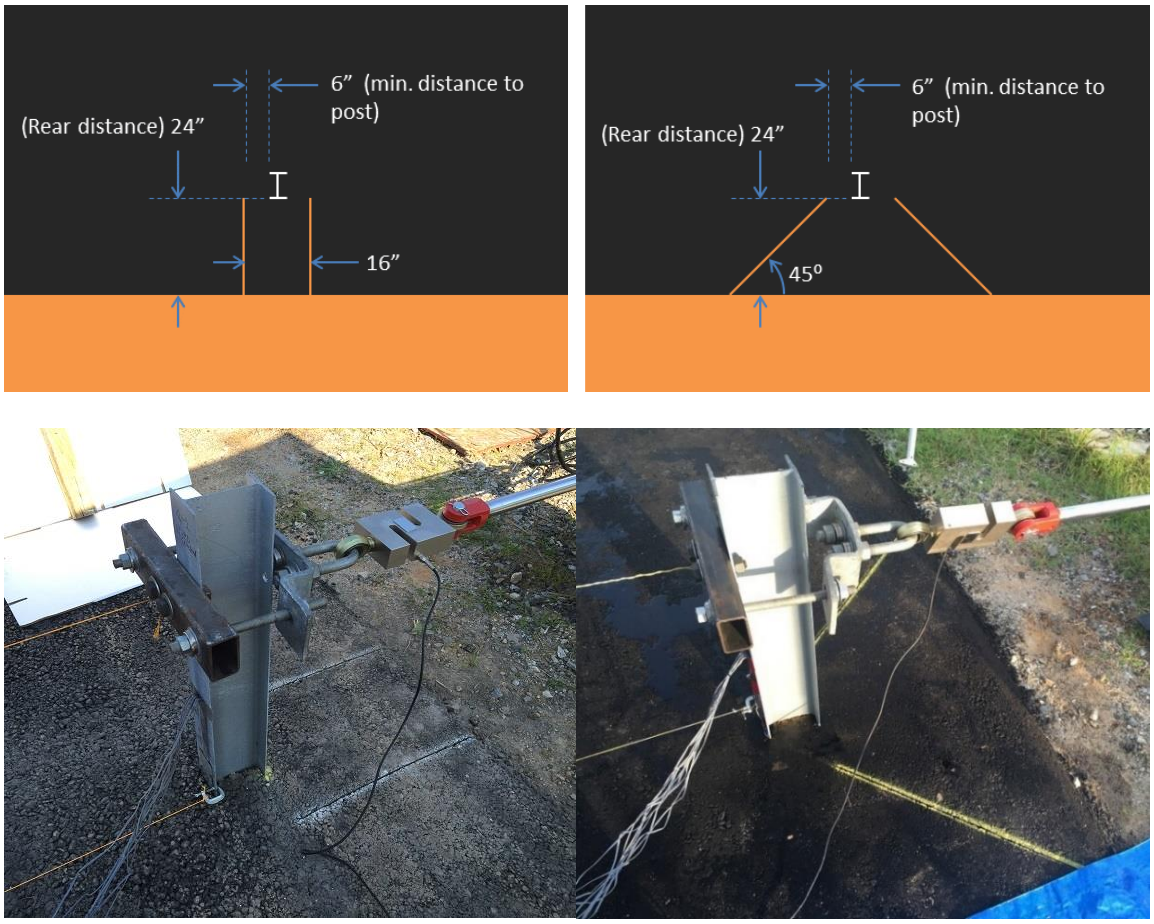

(a) (b)

Figure 3.12 Static test pre-cut mow strip configuration details and test setup: (a) parallel (P1), and (b) diagonal pre-cut (P2,3)

The influence of temperature and asphalt age was considered in the static test matrix. However, several experimental constraints and practical limitations precluded an investigation of low and high extremes of temperature as well as asphalt age.

Regarding temperature extremes, the lowest daily maximum temperature in Atlanta, GA, was recorded as 28°F, which was the only day below the freezing point during the static testing period (from 3/19/14 to 7/14/15) [63]. From the last 100 years (1917-2016)

of temperature records in Atlanta, GA, the 1st percentile of the daily maximum temperature is 50.5°F and the 99th percentile of the daily maximum temperature is 89.2°F [63], where each percentile can represent the winter and summer test temperatures, respectively. As such, test temperatures ranging from 50 to 90°F can be taken as a reasonable representation of local weather conditions for Atlanta, GA.

Regarding asphalt aging, several time-constraint factors related to the test preparation were critical. The static test program had a total of approximately 16 months of duration from the initial test site construction to the final test run. Because the outdoor test bed can contain up to 4 posts in a single round of tests, a total of 5 rounds were required to test all 19 posts. Additionally, the test bed needed to be restored after each round of tests for the next round test setup. The test bed restoration included multiple tasks such as post removal, soil compaction, asphalt placement, and post driving and typically took more than 4 weeks to be completed. Considering these, the oldest asphalt tested in the static program was set approximately 4 months from the date of asphalt placement.

Therefore, the static test program was governed by these constraints and tests were conducted under the temperature range of 50~90°F and an asphalt age range of 18~118 days. Nevertheless, the static test matrix successfully included experiments on identical test configuration at different test conditions. For example, tests T3 and T7 represent the most aged asphalt mow strips in a winter condition while tests T1, T2, T5, and T6 represent the least aged asphalt mow strips in a summer condition of Atlanta, GA.

3.3 Static test results

A total of 19 static tests were performed under the same test protocol described in Section 3.1. Lateral load of the post, displacements of the post at two locations (loading height and ground-level), and longitudinal strains along the post flange were measured and plotted. Three types of test result plots are presented in this section: (1) load-displacement plots, (2) work versus ground-level displacement plots, and (3) normalized maximum strain distribution plots.

The load-displacement plot, which can be referred to as the "P-Δ_p plot," where P indicates the applied load and Δ_p is the displacement at the elevation of the load, shows the overall structural response and performance of the subcomponent system. Specifically, the maximum load on the post and the corresponding displacement can be visualized by a P-Δ_p plot. The work versus ground-level displacement plot is referred to as the "W-Δ_g plot," where W is the work done by the applied load (calculated from the area under the P-Δ_p curve) and Δ_g is the displacement at ground or asphalt level, gives an indication of the relative stiffness of the subcomponent system.

Measured strain values at the maximum (peak) load can be illustrated via normalized maximum strain distribution plots, which are referred to as "strain distribution plots." All strain values in the plot were normalized by the yield strain – a value higher than 1.0 indicates that yielding occurred in the post at that gage location. The yield strain was determined as 0.00177 based on material testing (see Appendix A for details), where tension coupons were cut from the flange of a representative steel post and then tested under a specified test method - ASTM A370 [64]. The flexural stress and moment distribution in the post can be estimated by interpolating measured strain values.

Individual test records for all 19 posts are given in Appendix C. A test record sheet includes a test description, detailed drawings, photographs, P-Δ_p curve, W-Δ_g curve, strain plots, and maximum strain values measured at all gage locations.

3.3.1 Baseline tests

Three posts were tested with the baseline test setup as shown in Figure 3.8. The baseline results provide a lower bound for ground-level restraint on the post. Load-displacement (P-Δ_p, Figure 3.13), work versus ground-level displacement (W-Δ_g, Figure 3.14), and strain distribution (Figure 3.15) plots are presented. In the P-Δ_p plot, the average baseline response curve was computed from three test curves for further performance assessment. In the W-Δ_g plot, the results from tests B1 and B3 were almost identical. In the strain distribution plot, the 0-in. height denotes ground-level. Since strain gages used in the baseline tests were not protected by a metal shim, only a small number of gages survived after post driving.

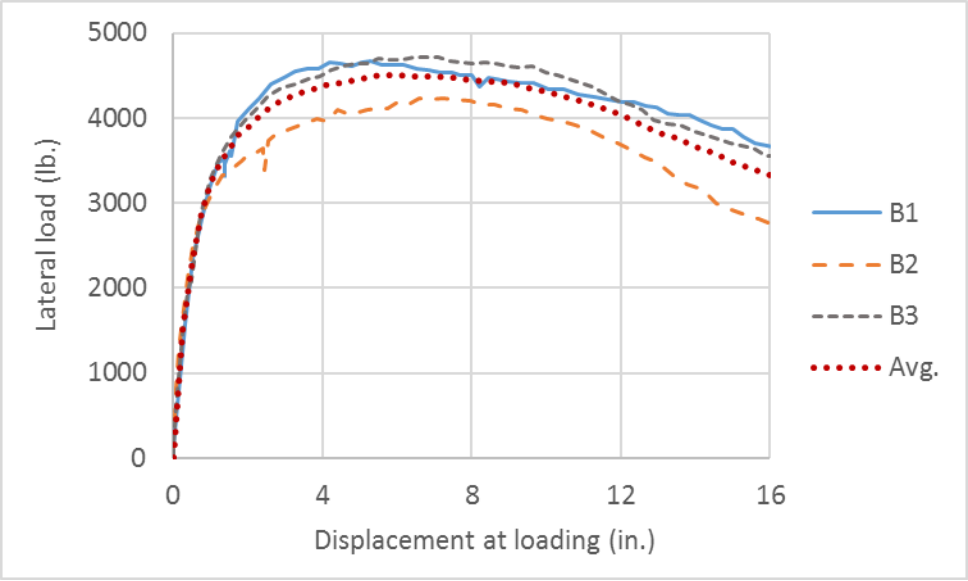

Figure 3.13 P-Δ_p curves of baseline tests (B1~3)

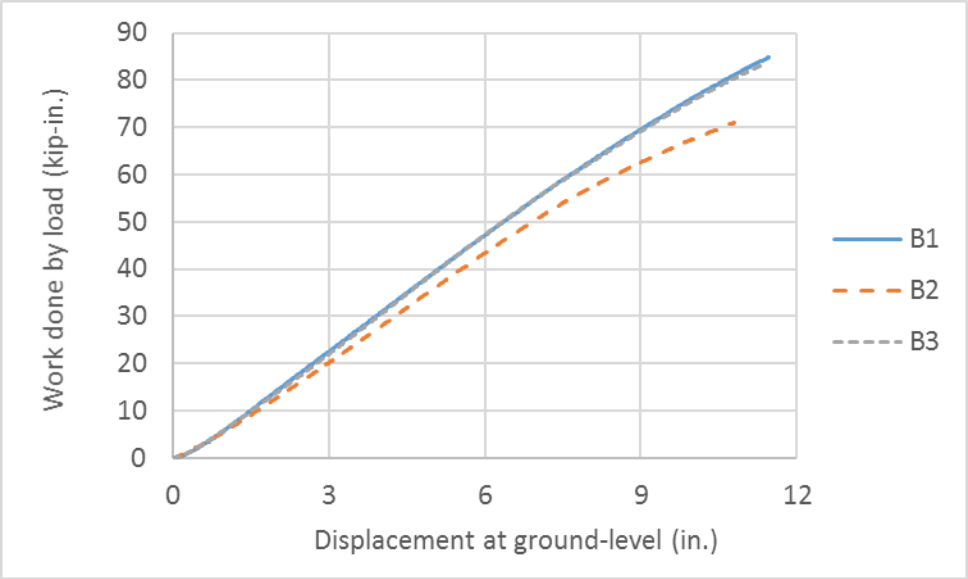

Figure 3.14 W-Δ_g curves of baseline tests (B1~3)

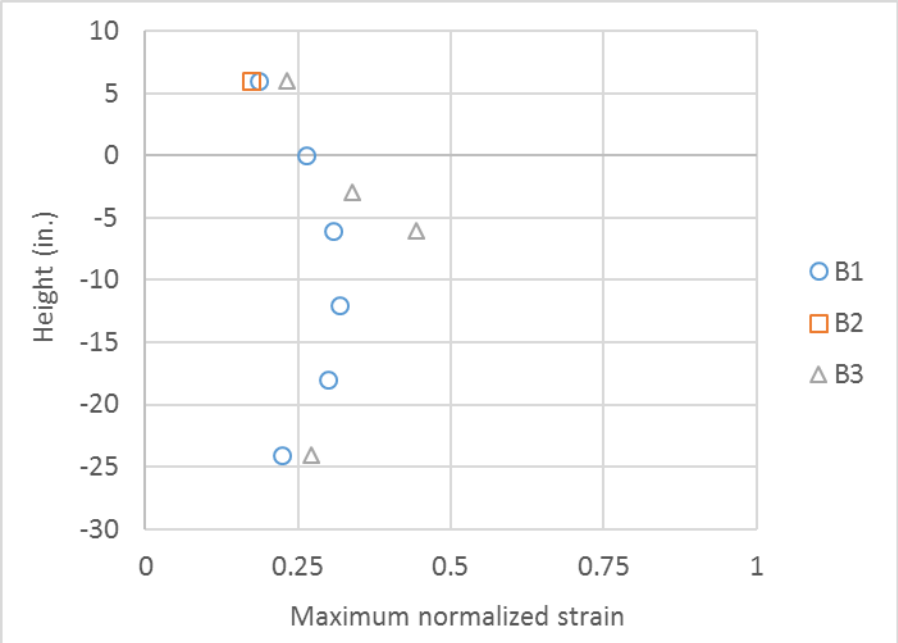

Figure 3.15 Strain distribution plots of baseline tests (B1~3)

3.3.2 Typical mow strip tests

Seven posts were tested with the typical mow strip configuration as shown in Figure 3.9. These tests were conducted with the same rear distance (24-in.) but under different test conditions including a variation in thickness (2- and 3.5-in.), test temperature (50, 75, and 90°F), and asphalt age (18, 40, and 118 days) as described in Table 3.2. Test results using a 2-in. thick mow strip test setup, T1 through T4, are presented and plotted in Figure 3.16 (P-Δ_p curves), Figure 3.18 (W-Δ_g curves), and Figure 3.20 (strain distribution plots). Test results using a 3.5-in. thick mow strip, T5 through T7, are presented in Figure 3.17 (P-Δ_p curves), Figure 3.19 (W-Δ_g curves), and Figure 3.21 (strain distribution plots). As expected for both 2- and 3.5-in. thickness mow strips, tests conducted with the most aged asphalt in a winter condition (T3 and T7) showed significantly higher lateral loads, stiffer slopes in the W-Δ_g plots, and higher strains along the post, compared to the tests conducted with the least aged asphalt in a summer condition (T1, T2, T5, and T6).

Table 3.2 Test geometry and condition in typical mow strip tests

Test number	Mow strip geometry		Test condition		Related figures for details
	Thickness (inch)	Rear distance (inch)	Test temperature (°F)	Asphalt age (day)	
T1, T2 T3 T4	2 2 2	24 24 24	90 50 75	18 118 40	Figure 3.9
T5, T6 T7	3.5 3.5	24 24	90 50	18 118	

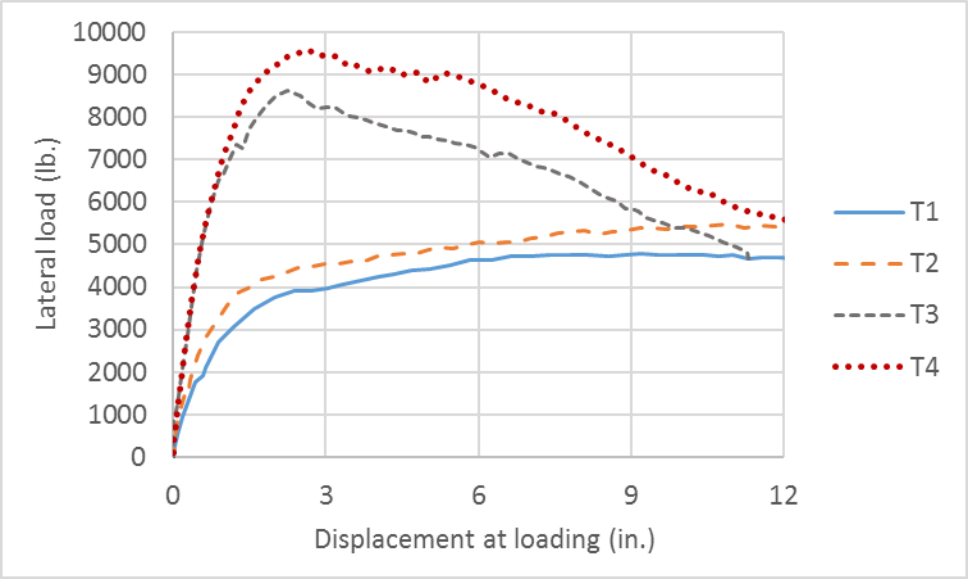

Figure 3.16 P-Δ_p curves of typical mow strip tests (T1~4: 2-in. thickness)

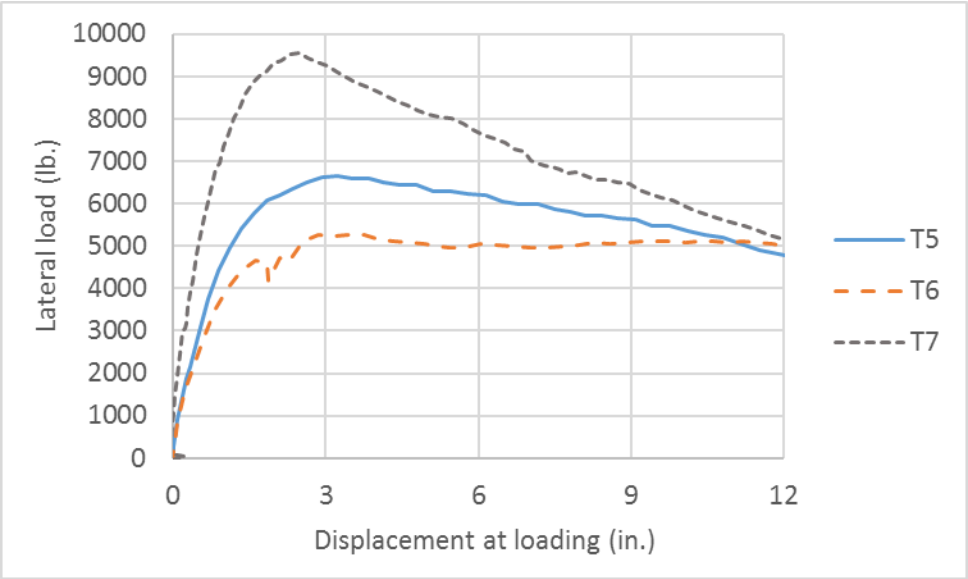

Figure 3.17 P-Δ_p curves of typical mow strip tests (T5~7: 3.5-in. thickness)

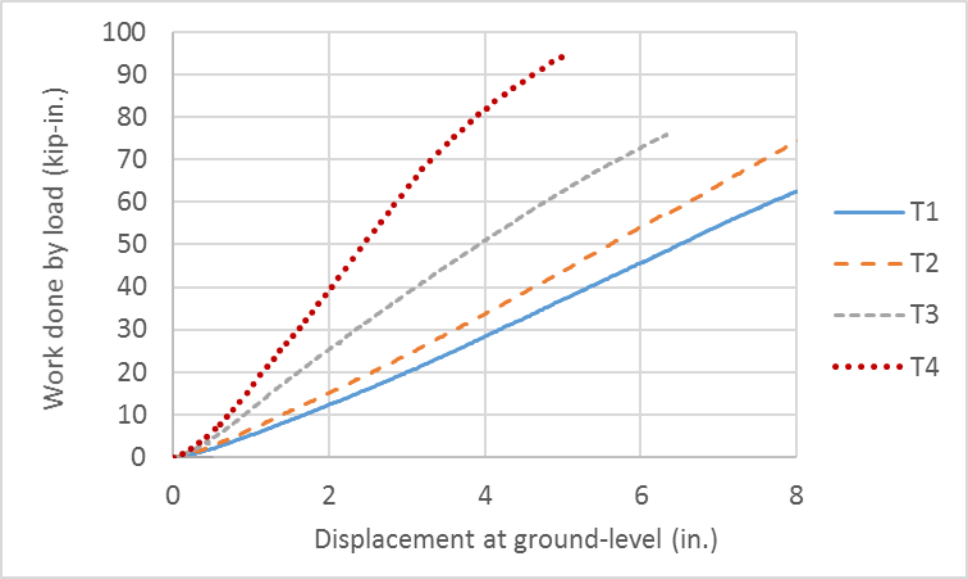

Figure 3.18 ***W*-Δ_g curves of typical mow strip tests (T1~4: 2-in. thickness)**

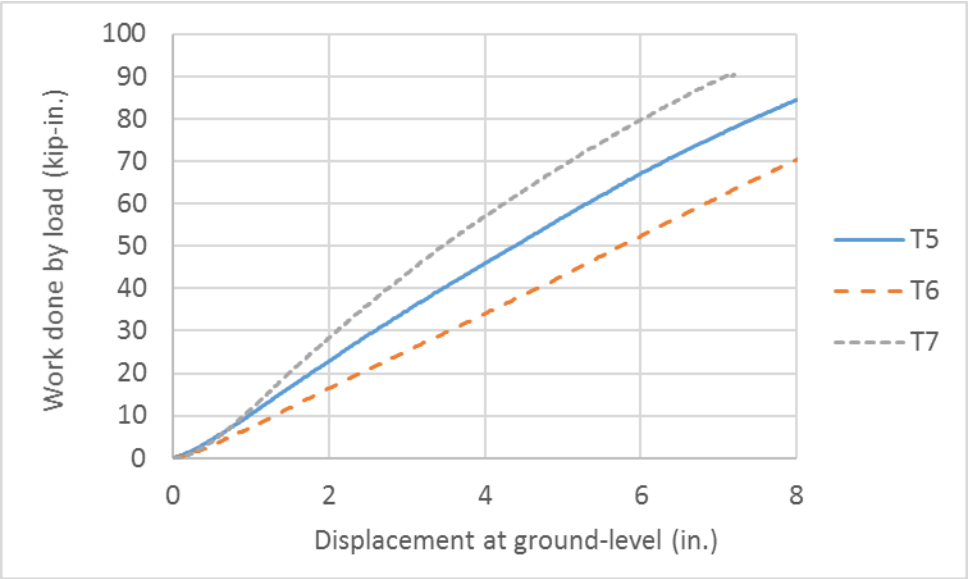

Figure 3.19 ***W*-Δ_g curves of typical mow strip tests (T5~7: 3.5-in. thickness)**

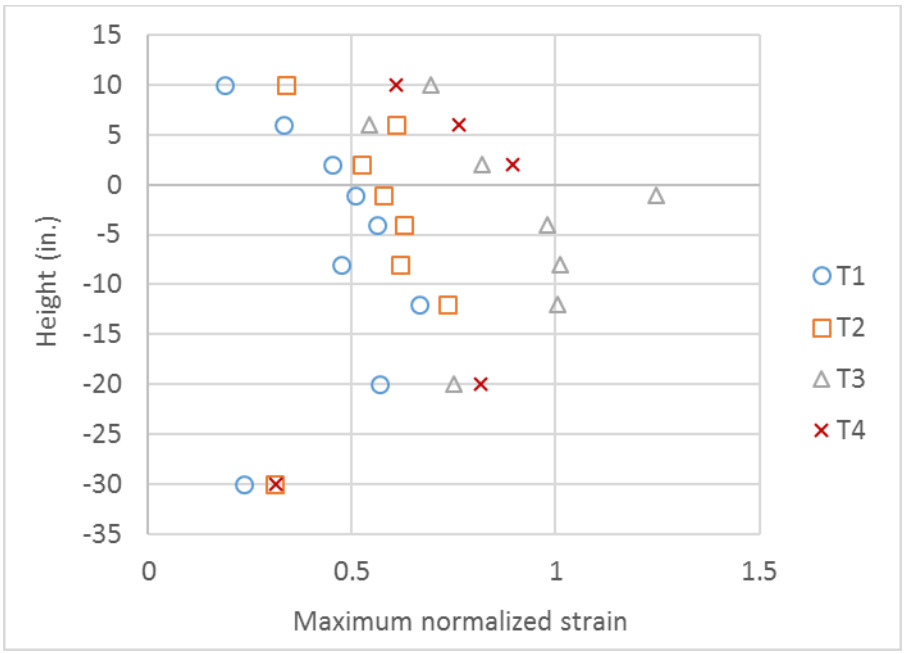

Figure 3.20 Strain distribution plots of typical mow strip tests (T1~4: 2-in. thickness)

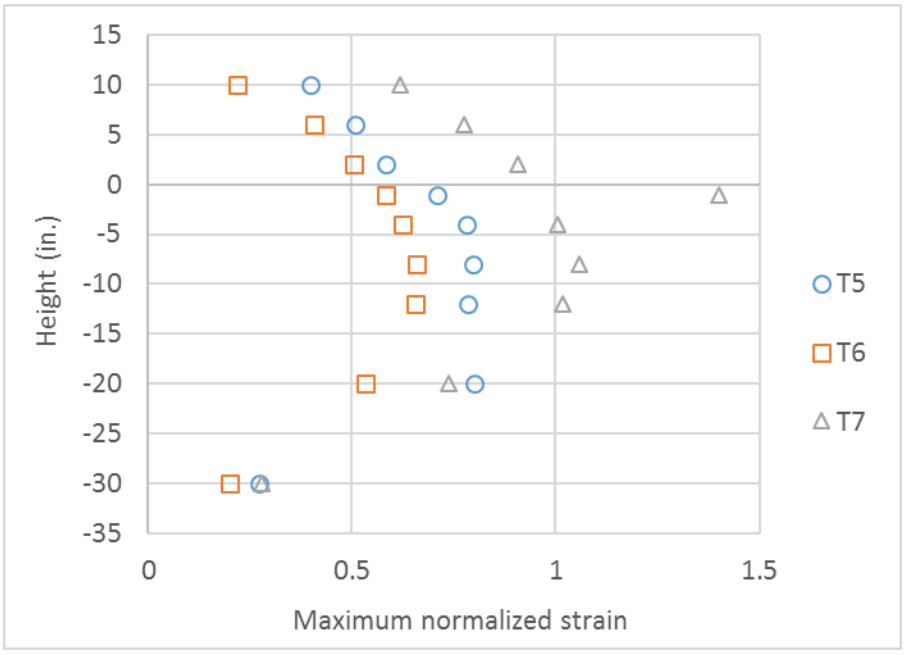

Figure 3.21 Strain distribution plots of typical mow strip tests (T5~7: 3.5-in. thickness)

3.3.3 Leave-out tests

Three posts incorporating a leave-out around the guardrail post were tested under the same test protocol and test configuration shown in Figure 3.10. Test results are presented and plotted in Figure 3.22 (P-Δ_p curves), Figure 3.23 (W-Δ_g curves), and Figure 3.24 (strain distribution plots). Specifically, the average leave-out P-Δ_p curve was computed from three test curves (L1~3) for further evaluation and discussion in Section 3.4 and 3.5. These test results will be used as a "target response" to compare to alternative mow strip installation methods.

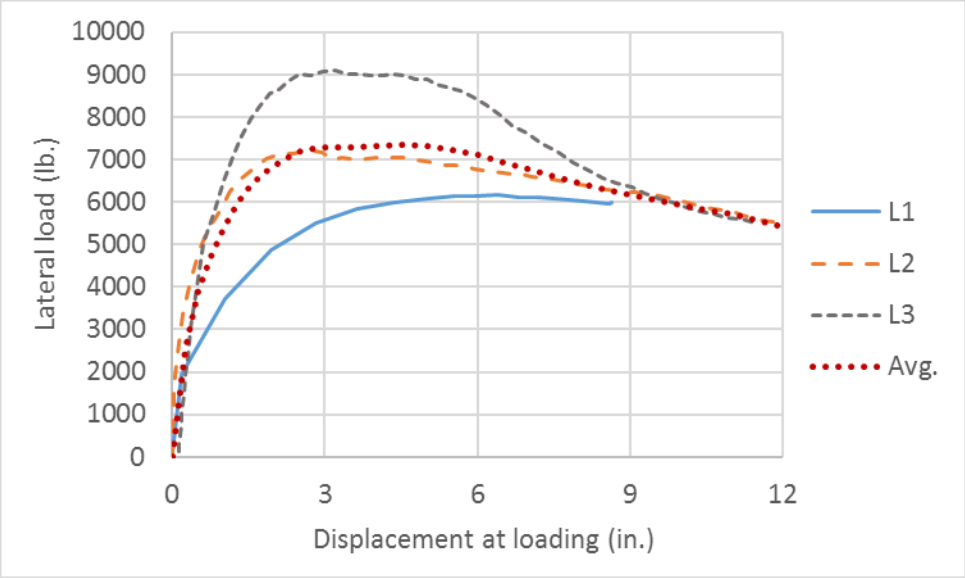

Figure 3.22 P-Δ_p curves of leave-out tests (L1~3)

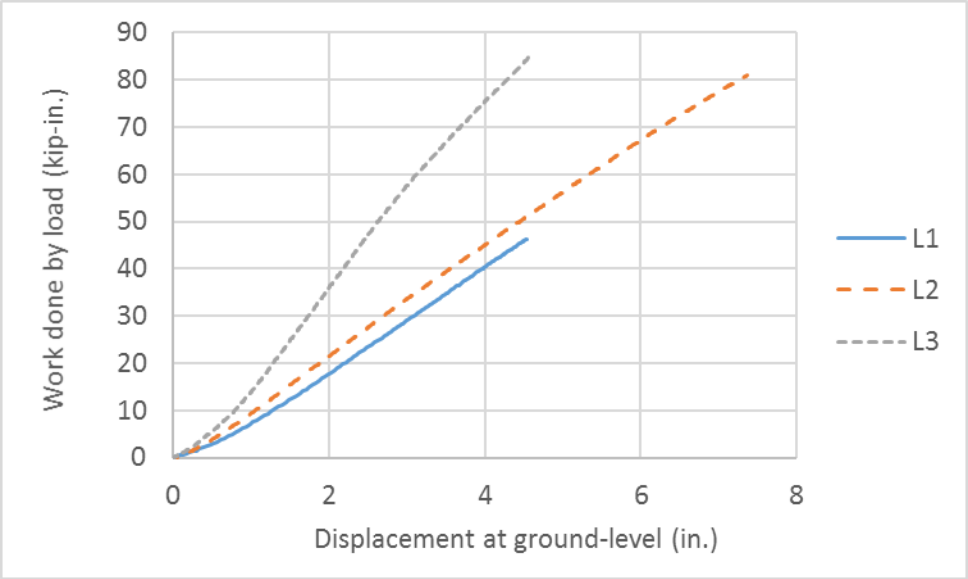

Figure 3.23 W-Δ_g curves of leave-out tests (L1~3)

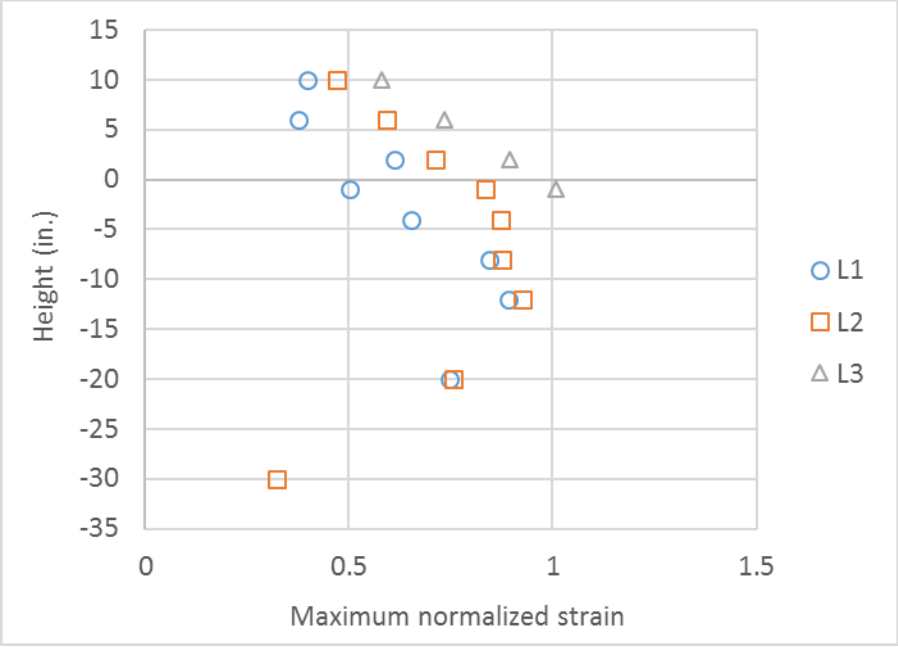

Figure 3.24 Strain distribution plots of leave-out tests (L1~3)

3.3.4 Tests on reduced rear distance mow strips

Three posts were tested with the reduced rear distance configurations shown in Figure 3.11. Test results are presented and plotted in Figure 3.25 (P-Δ_p curves), Figure 3.26 (W-Δ_g curves), and Figure 3.27 (strain distribution plots). Due to malfunction of instrumentation during the test, the R3 test results were not available.

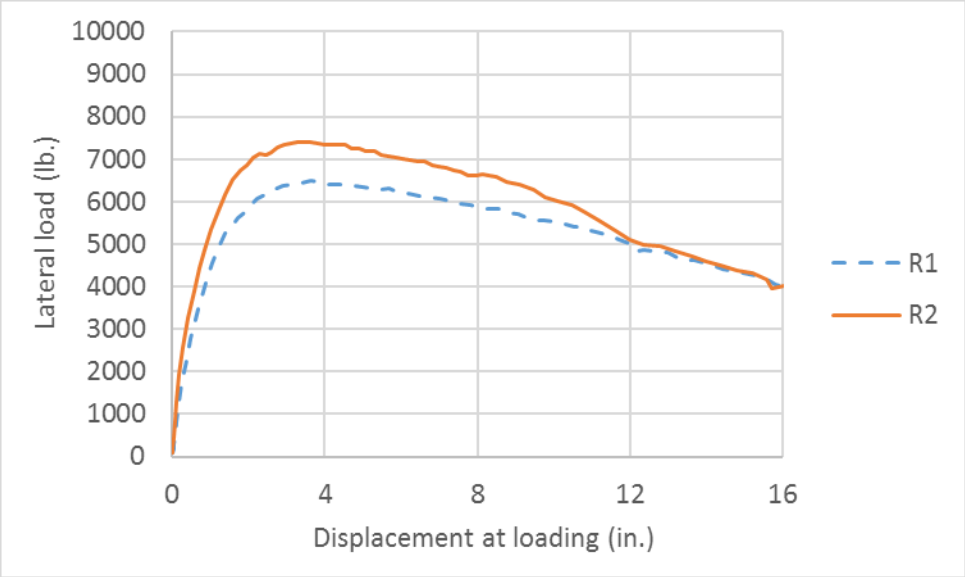

Figure 3.25 P-Δ_p curves of reduced RD tests (R1~2)

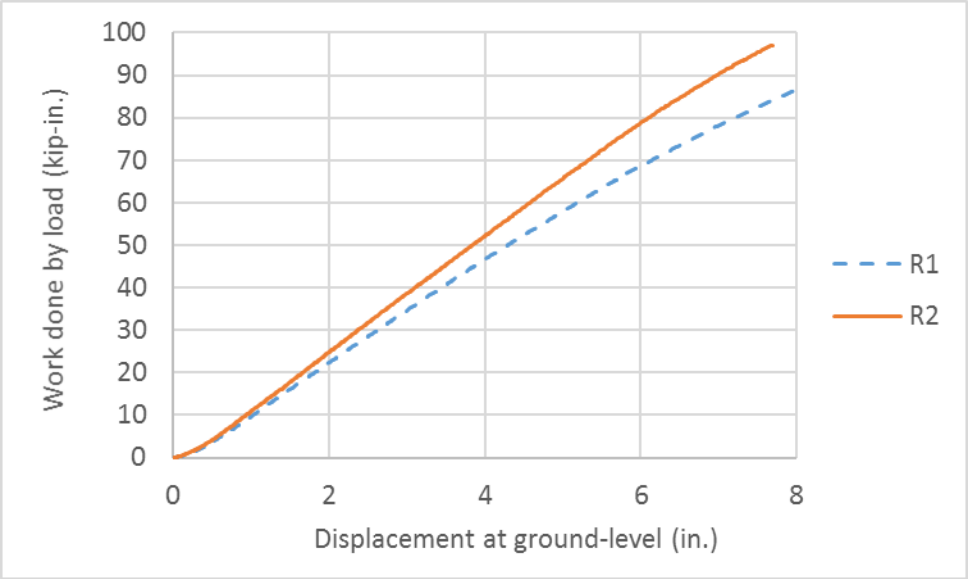

Figure 3.26 W-Δ_g curves of reduced RD tests (R1~2)

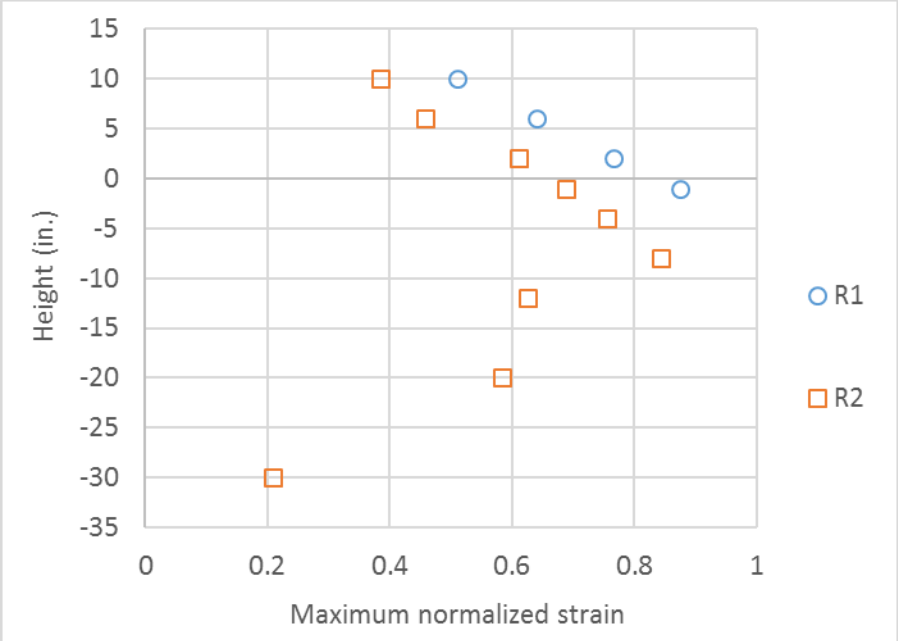

Figure 3.27 Strain distribution plots of reduced RD tests (R1~2)

3.3.5 Tests on pre-cut mow strips

Three posts were tested with the pre-cut mow strip configurations shown in Figure 3.12. Test results are presented and plotted in Figure 3.28 (P-Δ_p curves), Figure 3.29 (W-Δ_g curves), and Figure 3.30 (strain distribution plots). The parallel pre-cutting was applied in test P1 while the diagonal pre-cutting was applied in tests P2 and P3.

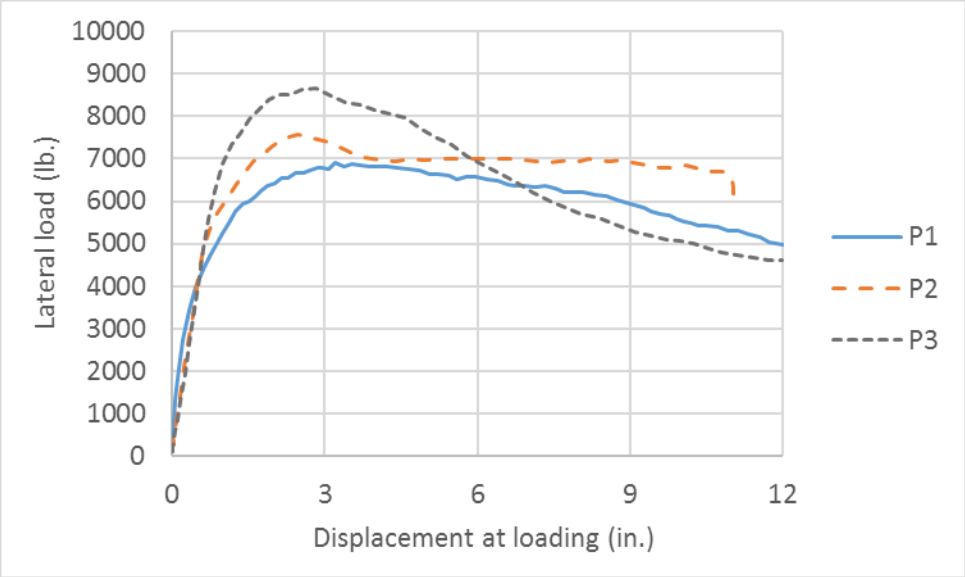

Figure 3.28 P-Δ_p curves of pre-cut tests (P1~3)

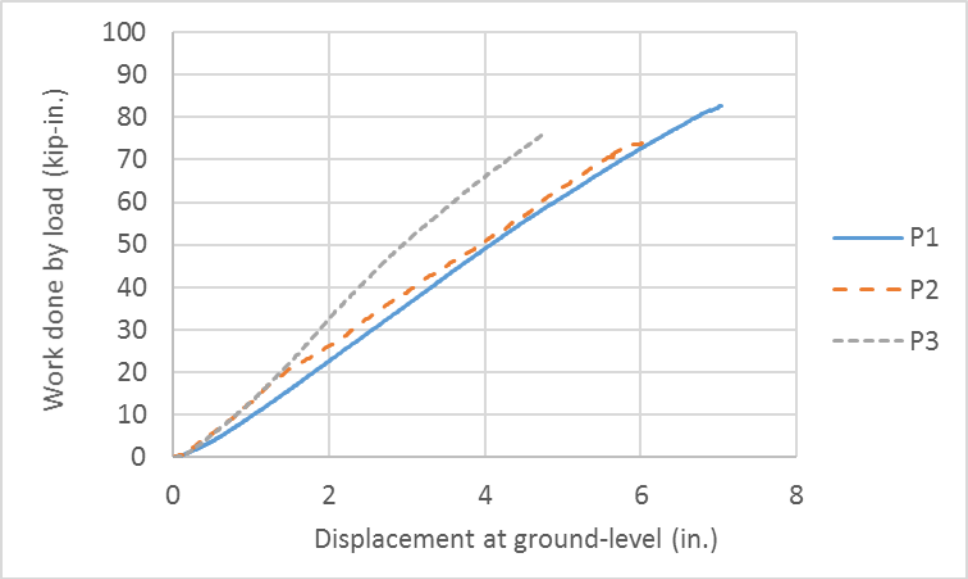

Figure 3.29 W-Δ_g curves of pre-cut tests (P1~3)

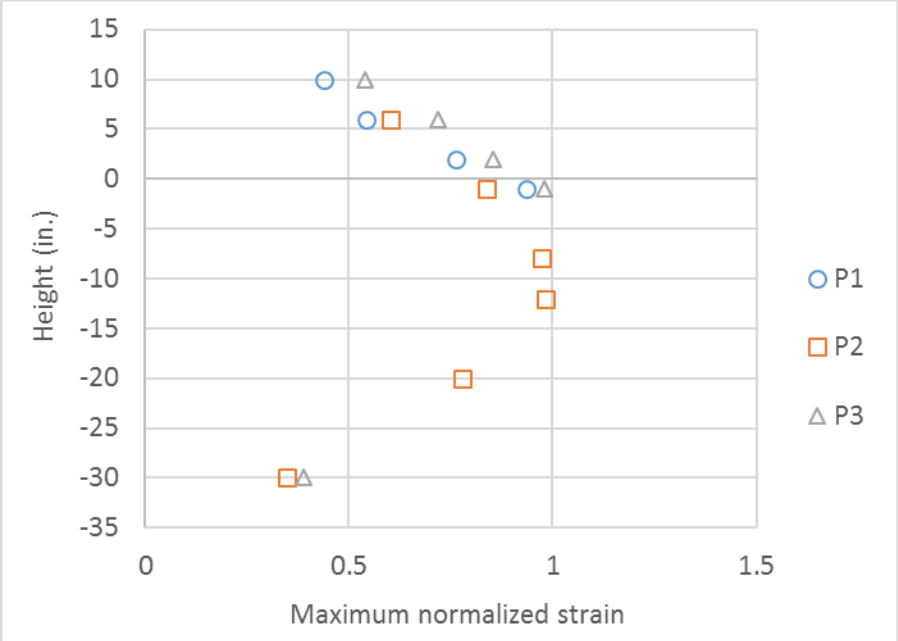

Figure 3.30 Strain distribution plots of pre-cut tests (P1~3)

3.3.6 Visual observations of asphalt rupture during static testing

The rupture mechanisms in the asphalt layers observed in the experimental program varied depending on the specific test setup. However, they provided an indication of the relative amount of restraint imparted to the post by the mow strip.

Figure 3.31 shows before and after conditions for a post tested with a typical mow strip configuration (test T7: asphalt thickness of 3.5 inch). This post installation resulted in higher relative restraint during the test. During the test, two large cracks appeared at the leading edge of the post flange and propagated in a direction diagonal to the edge of mow strip. Another major crack initiated at the edge of the mow strip and propagated toward the post as shown in Figure 3.31(b).

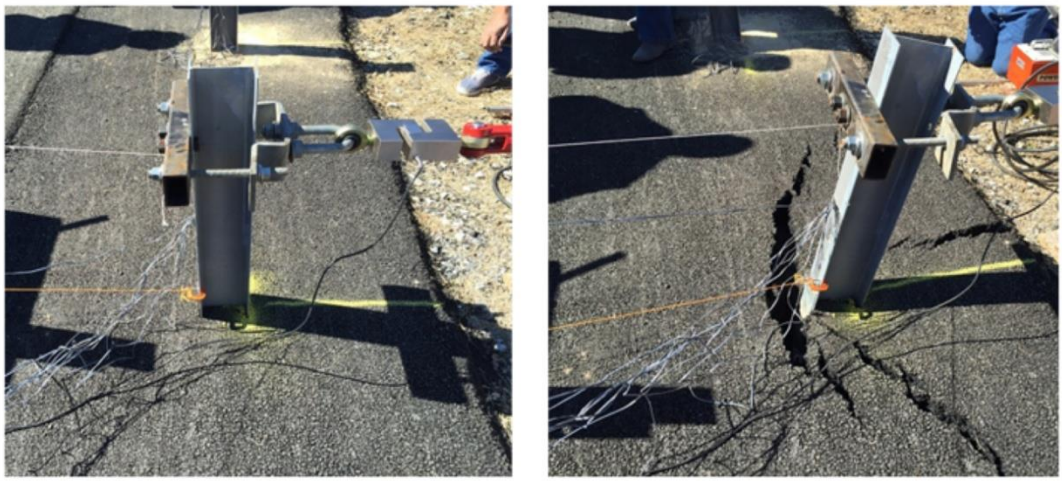

(a) (b)

Figure 3.31 Rupture in typical asphalt mow strip: (a) before-test; (b) after-test

Rupture mechanisms in the asphalt layer for tests with a pre-cut mow strip are indicative of a potentially significant lower level of restraint on the post compared to the

test T7 results. Figure 3.32 gives before and after conditions for a post tested with pre-installed cuts in the mow strip behind the post (test P1: parallel pre-cutting application). The cuts introduced in the mow strip prior to testing resulted in a more controlled and easily predictable asphalt rupture mechanism as shown in Figure 3.32(b). Since the separation of mow strip behind the post area was expedited by pre-cutting, ground-level restraint by the mow strip was limited.

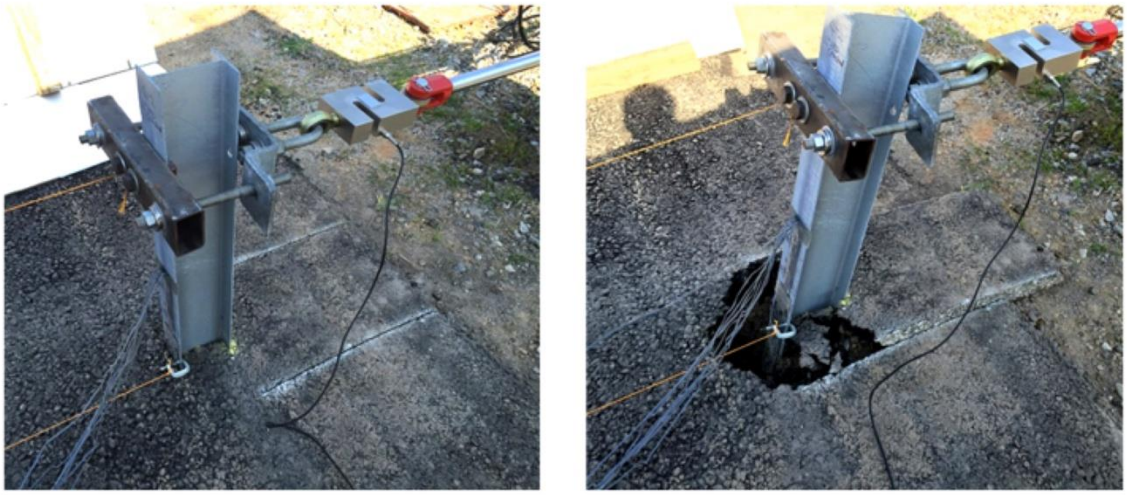

Figure 3.32 Rupture in pre-cut asphalt mow strip: (a) before-test; (b) after-test

3.4 Performance assessment criteria for static tests

The *AASHTO Roadside Design Guide* (RDG) uses qualitative observations to evaluate the performance of guardrail systems. A guardrail system is considered to exhibit good performance if a post is allowed to rotate in the soil, since post rotation absorbs some of the energy from an impact and reduces the chance of the premature

breaking and the plastic hinge formation of the guardrail post. However, the *RDG* classifies the mow strip as a rigid foundation. This classification fundamentally precludes assessing the relative impact of mow strip configuration on the behavior of the guardrail system with the asphalt layer considered as a deformable media, which can result in significant deformation and even failure in the mow strip itself.

As such, quantitative performance assessment criteria can be developed to evaluate the relative performance of posts installed with mow strips that have varying geometric or material parameters. The rationale for selecting the criteria is explained in Figure 3.33 and Figure 3.34, which give an illustration of the behavior of two laterally loaded posts with significantly different embedment conditions.

When a post embedded in a flexible material is subjected to a lateral load (P), bending of the post is negligible, and the ground-level displacement (Δ_g) is proportional to the displacement of the post at the loading height (Δ_p). On the other hand, when a post is embedded in a more rigid material such as rock, the post will have little or no ground-level displacement and exhibit plastic bending as the lateral load exceeds the yield load. The post with rigid embedment will carry a higher lateral load and have a higher longitudinal strain with reduced ground-level displacement.

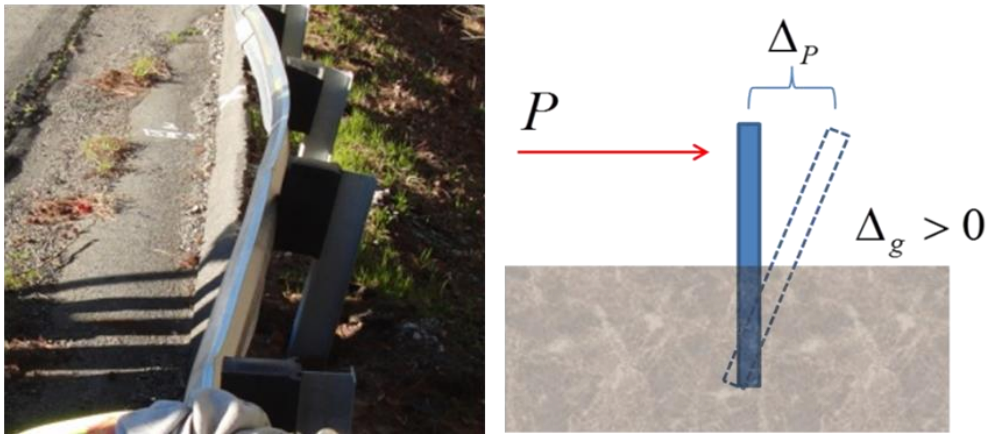

Figure 3.33 Desirable performance of post with relatively flexible embedment

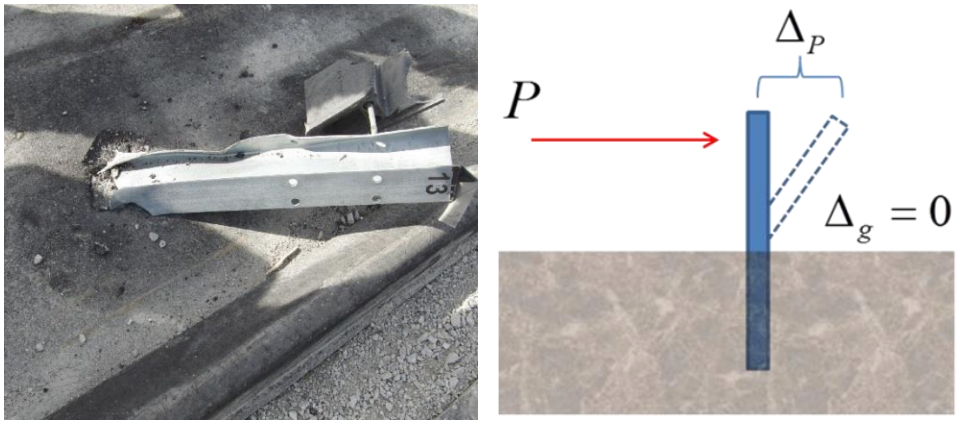

Figure 3.34 Undesirable performance of post with relatively rigid embedment

For the static test program, three quantitative assessment criteria were identified based on this description of desirable post behavior in the *RDG*: (1) peak applied force, (2) ground-level displacement, and (3) maximum post strain. One simple quantitative indication of relative post performance is to compare these values for different post/mow strip installations.

3.4.1 Peak applied force criterion

The peak force applied to the post is the simplest indicator of potentially excessive restraint of a post/mow strip system. In the static test results, a mow strip of greater thickness installed with more rear distance resulted in a higher peak force. Assuming static equilibrium at the peak load, this creates a higher bending moment and flexural stress in the post at the ground level. If analysis and test results indicate that an alternative mow strip design gives a similar or lower peak force under static loading compared to a mow strip with a leave-out, the alternative mow strip design may provide a similar level of restraint under dynamic loading.

3.4.2 Ground-level displacement criterion

The ground-level displacement of the post is an indicator of lateral restraint of the system. When two identical posts with varying embedment conditions are subjected to an equal amount of external work in the lateral direction, a post embedded in a relatively rigid material will exhibit less ground-level displacement. Hence, an alternative mow strip design can be considered providing a similar level of restraint if the alternative design yields a similar or higher ground-level displacement at the same given amount of the external work.

The amount of the work done by the external loading is assumed approximately equivalent to the dissipated energy of the system and a reference value of the energy dissipation for single guardrail post can be determined based on the *MASH* Test 3-10 condition [13]. The *MASH* Test 3-10 specifies a full-scale crash test condition and

parameters using a passenger car impacting a guardrail system as shown in Figure 3.35 and Table 3.3.

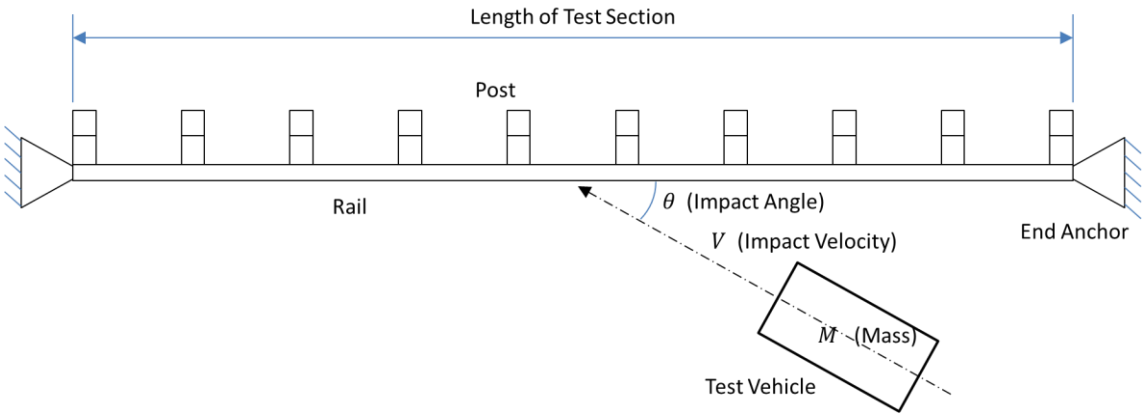

Figure 3.35 MASH 3-10 crash test condition (adapted from [13])

Table 3.3 MASH 3-10 crash test parameters [13]

Test condition	Values
Mass of a passenger car (m)	2420 lb.
Impact velocity (v)	62 mph
Impact angle (θ)	25°
Number of posts (n) (length of test section)	10

The lateral kinetic energy (E_K) contributing to the lateral displacement of the guardrail system can be calculated as shown in Equation (3-1). Assuming the lateral kinetic energy is distributed over 10 guardrail posts along the length of the test section, the average dissipated energy on each post ($E_{D,avg}$) can be estimated as 66.7 kip-in., as shown in Equation (3-2).

$$E_K = \frac{1}{2} m(v \sin \theta)^2 = 667 \text{ kip-in.} \quad (3\text{-}1)$$

$$E_{D,avg} = E_K / n = 66.7 \text{ kip-in.} \quad (3\text{-}2)$$

This value will be used as a reference value to compare ground-level displacements from different mow strip designs.

3.4.3 Maximum post strain criterion

The maximum longitudinal strain in the post flange is a third quantitative indicator of potential excessive restraint of a given post/mow strip system. A guardrail post embedded in a rigid material undergoes plastic hinging when the load increases significantly beyond the yield point for the material. For simplicity, a normalized maximum strain can be calculated from the maximum strain measured in the post divided by the yield strain. When yielding occurs during lateral loading, the normalized maximum strain exceeds 1.0. If computational analysis and experimental results indicate that an alternative mow strip design results in a similar or lower normalized strain than a mow strip design with a leave-out, the alternative design may provide a similar level of restraint under dynamic loading.

3.4.4 Summary of quantitative criteria

The three quantitative criteria are established and are summarized as follows:

- If a post/mow strip system has a similar or lower peak force compared to a mow strip incorporating a leave-out, it may also exhibit acceptable dynamic performance.

- If post/mow strip system has a similar or higher ground-level displacement at the reference value of external work/dissipated energy compared to a mow strip incorporating a leave-out, it may also exhibit acceptable dynamic performance.
- If a post/mow strip system has a similar or lower normalized maximum strain compared to a mow strip incorporating a leave-out, it may also exhibit acceptable dynamic performance.

These quantitative criteria can be used to evaluate whether a given post/mow strip configuration, subject to a controlled lateral loading, could potentially provide a similar or lower ground-level restraint compared to a post embedded in a leave-out incorporated mow strip. If a given post/mow strip system does not satisfy any of these criteria, it is reasonable to assume that configuration would potentially result in unacceptable performance not only under static loading but also under dynamic loading.

3.5 Influence of mow strip on structural performance of guardrail posts

3.5.1 Summary of test results under performance assessment criteria

Table 3.4 gives a summary of the test results from Section 3.3, including the three quantities determined as the performance assessment criteria: (1) the peak force applied on the post, (2) the ground-level displacement at the reference value of dissipated energy, and (3) the maximum strain at peak force normalized to the yield strain for steel. The average results of the leave-out-incorporated design (L1~3) were used as target performance values for checking the relative efficiency of mow strip design alternatives.

Table 3.4 Performance assessment criteria from static test results

Test number	Mow strip thickness (inch)	Mow strip rear distance (inch)	Peak applied force (lb.)	GL displacement at ref. (inch)	Maximum normalized strain at peak
B1~3 (average)	0	0	4554	9.01	0.402
T2	2	24	5491	7.26	0.758
T3	2	24	8672	5.37	1.321
T6	3.5	24	6663	5.97	0.842
T7	3.5	24	9553	4.98	1.482
L1~3 (average)	***3.5***	***24***	***7513***	***5.27***	***0.996***
R1	2	6	6492	5.82	0.895
R2	2	12	7429	5.07	0.930
P1	2	24	6912	5.46	0.989
P3	3.5	24	7577	5.43	1.039

Tests performed on posts installed with typical mow strips (T1~7) demonstrated the impact of service conditions. As expected, the graphs shown in Figure 3.36 indicate that tests T2 and T6 under summer conditions resulted in less restraint provided by the asphalt layer than those tested in winter conditions T3 and T7, respectively. Obviously, any addition of thickness or rear distance of the asphalt mow strip increases restraint compared to the baseline (B1~3) with no mow strip.

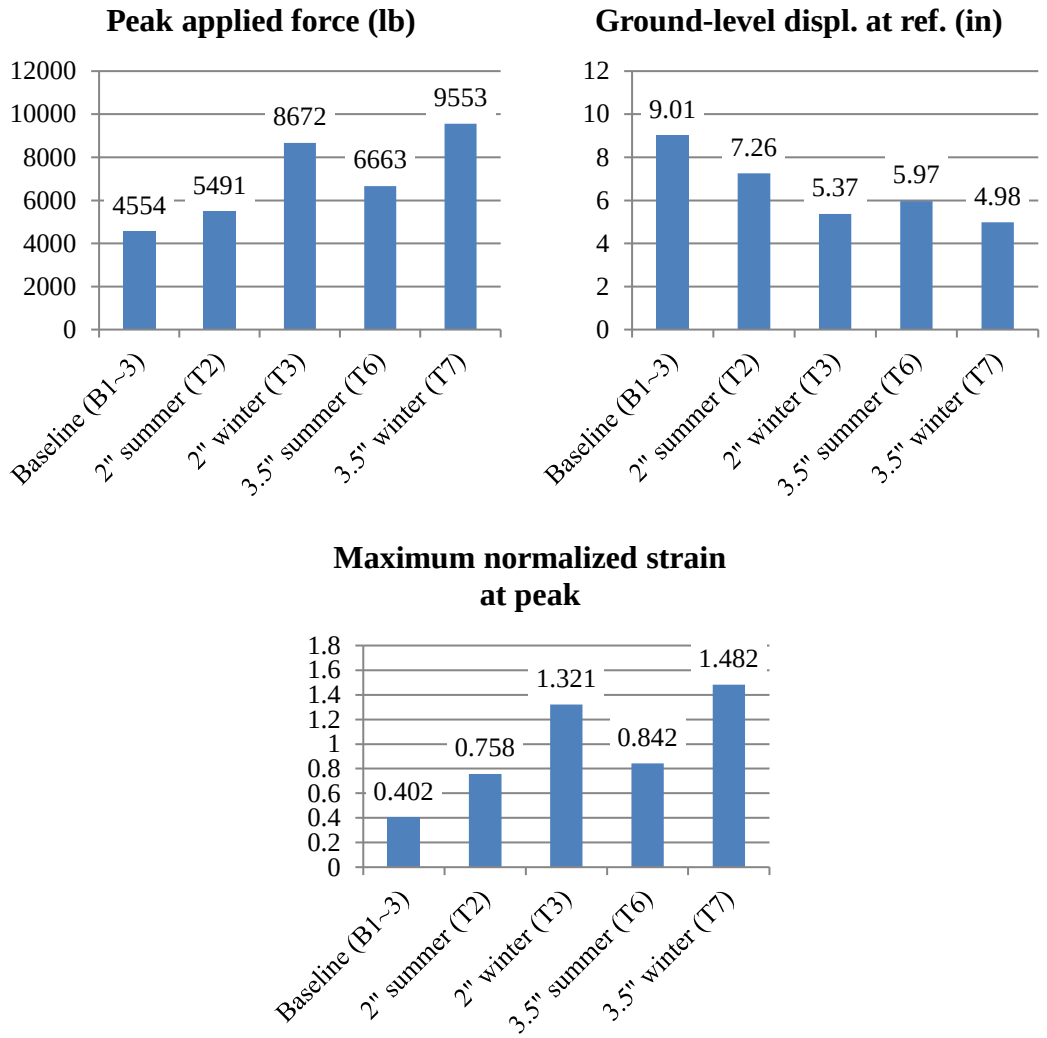

Note: mow strip rear distance 24" constant except baseline (B1~3)

Figure 3.36 Static test results: effect of service conditions

As mentioned earlier, the average values (peak applied forces, ground-displacements and maximum normalized strains) of the leave-out configuration (L1~3) were selected as target performance values (performance criteria) to assess the various mow strip designs. From all performance assessment criteria, the leave-out application mitigated the ground-

level restraint of the guardrail system – peak applied force and maximum normalized strain were reduced, and ground-level displacement was increased as shown in Table 3.4.

However, the static test results indicate that less ground-level restraint can be achieved not only by incorporating a leave-out but also by pre-cutting (P1~3), reducing the thickness (T3), rear distance (R3), or both (R1, 2) of the mow strip, compared to mow strip designs with no leave-out or other design modifications (T7). The performance assessment criteria showed that these alternatives reduced post restraint at the ground-level in a manner very similar to that exhibited by the leave-out-incorporated mow strip design.

The relative effectiveness of the rear distance reduction is shown in Table 3.5 and Figure 3.37. The average values of the leave-out configuration (L1~3) were decreased from the values of the typical mow strip (T3) by 13.4% for peak force, by 1.9% for ground-level displacement, and by 24.6% for maximum strain. By comparing corresponding values, the 6-in. rear-distance configuration (R1) showed better performance under all three criteria and the 12-in. configuration (R2) showed two performance criteria better than the average leave-out configuration.

The relative effectiveness of the pre-cutting is demonstrated in Table 3.6 and Figure 3.38. The average values of the leave-out configuration (L1~3) were decreased from the values of the typical mow strip (T7) by 21.4% for peak force and by 32.8% for maximum strain, but the ground-level displacement was increased by 5.8%. The diagonal pre-cut configuration (P3) showed a similar performance compared to the leave-out: the peak force was reduced by 20.7%, the maximum strain was reduced by 29.9%, and the ground-

level displacement was increased by 9.0%. However, the parallel pre-cut configuration (P1) showed relatively less restraint than the leave-out by satisfying all performance criteria. Therefore, it is shown that the selected alternative mow strip installation methods effectively reduce restraint under static loading and may potentially perform in an acceptable manner under dynamic loading.

Table 3.5 Static test results: effect of rear distance reduction

Test number	Rear distance	Peak applied force		Ground-level displacement. at ref.		Maximum normalized strain at peak	
		(lb.)	var.(%) from T3	(in.)	var.(%) from T3	(in./in.)	var.(%) from T3
T3	24 in.	8672	0	5.37	0	1.321	0
L1~3 (avg.)	24 in.	7513	-13.4%	5.27	-1.9%	0.996	-24.6%
R1	6 in.	6492	-25.1%	5.82	+8.4%	0.895	-32.2%
R2	12 in.	7429	-14.3%	5.07	-5.6%	0.930	-29.6%

Table 3.6 Static test results: effect of pre-cutting

Test number	Description	Peak applied force		Ground-level displacement. at ref.		Maximum normalized strain at peak	
		(lb.)	var.(%) from T7	(in.)	var.(%) from T7	(in./in.)	var.(%) from T7
T7	No treatment	9553	0	4.98	0	1.482	0
L1~3 (avg.)	Leave-out	7513	-21.4 %	5.27	+5.8 %	0.996	-32.8 %
P1	Parallel pre-cut	6912	-27.6 %	5.46	+9.6 %	0.989	-33.3 %
P3	Diagonal pre-cut	7577	-20.7 %	5.43	+9.0 %	1.039	-29.9 %

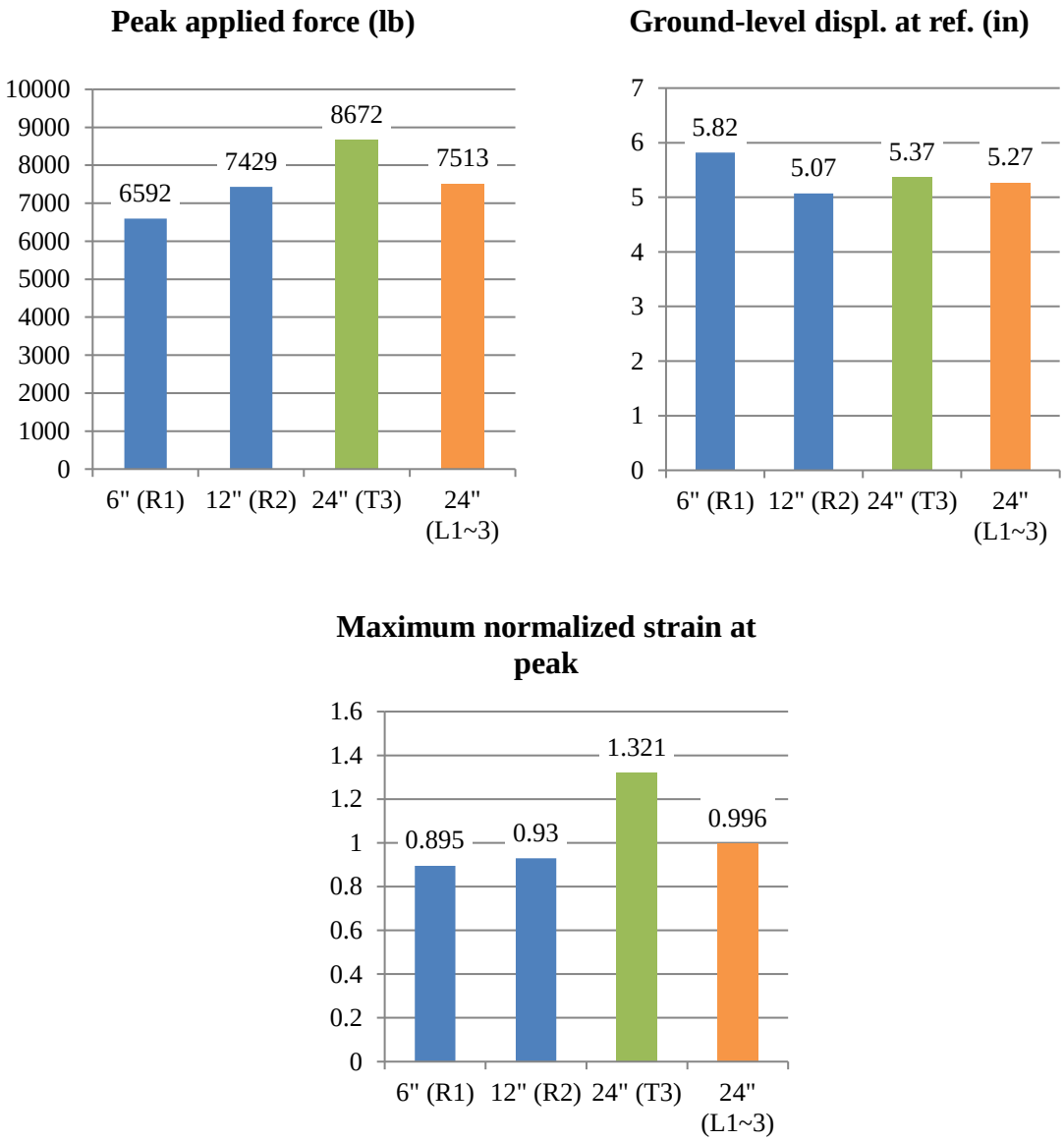

Note: mow strip thickness 2" constant except leave-out (L1~3)

Figure 3.37 Static test results: effect of rear distance reduction

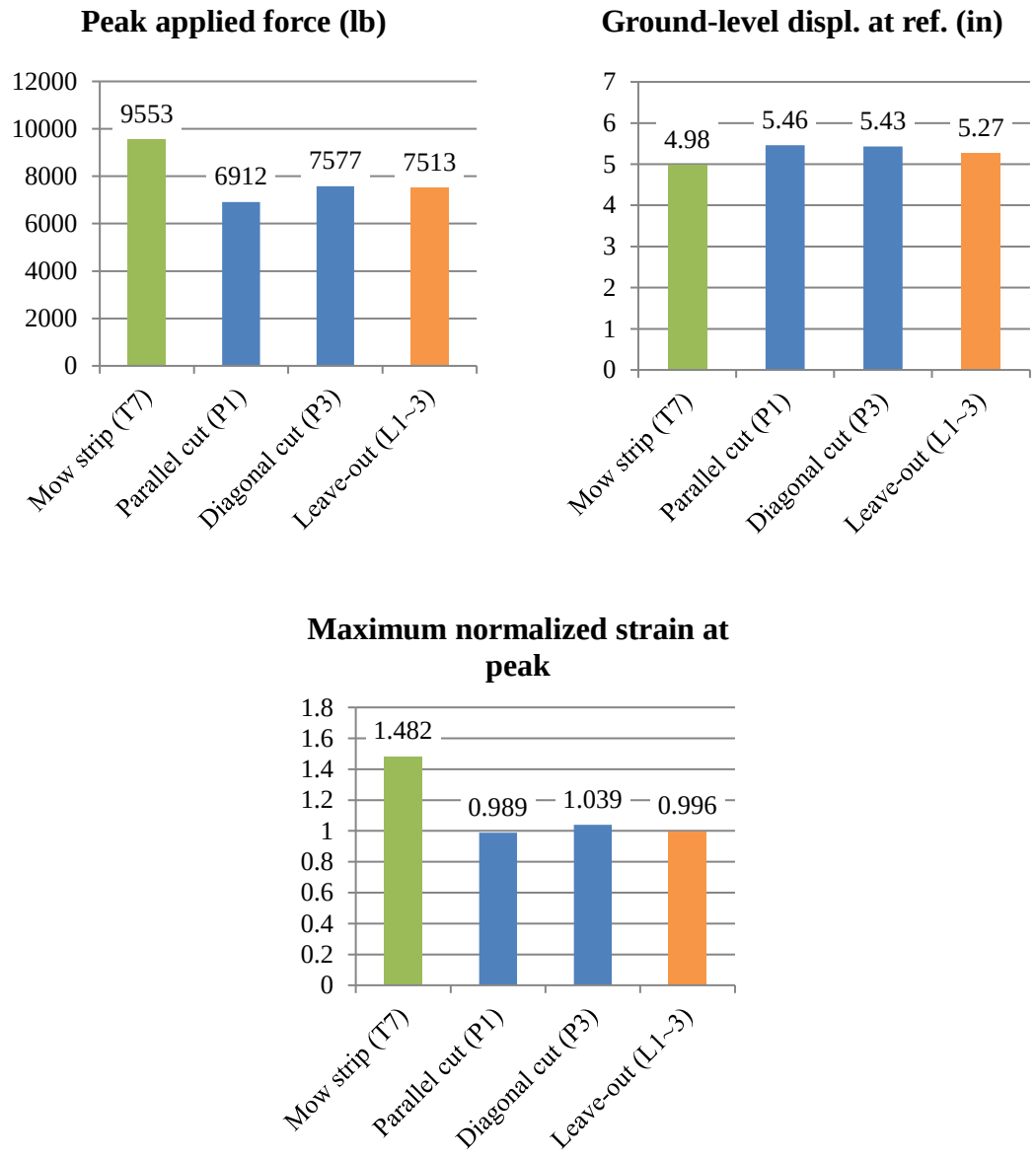

Note: mow strip thickness 3.5" constant except parallel cut (P1)

Figure 3.38 Static test results: effect of pre-cutting

3.5.2 Performance assessment compared with finite element simulation

The experimental results demonstrated that changing asphalt mow strip geometry influences post/mow strip system performance; the ground-level restraint of the asphalt layer on the post/mow strip system increases when the mow strip thickness and rear distance behind the post increase. However, the experimental results of this study can be combined with computer simulations via finite element analysis (FEA) to evaluate the performance of the system under static loading and the influence of geometric parameters (thickness and rear distance) in more efficient manner. The following general procedure has been used in previous research [62] to integrate the experimental and FEA investigations:

- The experimental results from the static test program and material testing provided the the target responses for the FEA model calibration.
- Experimental load-displacement curves (Figure 3.39) were the primary means of FEA model calibration. These curves represent test results with the lowest ambient temperature (50^0F) and the most aged asphalt condition (118 days) of entire static test program.
- The same failure mechanism (e.g., rupture, crack propagation) in the asphalt mow strip was observed in both experiments and FEA (Figure 3.40).

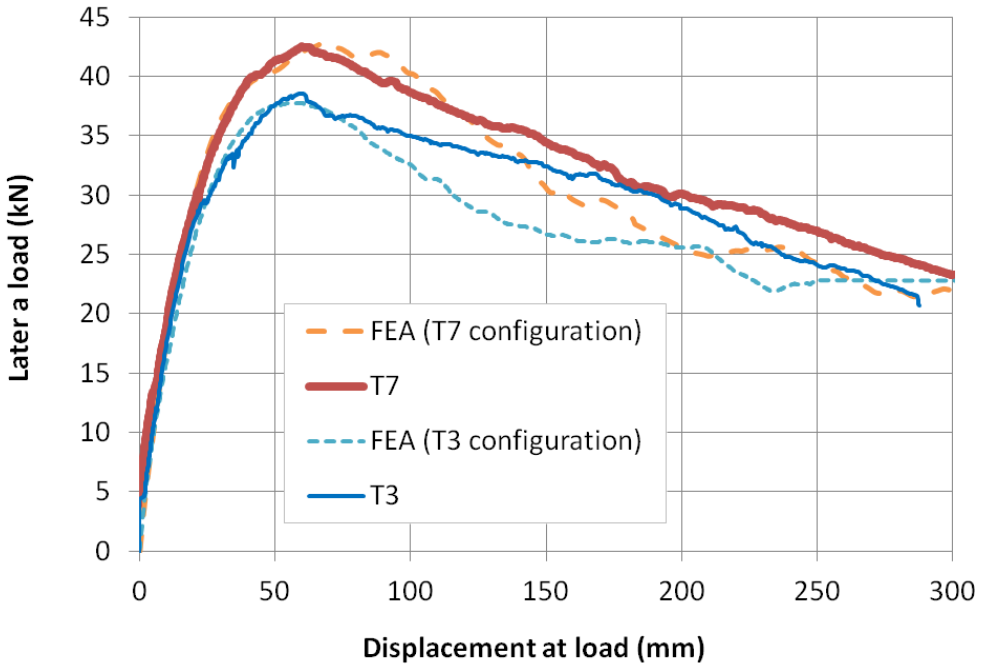

Figure 3.39 Comparison of static load-displacement curves for configurations with asphalt mow strip [62]

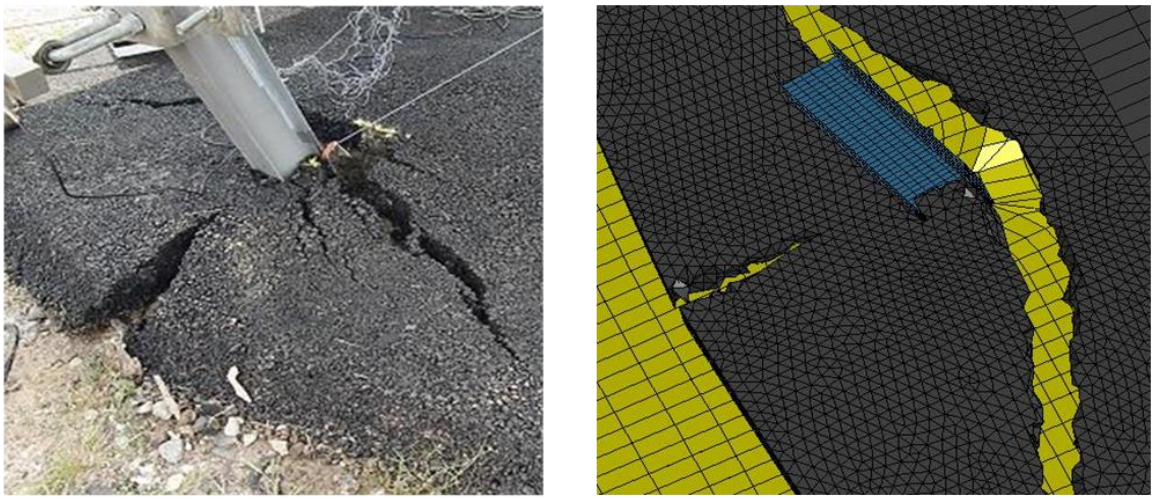

(a) (b)

Figure 3.40 Comparison of asphalt rupture: (a) in the experiment, and (b) in FEA simulation [62]

To determine a satisfactory range of mow strip geometry, a parametric study on the combination of different mow strip thicknesses and rear distances was performed using the FEA simulations [62]. Based on the survey results on common mow strip practice in the United States (Section 3.2), a combination of six thicknesses (ranging from 1 inch to 8 inches) and five rear distances (ranging from 0 inch to 48 inches) of asphalt mow strips were included in the parametric study. Simulation results on these 30 asphalt mow strip configurations are summarized and presented in Figure 3.41.

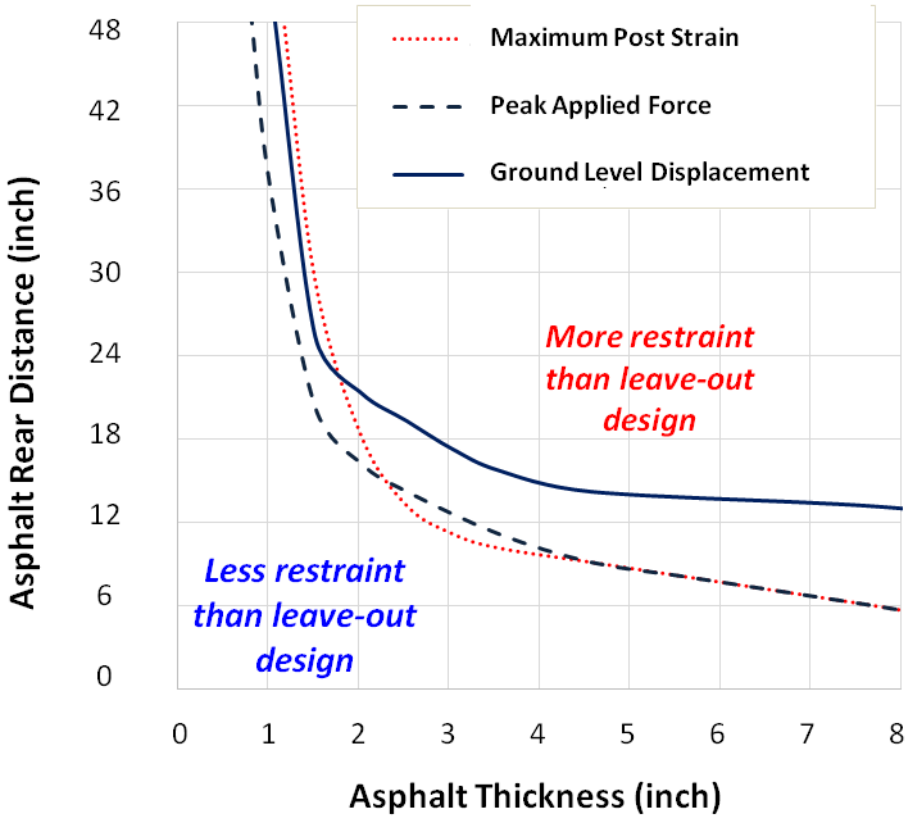

Figure 3.41 Graphical performance evaluation using all three criteria curves [62]

The three performance assessment criteria (peak applied force, ground-level displacement, and maximum post strain) were determined by the FEA simulation results in conjunction with the target performance values: the experimental results from static tests on the leave-out configuration (denoted as L1~3 in Table 3.4). These criteria, shown as three corresponding target performance curves, represent equivalent mow strip geometry combinations to a leave-out-incorporated design. They also inform whether a mow strip design would exhibit more ground-level restraint than the leave-out design or not. A mow strip design which satisfies all three performance criteria can be considered as a potentially acceptable alternative to the typical leave-out-incorporated design of the *AASHTO RDG*. For the static tests performed in the present work, the results indicate that two tested configurations with reduced rear distance (denoted as R1 and R2) are potential acceptable alternatives for exhibiting less ground-level restraint than a typical leave-out configuration.

3.6 Summary

The results of the static test program indicate that some alternative designs for asphalt mow strips result in lower levels of post restraint under static loading, compared to the typical mow strip installation practice in the United States. In addition, guardrail posts tested with alternative mow strip configurations demonstrated very similar structural performance to posts installed with leave-outs as recommended in the *AASHTO RDG*. As noted previously, the performance of presented structural system under static loading is not considered absolutely representative of the performance of that system under dynamic loading. However, results from the static experiments performed in this Chapter

were utilized to develop the dynamic test program presented in Chapter 5 as well as a semi-empirical analysis model presented in Chapter 6. The analysis model includes more detailed performance evaluation and design considerations.

CHAPTER 4
MATERIAL CHARACTERIZATION EXPERIMENTS FOR ASPHALT STRENGTH

This chapter presents the results of an investigation into the variability of asphalt strength used to evaluate the structural performance of the mow strip, focusing on two environmental parameters: temperature and age. Existing empirical design equations for pavement thickness are evaluated for suitability to be implemented in this study. Subsequently, an empirical procedure is proposed for estimating the failure of the asphalt material including the effects of temperature and aging. Finally, the development a cold mix asphalt supplemented with Portland cement is discussed for use in the dynamic test program outlined in Chapter 5.

4.1 Current design methods for asphalt pavements

A comprehensive series of methods for designing asphalt pavement structures is given in the *AASHTO Guide for Design of Pavement Structures* [65]; this is one of the most widely-used guidelines for pavement design in the United States. The asphalt pavement is generally referred to as "flexible pavement," while concrete pavement is usually referred to as "rigid pavement." The *AASHTO Guide* provides basic design equations to determine the required thickness for asphalt and concrete pavement structures. The design equation for the asphalt pavement is given in Equation (4-1) as follows:

$$\log_{10}(W_{18}) = Z_R S_0 + 9.36\ \log_{10}(SN+1) - 0.2 + \frac{\log_{10}\left[\frac{\Delta PSI}{4.2-1.5}\right]}{0.4 + \frac{1094}{(SN+1)^{5.19}}}$$

$$+ 2.32 \log_{10}(M_R) - 8.07 \qquad (4\text{-}1)$$

where W_{18} = predicted number of 18-kip equivalent single axle loads, Z_R = standard normal deviate (function of the design reliability level), S_0 = overall standard deviation of the traffic prediction and performance prediction, ΔPSI = total loss of serviceability due to traffic and other environmental factors during performance periods (usually 10~20 years or more), M_R = resilient modulus of soil base, and *SN* = structural number indicative of the total pavement thickness required (required structural capacity). Table 4.1 classifies the parameters of the Equation (4-1).

Table 4.1 Asphalt pavement design parameters in Equation (4-1)

Parameters	Classification	Sources
W_{18}	Traffic numbers	Traffic data
Z_R, S_0	Statistics	Road classification, reliability level
ΔPSI	Serviceability loss	Design performance periods (service life), traffic data, in-situ soil properties, environmental factors
SN, M_R	Structural values	Pavement/subbase thicknesses, elastic/resilient moduli, and linear coefficients

Once required traffic data, design performance periods, reliability level, in-situ soil properties and environmental factors are determined, a pavement designer can calculate the required structural number, *SN*, and then estimate the required thicknesses of asphalt

and soil layers. Specifically, the structural number, *SN*, can be expressed as shown in Equation (4-2) when the pavement structure consists of *n*-layers:

$$SN = \sum_{i=1}^{n} a_i D_i m_i \tag{4-2}$$

where a_i = *i*-th layer coefficient, D_i = *i*-th layer thickness, and m_i = *i*-th layer drainage coefficient. The details of these design parameters can be found in the *AASHTO Guide* [65].

However, this method may not be an appropriate choice for asphalt mow strip design as the mow strip is not intended to carry repeated traffic loads. Figure 4.1 illustrates a typical section for asphalt pavement structure in major roadways (e.g., interstate highways).

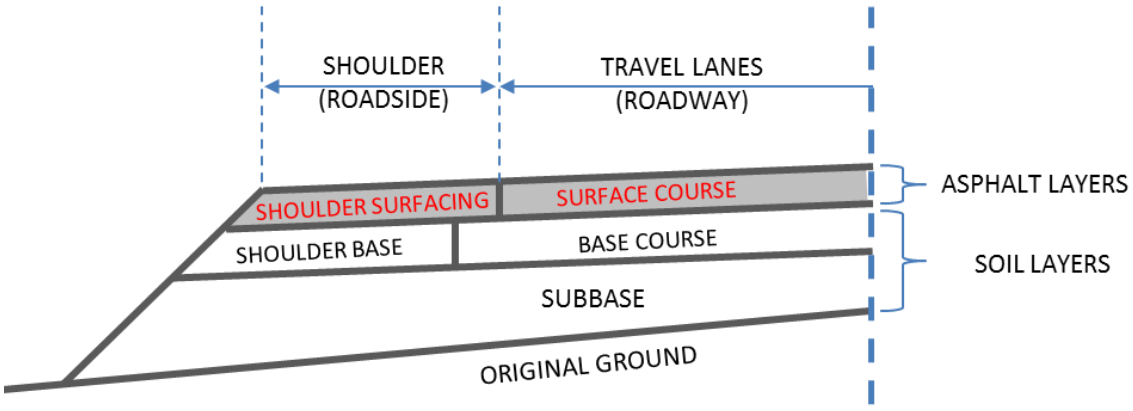

Figure 4.1 Typical section of asphalt pavement structure after [65]

Typical asphalt pavement layers consist of two parts: travel lanes (roadway) and shoulder (roadside or mow strip). These two parts can be designed, constructed, and

maintained separately. The roadside/shoulder portion of asphalt pavement may be subjected to a more moderate service condition than the traffic lanes under the traffic loading condition. On the other hand, the roadside pavement surrounding the guardrail posts plays an important role in the performance of the guardrail system in a vehicle crash.

The expected loading on the asphalt mow strip is different from that on the roadway pavement as illustrated in Figure 4.2. In the figure, the direction of traffic is designated as the *x*-direction, with the *y*-direction defined as the transverse direction of the road and the *z*-direction as the depth. As such, the axle loads applied to the roadway are in the z-direction similar to a punching shear load on a thin plate. A roadway pavement structure, designed for repeated vehicle axle loads, is designed so the material remains in the elastic range after multiple load applications. However, the loading on the mow strip by a guardrail post is an in-plane shear load along the *x*- and *y*- directions depending on the impact angle of the colliding vehicle. The impact loading on the mow strip is a one-time extreme loading and the mow strip structure may experience permanent deformation and potentially fracture. Therefore, a more complete investigation and characterization of asphalt strength under these loading conditions is needed to evaluate the performance of asphalt mow strips.

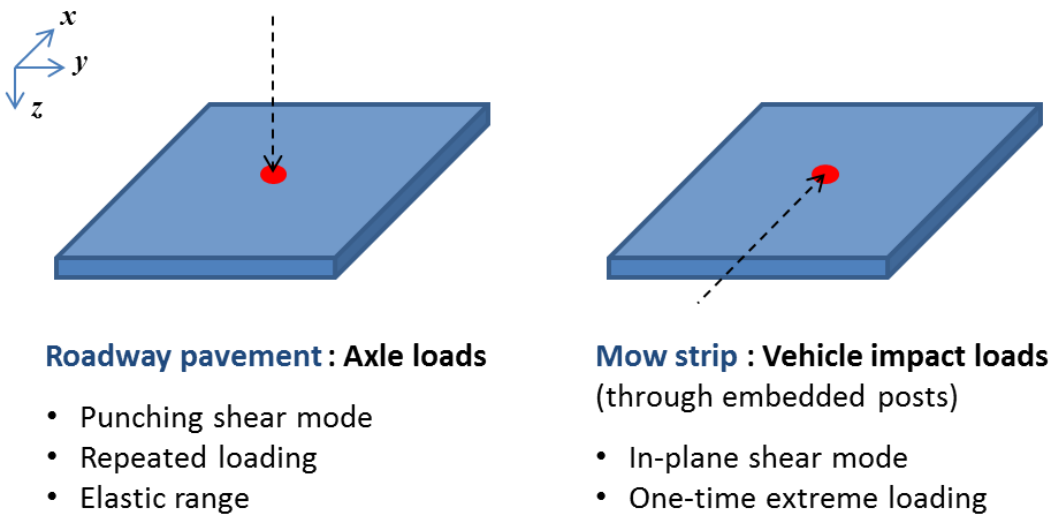

(a) (b)

Figure 4.2 Loads on asphalt pavements; (a) traffic lanes and (b) shoulders

4.2 Specimen testing for asphalt strength characterization

The expected load on the mow strip imparted by a vehicle impact will often lead to the failure of the mow strip in a single event. Thus, it is necessary to select a suitable failure criterion of asphalt for mow strip performance evaluation. A series of unconfined compression tests were conducted with various temperature and age conditions, with the results used to develop a simplified method to determine a failure criterion for the characterization of asphalt strength.

4.2.1 Mohr-Coulomb failure model

One of most widely-used material models for asphalt concrete is the Mohr-Coulomb (M-C) failure criterion model. The M-C model was first adopted by pavement

researchers in the early 1950s to evaluate the performance of asphalt mix designs [66, 67]. Later, studies conducted by Fwa et al. [10, 68] proposed a modified triaxial test method to determine the *C*-ϕ relationship at various temperature conditions. The cylindrical specimens 4 inches in diameter and 8 inches in height were mixed and compacted in the laboratory, and then tested less than 24 hours after asphalt compaction. However, this method is not adequate to evaluate the *C*-ϕ relationship for in-situ asphalt samples taken from mow strip since it is nearly impossible to retrieve a triaxial test specimen with the necessary 8-inch height from roadside asphalt layers whose thicknesses typically range from 2 to 5 inches. Additionally, experimental results on short-term aged laboratory specimens are unlikely to be indicative of aged asphalt in actual roadway conditions.

The Mohr-Coulomb (M-C) failure criterion model can be expressed as shown in Equation (4-3):

$$\tau - \sigma \tan \phi - C = 0 \tag{4-3}$$

where τ is the yield (failure) shear stress, σ is the normal stress, *C* is the cohesion stress, and ϕ is the internal friction angle. The stress condition of a cylindrical specimen under uniaxial compression with no circumferential confinement can be graphically illustrated with a Mohr's circle as shown in Figure 4.3. The axial stress σ_1, is the compressive strength ($\sigma_1 = f_c'$), the lateral stresses $\sigma_2 = \sigma_3$ are zero, and both the radius and the normal coordinate of the center of the circle are half of the compressive strength. The M-C failure envelope can be drawn as a line tangent to the circle as shown.

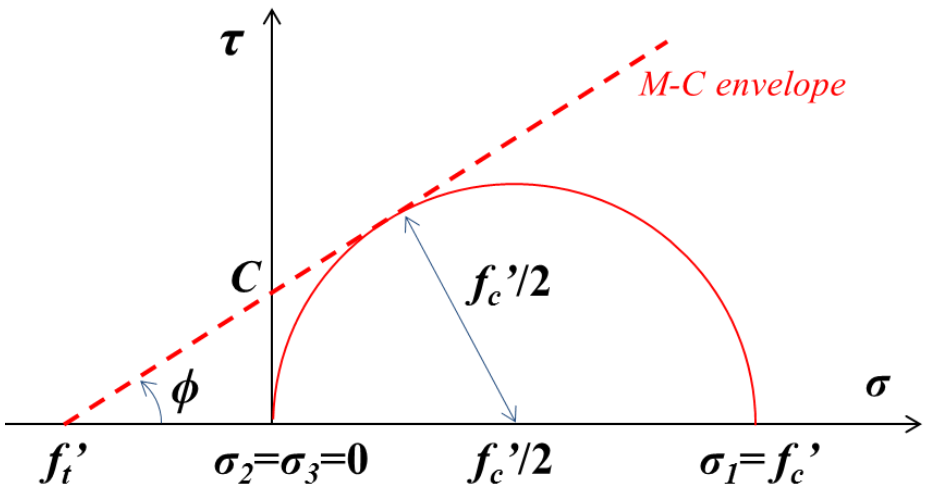

Figure 4.3 Mohr-Coulomb parameters from unconfined compression test

The tensile strength of the asphalt f_t' is not easily estimated from experiments because of the difficulty in applying uniaxial tension to the specimen. Instead, a series of equations can be written from trigonometric ratios from Figure 4.3 as follows:

$$f_t' = \frac{C}{\tan\phi} \tag{4-4}$$

$$\sin\phi = \frac{f_c'}{2f_t' + f_c'} \tag{4-5}$$

Equation (4-5) can be written as shown in Equation (4-6):

$$f_t' = \frac{f_c'}{2}\left(\frac{1}{\sin\phi} - 1\right) \tag{4-6}$$

Finally, the cohesion, *C*, can be written as a function of the internal friction angle ϕ and compressive strength f_c' by substituting f_t' in Equation (4-6) with Equation (4-4):

$$C = \frac{f_c'}{2}\left(\frac{1}{\cos\phi} - \tan\phi\right) \tag{4-7}$$

The cohesion is proportional to the compressive strength but varies with the internal friction angle. The cohesion ratio, defined as the cohesion value divided by the compressive strength (C/f_c'), is plotted in Figure 4.4.

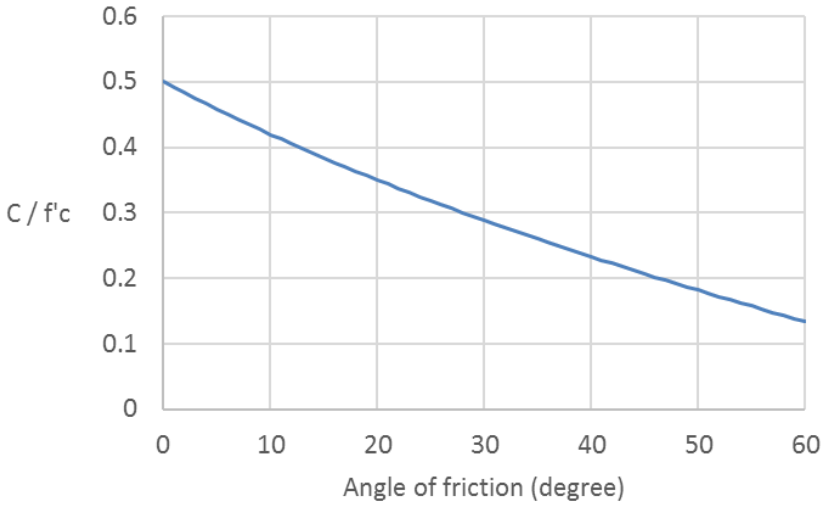

Figure 4.4 Cohesion ratio and angle of friction

To estimate the cohesion value of the M-C failure envelope from the uniaxial compressive tests on cylindrical specimens, the internal friction angle of asphalt ϕ is assumed to be 35 degrees. This value is taken from a representative value of satisfactory asphalt mix design criteria proposed by Smith [67]. Therefore, the cohesion value of asphalt *C* is estimated at approximately 26 percent of the compression strength as shown in Equation (4-8):

$$C = 0.2603\, f_c' \tag{4-8}$$

4.2.2 Experimental plan for asphalt material characterization

It is known that asphalt strength can vary significantly based on a number of different factors. As prior studies have reported, asphalt strength is highly sensitive to both temperature [10, 11] and age [8, 9, 69]. Specifically, the performance grade (PG) [70] in an asphalt mix design specifies the maximum and minimum pavement design temperatures to prevent rutting in high temperature and thermal cracking in low temperature. Observations from the static test program described in Chapter 3 showed there is a significant difference in the character of mow strip fracture between the summer and winter test conditions with the same test configuration (thickness: 2-in. and rear distance: 24 in.) as shown in Figure 4.5. Asphalt rupture in the summer test was accompanied by buckling and more deformation of the asphalt behind the post. However, the asphalt failure mode in the winter test was mostly a lateral rupture. The formation and propagation of cracks were more visible and distinct.

Figure 4.5 Difference in mow strip fracture between two tests

A series of compression tests were performed to attempt to estimate the effect of temperature and physical aging on asphalt strength for the specific material used in this research program. The hot mix asphalt (HMA) used in this research program was designed with a performance grade (PG) of PG 76-22 binder with 3/4-inch maximum aggregate size. This asphalt mix type is one of the most commonly used in road construction projects in Georgia. Test samples were cored from the asphalt pavement layer and were trimmed to approximately 4 inches in diameter and 4 inches in height as shown in Figure 4.6.

Figure 4.6 Asphalt test bed and representative cored specimens

It is well understood that both temperature and age effects on asphalt strength are not monotonic [71]. For this reason, three or more levels are required to analyze any curvilinear relationship between factors and their responses. In this study, three levels of temperature and eight levels of age condition were evaluated based on the practical limitations of specimen test settings and time constraints. Three test temperature levels were investigated: 32, 68, and 104 ^{0}F. Each level represents a common cold, moderate,

and elevated temperature condition, respectively. A total of 36 compression tests were performed at various age conditions of 26, 46, 67, 94, 105, 124, 159, and 182 days from the initial placement of the asphalt mow strip. For each age level, a minimum of three replicate specimens were tested.

Loading speed and moisture are two important control variables in this experimental setup as specified in the relevant testing specifications (*ASTM D1074* and *D1075* [72, 73]). To avoid dynamic or strain rate effects while testing, a loading rate of 0.2 in./min (5 mm/min) was used; this rate is specified in *ASTM D1074 – Standard Test Method for Compressive Strength of Bituminous Mixtures* [72]. As shown in Figure 4.7, all specimens were prepared at the same time and moved to an oven (for high temperature conditioning), a refrigerator (for low temperature conditioning), or to an environmental chamber whose temperature was kept constant at 68^{o}F.

Oven – high temperature conditioning (104^{o}F)

Refrigerator – low temperature conditioning (32^{o}F)

Figure 4.7 Temperature conditioning of cored specimens

Test specimens were loaded to failure in compression using a universal test machine as shown in Figure 4.8. Due to imperfections in the sample trimming process, not all specimens had completely horizontal top and bottom loading surfaces. A high strength steel ball was placed on top of the test specimen to minimize effects of stress concentration due to misalignment of the specimen in the testing machine. Specific details for test equipment used in the experiments are provided in Appendix B.

Figure 4.8 Test specimen in compressive failure

4.2.3 Test results

The compressive strength from each test was calculated from the maximum recorded load divided by the original cross-sectional area of the specimen. The cohesion value is estimated using Equation (4-8).

Table 4.2 and Table 4.3 show the unconfined compression test results for all specimens. The effect of temperature was notable: the compressive strength at the lowest temperature was approximately 10 times higher than the strength at the highest temperature. This result indicates the asphalt mow strip would behave in a more rigid fashion under extremely low temperature conditions. The effect of aging was not as significant as the temperature, but there was a slight positive correlation between the age and the strength/cohesion of the asphalt.

Table 4.2 Asphalt compression test results showing effect of aging

Test run	Age of specimen (day)	Test temperature (°F)	Number of specimens tested	Average compressive strength (psi)	Estimated cohesion value (psi)
1	26	68	3	156.8	40.82
2	46	68	3	185.6	48.31
3	46	68	3	191.6	49.87
4	67	68	3	217.5	56.62
5	67	68	3	251.0	65.34
6	94	68	3	225.1	58.59
7	105	68	3	224.3	58.39
8	124	68	3	236.5	61.56
9	124	68	3	214.7	55.89
10	124	68	3	270.2	70.33
11	159	68	3	204.5	53.23
12	182	68	3	255.6	66.53

Table 4.3 Asphalt compression test results showing effect of temperature

Test run	Age of specimen (day)	Test temperature (°F)	Number of specimens tested	Average compressive strength (psi)	Estimated cohesion value (psi)
1	67	32	3	718.2	187.0
2	67	68	3	217.5	56.63
3	67	68	3	251.0	65.34
4	67	104	3	74.03	19.27
5	182	32	2	876.0	228.0
6	182	68	3	255.7	66.55
7	182	104	2	45.45	11.83

4.3 Empirical models for the effect of temperature and age

Using the results from the compression tests on the specific asphalt material used in this study, the effect of temperature and age can be estimated empirically. General curve fitting techniques were used to determine the two empirical equations: a temperature-compressive strength relationship and an age-compressive strength relationship.

For the temperature model, a decaying power function was selected for maximizing the goodness of fit. The function showed a strong correlation with the test data - the regression coefficient R^2 was close to 1.0. The relationship between the temperature and compressive strength was estimated as shown in Equation (4-9) and Figure 4.9:

$$f_c'(T) = 218.4 \cdot (T/68.0)^{-1.695} \qquad (\mathrm{R}^2 = 0.9612) \qquad (4\text{-}9)$$

where f_c' is the compressive strength (psi) and T is the temperature (^{0}F).

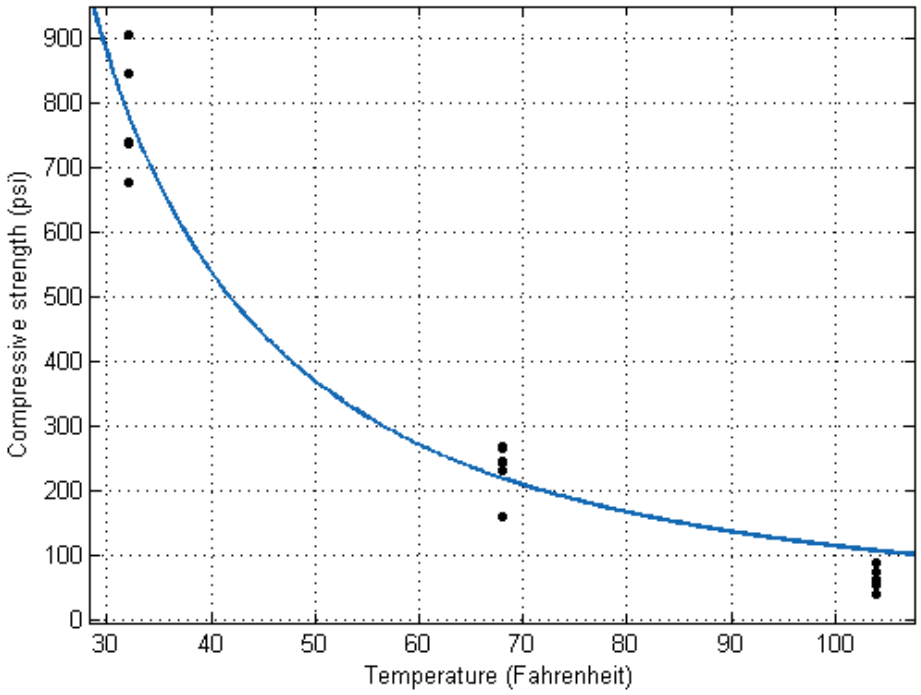

Figure 4.9 Empirical temperature-compressive strength model for asphalt

For the aging model, various types of functions were tested as the compressive strength had a relatively weak correlation with the age compared to the temperature model. After numerous iterations, a power function was selected to maximize the goodness of fit. The relationship between age and compressive strength is estimated using Equation (4-10) and graphically shown in Figure 4.10:

$$f_c'(t) = 98.77 \cdot t^{0.1788} \qquad (R^2 = 0.5011) \tag{4-10}$$

where f_c' is the compressive strength (psi) and *t* is the age of the asphalt material (day).

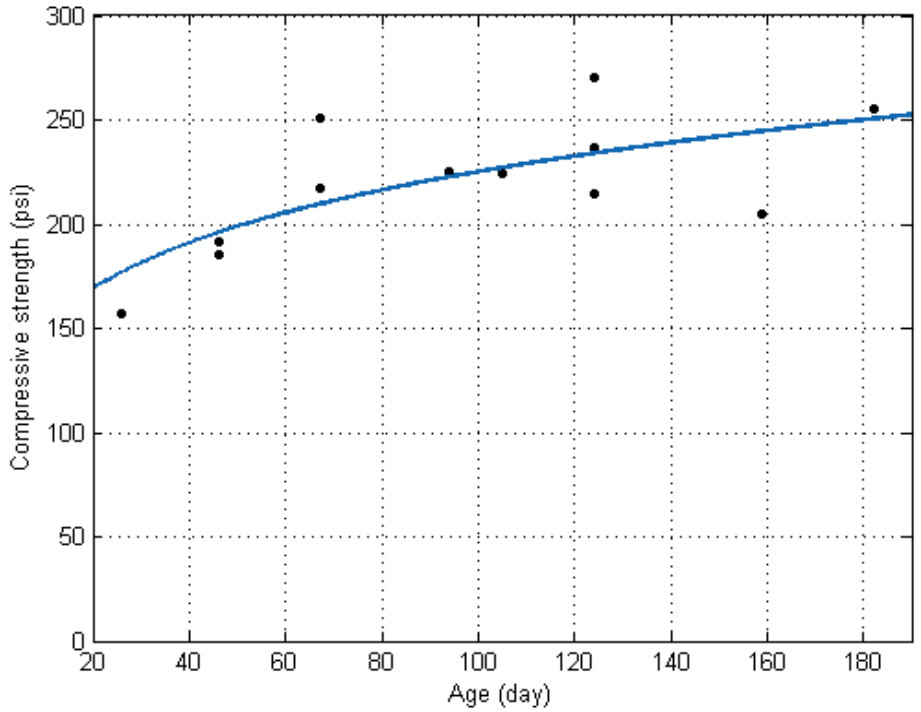

Figure 4.10 Empirical model of cohesion versus age for asphalt

4.4 Selection of equivalent asphalt material for dynamic testing

Due to practical limitations in the research program schedule, the hot mix asphalt mow strip used in the static test program could not be used for the dynamic testing program – there was not sufficient time in the program schedule to allow the hot mix material to age between test sessions. Hence, it was necessary to select an alternative type of asphalt material with equivalent strength developed in shorter amount of curing time (e.g, 14 days).

Recent experimental studies have proposed using modified cold mix asphalt (CMA) as an alternative to conventional hot mix asphalt (HMA). Niazi et al. [74] tested three additives (Portland cement, lime slurry, and hydrated lime) for increasing the strength of CMA; the authors found that adding Portland cement at a level of 2% by weight increased the indirect tensile strength by approximately 70 percent. Xu et al. [75] tested CMA with Portland cement added; the authors found a strong linear relationship between the amount added of cement and the resulting strengths (indirect tensile and flexural).

Based on this previous work, CMA supplemented with Portland cement was selected as an alternative asphalt mix for mow strip construction in the dynamic test program. A series of compression tests on CMA specimens were performed to determine the mixing ratio of Portland cement that would result in compressive strength values approximately equivalent to that seen in the static test program in a much shorter curing period. Using Equation (4-10), the target compressive strength was set to 232 psi, which represents the value of the stiffest mow strip among all static tests (the compressive strength of 118-day old HMA) performed as described in Chapter 3. In this study, four levels of cement content (4, 6, 8, and 10% by the total weight) and two levels of aging (7 and 14 days) were evaluated.

Cylindrical CMA specimens approximately 4 inches in diameter and 4 inches in height were prepared according to *ASTM T180* [61]. The CMA aggregates, Portland cement (Type I), and the minimum required amount of water were mixed together using a mechanical mixer. After a series of trial mix iterations, a water/cement (*w/c*) ratio of 0.33, which showed a decent workability in both mixing and compaction process, was selected as an optimal value. The mixed material was then moved to metal cylinder

molds, which were filled to approximately 1/5 of the cylinder height and compacted using a Proctor compaction hammer. These steps were repeated until the mold was filled completely (Figure 4.11). The molds were removed 24 hours after the final compaction to mitigate premature cracking or fracture of the CMA specimen.

Figure 4.11 Cold mix asphalt specimen preparation

The specimen test protocol throughout the CMA test program was same as the HMA test program described in the Section 4.2. Figure 4.12 shows representative pre- and post- test pictures. The compressive strength was calculated from the maximum recorded load divided by the original cross-sectional area of the specimen. Table 4.4 and Figure 4.13 present the test results on various CMA mix types.

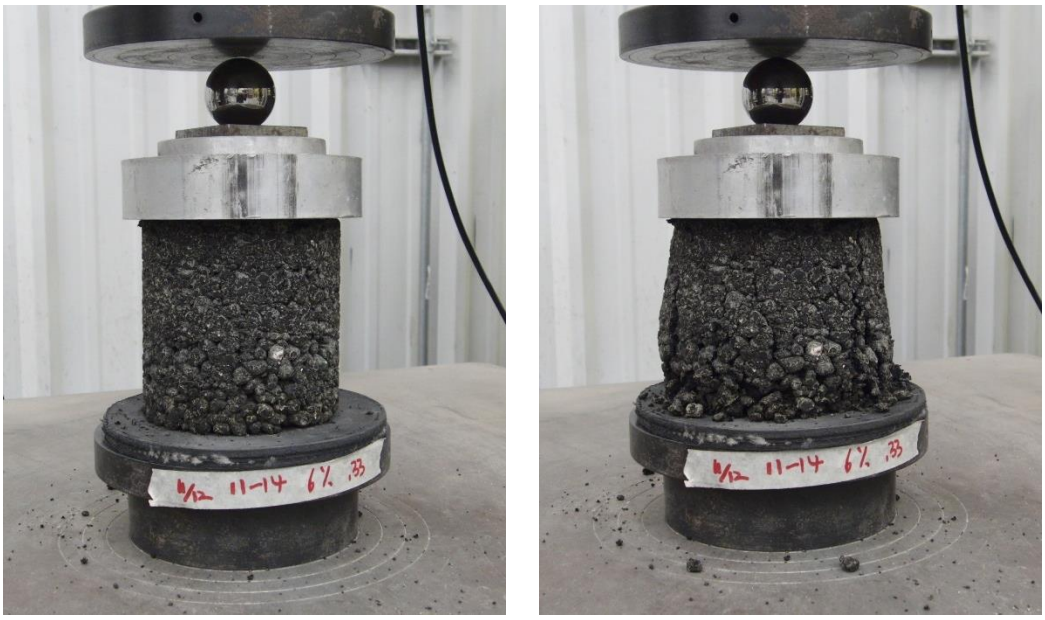

(a) (b)

Figure 4.12 Unconfined compression test pictures of CMA specimen (a) pre- and (b) post-test

Table 4.4 CMA test results for various mixing ratios

Asphalt age (day)	Cement content	Average compressive strength (psi)	No. of specimen tested	Test temperature (^{0}F)
7	4%	79.1	2	72
	6%	105.5	2	72
	8%	142.3	2	72
	10%	182.6	2	69
14	4%	83.7	3	71
	6%	126.7	2	71
	8%	184.3	2	71
	10%	251.7	6	67

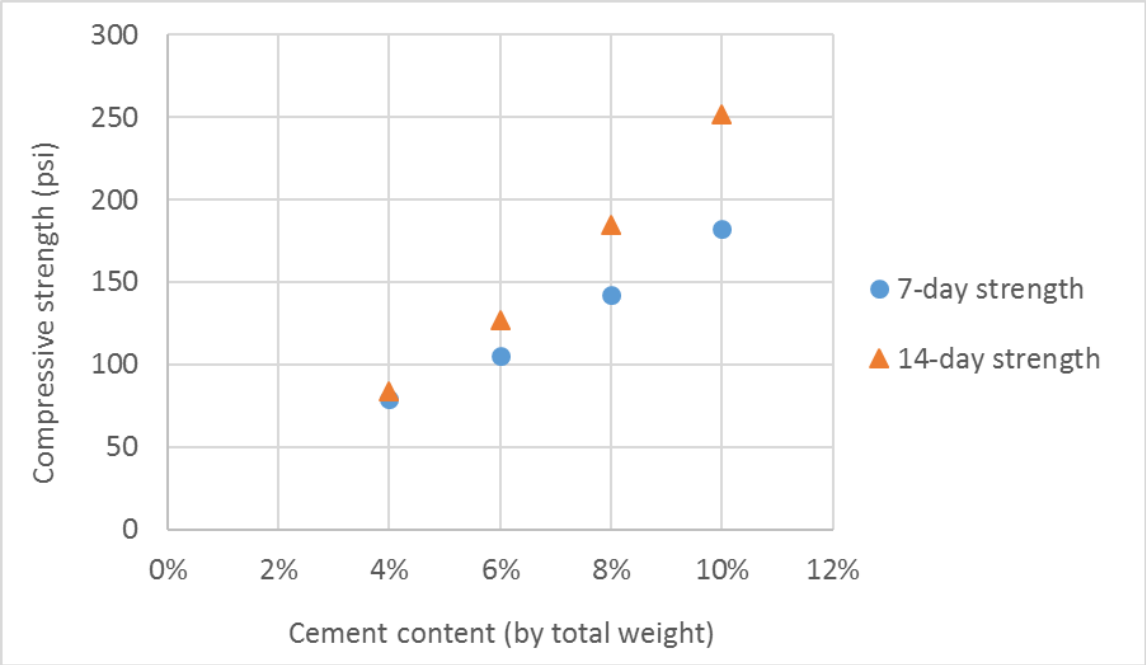

Figure 4.13 CMA test results: compressive strength vs. cement content

As found by previous researchers [75], a strong linear trend between the strength and the cement content was observed both in the 7- and 14-day results. Specifically, the 14-day compressive strength of CMA supplemented with 10% Portland cement by weight slightly exceeded (252 psi) the target compressive strength of 232 psi. Therefore, this material mixture was selected for use in the construction of mow strips for the dynamic test program as a conservative approximation of the HMA asphalt used in the static test program.

4.5 Summary

The characterization of asphalt material used in the experimental program was a critical process to evaluate the structural performance of the mow strip. An empirical method based on the Mohr-Coulomb failure criterion was discussed for estimating the compressive strength and cohesion of the asphalt material. Compression tests on specimens were conducted to investigate the effect of temperature and asphalt aging. Empirical models including the effects of temperature and age for asphalt material used in the static test program were presented. Additionally, the experimental procedure of selecting an equivalent asphalt mix for dynamic testing presented in Chapter 5 was discussed. Results from the experiments performed in this Chapter are also utilized in Chapter 6 to calibrate a semi-empirical analysis model for performance assessment of various mow strip design alternatives.

CHAPTER 5
DYNAMIC TESTS FOR PERFORMANCE ASSESSMENT OF GUARDRAIL POSTS

This chapter presents a novel dynamic subcomponent test method using a high-speed hydraulic actuator in the performance assessment of guardrail posts in asphalt layers. A total of 14 dynamic impact tests were conducted under various mow strip designs and configurations. Experimental data from accelerometers and high-speed cameras were utilized to quantify the relative ground-level restraint of the guardrail post driven through the asphalt mow strip. A series of quantitative performance criteria were selected to evaluate the structural performance of the subcomponent system. These experimental results were used as one of assessment tools in this study to aid in the understanding of the effect of mow strip design variables on guardrail post performance.

5.1 Development of dynamic impact test protocol using high-speed hydraulic actuator

Historically, in lieu of performing costly full-scale vehicle crash tests, the dynamic performance of guardrail subcomponents has been examined through four different dynamic test methods – the gravitational pendulum, drop mass, reduced-scale models, and bogie vehicles [13]. The most common method employed is the bogie vehicle method which has been primarily used for tests on guardrail posts of various designs and other roadside safety hardware subcomponents as described in Chapter 2.

However, a dynamic test method using a high-speed hydraulic actuator can be employed in testing various roadside safety hardware subcomponents as an alternative methodology. The test method with the hydraulic actuator features several advantages over the existing bogie vehicle method; (1) the amount of impact energy transferred from the actuator can be readily controlled or estimated; (2) the actuator allows the user to control, measure, and replicate the impact features more precisely and safely; (3) supplementary instrumentation on the test specimen and on the actuator itself is available; and (4) testing under controlled indoor conditions allows a user to minimize the variability in ambient conditions such as the moisture content in the soil base around the post and under the mow strip.

5.1.1 High-speed hydraulic actuator

The high-speed hydraulic actuator, located in the Structural Engineering and Mechanics and Materials (SEMM) Laboratory of Georgia Institute of Technology, was designed to produce an impulse by impacting the test specimen in a controlled manner [76]. The actuator used in the dynamic test program, which is capable of producing a computer-controlled impact up to 73.5 mph velocity or 890 kip-in. of kinetic energy with a repeatability in velocity of no greater than 4% [77]. The desired impact condition is achieved through the precise timing of valve opening and pressure control in the actuator system along with appropriate loading fixture design. The actuator system can be programmed to simulate an equivalent vehicle impact condition by providing a specific amount of kinetic energy and initial impact velocity.

Figure 5.1 shows a schematic illustration of the hydraulic system which consists of an actuator, control valves, accumulators, and transducers [78]. The flyer mass is located next to the impactor plate attached to the piston rod of the hydraulic actuator. To simulate the 1-D movement of a vehicle with a constant velocity as closely as possible, a rail system securely guides the flyer mass that is accelerated by the impactor plate, released at the desired velocity, and subsequently impacts the target structure at the desired impact height. During the test, the pressure valve openings are precisely controlled by the main control computer to accelerate the piston rod and flyer mass to the desired impact velocity [77].

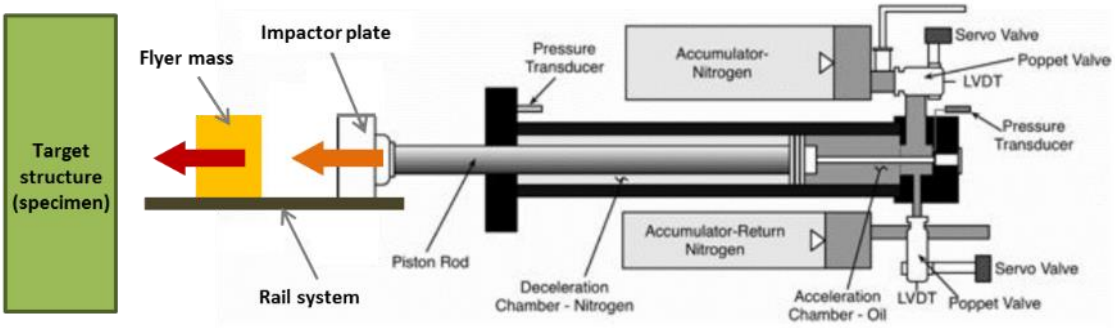

Figure 5.1 Schematic of dynamic impact test using hydraulic system (after [77] and [78])

5.1.2 Dynamic test bed construction

Test containers

To provide the most flexibility for specimen preparation as well as the testing schedule, a moveable test bed was constructed that could be relocated in and out of the Laboratory testing area as needed. Three test beds were fabricated using three steel front

load sanitation containers. The size of the containers (6-cubic yard dumpster), shown in Figure 5.2, was selected after a soil influence zone analysis using visual observation and finite element simulation in a previous study [62] so that the container boundary effect could be lessened in the dynamic tests.

Prior to soil placement, these containers were reinforced by welding additional steel sections around and under the container as shown in Figure 5.3. This reinforcement was necessary for multiple uses of the test bed in this dynamic test program because the original unreinforced dumpster was not designed to carry lateral impact loads on the sidewall as well as the dead weight of the compacted soil. After being reinforced, the container can be towed into position, laterally supported by a supporting frame system, and then anchored down to the Laboratory Strong Floor for dynamic testing. The movable test bed concept allows a test user to significantly reduce the preparation time between dynamic tests in the Laboratory.

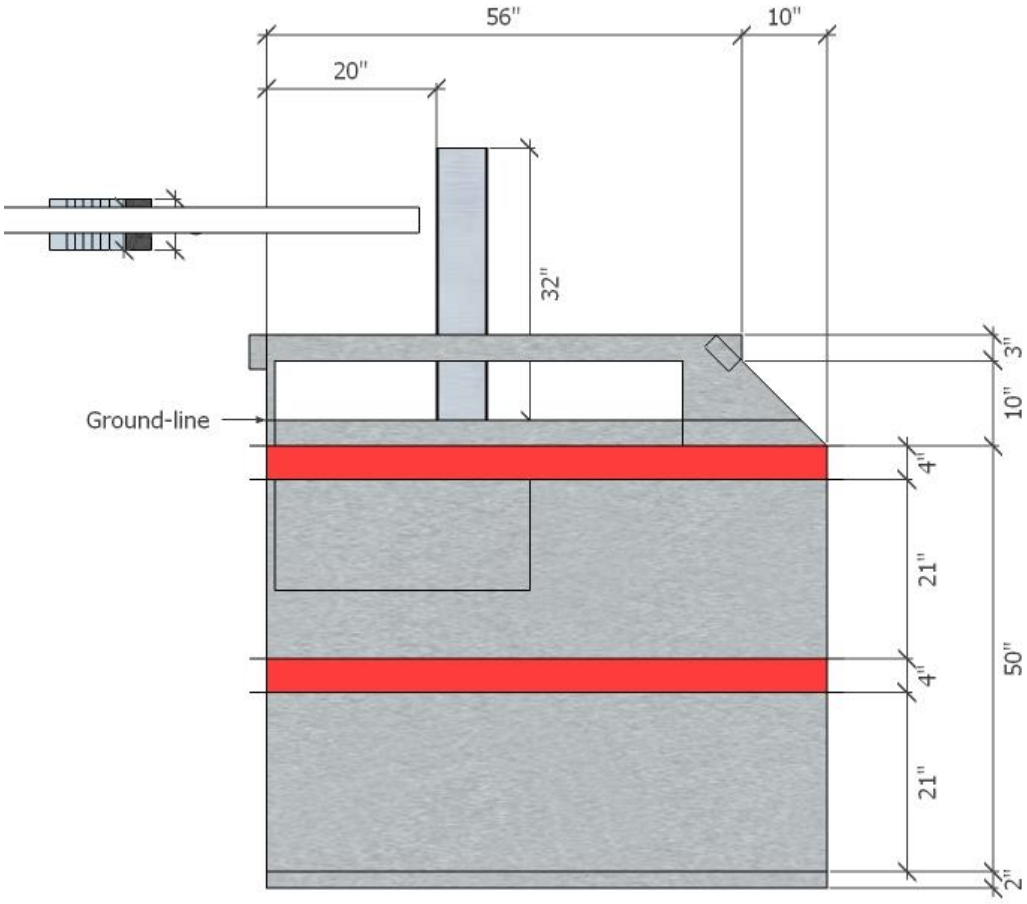

Figure 5.2 Dimension of dynamic test bed (6-cubic yard dumpster)

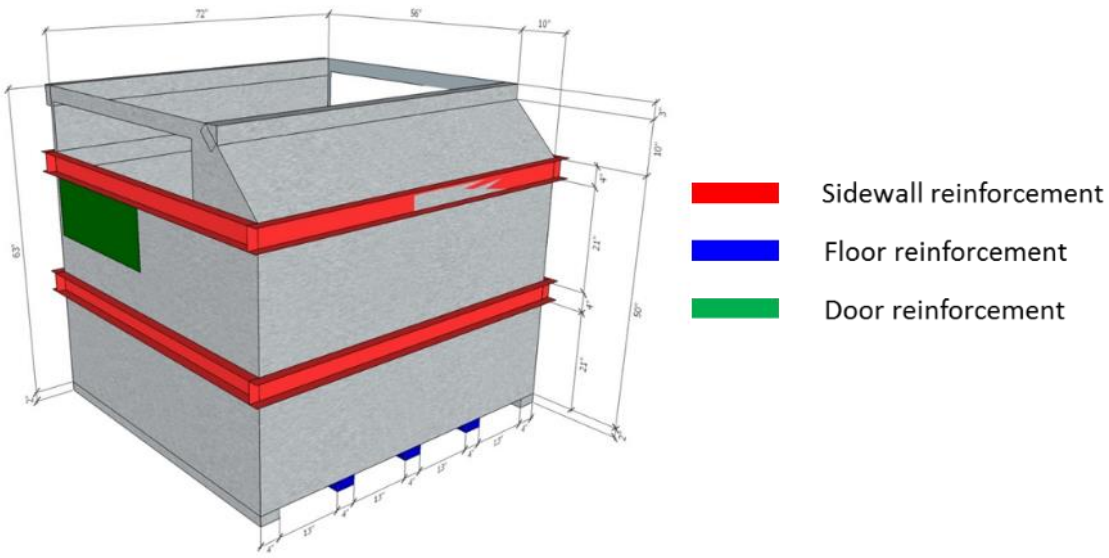

(a)

(b)

Figure 5.3 Steel container reinforcement; (a) drawing, and (b) fabrication picture

Soil and asphalt placement

After container fabrication was completed, the same type of base soil used in the static test program was placed and compacted to meet the grading requirements in accordance with *MASH* guidelines [13]. Then, the asphalt mow strip was installed over the compacted soil. In order to provide shear resistance along the side boundary of the asphalt mow strip, metal shear studs were welded on the sidewalls of the container (Figure 5.4(a)). These shear studs were located at the middle of the mow strip thickness every 5-inches along the sidewalls. Both soil and asphalt layers were compacted using a plate vibratory compactor (Figure 5.4(b)).

(a) (b)

Figure 5.4 Asphalt mow strip installation: (a) shear studs, (b) compaction

Due to practical limitations in the research program schedule, the hot mix asphalt used in the static test program could not be used for the dynamic testing program – there was not sufficient time to allow the hot mix material to age between test sessions. As such, a cold mix asphalt (CMA) was used for the mow strips in the dynamic test program.

In order to provide a strength and stiffness in the restraint layer similar to that seen in the static test program, Portland cement and water were added to the cold mix asphalt and a Portland cement ratio of 10 % by weight and 0.33 *w/c* (water/cement) ratio was selected as an acceptable mix design for the mow strips used in the dynamic test program. Discussion and details on all performed asphalt specimen tests are presented in Chapter 4.

For each mow strip test bed construction, 4 in. by 4 in. cylindrical specimens were prepared at the same time based on the method specified in *ASTM T-180* [61]. Table 5.1 shows uniaxial compression test results of the specimens made from four different cold mix batches. The average compressive strength at approximately 2 weeks was 239.3 psi and exceeded the target strength of 232 psi, which was determined as presented in Chapter 4. Hence, it can be asserted that the mow strip strength and stiffness were similar to structural properties of asphalt used in the static test program under the same temperature.

Table 5.1 Cold mix asphalt compression test results

No. of batch	Average compressive strength (psi)	No. of specimen tested	Test temperature (^{0}F)	Asphalt age (day)
1	273.6	3	66	14
2	229.7	3	68	13
3	248.0	2	71	13
4	193.8	2	69	11
Average	239.3	-	68.2	12.9

Guardrail post installation

The hydraulic post-rammer vehicle owned by the Georgia Department of Transportation used in the static test program was not suitable for driving the posts safely into the test container due to the elevation of the container above ground level. Instead, a vertical static load was applied using a hydraulic loading system in the laboratory as shown in Figure 5.5. The maximum loading capacity of 100 kips and the quasi-static loading rate of approximately 0.5 in./sec enabled both safe application of the loading and continuous monitoring of the slope and orientation of the post while driving. The slope and orientation of the post was carefully controlled so that the post could be driven in a perpendicular fashion. The maximum driving angle of the post did not exceed 1 degree from the perpendicular direction relative to the ground surface.

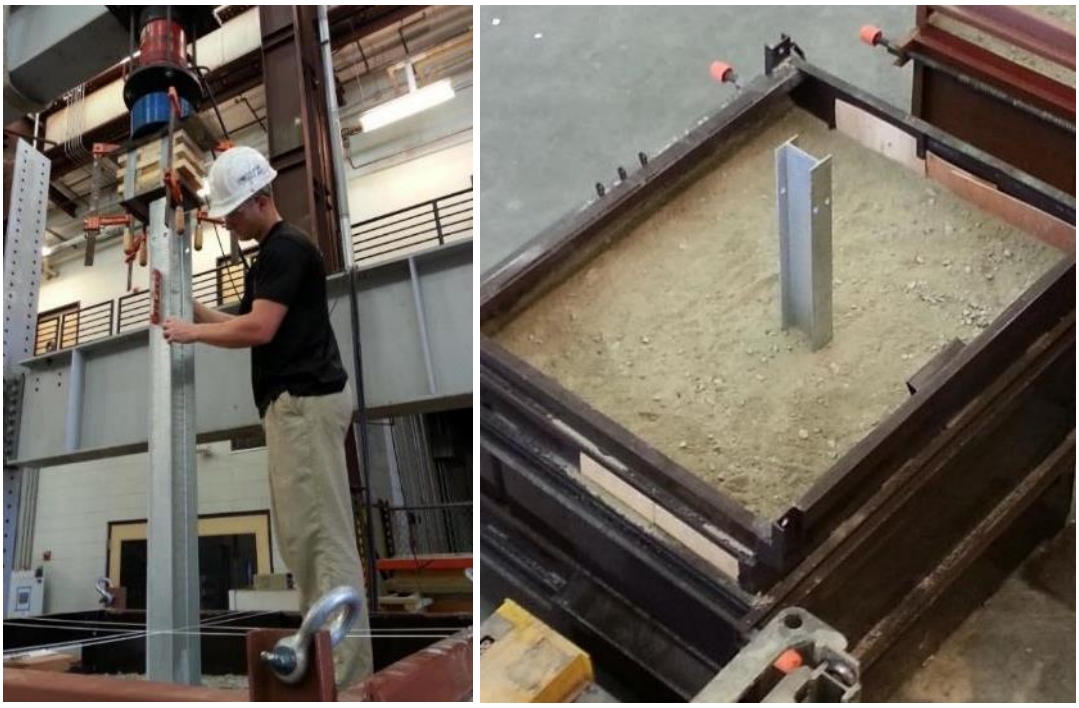

Figure 5.5 Post driving for dynamic test bed

Flyer mass

A flyer mass unit was precisely designed and fabricated for applying the impact to the post as desired. As shown in Figure 5.6, the flyer mass consists of: (1) two wing steel plates (6”x36”x1”: Height x Width x Thickness) to use as guides on the impact rail system, (2) middle steel plates (6”x10”x1”) located between the wing plates to allow for adjustment of the mass, (3) front and rear steel plates (6”x10”x2”) with threaded holes and recessed slots, and (4) four threaded rods and nuts (0.5” diameter) for connecting all the parts into one rigid body. By changing the number of middle plates, the mass can be adjusted from 175 to 350 lbs. One of the middle plates has a mounting slot on the top side so that an accelerometer can be safely mounted. Detailed drawings for the flyer mass are given in Appendix D. Additionally, a steel safety chain system (Figure 5.7) was employed to restrain the motion of the flyer subsequent to post-flyer impact. The safety chain was effective in preventing damage to the test setup (e.g., hydraulic actuator) as well as for allowing the reuse of the test components for multiple experiments.

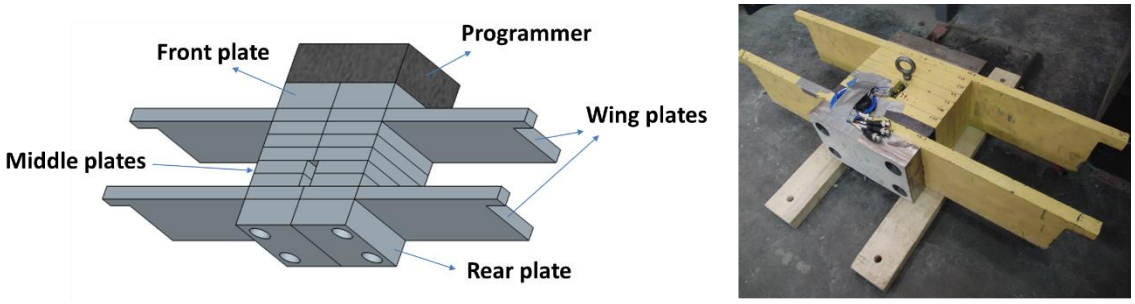

Figure 5.6 Adjustable flyer mass

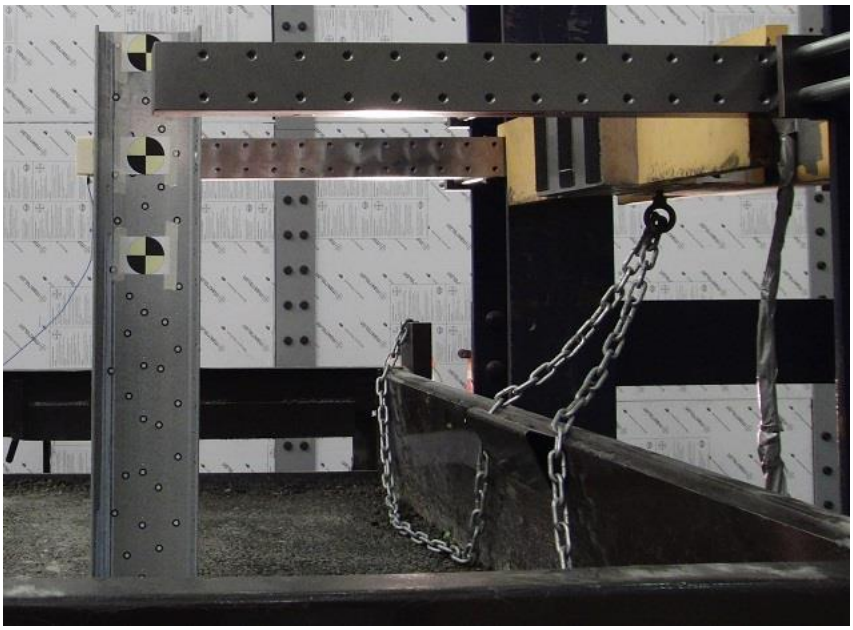

Figure 5.7 Safety chain system

5.1.3 Loading calibration with mock-up experiments

The magnitude and duration of the dynamic impact loading can be tailored not only by controlling the hydraulic setting but also by placing a relatively-weak and deformable medium (e.g., urethane foam) on the impact side of the flyer mass as shown in Figure 5.6. This deformable medium can be called as a programmer which is equivalent to a shock absorber in vehicles. A programmer transfers the energy and momentum of the hydraulic force to the test specimen. It also reduces the magnitude of acceleration so that the peak acceleration can be within the measurement range of accelerometers.

Equation (5-1) explains the general concept of the dynamic impact testing including a programmer-attached flyer mass. The net force, $F(t)_{net}$, acting on the flyer mass during the collision is equal to the product of its mass, m, and acceleration, $a(t)$, which is

measured by accelerometers located on the non-impact side of the flyer. The actual force on the test specimen (guardrail post), $F(t)_{specimen}$, can be adjusted by a modification factor, $\beta(v)$, related to the programmer (e.g., geometry and/or material), which is primarily a function of velocity, v.

$$F(t)_{net} = ma(t) = \beta(v)F(t)_{specimen} \tag{5-1}$$

Thus, as shown in Equation (5-2), the dynamic force on the specimen can be manipulated by the adjustment and calibration of the mass and the programmer of the impacting module.

$$F(t)_{specimen} = \frac{ma(t)}{\beta(v)} \tag{5-2}$$

In this study, a series of "mock-up" tests, classified as one-dimensional (1-D) momentum transfer experiments, were conducted to calibrate the forces from the hydraulic system. It was critical to confirm if a dynamic test with the most restrained condition of the post could be conducted safely within a reasonable range of accelerations. Hence, the mock-up test was designed to approximate a post in the most restrained condition. The mock-up test configuration includes a standard steel post with two fixed supports to the rigid steel frame using bolted connections as shown in Figure 5.8.

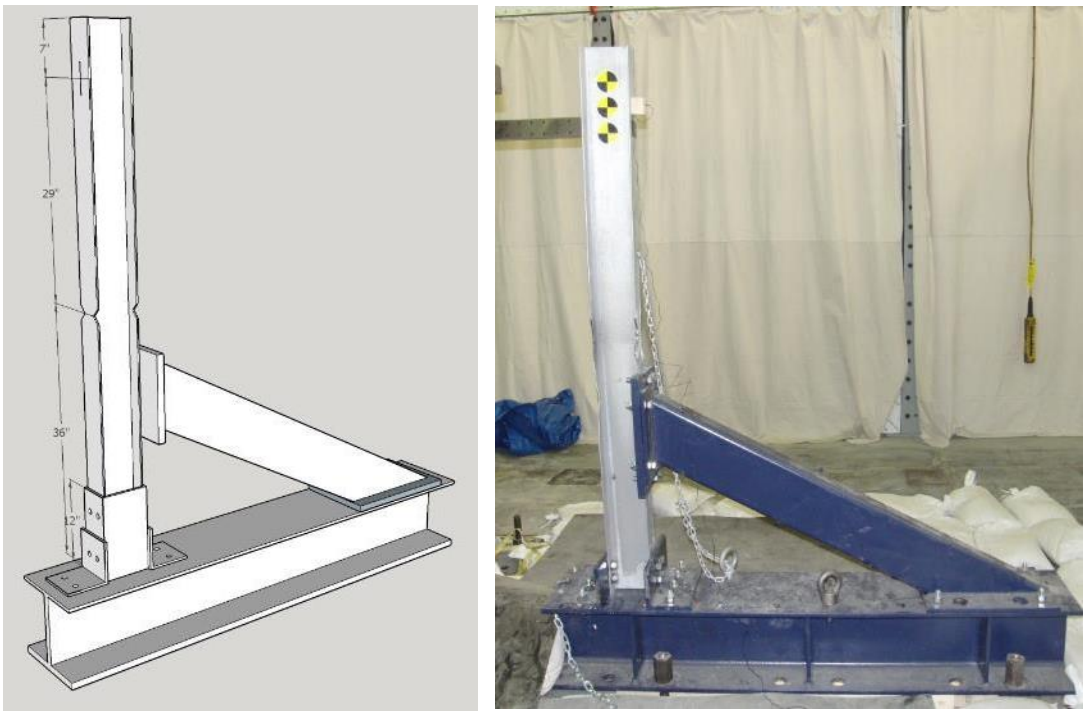

(a) (b)

Figure 5.8 Mock-up test on post with rigid connection: (a) drawing, and (b) experimental setup

Various impact speeds and programmer designs were tested to determine the appropriate hydraulic control needed to achieve the desired dynamic impact load in the dynamic test program. Table 5.2 summarizes results from the mock-up tests, and Figure 5.9 shows the flyer raw acceleration curves. It was determined from the M1 test that the 4" thick neoprene rubber programmer design was not suitable due to its high acceleration response. In the M2 and M3 tests, two different types of medium-density (10 lb./ft^3) urethane foam programmers were tested and a significant reduction in accelerations was observed compared to the M1 results. The M4 test indicated that using a low-density (6 lb./ft^3) urethane foam is more effective way to reduce the flyer acceleration and to

increase the deformation of the programmer. Based on these results, a reference FEA model was constructed and calibrated in a parallel study [12]. The FEA simulation for the M4 test shows reasonable agreement in both the maximum acceleration of the flyer and deformation of the programmer. Figure 5.10 compares the two deformed shapes of the programmer, one from the experiment and the other from the FEA simulation.

Table 5.2 Mock-up test summary

Test number	Impact speed (mph)	Programmer design and thickness	Max. acceleration of flyer mass (g)		Max. deformation of programmer (in.)	
			Exp.	FEA[12]	Exp.	FEA[12]
M1	13.0	(1): 4”	500	-	0	-
M2	13.0	(2): 4”	54	-	0.2	-
M3	13.0	(3): 6”	46	-	0	-
M4	21.6	(4): 5”	52	65	1.6	1.46

(1) 4” thick neoprene rubber
(2) 3” thick medium density (10 lb./ft^3) urethane foam + 1” thick neoprene rubber
(3) 2” floral foam + 3” thick medium density urethane foam + 1” thick neoprene rubber
(4) 4” thick low density (6 lb./ft^3) urethane foam + 1” thick neoprene rubber

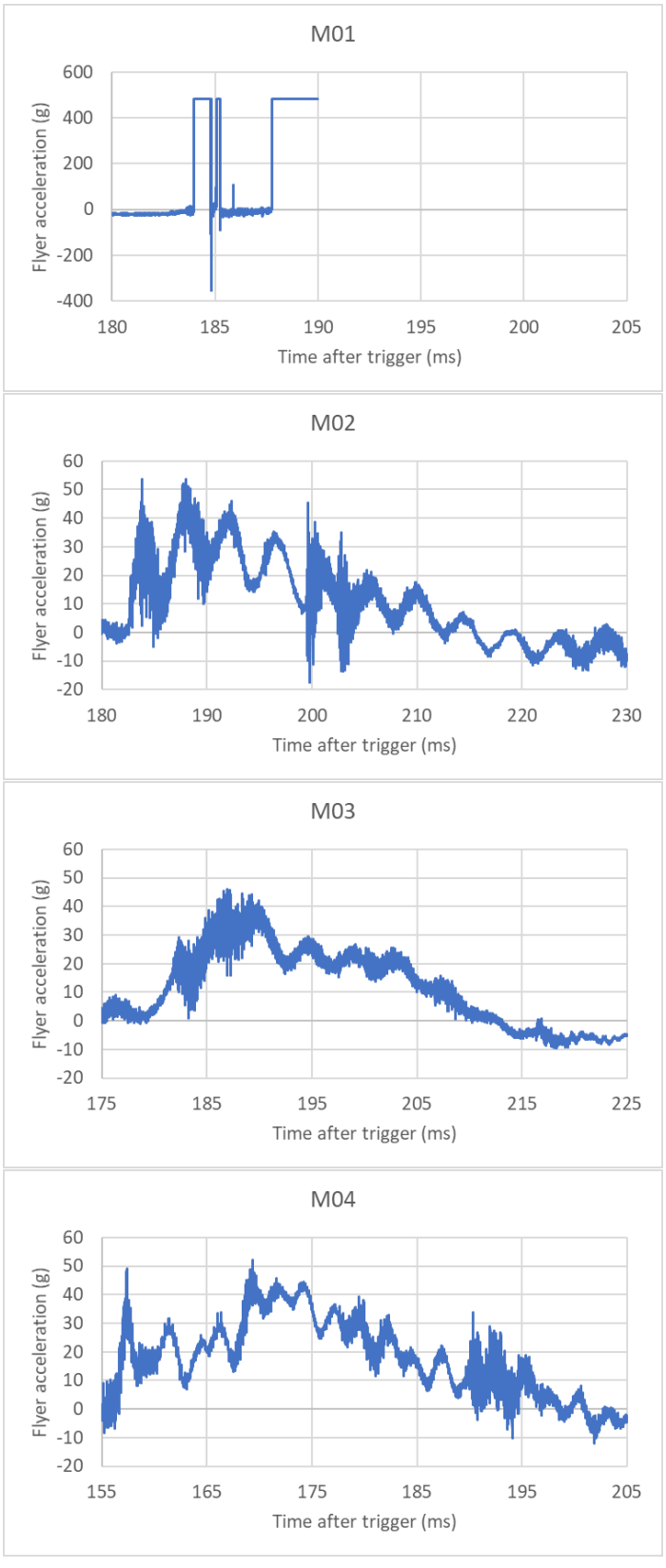

Figure 5.9 Mock-up test flyer raw accelerations

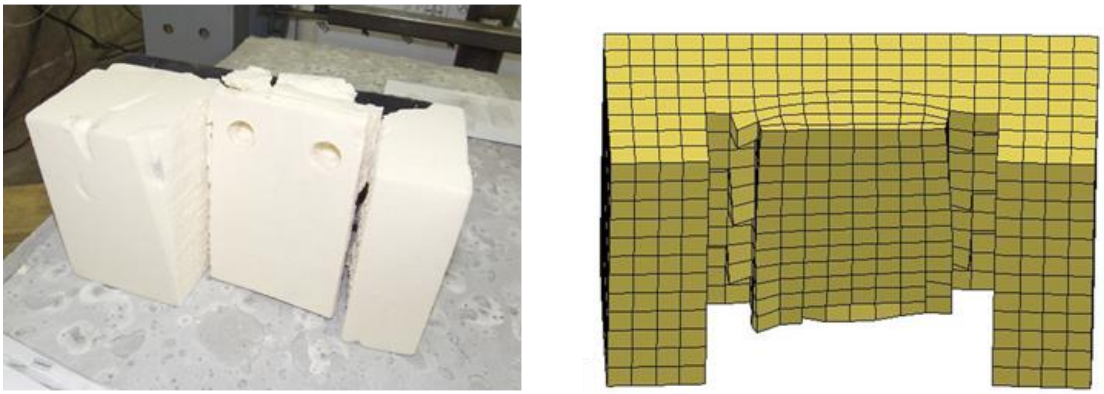

(a) (b)

Figure 5.10 Comparison of programmer deformation after impact (test M4): (a) experiment, and (b) FEA [12]

The calibrated FEA model guided the selection of programmer design for further dynamic experiments. Since the maximum acceleration of the flyer was still higher than that in typical full-scale crash tests as well as the *MASH* maximum acceleration requirement of 20.49 g, it was necessary to increase the thickness of the programmer material. Based on the FEA simulation results on combinations of various thicknesses and candidate materials [12], a programmer of 9 in. thick, consisting of two 4 in. thick low density urethane foams (6-lb./ft^3) and 1 in. thick neoprene rubber pad (Figure 5.11) was selected.

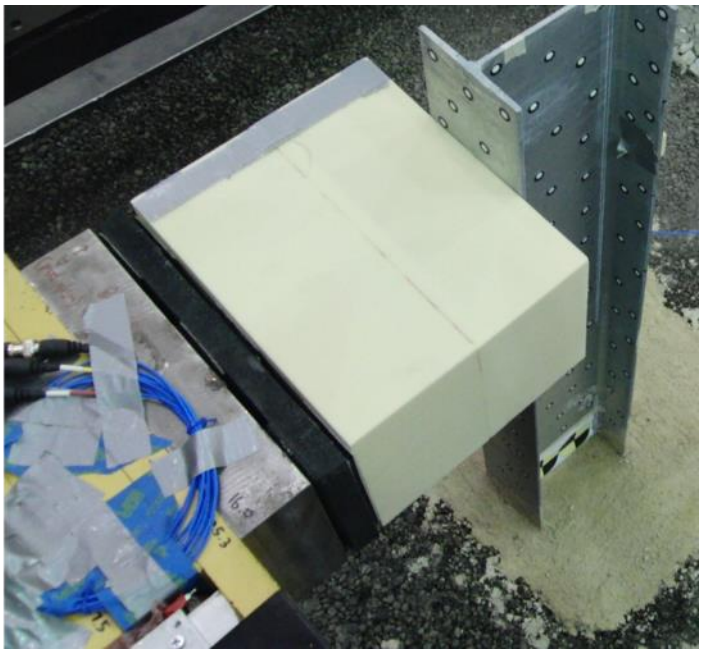

Figure 5.11 Final programmer design used in dynamic test program

5.1.4 Test instrumentation and data processing

Accelerometers

Shock-accelerometers ranging up to 5,000 g acceleration (PCB© 356B20) were installed on opposite sides of the impact surface - one on the flyer mass and the other on the post. The locations of the accelerometers are shown in Figure 5.12. To minimize damage to the instrumentation, accelerometer 1 (flyer mass) was mounted at a secured position on the top of the flyer and accelerometer 2 (guardrail post) was mounted on the opposite side flange. A high-speed portable data acquisition system (Synergy© P) was used to record all acceleration data at a sampling rate of 100 kHz. A detailed list of equipment used in the experimental program is given in Appendix B.

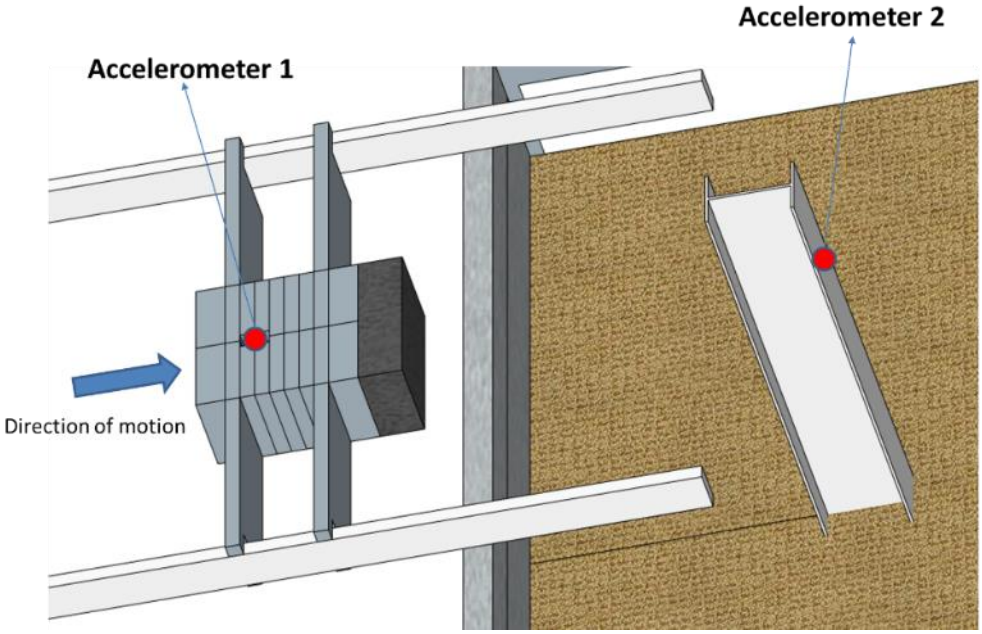

Figure 5.12 Location of accelerometers for dynamic testing

Acceleration data processing

Acceleration data were processed using a digital low pass filter. Specifically, the CFC 60 filter, specified in the SAE J211-1 [79], was used in this research. This filter is one of most widely used filters in automotive engineering for processing impact signals, and is recommended in *MASH*. This filtering process is necessary to remove high-frequency noises which can conceal the underlying trend in the signal. This filtering method was used in plotting acceleration-time history curves for all performed tests. Figure 5.13 gives an example of the raw and filtered acceleration curves.

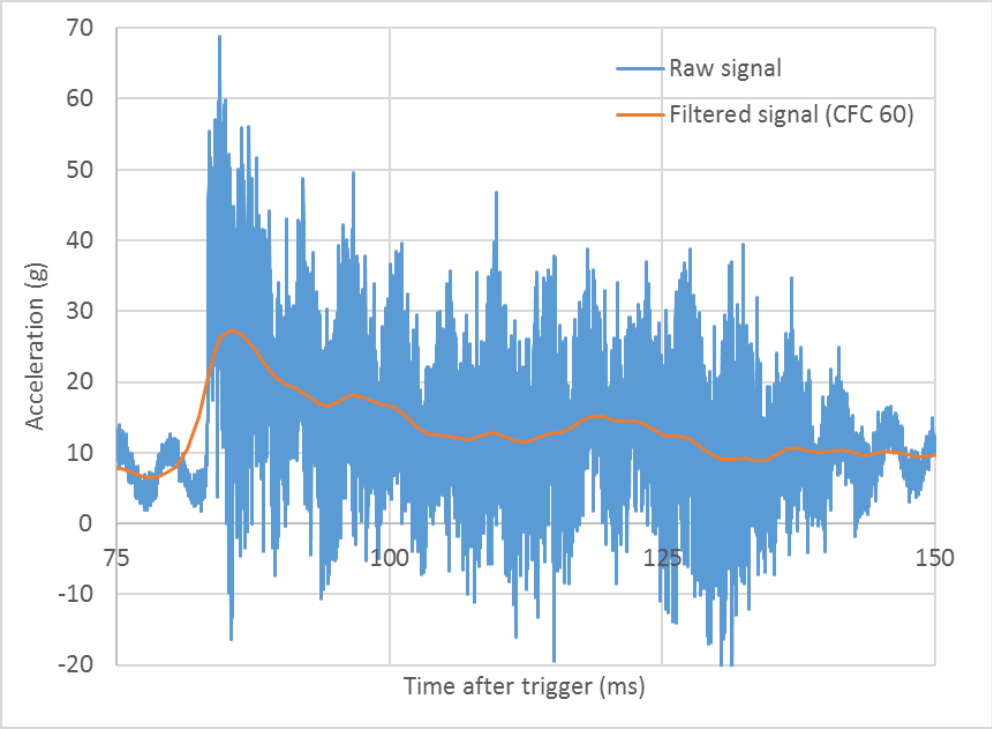

Figure 5.13 Example of raw and filtered acceleration signals

The first few dynamic tests were conducted with the accelerometer cables provided by the manufacturer with no protection/reinforcement. However, a significant amount of low-frequency noise in the acceleration data was recorded due to the vibration of accelerometer cables while the flyer was moving, which made the behavior of the flyer difficult to capture. To address this issue, more robust shielded extension cables were used and attached on the flyer with proper adhesive reinforcement as shown in Figure 5.14. The flyer acceleration was successfully captured in later tests using this approach. Figure 5.15 shows the filtered acceleration records from two different tests (before and after the treatment) but from the same test configuration.

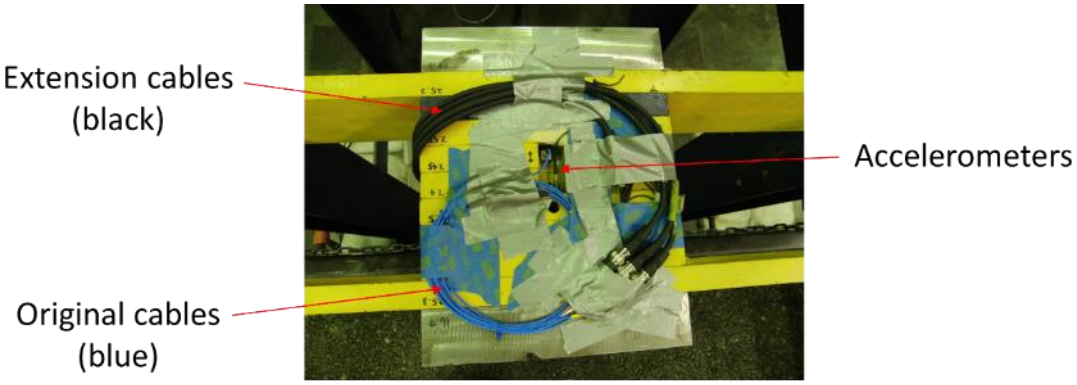

Figure 5.14 Protection and reinforcement for accelerometer cables

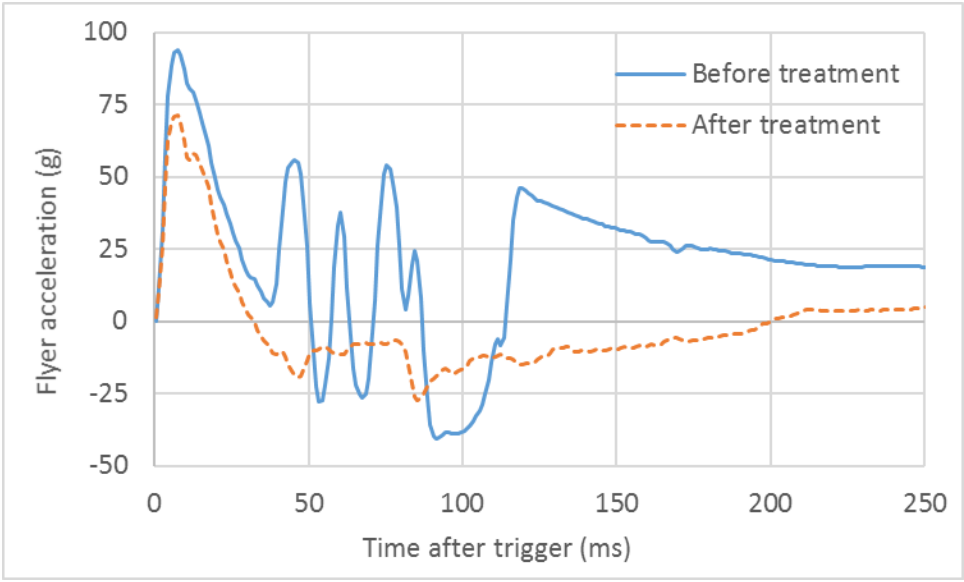

Figure 5.15 Removal of low-frequency noises from flyer acceleration

High-speed cameras

Two high-speed cameras (Phantom© Miro M310 and Miro C110) were used for both qualitative and quantitative evaluation of the structural behavior of the post. These cameras can provide video recording at both impact height and ground-level with an acceptable framerate (1,000 frames/second) and resolution (0.6 mm/pixel) during each

test. Figure 5.16 shows the location of both cameras and their corresponding fields of view. The recorded images can be analyzed with motion tracking software to provide detailed displacement information for the flyer mass, guardrail post, and surrounding asphalt. A detailed description of the high-speed cameras used in the dynamic testing program is given in Appendix B.

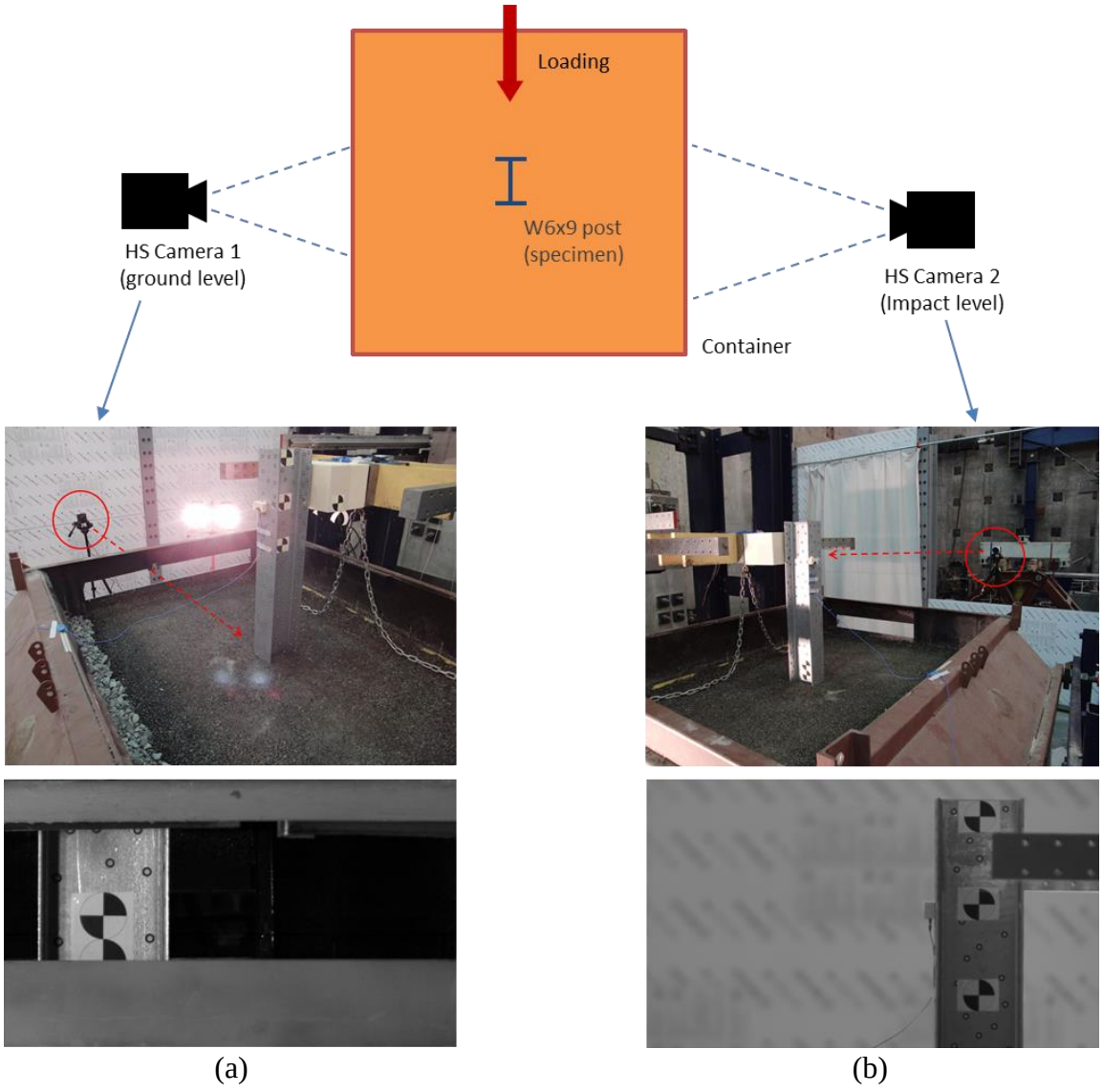

Figure 5.16 High-speed camera setup and images: (a) ground level, (b) impact level

Displacements from high-speed images

High-speed images can be utilized for plotting displacement-time history curves via PCC© [80], a software package featuring not only high-speed camera control but also motion tracking on high-speed images. Figure 5.17 shows an example of motion tracking based on the recorded images focused on targets located around the impact point and the flyer. Displacement-time history curves for three targets marked in this example are plotted in Figure 5.18.

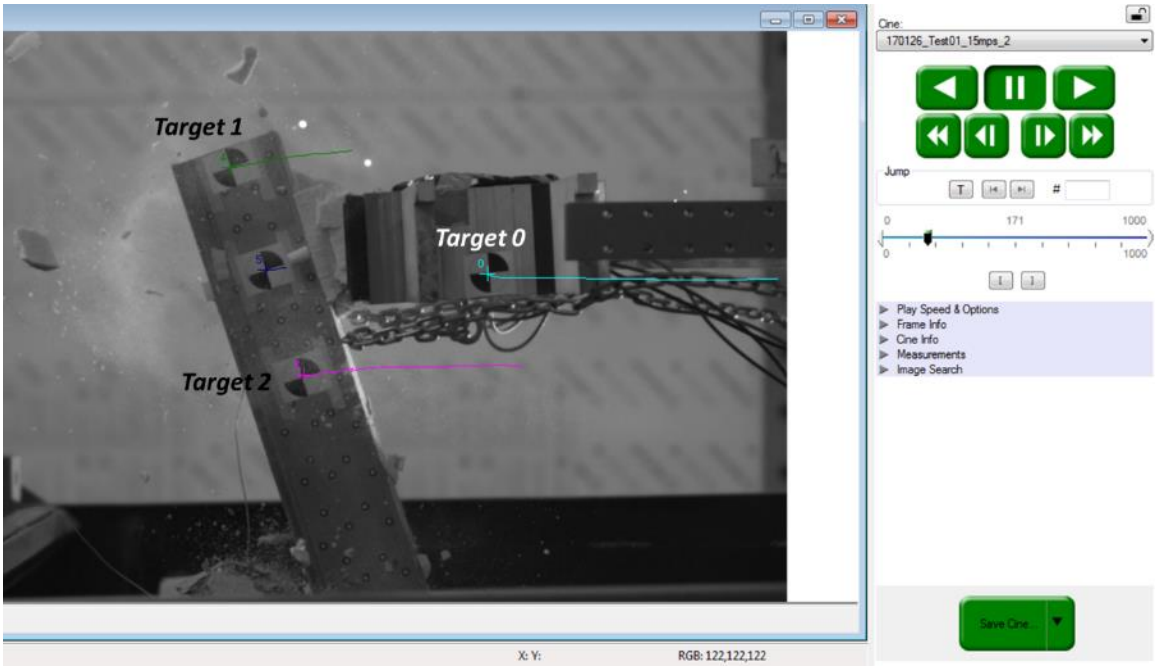

Figure 5.17 Example of motion tracking for displacements using PCC [80]

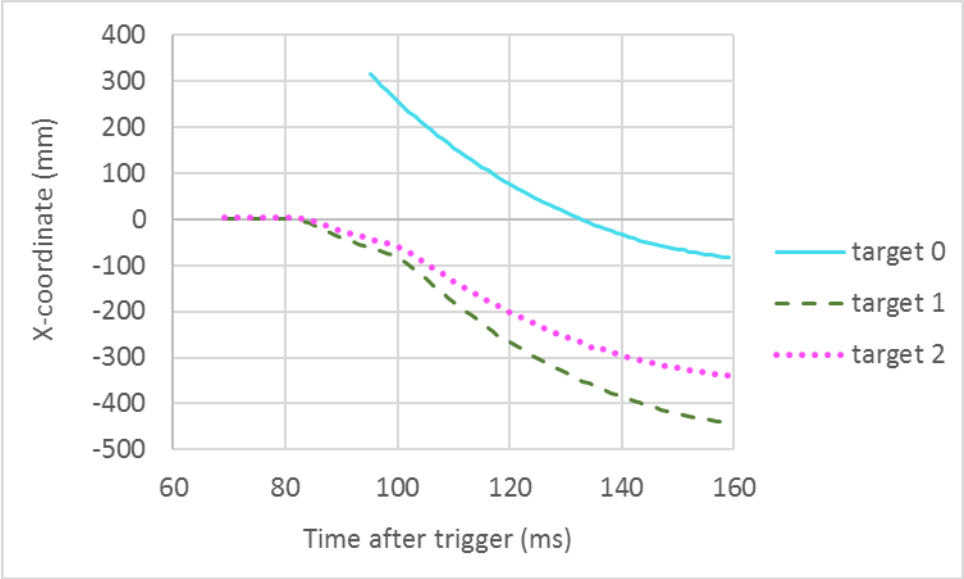

Figure 5.18 Example of target position-time history plots for multiple targets

Figure 5.19 shows an example of sequential photographs taken every 30 ms after the impact between flyer and post. A noticeable point occurs when the flyer started rotating horizontally when the post has nearly reached its maximum dynamic displacement (see pictures taken at 203 and 233 ms). This resulted from the accumulation of small imperfections and asymmetry in the test setup and specimen orientation. Because of this rotational movement of the flyer observed in several tests, the lateral displacement of flyer via motion tracking and the acceleration of flyer from the accelerometers were less accurate/reliable after the maximum dynamic displacement of the post occurred.

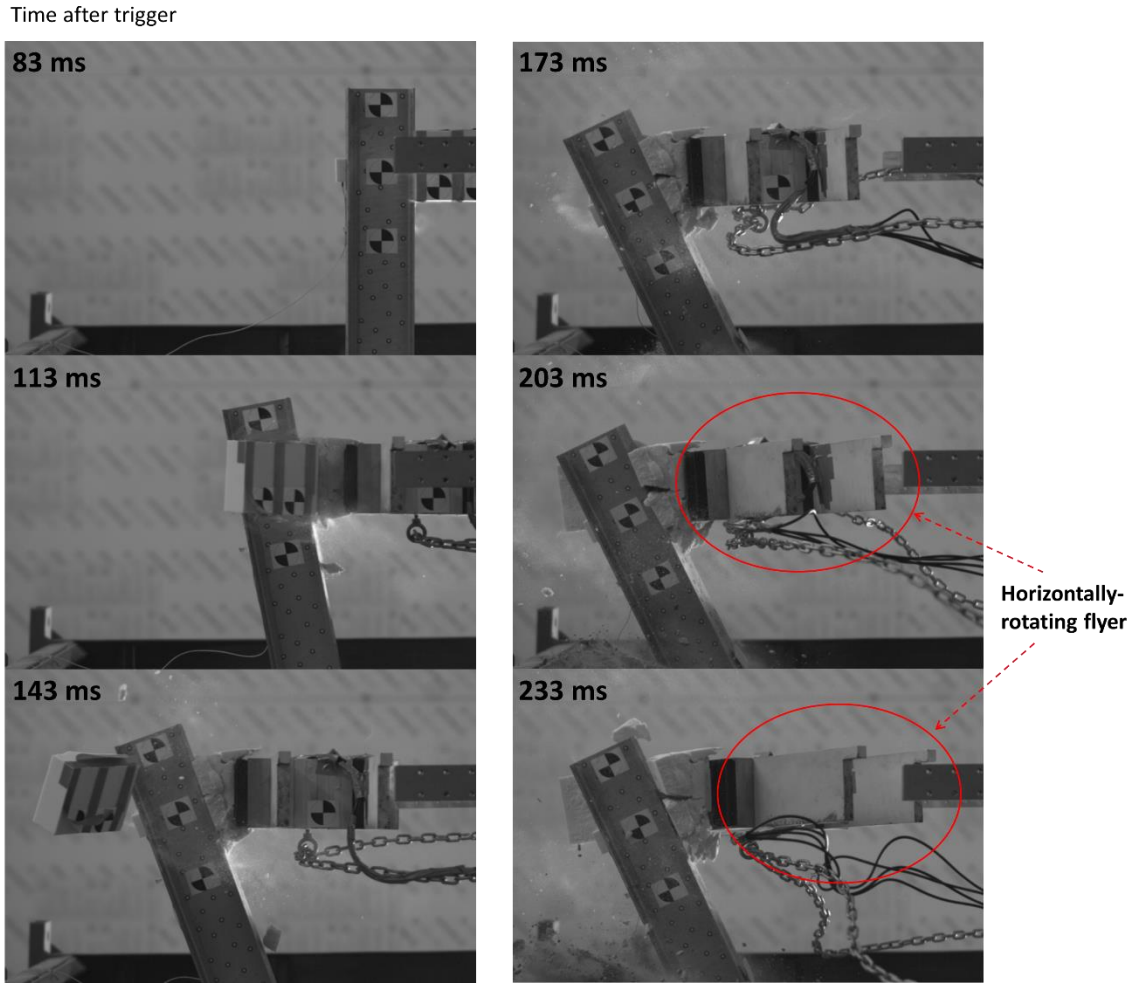

Figure 5.19 Sequential photographs for behavior of flyer and post after impact

5.2 Dynamic test program

5.2.1 Test input parameters

One of the most critical steps for dynamic impact testing is to determine a reference dynamic loading condition with test input parameters. As a first step, the reference kinetic energy level for dynamic tests was determined using the crash test parameters of *MASH* Test 3-11 [13]. The *MASH* Test 3-11 configuration specifies a test section and conditions for full-scale crash tests using a pickup truck impacting a guardrail system as shown in Figure 5.20 and Table 5.3. The test guideline specifies a dynamic load in terms of mass (m), impact angle (θ), and velocity (v) of the testing vehicle for the entire guardrail system. Hence, a dynamic impact load profile (e.g., load-time history curve) for single guardrail post is not available from the test guideline or available test reports from other roadside testing agencies.

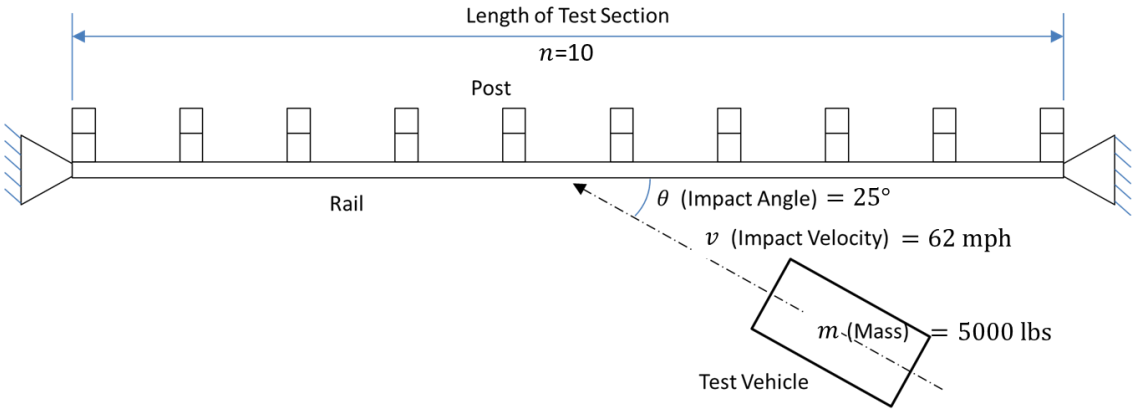

Figure 5.20 MASH 3-11 crash test condition (adapted from [13])

Table 5.3 MASH 3-11 crash test parameters [13]

Test condition	Values
Weight of a pickup truck (m)	5000 lb.
Impact velocity (v)	62 mph
Impact angle (θ)	25°
Number of posts (n) (length of test section)	10

The total lateral kinetic energy (E_K) contributing to the lateral displacement of the guardrail system can be calculated as shown in Equation (5-3). By assuming the lateral kinetic energy is distributed over 10 guardrail posts along the length of the test section, the average kinetic energy input on single post ($E_{K,avg}$) can be estimated as 137.9 kip-in. as shown in Equation (5-4). This value can be used as the reference kinetic energy input for test configurations including a single post.

$$E_K = \frac{1}{2} m (v \sin\theta)^2 = 1379 \text{ kip-in.} \quad (5\text{-}3)$$

$$E_{K,avg} = E_K / n = 137.9 \text{ kip-in.} \quad (5\text{-}4)$$

Even though numerous combinations of velocity and mass can yield the reference kinetic energy, both the maximum capacity of hydraulic actuator and the upper limit of the flyer dimension to avoid potential interference between test components were considered for conducting a dynamic test safely. As such, an impact velocity of 32.4 mph and flyer mass of 305 lbs. were selected as the most feasible dynamic test input parameters for the test program. Utilizing the test input parameters and methodology described in the previous section, experiments on guardrail post specimens with various

test configurations were planned by using the generalized dynamic test setup shown in Figure 5.21.

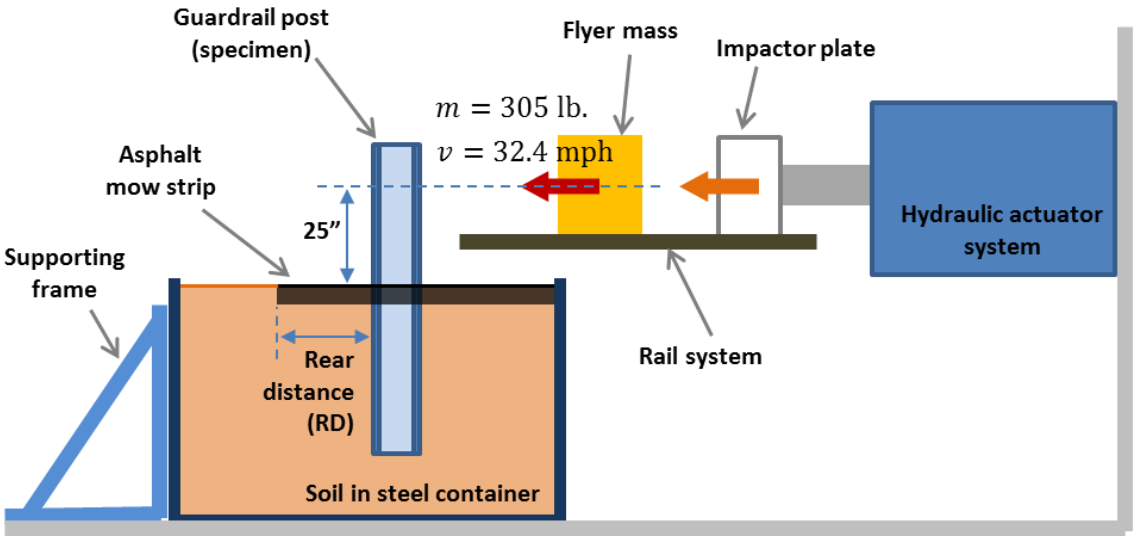

Figure 5.21 Schematic illustration of dynamic test configuration

5.2.2 Dynamic test matrix

A dynamic test matrix is given in Table 5.4. The test program classifies each test into one of three categories: basic configuration, treatment behind post, and variation in dimensions. Test setup photographs for all test categories are shown in Figure 5.22. An impact velocity of 32.4 mph and flyer mass of 305 lb. were used throughout the entire test program.

Table 5.4 Dynamic test matrix

Test Category	Test Configuration	Mow Strip Dimension		Test Date (Test Number)	Test Condition	
		Thick.	RD*		Temp.	Asphalt Age
Basic Configuration	Baseline	0	0	9/12/16 (#1) 9/29/16 (#2) 1/26/17 (#13)	85 ^{0}F 75 ^{0}F 71 ^{0}F	- - -
	Typical mow strip	3.5”	24”	10/27/16 (#3) 12/19/16 (#6)	79 ^{0}F 66 ^{0}F	15 days 16 days
Treatment Behind Post	Leave-out	3.5”	24”	10/28/16 (#5) 1/26/17 (#12)	82 ^{0}F 71 ^{0}F	15 days 13 days
	Pre-cut (parallel)			10/27/16 (#4) 12/20/16 (#8)	79 ^{0}F 68 ^{0}F	13 days 13 days
	Pre-cut (diagonal)			1/5/17 (#10)	71 ^{0}F	16 days
Variation in Dimension	Thin	1.5”	24”	1/5/17 (#9)	71 ^{0}F	16 days
	Thick	5.5”	24”	1/6/17 (#11)	71 ^{0}F	16 days
	Reduced RD	3.5”	12”	12/19/16 (#7)	68 ^{0}F	13 days
	Thick and reduced RD	5.5”	12”	1/27/17 (#14)	69 ^{0}F	11 days

* *RD* = rear distance of mow strip behind trailing flange of post (see Figure 5.21)

A total of five tests are classified as “basic configuration” category in Table 5.4. The baseline configuration denotes a test configuration with no mow strip and with the least amount of ground-level restraint. The main purpose of this test was to provide a lower bound for system response regarding to the ground-level restraint. The typical mow strip configuration (3.5” thick and 24” rear distance) was identified as one of the most common mow strip dimensions in U.S. roadways. The typical configuration represents a test configuration with a moderate-rigid ground-level restraint where other mow strip configurations can be compared to.

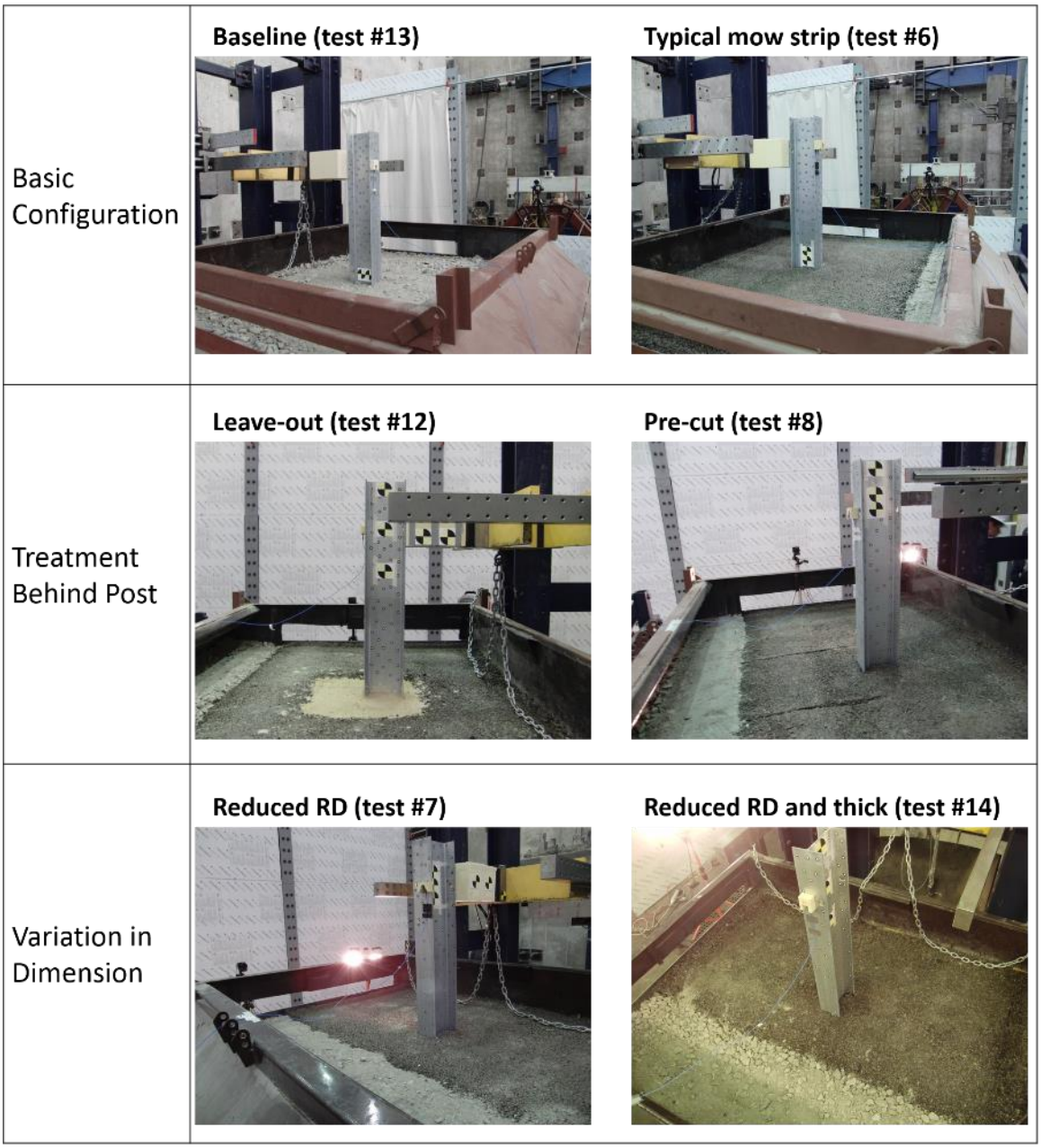

Figure 5.22 Representative dynamic test setup photographs by test category

The “treatment behind post” category in Table 5.4 includes a total of five tests. Thickness and rear distance in these tests were set equal to the typical mow strip configuration (3.5” thick and 24” rear distance). As shown in Figure 5.23, two treatment techniques were applied at the mow strip area behind the post intended to reduce ground-level restraint. Two tests including a leave-out application (based on recommendations in the *AASHTO Roadside Design Guide*) were conducted to establish a reference performance level for a post struck by the impactor. The 28-day compressive strength of the grout materials used with the leave-out were less than 120 psi, which satisfies the *AASHTO RDG* recommendation. Next, three pre-cut mow strip configurations (as explained in Section 3.2.2) were tested as an alternative to the leave-out treatment.

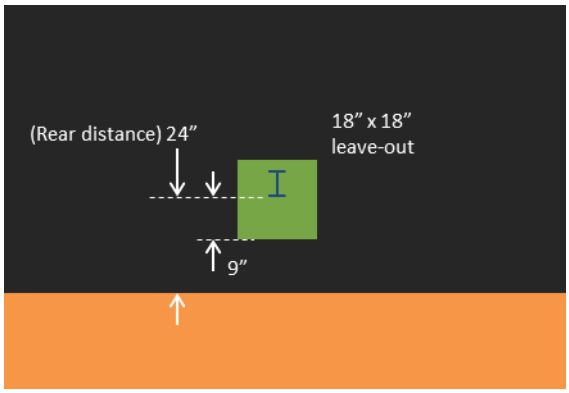

(a)

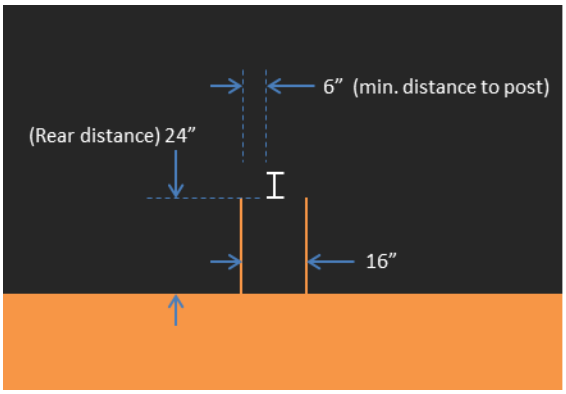

(b)

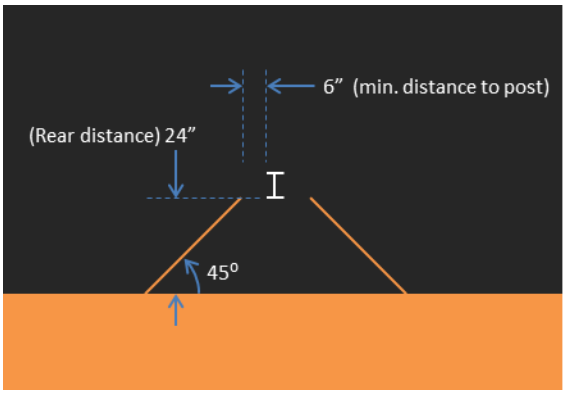

(c)

Figure 5.23 Tested mow strips with treatment behind post: (a) leave-out, (b) parallel pre-cut, and (c) diagonal pre-cut

A total of four tests are classified in the “variation in dimension” category in Table 5.4. The main purpose of these tests was to provide a quantitative guideline on the variability in ground-level restraint caused by changes in mow strip geometric parameters. Three mow strip thicknesses (1.5”, 3.5”, and 5.5”) and two rear distances (12” and 24”) were considered in the development of the test matrix; ultimately, 4 cases (1.5” x 24”, 5.5” x 24”, 3.5” x 12”, and 5.5” x 24”) were tested under the dynamic test protocol.

5.3 Dynamic test results

5.3.1 Basic configuration tests

In baseline tests with no mow strip, the guardrail post could contain the flyer mass and redirect it to a gradual stop in conjunction with lateral deflection of the post. Figure 5.24 shows sequential photographs of test #13 from the high-speed camera. Figure 5.25 shows a representative baseline test setup (test #13) and the overall displacement of the post and the deformation of the soil foundation. The maximum post displacement at the impact height was 23.11 in. at 109 ms after the initial impact. The flyer started rotating horizontally after maximum displacement and landed on the ground of the impact side. The post displacement at the ground-level was measured 10.83 in. and there was no post bending or local yielding in the post section due to ground-level restraint. The acceleration response showed that the peak flyer acceleration of 27.4 g occurred at 3 ms and the acceleration slowly decreased after the peak while the flyer and the post were in contact.

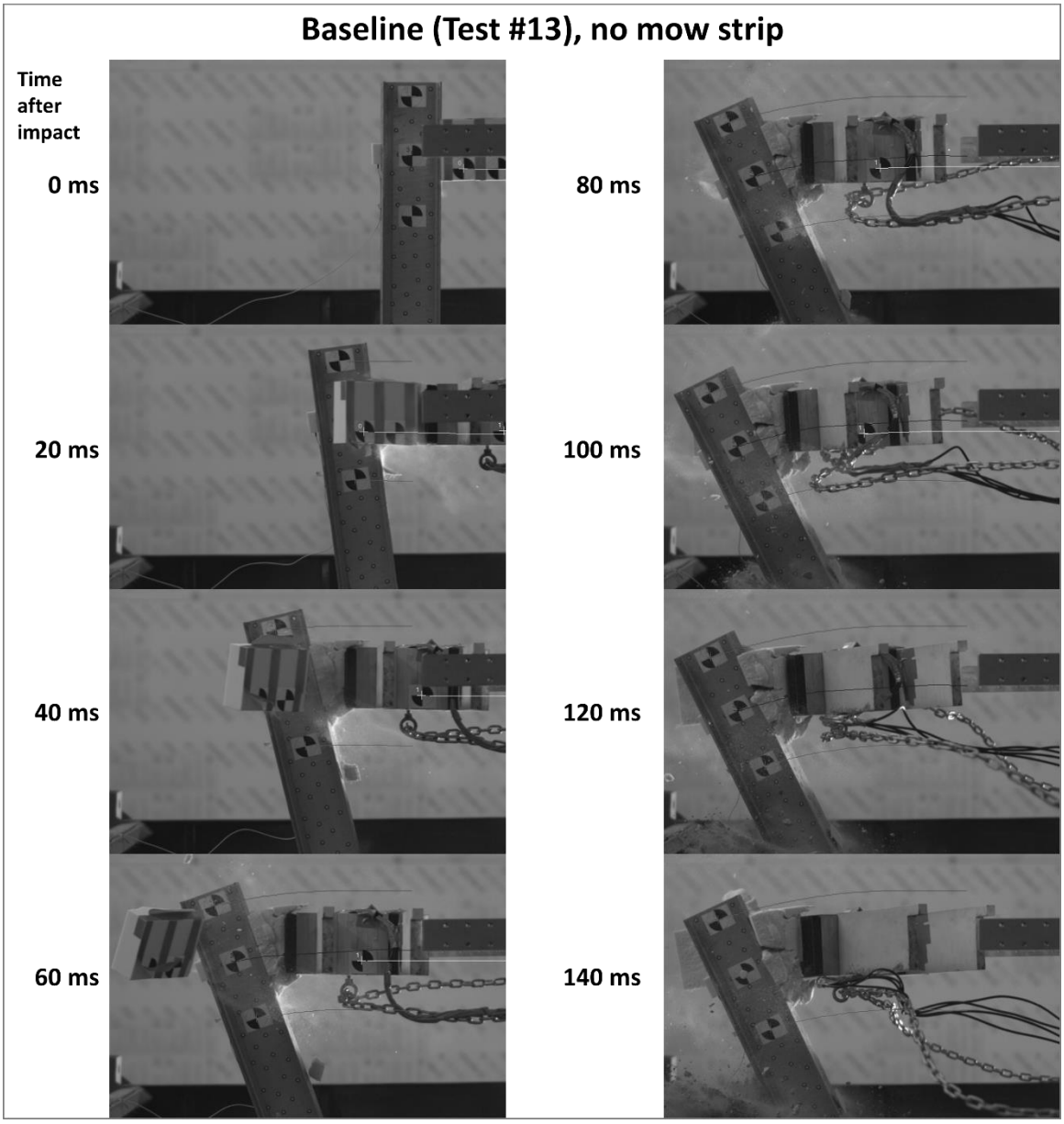

Figure 5.24 Baseline test (test #13): sequential photographs for post displacements

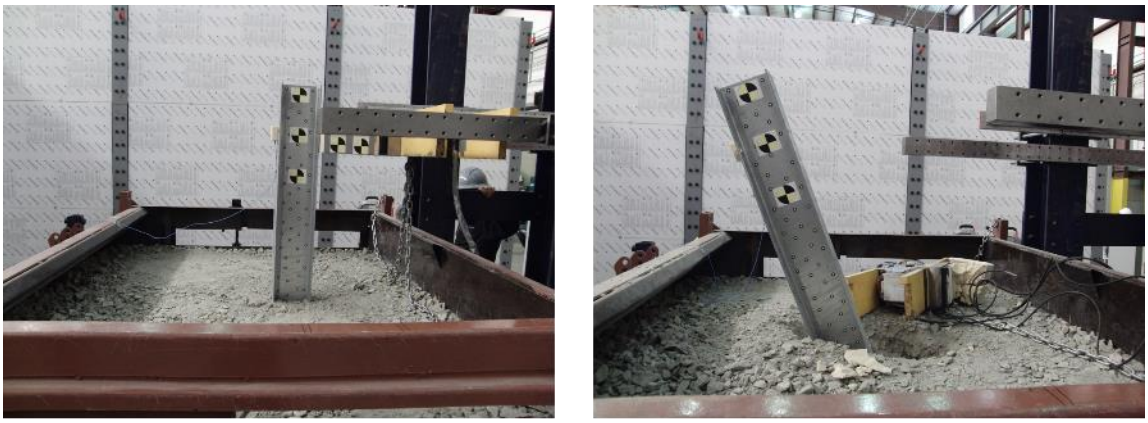

(a) Test setup before impact

(b) After impact (side view)

(c) After impact (top view)

(d) Deformation at ground-level

Figure 5.25 Baseline test (test #13): overall damage after impact

In typical mow strip tests, the embedded guardrail post successfully redirected the flyer mass to the impact side. Figure 5.26 shows a representative test setup (test #6), the overall displacement of the post, and the deformation of the mow strip. The mow strip on the rear side was completely fractured by the impact: two diagonal crack lines propagated from the post flanges and one crack line propagated along the direction of the impact. However, there was no significant bending or local yielding in the post due to ground-

level restraint by the mow strip. Figure 5.27 shows the sequential photographs of test #6 from the high-speed camera. The maximum post displacement at the impact height was 13.71 in. at 96 ms after the initial impact while the post displacement at the ground-level was measured at 5.12 in. The flyer was decelerated by the post and safely landed on the rails after maximum displacement. The acceleration response showed that the peak flyer acceleration of 42.5 g occurred at 19 ms and the acceleration rapidly decreased after the peak compared to the baseline results.

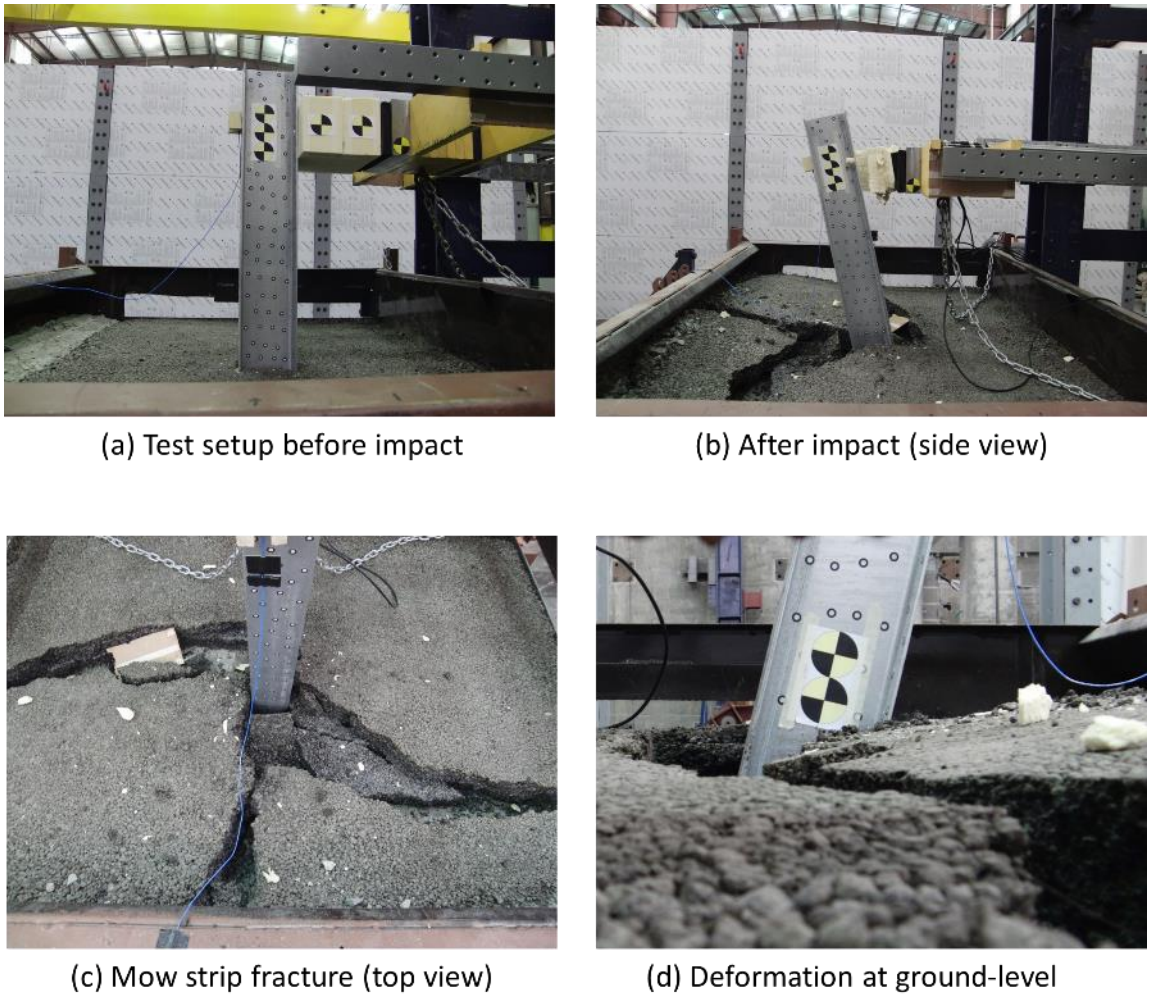

(a) Test setup before impact

(b) After impact (side view)

(c) Mow strip fracture (top view)

(d) Deformation at ground-level

Figure 5.26 Typical mow strip test (test #6): overall damage after impact

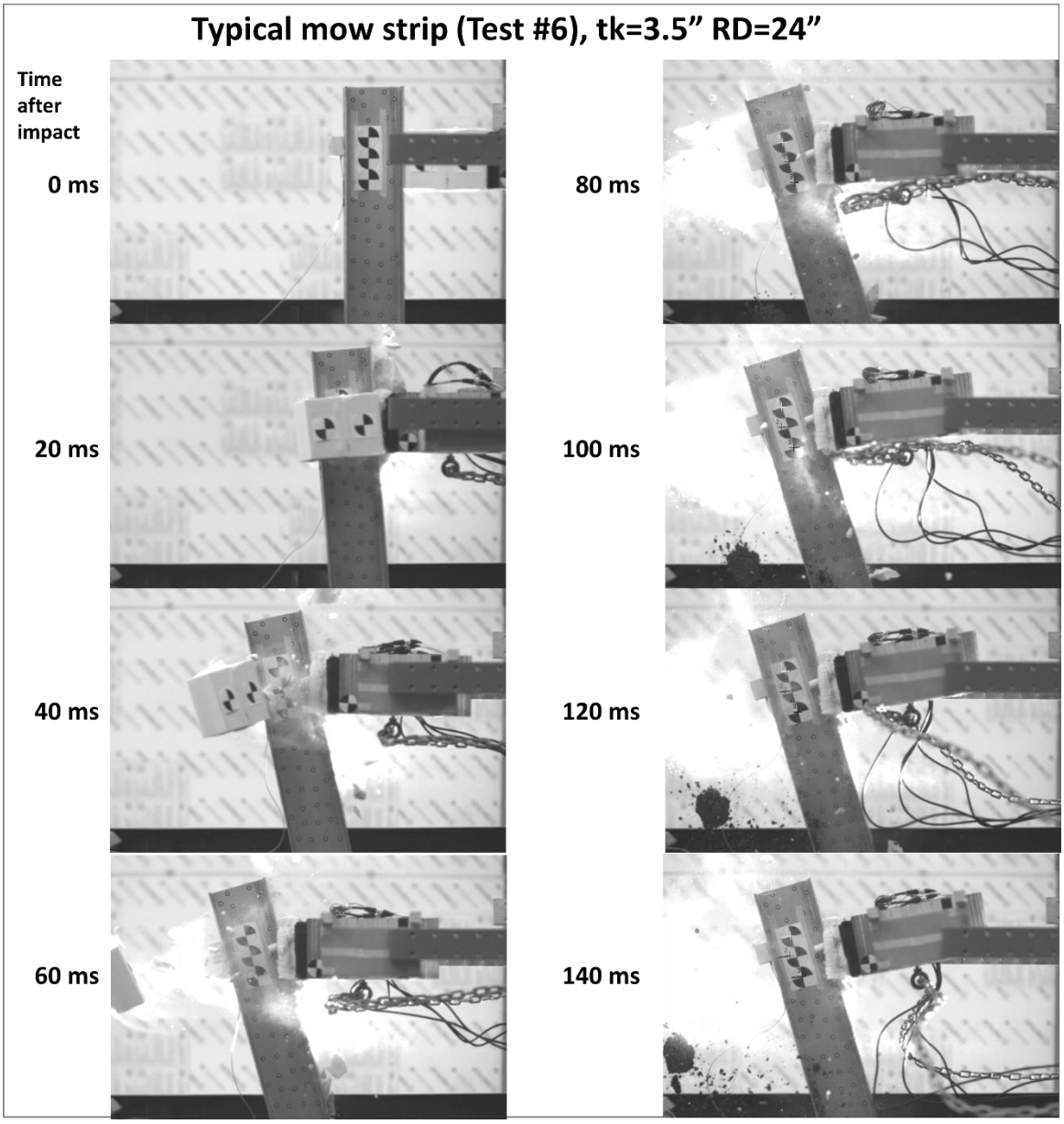

Figure 5.27 Typical mow strip test (test #6): sequential photographs for post displacements

Acceleration curves from representative tests in the basic configuration category are shown in Figure 5.28. Displacement measurements from high-speed images are plotted in Figure 5.29. Impact details based on the acceleration and displacement responses are summarized in Table 5.5.

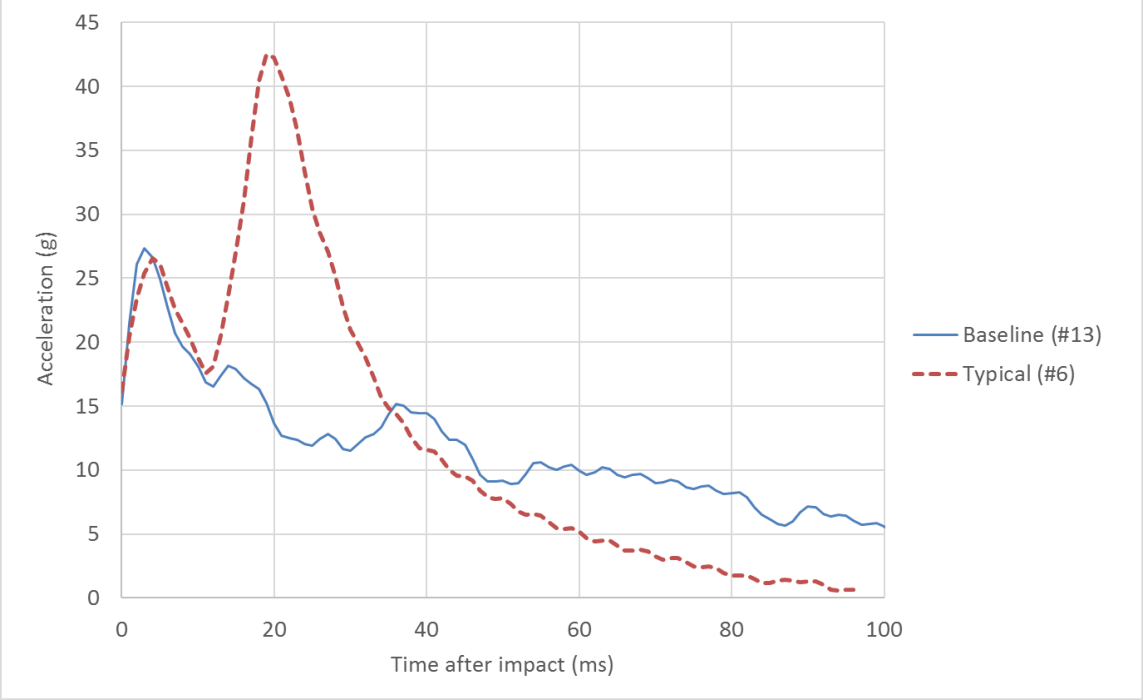

Figure 5.28 Basic configuration tests: acceleration-time history

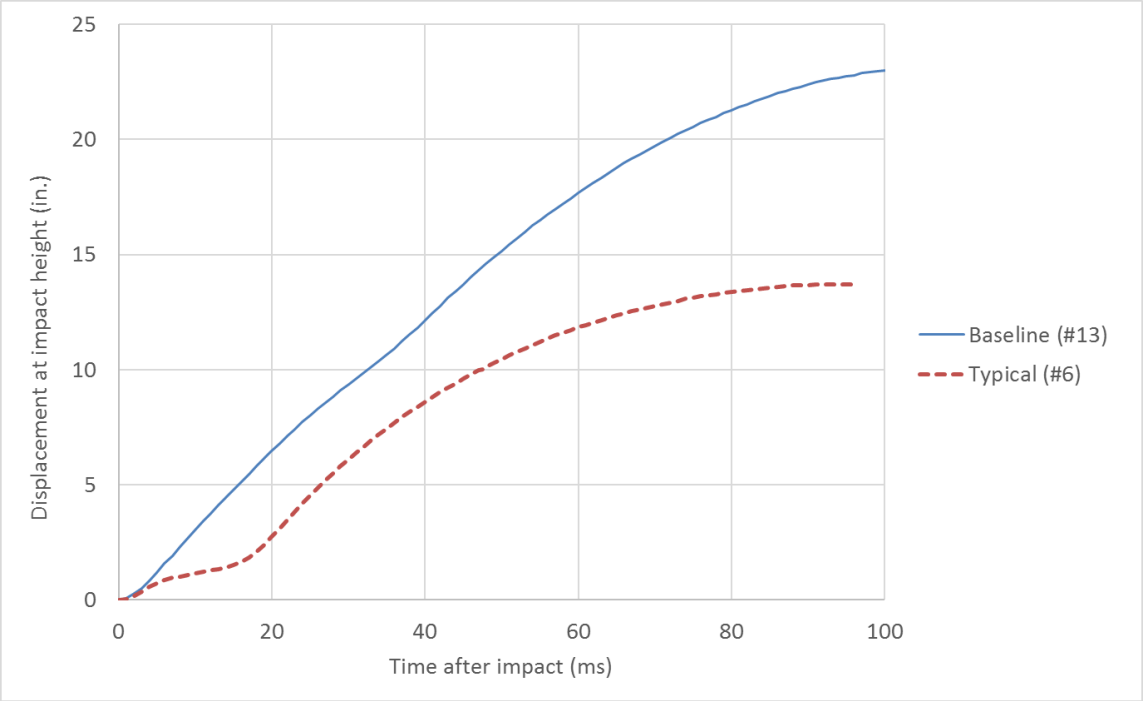

Figure 5.29 Basic configuration tests: displacement-time history

Table 5.5 Basic configuration tests: impact details

Test Configuration	Mow Strip Dimension		Peak accel. (g)	Time at peak accel.(ms)	Max. displ. (in.)	Time at max. displ. (ms)
	Thick.	RD				
Baseline	0	0	27.4	3	23.11	109
Typical mow strip	3.5”	24”	42.5	19	13.71	96

5.3.2 Tests with treatment behind post

In the leave-out mow strip test, the flyer mass was successfully decelerated by the post and dropped on the impact side of the mow strip/leave-out zone. Figure 5.30 shows the sequential photographs of test #12 from the high-speed camera. Figure 5.31 shows the leave-out test setup (test #12), the overall displacement of the post, and the deformation of the grout-leave out with surrounding mow strip. The leave-out zone behind the post was completely crushed and the mow strip on the rear side was also fractured by the impact. Two diagonal cracks propagated from two rear-side corners of leave-out and another crack split the mow strip along the direction of impact. No significant local damage in the post was observed. The maximum post displacement at the impact height was 15.91 in. at 92 ms after the initial impact while the post displacement at the ground-level was measured at 6.69 in. The flyer was decelerated by the post and redirected to the front side of the mow strip after maximum displacement. The peak flyer acceleration of 32.4 g was recorded at 21 ms, which was lower than the typical mow strip test (42.5 g) but higher than the baseline test (27.4 g).

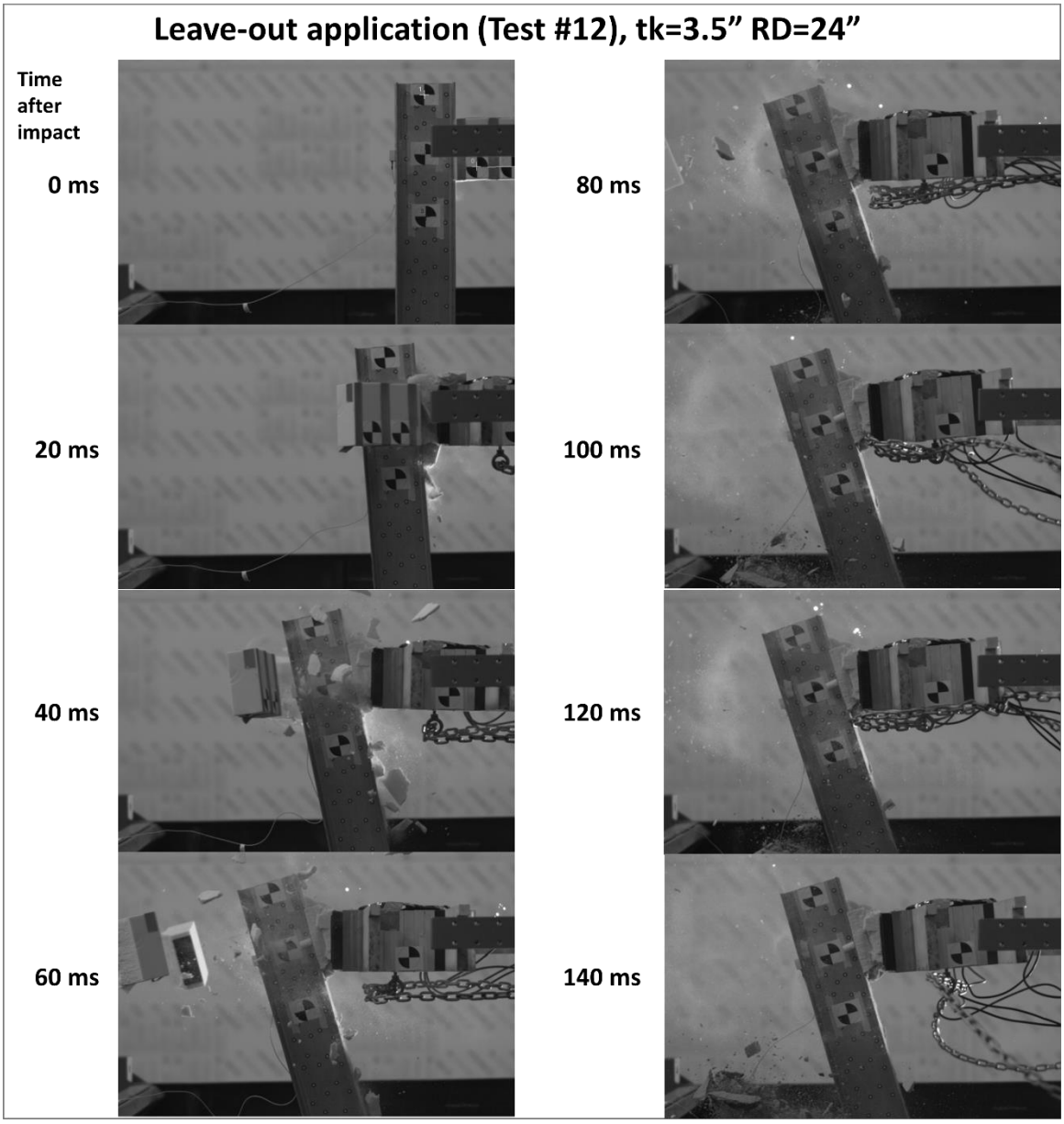

Figure 5.30 Sequential photographs for leave-out configuration

(a) Test setup before impact

(b) After impact (side view)

(c) Mow strip fracture (top view)

(d) Deformation at ground-level

Figure 5.31 Leave-out test (test #12): overall damage after impact

In pre-cut configuration tests, the lateral restraint by the guardrail post was reduced by applying one of the pre-cutting patterns shown in Figure 5.23. The guardrail posts were able to contain the flyer mass and redirect it to the front side of the ground. Figure 5.32 shows the pre-cut test setup (test #8), the overall displacement of the post, and the fracture mode of the mow strip. Figure 5.33 shows the sequential photographs of test #8 from the high-speed camera. The maximum post displacement at the impact height was

22.0 in. at 123 ms after the initial impact and the ground-level displacement was measured at 9.49 in. The peak flyer acceleration of 29.6 g was recorded at 21 ms. As expected, the fracture of mow strip behind the post was guided by the pre-cuts. There was no remarkable damage in the mow strip outside the pre-cut area as well as in the guardrail post near the ground level.

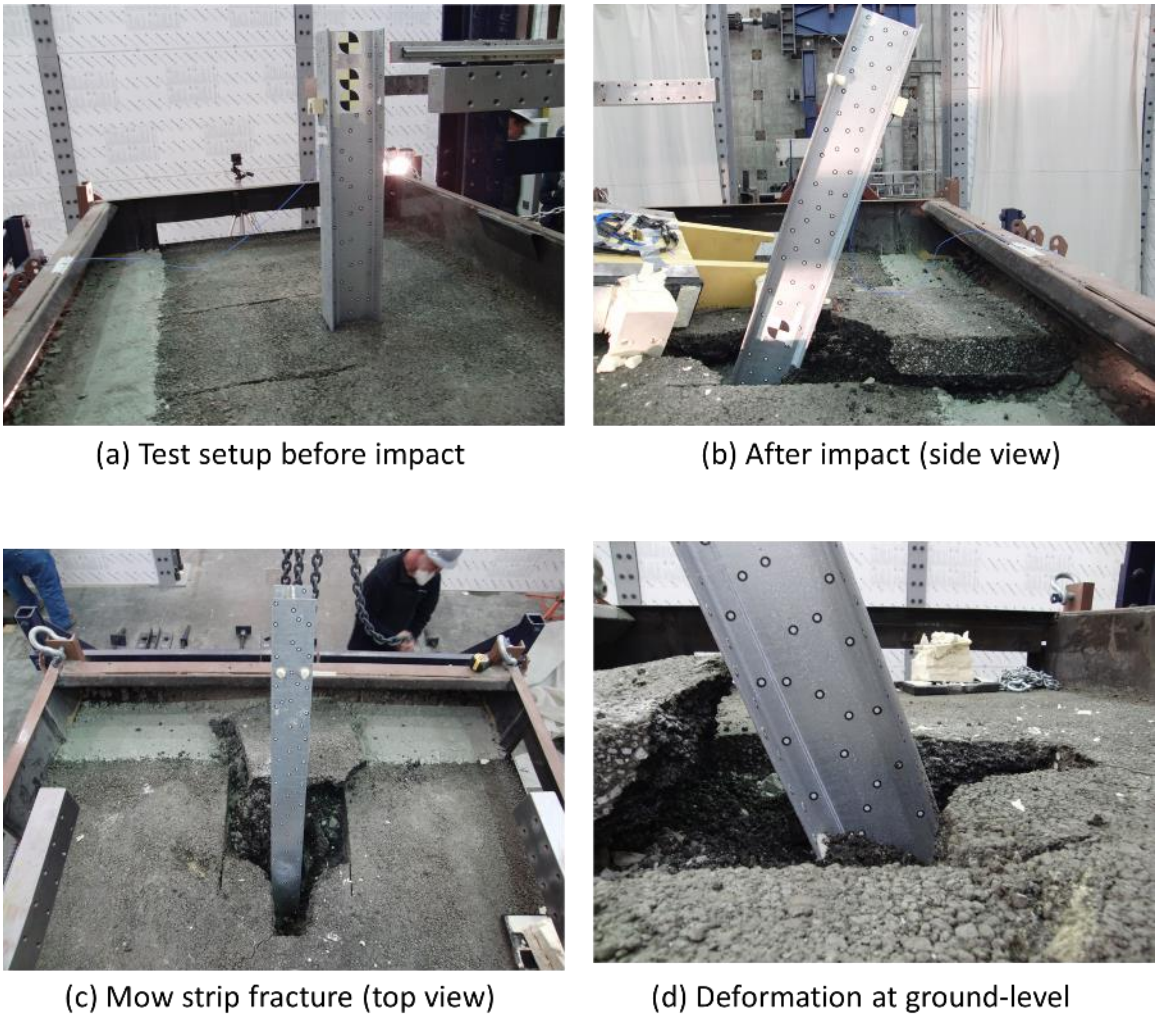

(a) Test setup before impact

(b) After impact (side view)

(c) Mow strip fracture (top view)

(d) Deformation at ground-level

Figure 5.32 Pre-cut test (test #8): overall damage after impact

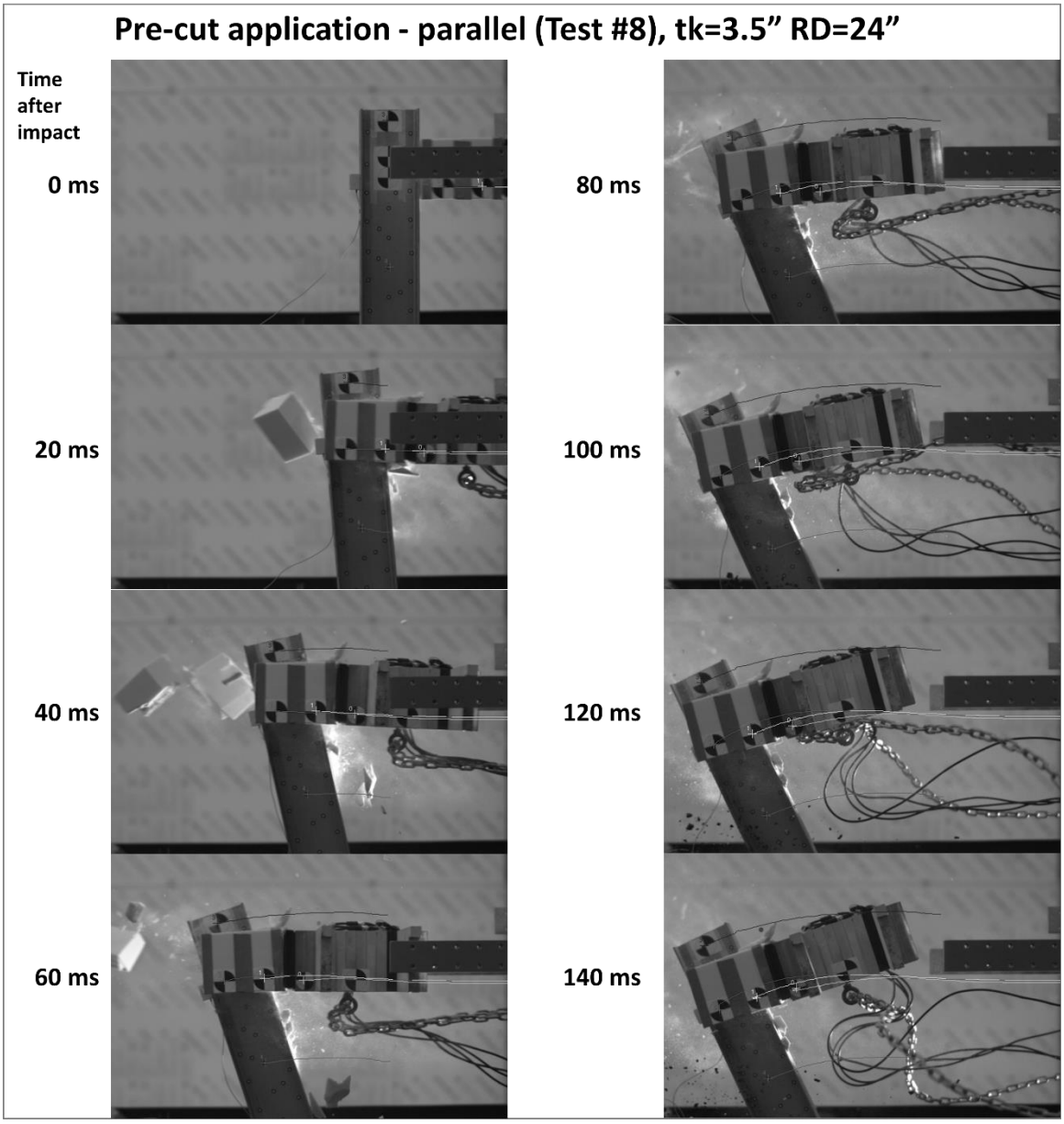

Figure 5.33 Pre-cut test (test #8): sequential photographs for post displacements

Acceleration curves from this test category are shown in Figure 5.34. Displacement measurements from high-speed images are plotted in Figure 5.35 and impact details based on the acceleration and displacement responses are shown in Table 5.6.

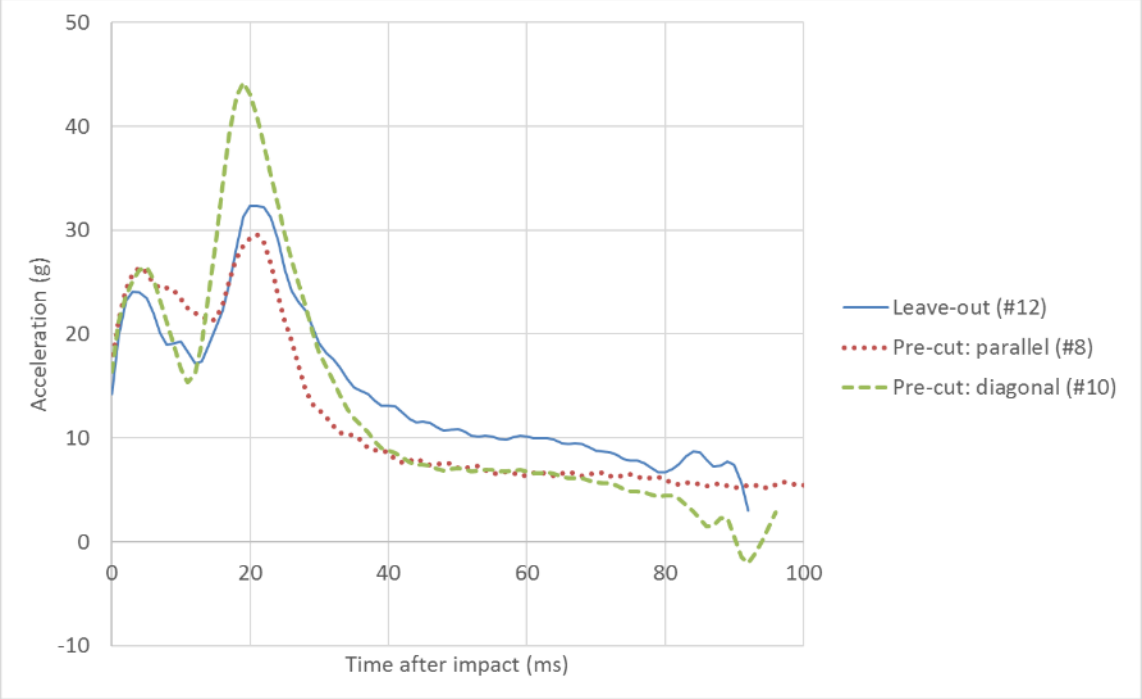

Figure 5.34 Treatment behind post tests: acceleration-time history

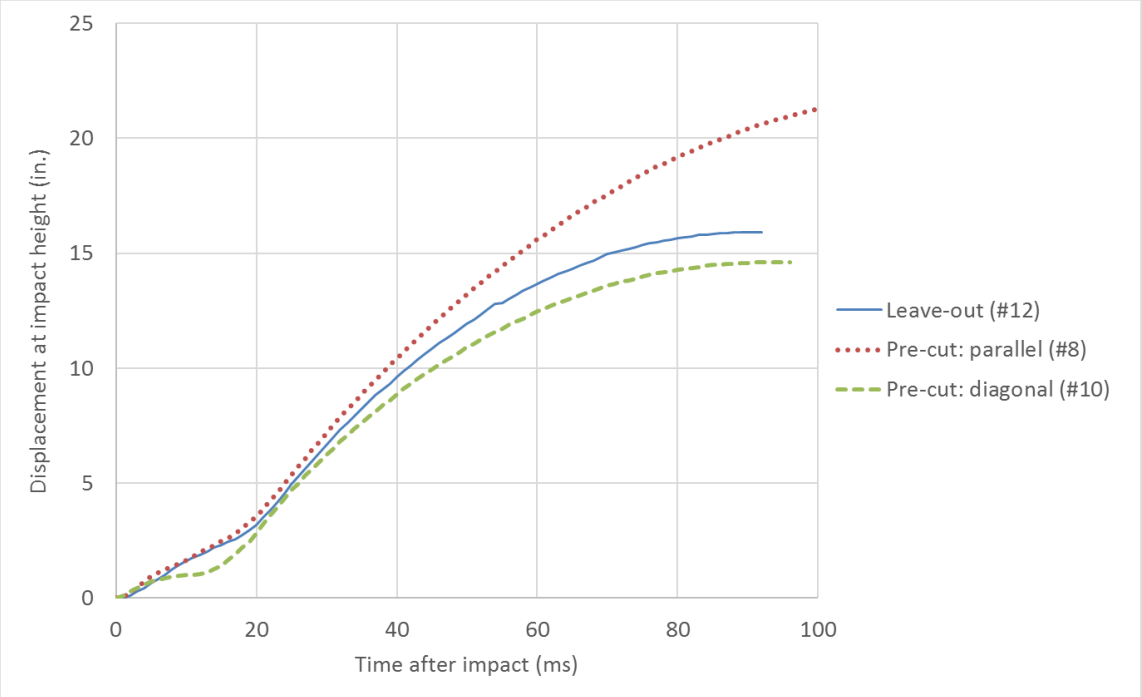

Figure 5.35 Treatment behind post tests: displacement-time history

Table 5.6 Treatment behind post tests: impact details

Test Configuration	Mow Strip Dimension		Peak accel. (g)	Time at peak accel.(ms)	Max. displ. (in.)	Time at max. displ. (ms)
	Thick.	RD				
Leave-out	3.5”	24”	32.4	21	15.91	92
Pre-cut (parallel)			29.6	21	22.00	123
Pre-cut (diagonal)			44.2	19	14.61	96

5.3.3 Tests with variation in dimension

In the variation in dimension test category, the thick mow strip test (#11) and the reduced rear distance test (#7) are addressed as a representative case of each geometric parameter. The thick mow strip test was conducted as the most restrained among all test configurations. The guardrail post could contain the flyer mass until its maximum dynamic displacement and pushed the flyer back to the rail. Figure 5.36 shows the sequential photographs of the thick mow strip test (#11). The maximum post displacement at the impact height was 10.45 in. at 81 ms after the initial impact and the post displacement at the ground-level was measured at 4.21 in. The acceleration response showed that the peak flyer acceleration of 53.5 g occurred at 18 ms and the acceleration rapidly decreased after the peak. Figure 5.37 shows the test setup (#11), the overall displacement of the post, and the deformation of the mow strip. The mow strip on the rear side was fractured by the impact and two distinct crack lines were formed from the rear side flange of the post. Due to excessive restraint by the mow strip, plastic deformation of the post near the ground level was clearly observed as shown in Figure 5.37(d).

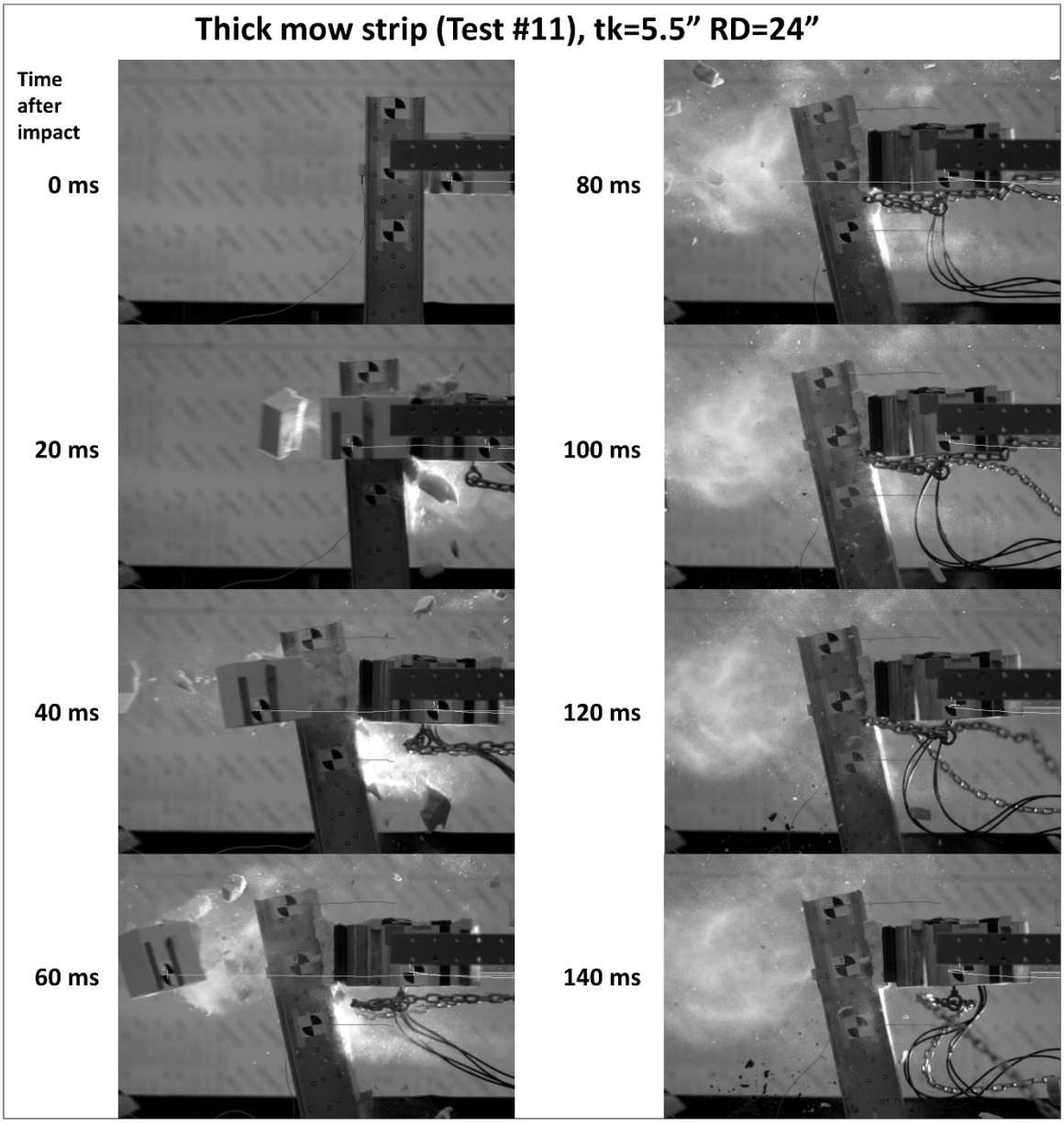

Figure 5.36 Thick mow strip test (test #11): sequential photographs for post displacements

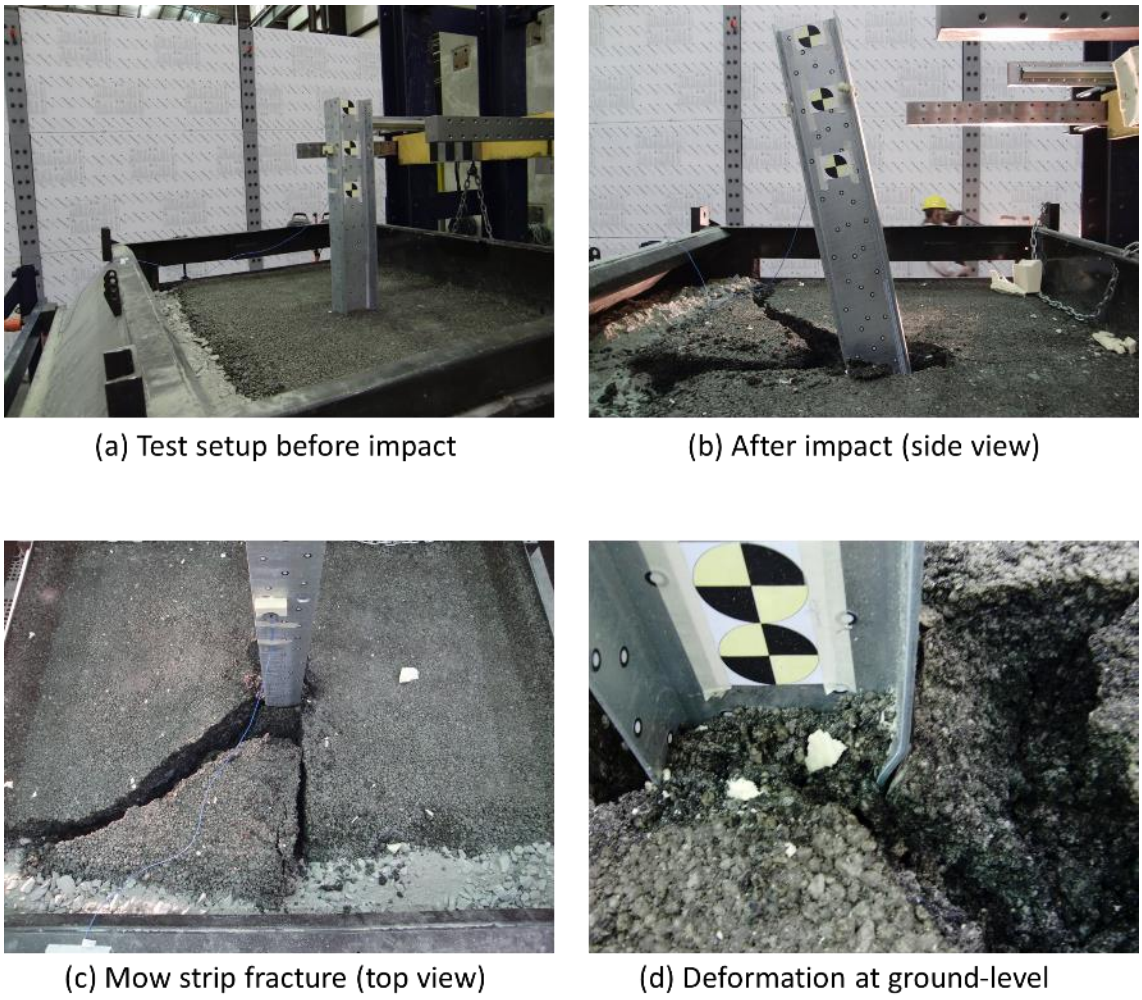

Figure 5.37 Thick mow strip test (test #11): overall damage after impact

In the reduced rear distance (RD) test, the post contained the flyer with a significant level of translation. Figure 5.38 shows the test setup (test #7), the overall displacement of the post, and the mow strip fracture. Apparently, the mow strip fracture shape in the reduced RD test did not involve major crack lines, which is a common fracture shape observed from the 24 in. wide mow strip tests. The rear side mow strip was scattered with small pieces by the impact which may indicate a lower level of ground-level

restraint due to the reduction of RD. Figure 5.39 shows the sequential photographs of test #7 from the high-speed camera. The maximum post displacement at the impact height was 25.81 in. at 131 ms after the impact and the ground-level displacement was measured at 11.73 in. The peak flyer acceleration of 26.6 g was recorded at 4 ms. and the acceleration slowly decreased after the peak while the flyer and the post were in contact.

(a) Test setup before impact

(b) After impact (side view)

(c) Mow strip fracture (top view)

(d) Deformation at ground-level

Figure 5.38 Reduced RD test (test #7): overall damage after impact

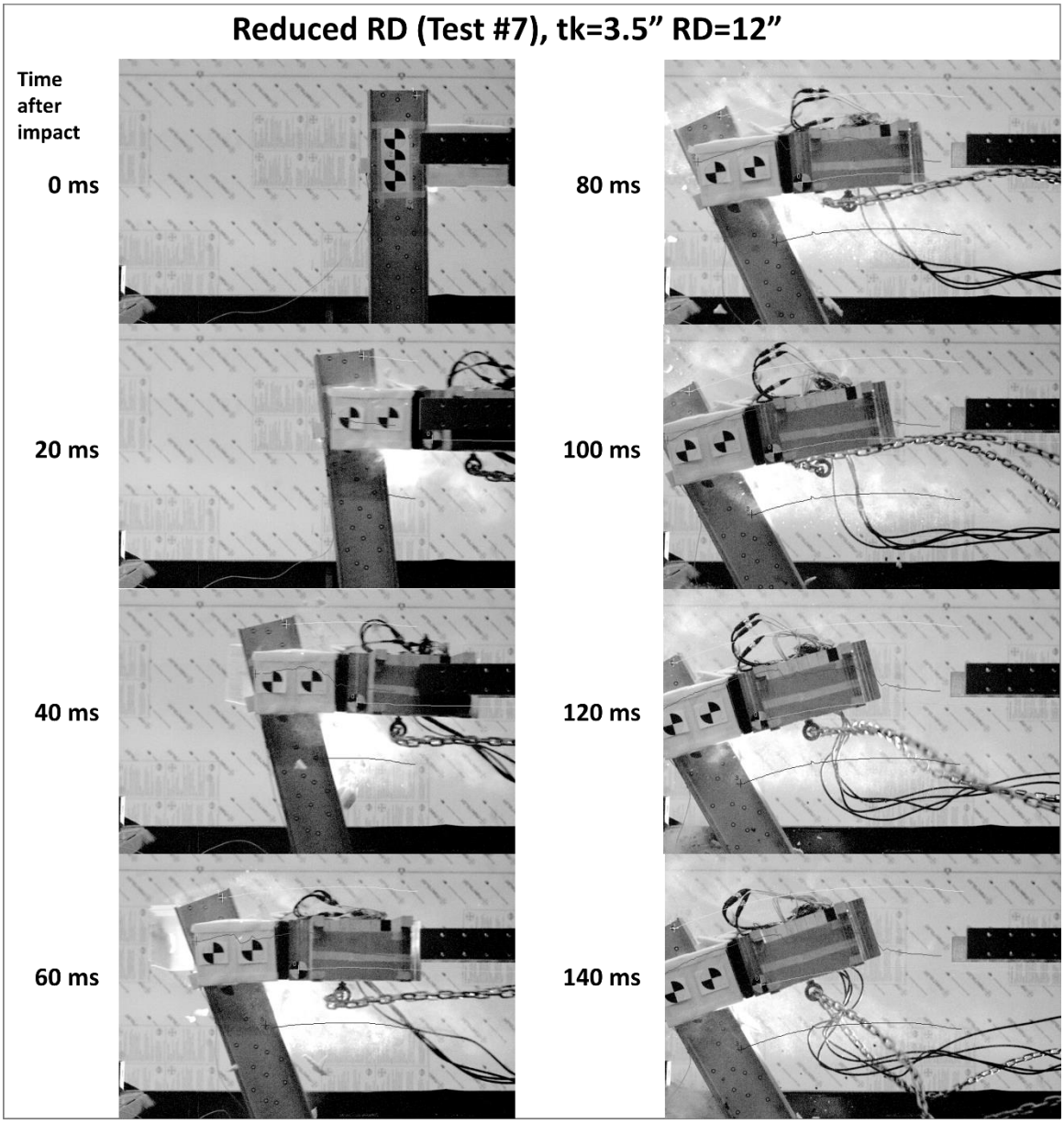

Figure 5.39 Reduced RD test (test #7): sequential photographs for post displacements

Acceleration curves from this test category are shown in Figure 5.40. Displacement measurements from high-speed images are plotted in Figure 5.41 and impact details based on the acceleration and displacement responses are shown in Table 5.7.

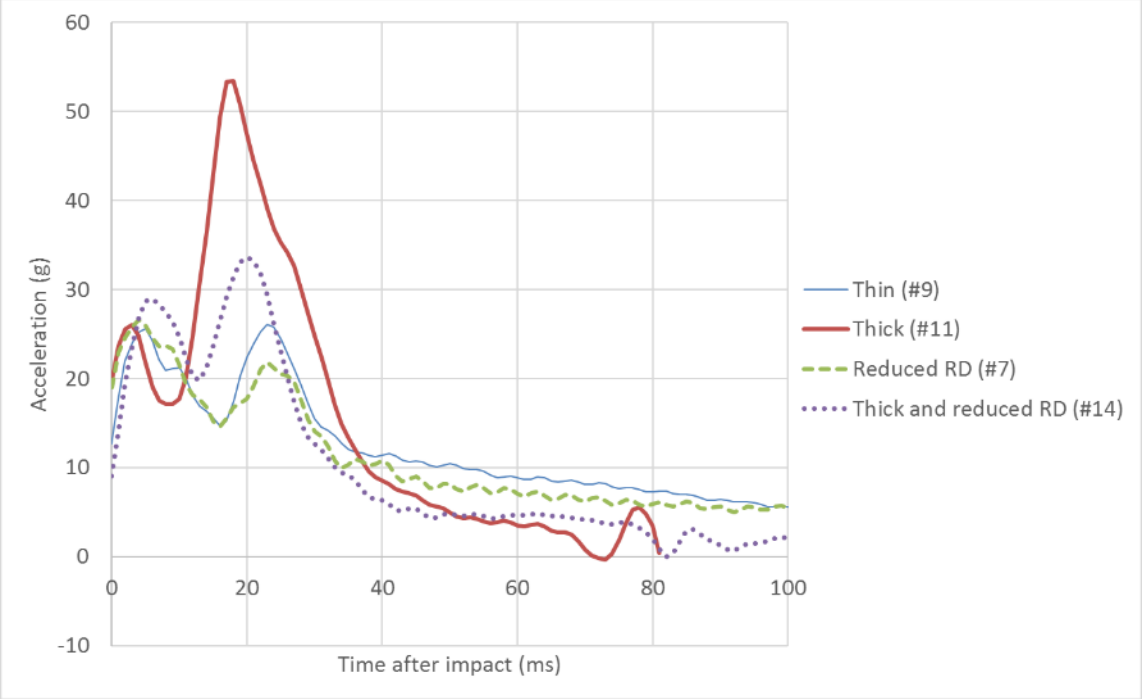

Figure 5.40 Variation in dimension tests: acceleration-time history

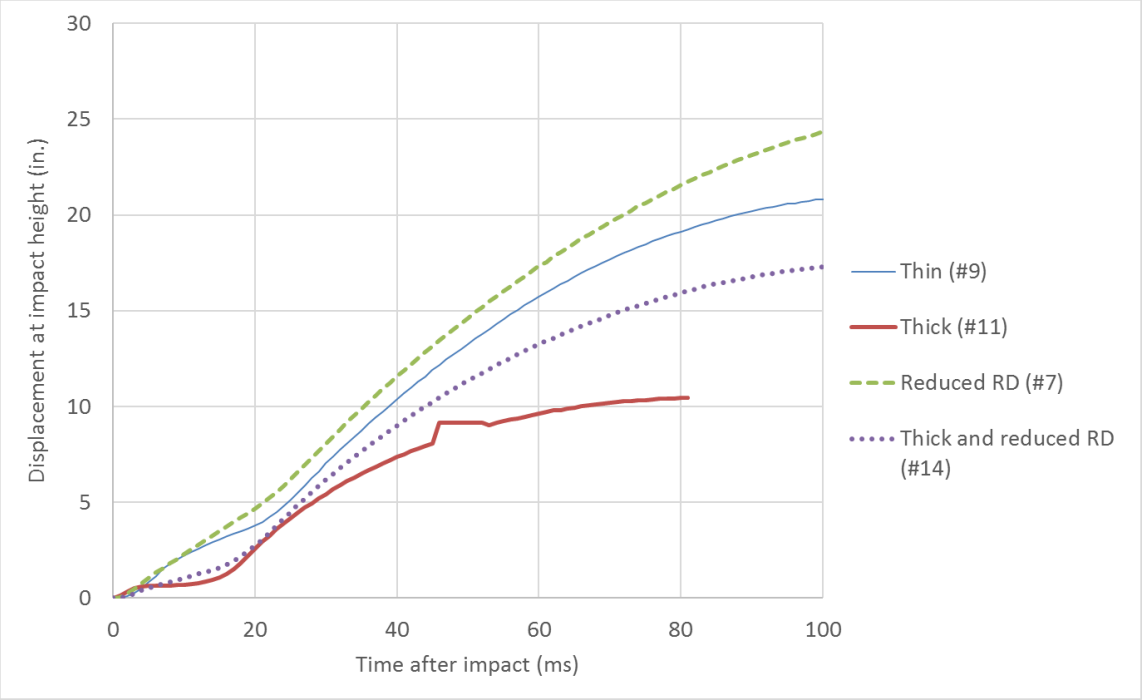

Figure 5.41 Variation in dimension tests: displacement-time history

Table 5.7 Variation in dimension tests: impact details

Test Configuration	Mow Strip Dimension		Test Number	Peak accel. (g)	Time at peak accel.(ms)	Max. displ. (in.)	Time at max. displ. (ms)
	Thick.	RD					
Thin	1.5”	24”	#9	26.1	23	21.08	112
Thick	5.5”	24”	#11	53.5	18	10.45	81
Reduced RD	3.5”	12”	#7	26.6	4	25.81	131
Thick and Reduced RD	5.5”	12”	#14	33.7	20	17.52	112

5.4 Performance assessment criteria for dynamic tests

In Section 3.4, a comprehensive discussion on the desirable performance of guardrail post was made based on the observations from prior guardrail studies and the statements in the *AASHTO Roadside Design Guide* (RDG). Guardrail posts in a typical guardrail system are required to rotate and translate under impact conditions. At the same time, the impacting vehicle needs to be contained by the guardrail system and decelerated in a controlled manner.

Based on this performance description, a total of four dynamic assessment criteria were selected to evaluate the influence of varying mow strip installations on the performance of the post: peak dynamic force, effective dynamic force, ground-level displacement, and impact-height displacement. Each criterion was selected to be a quantitative measure of ground-level restraint and informative/applicable to full-scale tests. These assessment criteria can be determined by using experimental data: accelerations and displacements.

Figure 5.42 illustrates a sequential progression of the dynamic impact test from the release of the flyer to the maximum displacement of the post. Acceleration, velocity, and displacement of each test component can be used to determine the state of the dynamic behavior and the relative stiffness of different mow strip configurations.

			Note
$t < 0$	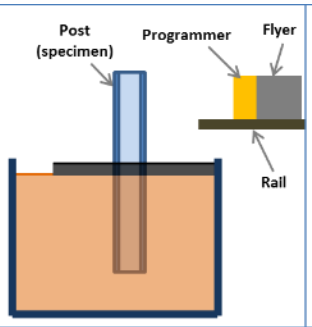	$v = v_{impact}$ $a_{flyer} = 0$ $a_{post} = 0$ $\Delta_{post} = 0$	The flyer is released from the hydraulic ram and traveling along the rail. Ideally, the velocity is constant and accelerations are zero
$t = 0^+$ *(impact)*	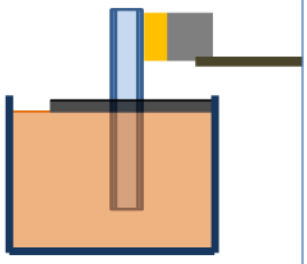	$v = v_{impact}$ $a_{flyer} < 0$ $a_{post} > 0$ $\Delta_{post} = 0$	The flyer impacts the post and load is applied through the transfer of momentum. The flyer and post accelerations occur in opposite direction. The programmer is undeformed.
$0 < t < t_{max}$	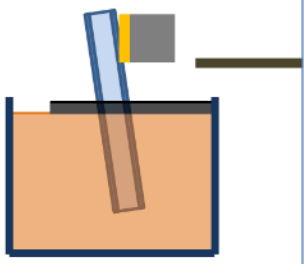	$0 < v < v_{impact}$ $a_{flyer} < 0$ $a_{post} > 0$ $0 < \Delta_{post} < \Delta_{max}$	The programmer is completely deformed by compression. The flyer is slowed down by the restraint of the embedded post. The post is translating and rotating by the kinetic energy of the flyer.
$t = t_{max}$ *(max. displ. of post)*	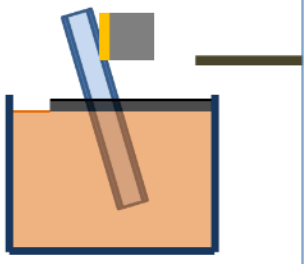	$v = 0$ $a_{flyer} < 0$ $a_{post} > 0$ $\Delta_{post} = \Delta_{max}$	The post reaches its maximum displacement and the velocity of flyer is zero. Both the flyer and the post are about to move reversely. Both accelerations are low but not zero.

Figure 5.42 Sequential progression of dynamic impact test and detailed descriptions

5.4.1 Peak dynamic force

In an impact condition, a dynamic load is generally difficult to measure using conventional load cells. Instead, the dynamic force, $F(t)$, can be estimated from the product of acceleration, $a(t)$, and mass, *m*, of the flyer using Newton's second law of motion:

$$F(t) = ma(t) \tag{5-5}$$

Because the mass of the flyer remains constant, higher dynamic force yields higher acceleration of the impacting vehicle. Therefore, lower peak dynamic force is a more desirable response when the same amount of kinetic energy/impulse is used.

5.4.2 Ground-level displacement

As a direct measure of ground-level restraint, the ground-level displacement can be estimated from the high-speed images focused on ground-level targets and their processing through motion tracking software. Since applied kinetic energy in this dynamic test program is controlled to be consistent (137.9 kip-in), a guardrail post which translates farther potentially has a greater chance of stopping an impacting vehicle in a safer fashion by dissipating its kinetic energy. Therefore, larger ground-level displacement indicates lower ground-level restraint. In this test program, residual ground-level displacements were used for comparison among the various mow strip installation methods tested.

5.4.3 Impact height displacement

The impact height displacement, usually referred to as "maximum dynamic displacement" or "dynamic crush", is a widely-used criterion for initial evaluation of guardrail systems [3] or vehicles in crash tests [81]. Generally, displacements at impact height have a strong correlation with the flexibility of the system. A stiffer guardrail system yields less dynamic deformation on the guardrail side but results in more deformation of the vehicle. The impact height displacement can be a simple but critical measure of the overall system response regardless of testing dimensions.

5.4.4 Effective dynamic force

An effective dynamic force, F_{eff} , can be defined as the average required force to displace the post up to a reference displacement, Δ^*. The effective dynamic force criterion represents a measure of the overall ground-level restraint of a post while being displaced to the reference point by an impact. This criterion can be written as shown in Equation (5-6):

$$F_{eff} = \frac{1}{\Delta^*}\int_0^{\Delta^*} F(t)d\Delta \tag{5-6}$$

where $F(t)$ is the dynamic force acting on the impact plane. The lower effective dynamic force, generally resulting from lower acceleration during the impact, indicates that a system has less ground-level restraint. When a series of dynamic tests are conducted under the same test protocol, a reference point can be designated as the maximum (or close to the maximum) dynamic displacement of the most restrained test

configuration – the minimum of the maximum dynamic displacement among all tests. This allows a user to evaluate the relative performance of all performed dynamic tests with the maximum amount of test measurement data. In this study, the reference point of 10-in. was selected for performance assessment, which is the closest smaller integer to the minimum of the maximum displacement 10.45 in. recorded in the test with the highest ground-level restraint (test #9: thick mow strip configuration).

5.5 Effect of mow strip design parameters

5.5.1 Summary of dynamic test results

In this section, mow strip design parameters are analyzed using the dynamic performance assessment criteria identified in Section 5.4. Table 5.8 gives a summary of the results from dynamic tests performed in the present work, including: (1) peak dynamic force, (2) effective dynamic force ($\Delta^* = 10$ in.), (3) impact height displacement, and (4) ground-level displacement. Results from tests performed using the leave-out (LO) configuration are designated as the "target performance value" for checking the relative efficiency of other tested alternative designs.

Table 5.8 Performance assessment criteria from dynamic tests

Test Configuration	Mow Strip Dimension		Dynamic forces (lb.)		Displacements (in.)	
	Thick.	RD	Peak	Effective	Impact height (maximum)	Ground-level (residual)
Baseline	0	0	8154	5066	23.11	10.83
Typical mow strip	3.5”	24”	12677	7269	13.71	5.12
Leave-out	3.5”	24”	***9650***	***6419***	***15.91***	***6.69***
Pre-cut (parallel)			8821	5760	22.00	9.49
Pre-cut (diagonal)			13181	7066	14.61	5.79
Thin	1.5”	24”	7771	5624	21.08	10.51
Thick	5.5”	24”	15931	7566	10.45	4.21
Reduced RD	3.5”	12”	7922	5122	25.81	11.73
Thick and Reduced RD	5.5”	12”	10030	5517	17.52	8.23

5.5.2 Effect of thickness

A total of five test configurations – consisting of the baseline, the leave-out, and three different mow strip thicknesses (thin: 1.5”, typical: 3.5”, and thick: 5.5”) – are selected for investigating the effect of mow strip thickness on relative restraint imparted by an asphalt layer. Figure 5.43 shows four assessment criteria with a strong linear trend between thickness and ground-level restraint. Under all four criteria, the target performance values (Leave-out: 3.5” thick mow strip with leave-out application) are located between the performance values of 1.5” and 3.5” thick mow strip configurations. The thin mow strip configuration (1.5”) shows lower peak and effective dynamic forces than the target but larger displacements at both the impact point and the ground-level.

Force-displacement curves can efficiently visualize relative ground-level restraint. The curves can be drawn from the combination of the acceleration-time and displacement-time history curves shown in Section 5.2. Figure 5.44 displays the force-displacement curves of the five test configurations. It can be seen that the most restrained configuration is 5.5" and the leave-out has more restraint than the 1.5" but less than the 3.5" mow strip thicknesses. The results presented here indicate that the leave-out mow strip configuration may not result in significantly less ground-level restraint than a 1.5" thick mow strip configuration under all four assessment criteria. The limited data appear to indicate that a mow strip thickness of approximately 2.7" would exhibit roughly equivalent performance to the leave-out; this of course cannot be definitively asserted without more test repetitions.

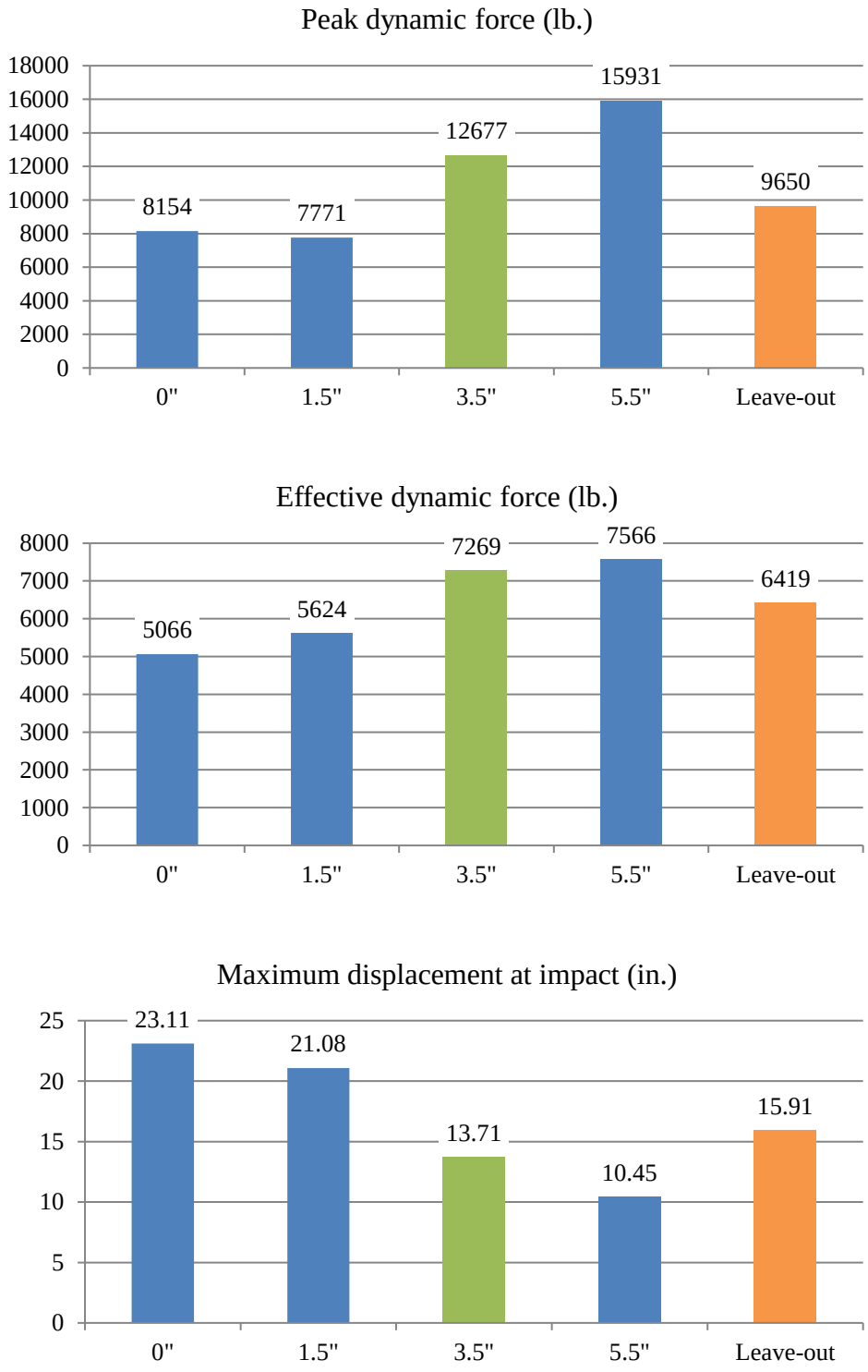

Note: RD=24” constant

Figure 5.43 Assessment criteria: effect of thickness

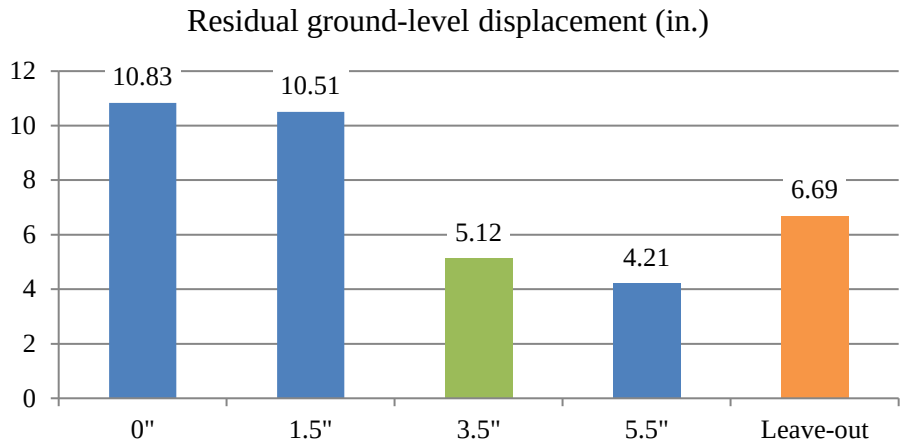

Note: RD=24” constant

Figure 5.43 (continued).

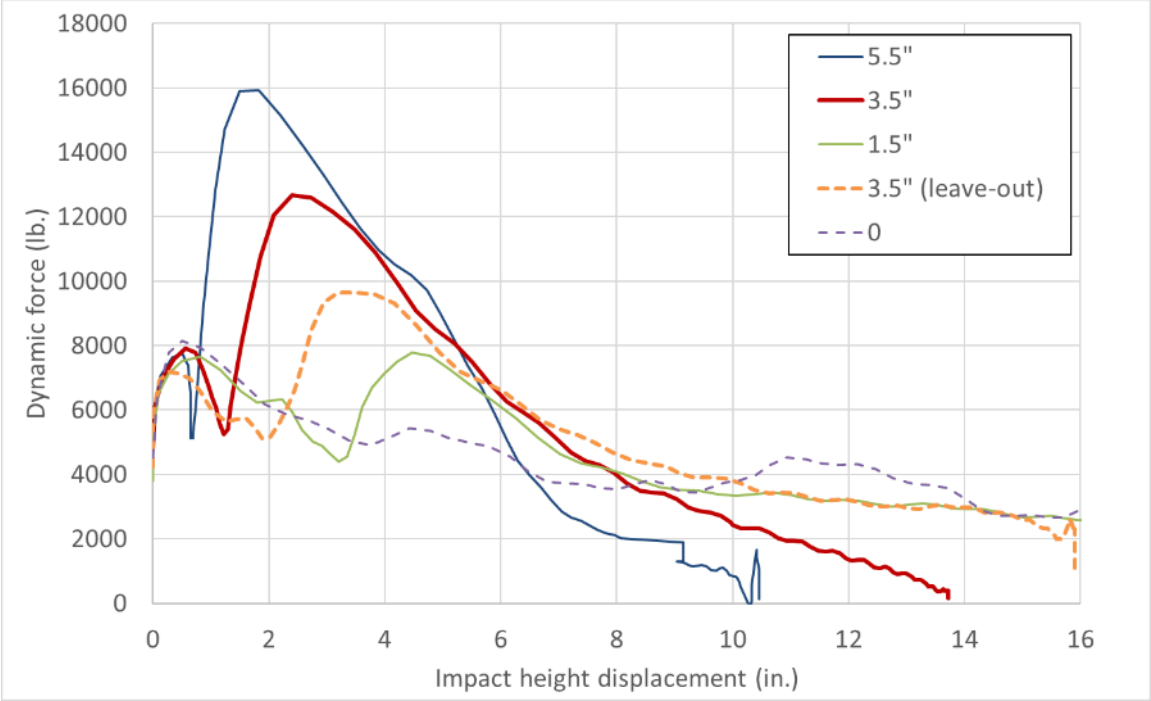

Figure 5.44 Force-displacement curves: effect of thickness

5.5.3 Effect of rear distance

A total of five test configurations are chosen for investigating the effect of mow strip rear distance (RD). Two reduced RD (RD=12") tests are paired with the typical RD tests (RD=24") for two thicknesses (typical: 3.5" and thick: 5.5") and the leave-out test is included as the target performance value. The effect of rear distance is also very significant in terms of its influence on ground-level restraint. Figure 5.45 shows four assessment criteria and a strong linear correlation between rear distance and ground-level restraint for the two mow strip thicknesses (3.5" and 5.5"). It is shown that the rear distance reduction by 12" improves the performance under all four criteria: (1) peak dynamic force decreased by 37%, (2) effective dynamic force decreased by 28%, (3) maximum displacement at impact increased by 44%, and (4) residual ground-level displacement increased by 53%. Specifically, the 5.5" thick and reduced RD configuration shows lower peak and effective dynamic forces than the target (leave-out) but larger displacements at both the impact point and the ground-level. Dynamic force-displacement curves shown in Figure 5.46 also exhibit this correlation. It can be seen that the least restrained configuration is the reduced RD (with 3.5" thick mow strip) and the thick and reduced RD configuration (with 5.5" thick mow strip) has similar or slightly less level of the restraint compared to the leave-out. The results presented here indicate that the leave-out mow strip configuration may not result in significantly less ground-level restraint than a 12" wide mow strip configuration under all four assessment criteria.

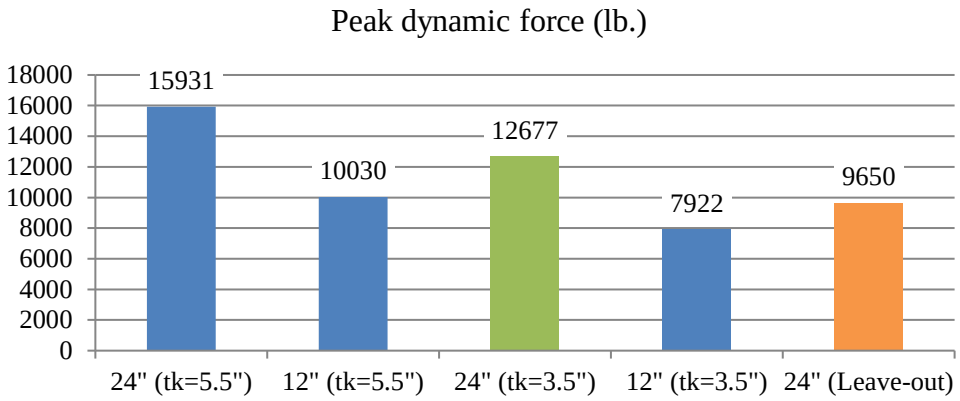

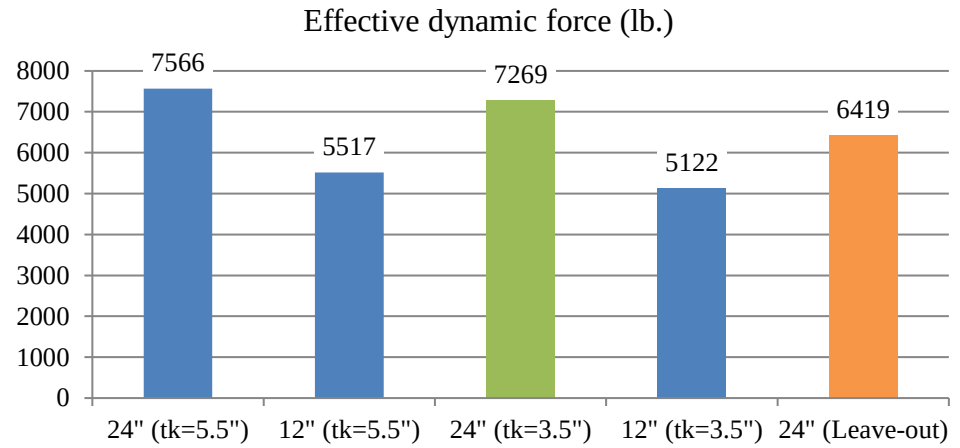

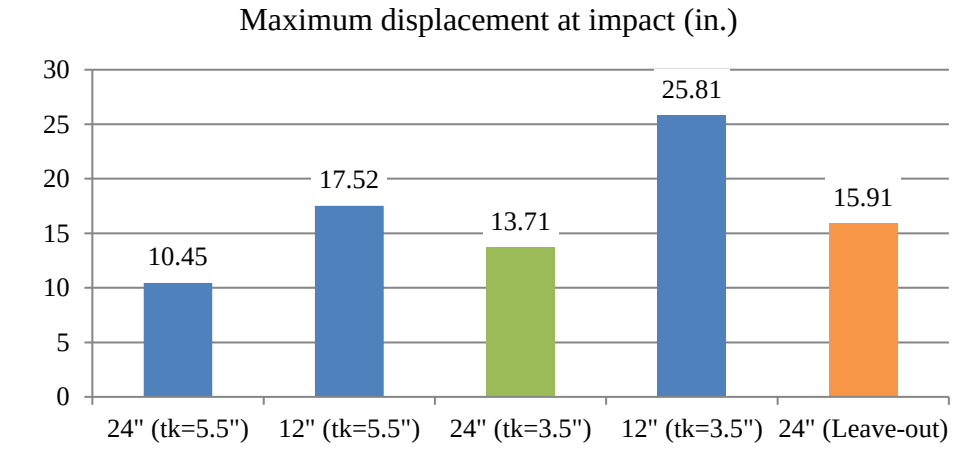

Note: tk: mow strip thickness

Figure 5.45 Assessment criteria: effect of rear distance

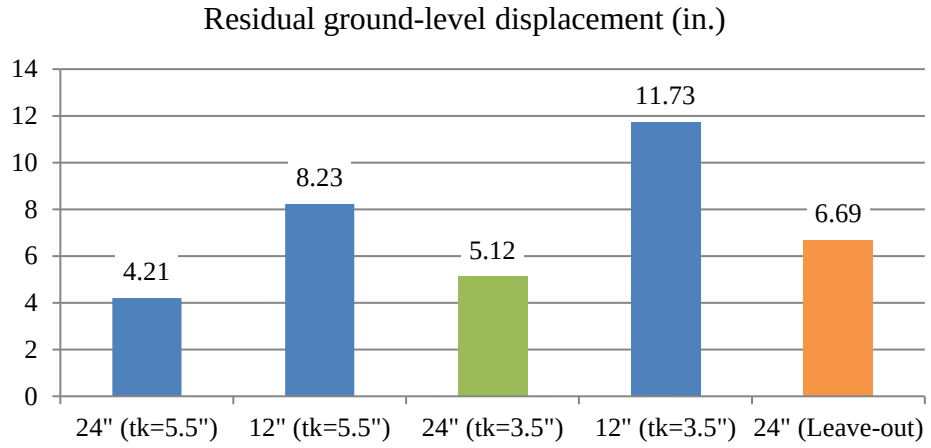

Note: tk: mow strip thickness

Figure 5.45 (continued).

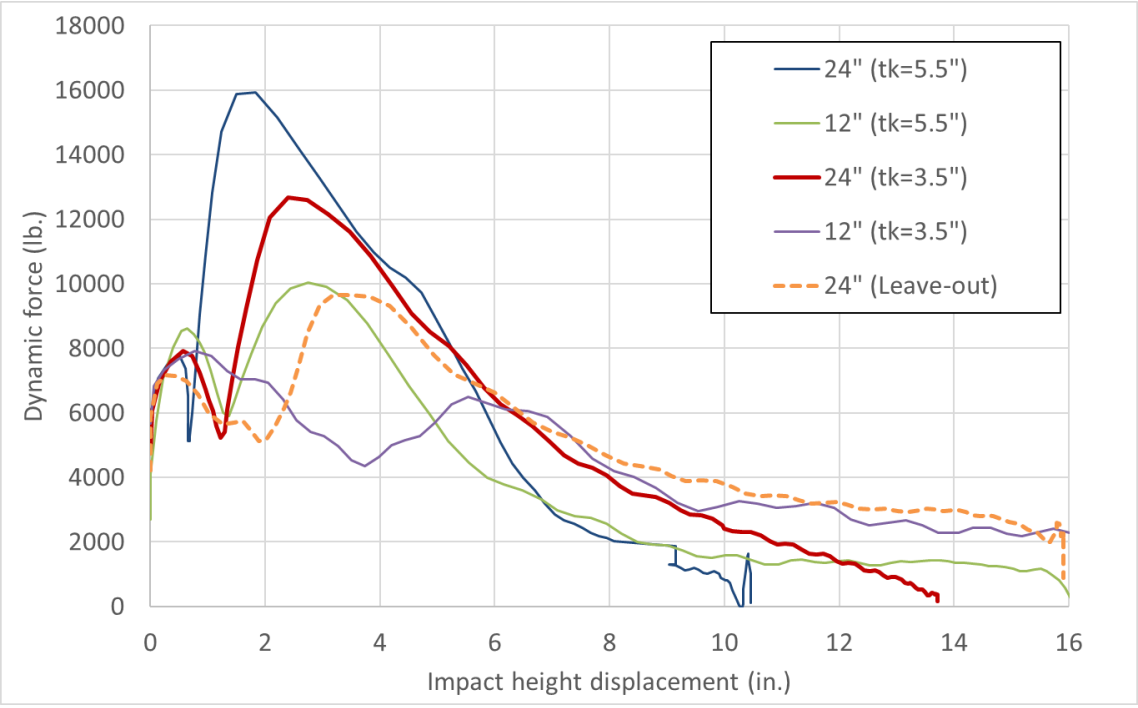

Figure 5.46 Force-displacement curves: effect of rear distance

5.5.4 Effect of pre-cutting

A total of four test configurations are selected for investigating the effect of pre-cutting. The typical mow strip (t_k=3.5, RD=24”), the leave-out, and two pre-cut configurations are compared under the performance assessment criteria to check if pre-cutting can be an effective solution for existing mow strips with excessive ground-level restraint. Figure 5.47 shows four assessment criteria and Figure 5.48 shows the dynamic force-displacement curves. The parallel pre-cut application significantly improves the performance under all four criteria: (1) peak dynamic force decreased by 30%, (2) effective dynamic force decreased by 21%, (3) maximum displacement at impact increased by 38%, and (4) residual ground-level displacement increased by 46%. The diagonal pre-cut application also improves the performance but not as effectively as the parallel pre-cut: (1) peak dynamic force increased by 4%, (2) effective dynamic force decreased by 3%, (3) maximum displacement at impact increased by 6%, and (4) residual ground-level displacement increased by 12%. As mentioned earlier, these results of course cannot be definitively asserted without more test repetitions.

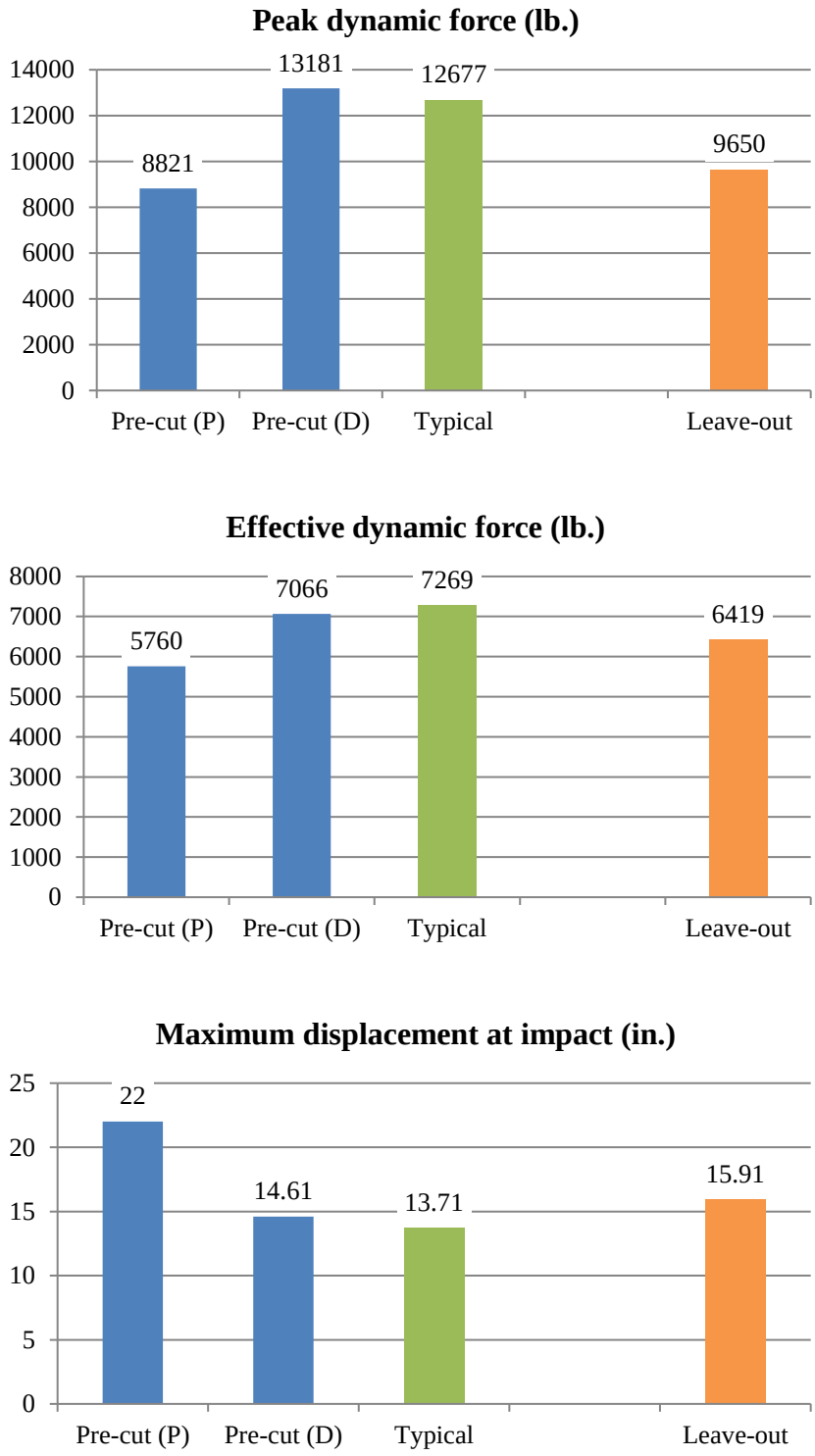

Note: mow strip thickness 3.5” / rear distance 24” (constant)

Figure 5.47 Assessment criteria: effect of pre-cut

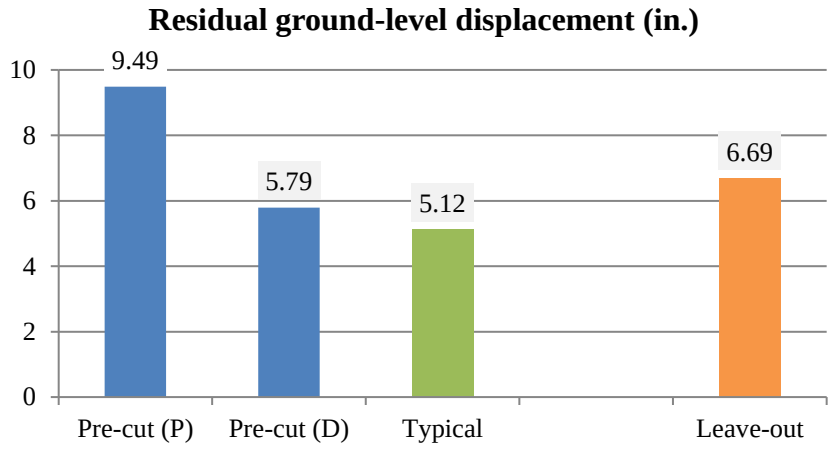

Note: mow strip thickness 3.5” / rear distance 24” (constant)

Figure 5.47 (continued).

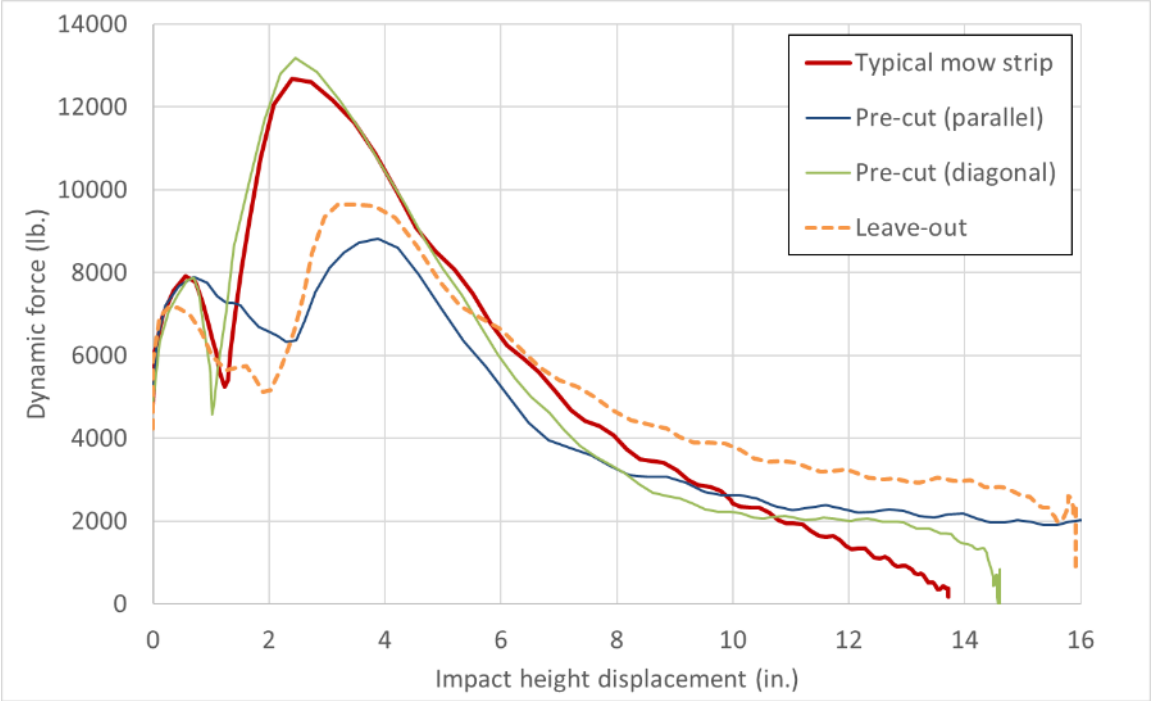

Figure 5.48 Force-displacement curves: effect of pre-cut

5.5.5 Performance ranking for various mow strip designs

Each dynamic performance criterion represents a quantitative measure of ground-level restraint, and it is possible to rank various mow strip designs under these criteria. Because all dynamic tests were conducted with little variation in soil and asphalt conditions compared to those in the static tests, a performance ranking based on the dynamic test results can be informative for planning full-scale crash tests. Table 5.9 shows the individual and overall performance ranking of various mow strip designs. The reduced RD configuration is determined to have the least amount of the ground-level restraint. The thin, the parallel pre-cut, and the thick and reduced RD configurations are determined to have less restraint than the leave-out configuration.

Table 5.9 Performance ranking for various mow strip designs

Test Configuration	Individual ranking				Overall ranking
	Peak dynamic force	Effective dynamic force	Max. displ. at impact height	Residual ground-level displ.	
Typical mow strip	6	7	7	7	7
Leave-out	*4*	*5*	*5*	*5*	*5*
Pre-cut (parallel)	3	4	2	3	3
Pre-cut (diagonal)	7	6	6	6	6
Thin	**1**	3	3	2	2
Thick	**8**	**8**	**8**	**8**	**8**
Reduced RD	2	**1**	**1**	**1**	**1**
Thick and Reduced RD	5	2	4	4	4

Note: 1= lowest, 8= highest ground-level restraint

5.6 Summary

This chapter introduced a new dynamic subcomponent test protocol for testing guardrail systems using a high-speed hydraulic actuator. A total of 14 dynamic impact tests were conducted based on the protocol and the test results were utilized in the performance assessment of guardrail posts embedded in various type of asphalt layers. The performance assessment using relevant quantitative criteria and dynamic test results demonstrated that either reducing specific geometric parameters of the mow strip compared to the typical configuration or the application of pre-cutting can reduce potential excessive restraint by the mow strip.

CHAPTER 6
PERFORMANCE EVALUATION USING EMPIRICAL ANALYSIS MODEL

6.1 Overview

In the present work, the performance of guardrail posts installed in asphalt mow strips are evaluated based on: (1) subcomponent test results, (2) asphalt specimen test results, and (3) calibrated empirical analysis models. Figure 6.1 illustrates the three-stage performance evaluation procedure to develop an example of mow strip design guideline. Chapters 3, 4 and 5 detail the experimental program undertaken in the present work, and the results of this investigation. The experimental program obviously could not include all existing mow strip design variations in geometry and material properties. As such, this chapter presents the development of a semi-empirical analysis model to assess a broader range of design combinations.

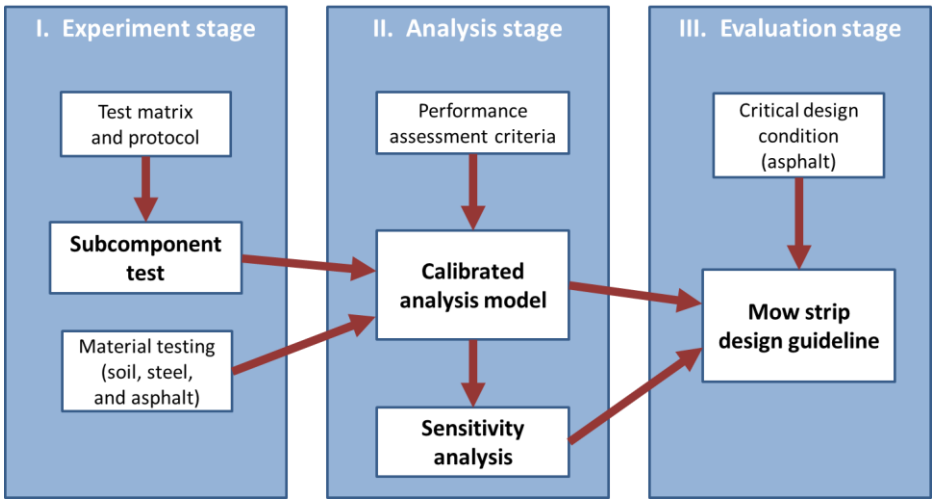

Figure 6.1 Performance evaluation procedure for mow strip design and evaluation

The analysis model is constructed to predict how a design change affects relative ground-level restraint and structural performance based on predetermined performance evaluation criteria. This model is used to perform sensitivity analyses on major design parameters to assess their influence on the performance of the post embedded in an asphalt layer.

In the evaluation stage, a generalized method for mow strip design is discussed which can be used not only in a few specific design cases but could also be applicable to a broader range of design conditions. The variation in asphalt compressive and shear strength, influenced by environmental factors (e.g., temperature, age) is addressed and the critical design condition is specified for developing design guidelines. The design guidelines/criteria are presented as a series of contour plots, which enables a user to select more than one mow strip alternative demonstrating effective static and dynamic structural performance of guardrail posts.

6.2 Development of empirical analysis model

6.2.1 Model description

A simplified analysis model consisting of a beam and springs can be used to represent a guardrail post embedded in a mow strip. As shown in Figure 6.2, the embedded soil and the asphalt layer around the guardrail post can be modeled with a series of discrete non-linear springs with varying stiffnesses in both the y- (lateral) and z- (depth) directions. The model, written in MATLAB©, is developed to perform a monotonic

pushover analysis which yields a load-deflection (p-y) relation, bending moment distribution, and the deflected shape of the post. The static equilibrium and energy conservation conditions are checked throughout the post deflection. For the calibration of model parameters, the material properties and geometric configuration of the guardrail subcomponent system described in Chapters 4 and 5 were adopted. The lateral resistance/stiffness of the soil (k_s) and the asphalt mow strip (k_a) were modeled separately using two distinct constitutive relationships. The inclusion of pertinent section and material properties of the steel post allows the model to predict the formation of a plastic hinge at the maximum bending moment location as well as the overall deformation of the post.

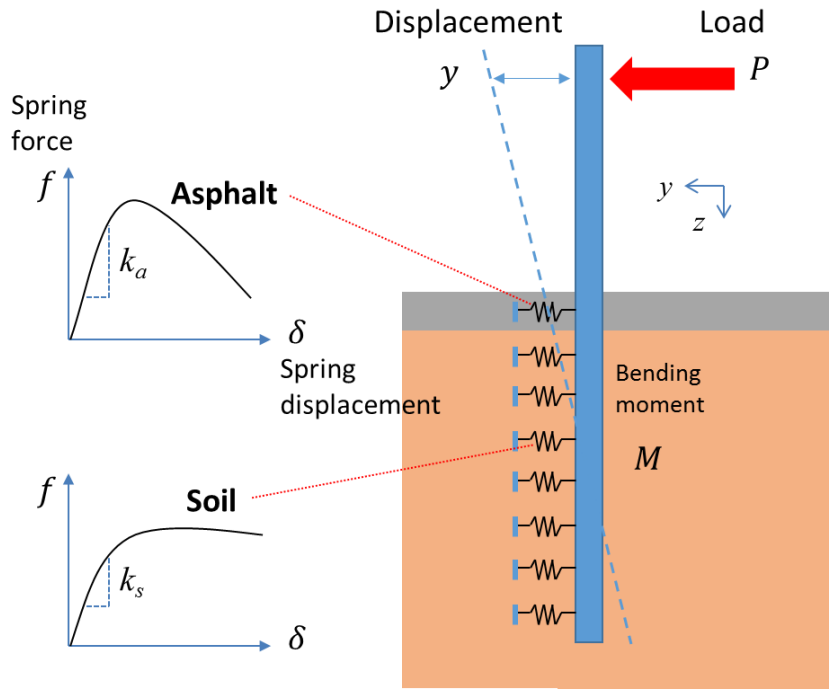

Figure 6.2 Schematic illustration of the two-dimensional analysis model

The model is developed based on static material properties; as such, it is limited to the static analysis as developed. However, a user can extend this model using dynamic material properties and constitutive relationships (to include rate dependence) if they are determined with reasonable accuracy. Details on these model features are discussed in the following sections.

6.2.2 Method of analysis

Step 1

First, a displacement profile of the beam is determined to satisfy the static equilibrium condition. If elastic bending of the beam is not considered in this step, displacements (δ_i) at all spring locations ($i = 1, 2, \ldots, N$) can be computed by assuming a small displacement at the loading height (y) and slope of the beam as shown in Figure 6.3.

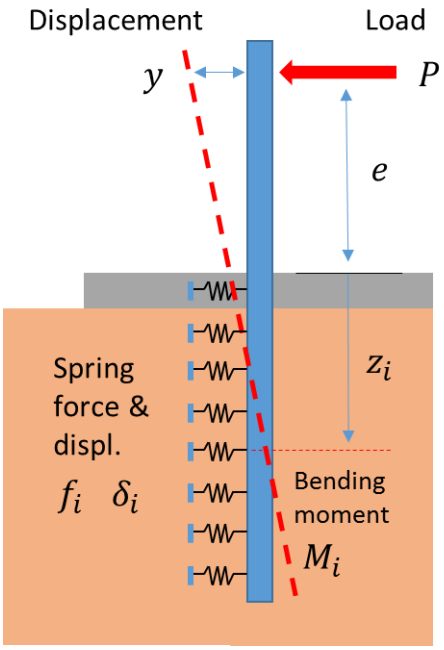

Figure 6.3 Analysis model before plastic hinge formation

All spring forces (f_i) are calculated by constitutive relationships of the soil and asphalt layers which will be discussed in later sections. The sum of all spring forces must be equal to the applied load (*P*) in this system for static equilibrium. Also, a bending moment profile (M_i) along the entire beam can be obtained from the spring force distribution. These relationships are expressed in Equations (6-1) and (6-2):

$$P - \sum_{i=1}^{N} f_i = 0 \tag{6-1}$$

$$\sum_{i=1}^{N} f_i(e + z_i) = 0 \tag{6-2}$$

where *e* is the eccentricity of loading (loading height) and z_i is the depth of the spring. The loading height displacement can be increased step by step and the analysis can be repeated as needed.

Step 2

In this step, an updated displacement/flexure profile of the beam is determined using an energy conservation relationship. For each displacement increment, the amount of the total strain energy in the system shall be equal to the amount of work done by the applied load *P*. This relationship can be written as Equation (6-3):

$$P \cdot y = \sum_{i=1}^{N} f_i \, \delta_i + \int_{beam} M\kappa \, dz \tag{6-3}$$

where y = displacement at the loading point, *M* = bending moment, and κ = curvature of the beam. In Equation (6-3), the left-hand side denotes the work done by lateral load and the right-hand side denotes the sum of strain energy consisting of the strain energy stored in the lateral springs (both soil and asphalt) by compression and the beam (guardrail post)

by flexure. The external work done and the strain energy in the springs can be computed by multiplying the load by the corresponding displacement. The strain energy of the beam can be calculated from the integration of the bending moment versus curvature profiles along the beam. This elastic analysis method is assumed valid until the maximum bending moment reaches the specified yield moment (M_y) of the beam section.

Step 3

In this step, a plastic deformation of the beam is computed if necessary. When the maximum bending moment in the steel beam exceeds the elastic limit, the maximum moment is likely to occur at the asphalt mow strip, a relatively stiff layer compared to the soil layers. In the present work, the location of the plastic hinge is assumed to be concentrated near the ground level where the bending moment is maximized. Figure 6.4 illustrates the schematic diagram of analysis model after plastic hinge formation.

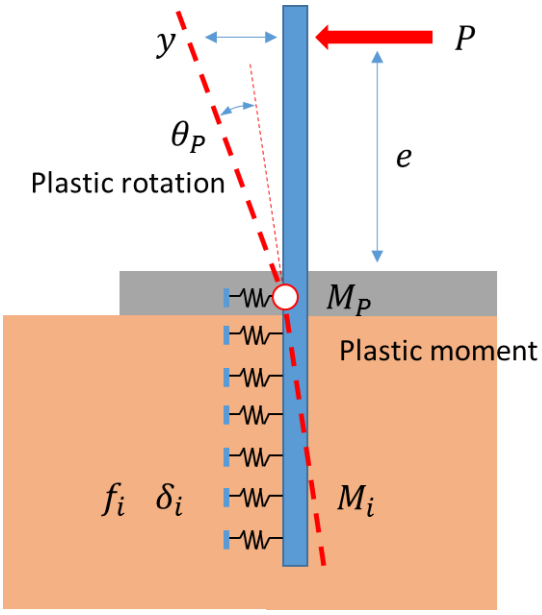

Figure 6.4 Analysis model including plastic hinge formation

A generalized bilinear moment-rotation relation for the plastic behavior of the steel post can be specified as shown in Figure 6.5. The rotation of the post is set proportional to the bending moment until reaching the yield moment M_y. After yield, the plastic bending will continue until the rotation reaches the plastic rotation θ_P. The magnitude of the plastic rotation can be assumed as a multiple of the yield rotation θ_y using the plastic amplification factor α. The yield rotation θ_y is calculated based on the assumption that the beam would behave as a cantilever beam when a stiff layer at the ground level restrains the rigid body translation/rotation of the post. This can be expressed as shown in Equation (6-4):

$$\theta_y = \frac{M_y e}{3EI} \tag{6-4}$$

where E = Young's modulus of steel, I = section moment of inertia, M_y = yield moment of the steel section, and e = eccentricity of load.

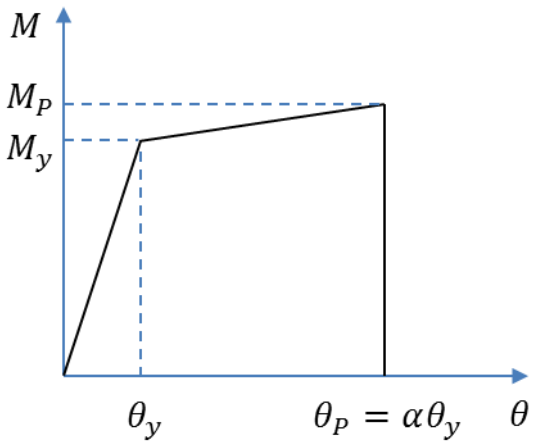

Figure 6.5 Plastic moment-rotation relation for static analysis model

At present, there is no specific methodology for selecting the amplification factor for this type of pushover analysis including a guardrail post. However, as a reference, the PreStandard and Commentary for the Seismic Rehabilitation of Buildings (FEMA 356) [82] permits using the factor $\alpha = 4$ if a wide-flange section satisfies the flange or web slenderness criteria as shown in Equation (6-6):

$$\theta_P = 4\theta_y \tag{6-5}$$

$$\frac{b_f}{2t_f} \geq \frac{65}{\sqrt{\sigma_y}} \quad or \quad \frac{h}{t_w} \geq \frac{640}{\sqrt{\sigma_y}} \tag{6-6}$$

where b_f = flange width, t_f = flange thickness, h = section height, t_w = web thickness, and σ_y = yield strength of steel.

The plastic moment-rotation relationship (Figure 6.5) used in the analysis model assumes the plastic rotation (θ_P) as a limit state for the steel post where the moment capacity of the post section becomes zero at the plastic hinge location. The pushover analysis is terminated at this limit state because the post is assumed no longer able to support a lateral load and thus becomes unstable. In real-world crash events, a steel post would experience lateral torsional buckling in addition to hinging at the ground-line, which is a commonly observed failure mode of steel post in roadside crash sites as shown in Figure 6.6. Since this type of post failure mode is considered undesirable for guardrail systems, it is reasonable to terminate the analysis at the plastic rotation and neglect the after-plastic rotation capacity of the steel post.

Figure 6.6 Buckled steel post installed with mow strip after a vehicle impact

6.2.3 Soil lateral resistance modeling

The p-y curve method considering nonlinear soil response is a widely-used method in the design of laterally-loaded piles. In particular, the p-y curve suggested by the Recommended Practice of the American Petroleum Institute (API) [83] is one of the most widely-used methods and has been justified by numerous field and laboratory experiments [84]. This recommendation contains possible loading cases and analysis models for embedded piles with various soil types. Lateral soil resistance deflection (p-y) relationships of laterally-loaded piles are most relevant to the tested guardrail system under static loading. Based on the *MASH* compliant soil condition specified in Chapter 3, a lateral soil resistance deflection (p-y) curve of laterally-loaded piles for sand (cohesionless soil) proposed by O'Neill and Murchinson [85] can be adopted. The ultimate lateral bearing capacity p_u for sand may be determined using Equation (6-7):

$$p_u = min[(c_1 H + c_2 D)\gamma H\ , c_3 D\gamma H] \qquad (6\text{-}7)$$

where γ is the effective soil weight, H is the depth, D is the size factor of the pile, and c_1, c_2, c_3 are coefficients determined from Figure 6.7 as function of ϕ_s, which is the angle of internal friction of the soil.

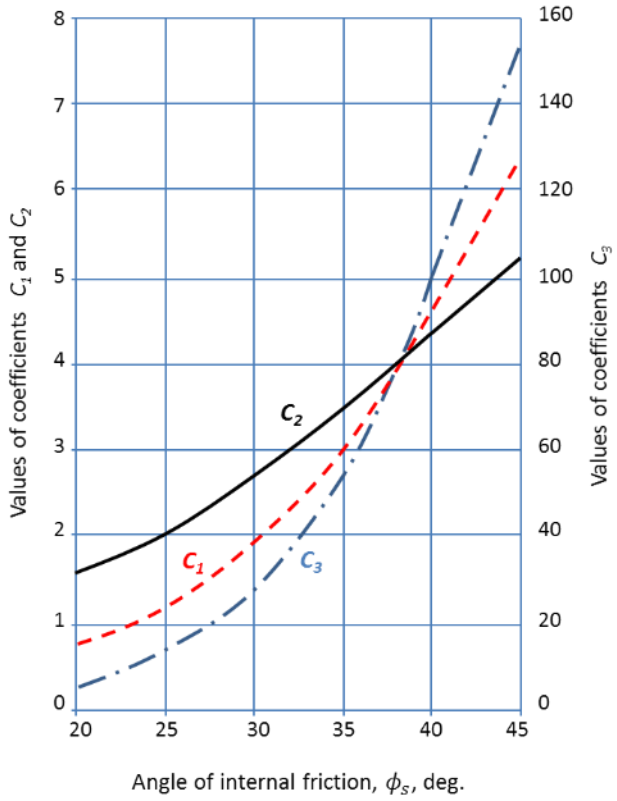

Figure 6.7 Coefficients as function of internal friction angle (after [83])

The lateral load-displacement (p-y) relationship can be approximated as a hyperbolic tangent nonlinear curve. When a depth H and a lateral displacement y is specified, the resulting load p can be calculated using Equations (6-8) and (6-9):

$$p = Ap_u tanh\left(\frac{kHy}{Ap_u}\right) \tag{6-8}$$

$$A = min\left[\left(3.0 - 0.8\frac{H}{D}\right), 0.9\right] \tag{6-9}$$

where A is a dimensionless factor for the static loading condition and k is the initial modulus of subgrade reaction which is determined from Figure 6.8 as function of the angle of internal friction, ϕ_s.

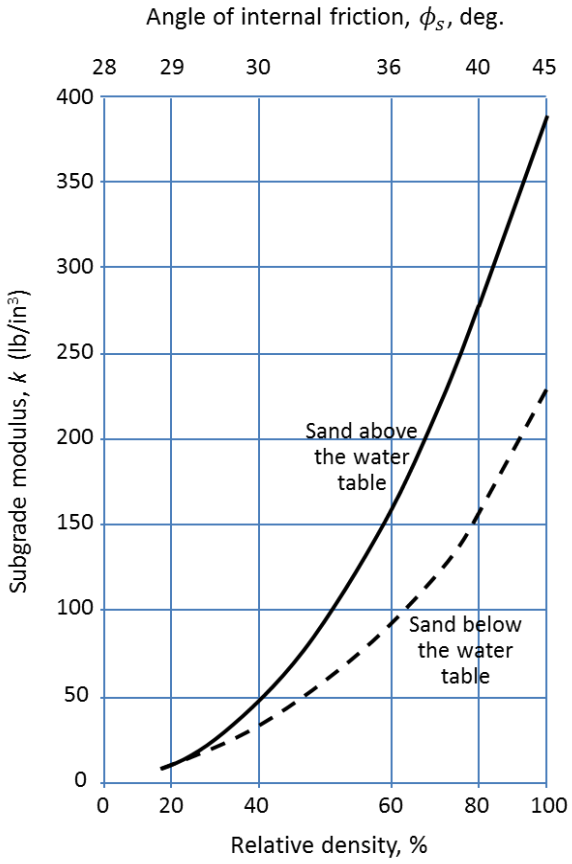

Figure 6.8 Modulus of subgrade reaction plot after [83]

6.2.4 Asphalt lateral resistance modeling

As discussed in Chapter 4, the expected load on a pavement layer can be classified into two categories: (1) punching-shear load, and (2) in-plane shear load. The punching shear load typically results from axle loads by traffic which most designers consider in roadway pavement design. The magnitude of this type of loading is usually within the elastic range. However, in-plane shear loads on the asphalt layer are typically not considered in pavement design. When a lateral load is applied to the mow strip and a guardrail post is assumed to be rigid, a significant shear crack will appear and propagate. The lateral load capacity of the mow strip diminishes after the first crack formation (rupture) and goes to zero when the rear part of the mow strip becomes detached from the main body of the asphalt layer.

An empirical constitutive model of load-displacement is adopted in the development of the model in the present work. Bakhtiary [12] proposed an empirical nonlinear spring model for the lateral restraint of the asphalt layer, calibrated based on previous experimental research presented in Lee et al. [86] The spring force-displacement (f- δ) model is expressed with the following equations:

$$f = \left[-\left(\frac{\delta}{\delta_1}\right)^2 + 2\frac{\delta}{\delta_1}\right] f_{max} \qquad \delta \leq \delta_1 \tag{6-10a}$$

$$f = \frac{(\delta_2 - \delta) f_{max}}{(\delta_2 - \delta_1)} \qquad \delta_1 < \delta < \delta_2 \tag{6-10b}$$

$$f = 0 \qquad \delta \geq \delta_2 \tag{6-10c}$$

where δ_1 is the lateral displacement at which the maximum (peak) force f_{max} occurs, and δ_2 is the lateral displacement at which the asphalt layer no longer provides any lateral resistance. These parameters can be expressed with the following predictive equations [12]:

$$f_{max} = C\,(r+h)(2.87 - 0.025\,\phi_a) \tag{6-11}$$

$$\delta_1 = 53.62\frac{C}{G} \tag{6-12}$$

$$\delta_2 = \delta_1 + 15.12\,\frac{C\,(r+h)}{G} \tag{6-13}$$

where r is the rear distance, h is the depth of post cross section, C is the cohesion of asphalt, ϕ_a is the friction angle of asphalt (in degree), and G is the shear modulus of asphalt. Figure 6.9 shows a representative curve from Equation (6-10) with given parameters of C = 72.5 psi, ϕ_a = 35 deg., G = 7250 psi, r = 24 in., and h = 6 in.

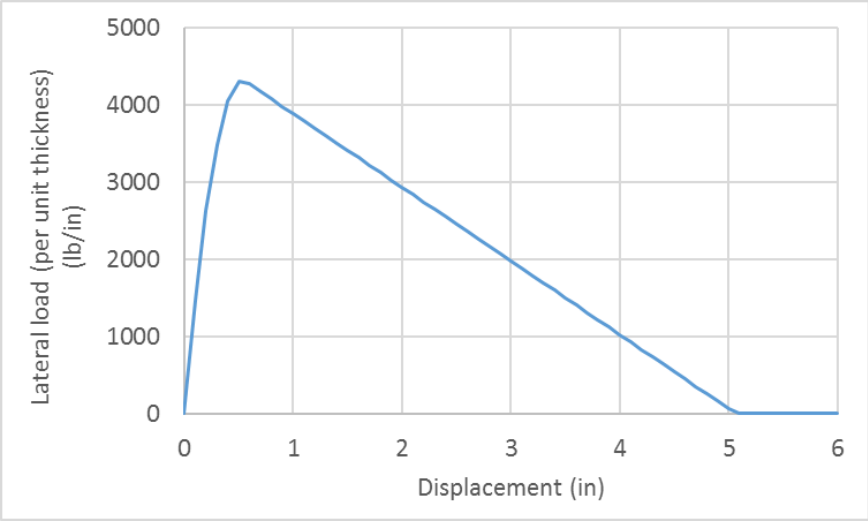

Figure 6.9 A representative *f-δ* curve for an asphalt mow strip (after [12])

6.3 Model validation

6.3.1 Determination of model constants

To make use of the analysis model, it is necessary to determine the material and geometric constants for the post when embedded in an asphalt layer. Table 6.1 summarizes the model constants used in this study.

Table 6.1 Constants in the analysis model

Category	Constant	Value	Source
Post	Yield stress, σ_y	51.4 ksi	Laboratory test
	Yield moment, M_y	285 kip-in	W6x9 section property
	Plastic moment, M_P	320 kip-in	W6x9 section property
	Elastic modulus, E	29,000 ksi	Common value
	Area moment of inertia, I	16.4 in^4	W6x9 section property
Soil	Density, ρ	144 lb/ft^3	Laboratory test
	Friction angle of soil, ϕ_s	45 deg.	Laboratory test
	Soil coefficient, c_1	6.28	API [83]
	Soil coefficient, c_2	5.25	API [83]
	Soil coefficient, c_3	153	API [83]
	Subgrade reaction, k	381 lb/in^3	API [83]
Asphalt	Friction angle of asphalt, ϕ_a	35 deg.	Smith [67]
	Shear modulus, G	7250 psi	Lee et al. [86]

The yield stress of steel was determined based on tensile coupon tests conducted according to ASTM A370 [64] (see Appendix A for details). The yield moment, plastic moment, and moment of inertia were determined using classic methods of mechanics for the W6x9 section used as the post. The soil density and friction angle were determined from laboratory soil testing results shown in Appendix A. Using the value of the friction

angle, soil spring coefficients were determined from the API chart [83] as discussed above. The asphalt friction angle was determined from the representative value of satisfactory asphalt mix design criteria proposed by Smith [67]. The shear modulus is a critical factor in pavement design in elastic loading range but the influence of shear modulus on the rupture capacity of mow strip is less significant [12]. Hence, the value of 7250 psi was selected from the study proposed by Lee et al. [86]

6.3.2 Model calibration using experimental results

The present model contains parameters that must be determined through a system calibration, which means these parameters can be tuned to maximize the correlation between the experimental responses and the model. Table 6.2 shows the parameters calibrated through the system calibration. Three calibration factors were iteratively adjusted to reflect the test results and each parameter will be discussed in detail.

Table 6.2 Calibrated model parameters

Parameter	Value	Influenced by
Post size factor, *D*	19.0	- Post section size/shape - Soil type/condition
Asphalt peak force correction factor, λ_f	0.90	- Asphalt material - Test site condition
Asphalt peak displacement correction factor, λ_δ	0.68	- Asphalt material - Test site condition

The post size factor, *D*, from Equation (6-7) and (6-9), determines the ultimate lateral resistance of the soil springs. This parameter depends on the shape of the post, the soil type and condition (e.g., relative density, moisture) of the experiment site. Since the parameter does not include any effect from the asphalt mow strip, the baseline experimental results were a target to estimate this value. Various values were tried iteratively and finally D = 19.0 showed reasonable agreement. Figure 6.10 shows the comparison of load-displacement curves between the experiment and post size factor calibrated model results.

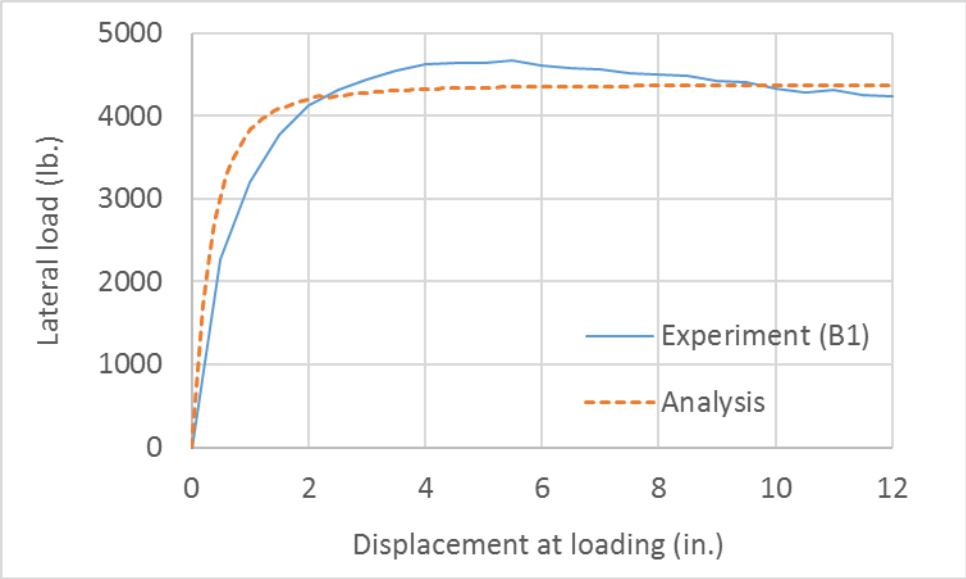

Figure 6.10 Comparison of load-displacement curves for baseline test (test B1)

The asphalt spring model described in the previous section may demonstrate discrepancies compared to the experimental results because this model cannot capture in-situ asphalt conditions such as moisture, void ratio, and friction between the asphalt-soil interface. Hence, a simple calibration method was introduced to correlate the

experimental and analytical results. Two parameters were introduced to adjust the maximum (peak) force (f_{max}) and corresponding displacement of the asphalt layer (y_1) as shown in Equation (6-14) and (6-15):

$$f_{max,eff} = \lambda_f \cdot f_{max} \tag{6-14}$$

$$\delta_{1,eff} = \lambda_\delta \cdot \delta_1 \tag{6-15}$$

where $f_{max,eff}$ is the effective asphalt peak force, λ_f is the asphalt peak force correction factor, $\delta_{1,eff}$ is the lateral displacement at which the asphalt peak force occurs with $f_{max,eff}$, and λ_δ is the lateral displacement correction factor. To calibrate the two correction factors, test results for four different test conditions were used. The four reference tests included two different geometry (thicknesses of 2" and 3.5") and two different test conditions (summer and winter). Cohesion values for the asphalt material were determined using Equations (4-8), (4-9), and (4-10). As such, a force correction factor of λ_f= 0.90 and a displacement correction factor of λ_δ= 0.68 were determined. The model showed reasonable agreement overall with the experimental data as shown in Figure 6.11, Figure 6.12, Figure 6.13, and Figure 6.14. Table 6.3 gives a comparison of the structural performance between the experimental and model results for various test setups using the quantitative performance criteria. Under the peak applied force, and ground-level displacement (at the reference value of dissipated energy of 66.7 kip-in.) criteria, the difference between the experiment and analysis is approximately 10 percent.

Table 6.3 Summary of model calibration results

Test description	Mow strip t_k x RD	Cohesion estimate (psi)	Peak force (lb.)		GL displ. (in.)	
			Exp.	Analysis [var]	Exp.	Analysis [var]
B1 (baseline)	0” x 0”	-	4673	4373 [- 6.4 %]	8.58	8.65 [+ 0.8 %]
T2 (summer)	2” x 24”	26.8	5491	5635 [+ 2.6 %]	7.26	7.09 [- 2.3 %]
T3 (winter)	2” x 24”	101.6	8672	7786 [- 10.2 %]	5.37	5.71 [+ 6.3 %]
T6 (summer)	3.5” x 24”	26.8	6663	6467 [- 2.9 %]	5.97	6.32 [+ 5.9 %]
T7 (winter)	3.5” x 24”	101.6	9553	10250 [+ 7.3 %]	4.98	4.32 [- 13.3 %]

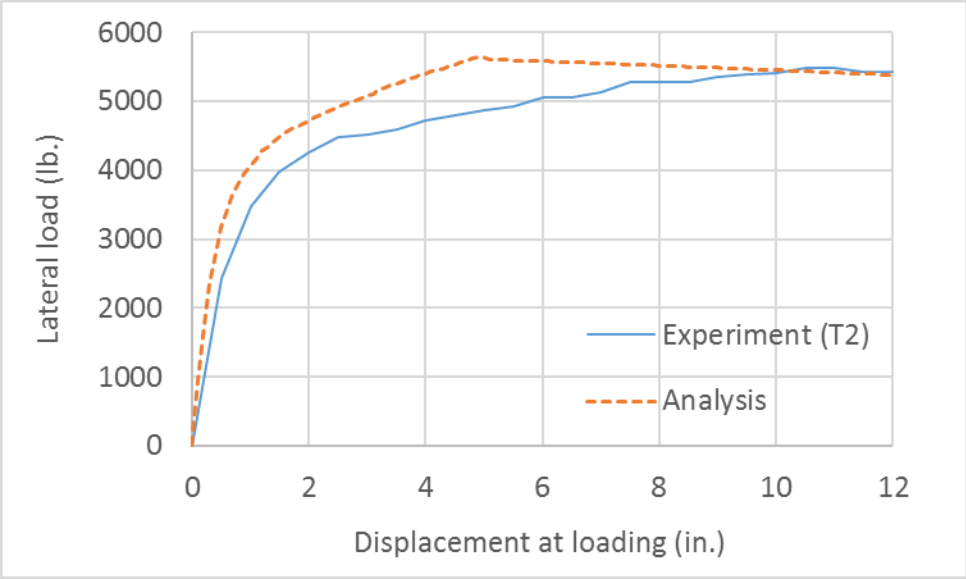

Figure 6.11 Comparison of load-displacement curves for test T2 (summer, t_k=2” and RD=24”)

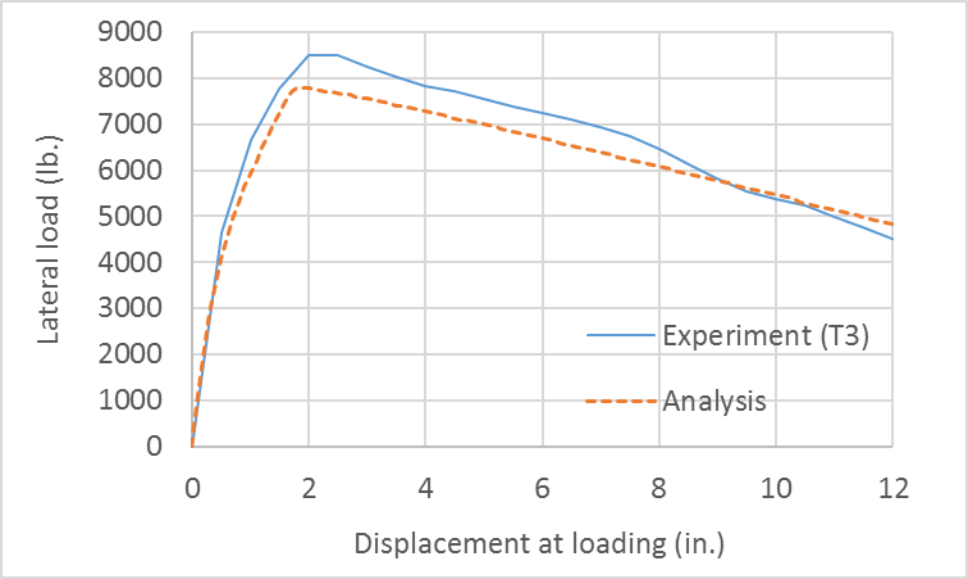

Figure 6.12 Comparison of load-displacement curves for test T3 (winter, t_k=2" and RD=24")

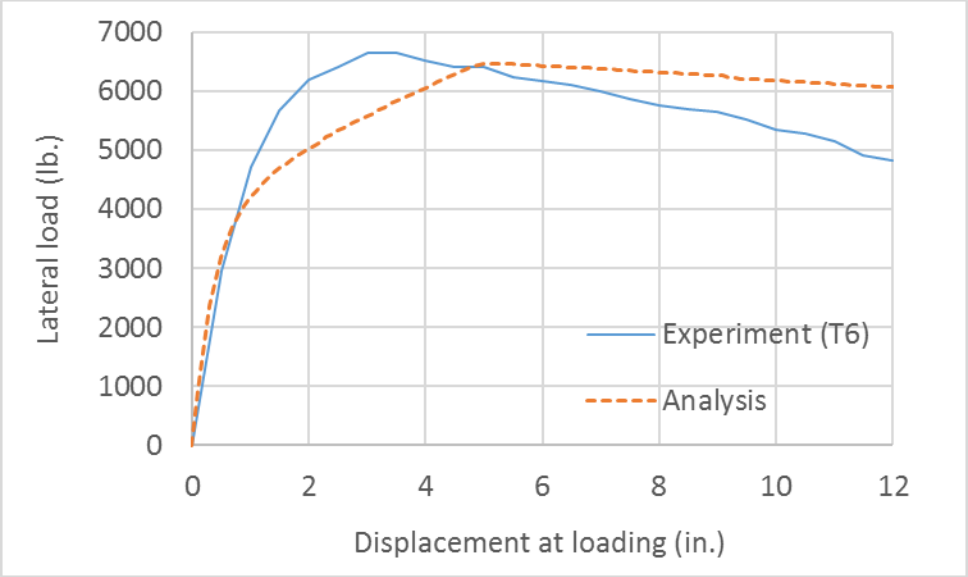

Figure 6.13 Comparison of load-displacement curves for test T6 (summer, t_k=3.5" and RD=24")

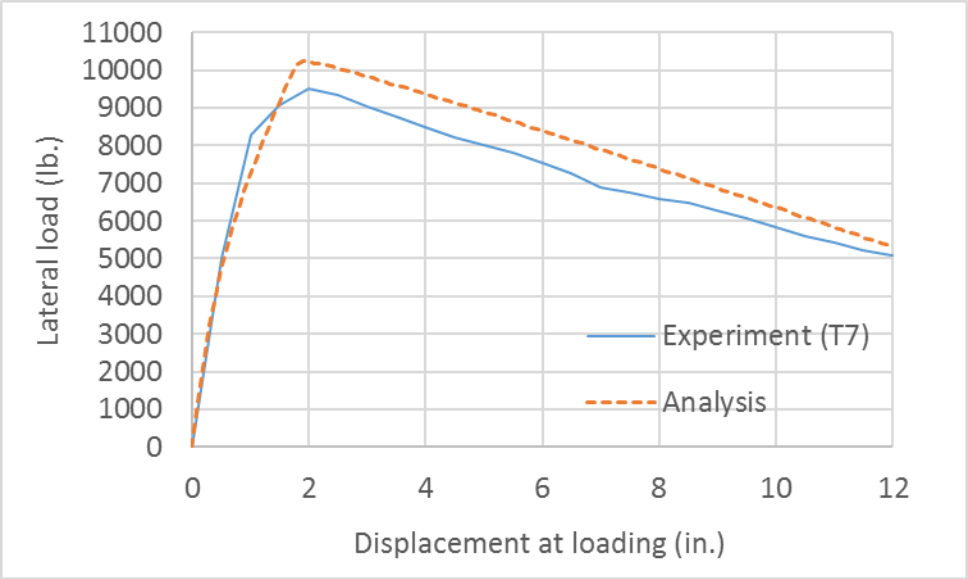

Figure 6.14 Comparison of load-displacement curves for test T7 (winter, t_k=3.5" and RD=24")

6.3.3 Convergence check

As the lateral resistance of the soil and asphalt layers are modeled as discrete springs, it is necessary to check if the number of springs affects the analysis result. For this purpose, a test configuration with a 4-inch thick and 24-inch wide mow strip was selected. A series of analyses were performed to check if the analysis results are converging and consistent under different numbers of springs. The results showed a reasonable trend of convergence in all performance criteria while the CPU time shows a strong positive correlation with an increasing number of springs. The minimum resolution of mow strip thickness variation in the analysis model is set to 0.5 inch. Therefore, the distance between two adjacent springs in this study were set to 0.5 inch, which means a total of 80 springs are used for the embedment depth of 40-inch.

Table 6.4 Effect of number of springs under performance evaluation criteria

Total number of springs	10	20	40	80	160
Distance between springs (in.)	4.0	2.0	1.0	0.5	0.25
Peak applied force (lb.)	9106	9087	9072	9073	9073
Ground-level displacement (in.)	4.766	4.707	4.704	4.703	4.704
Maximum normalized strain	0.9499	0.9130	0.8942	0.8856	0.8813
CPU time (s)	8.0	8.9	9.8	11.8	15.7

6.4 Sensitivity analysis on design variables

The subcomponent system in this study contains a number of design variables related to the asphalt layer. Unlike the full-scale experiment setup, the analysis model enables a user to apply a small deviation on a specific design variable while keeping all other remaining variables constant. Based on the sensitivity analysis, these design variables can be prioritized under certain evaluation criteria and aid the user in determining the optimal set of design variables. In this section, a total of four main design variables were investigated: thickness, rear distance, temperature, and age. These variables were initially considered in the development of the static and dynamic test matrices. The reference values of design variables and other factors were set as shown in Table 6.5 and used in the sensitivity analysis unless noted otherwise.

Table 6.5 Default values of design variables in sensitivity analysis

Design parameter	Value
Thickness	4 in.
Rear distance	24 in.
Temperature	68 °F
Age	120 days
Embedment depth	40 in.
Post type	Standard steel: W6x9

6.4.1 Effect of thickness and rear distance

Based on the mow strip survey, the range of mow strip geometry was set ranging from 1 to 8 inches of thickness and from 6 to 48 inches of rear distance. Figure 6.15 shows load-displacement curves for four representative thickness cases (2, 4, 6, and 8 in.) with a default rear distance (24 in.). Figure 6.16 shows the analysis results for various asphalt layer thicknesses in terms of the three static performance criteria. It can be observed that thickness has a strong impact on the level of restraint when all other design variables held constant. Figure 6.15 indicates that the 8-in. thick case demonstrates premature failure of the system due to plastic hinge formation in the post. The 7- and 8-in. thick asphalt mow strip cases also show significantly reduced ground-level displacements (Figure 6.16(b)) which is an indication of excessive ground-level restraint. The maximum flange stress exceeds the yielding stress in the asphalt layer for thicknesses above 6-inches (Figure 6.16(c)).

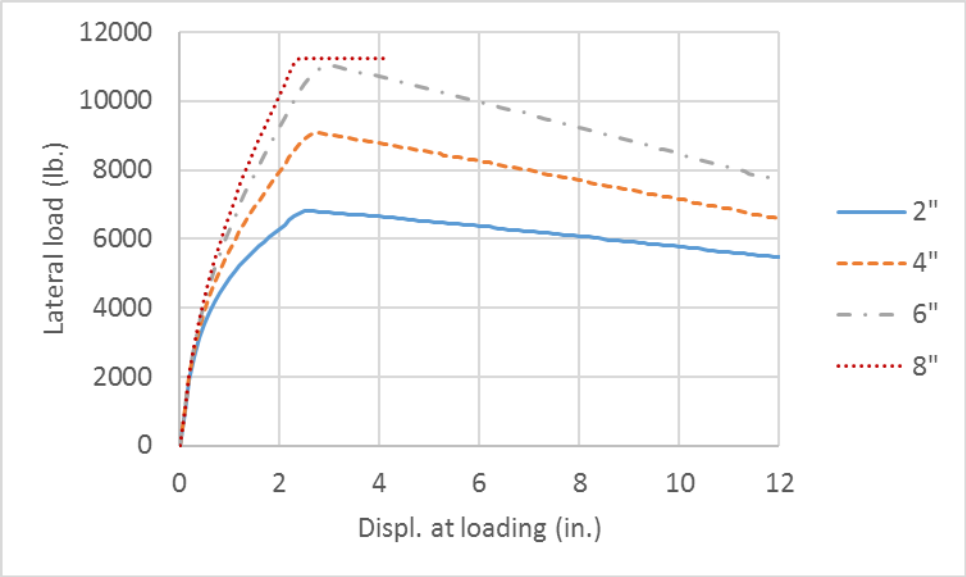

Figure 6.15 Effect of thickness on post restraint shown via load-displacement

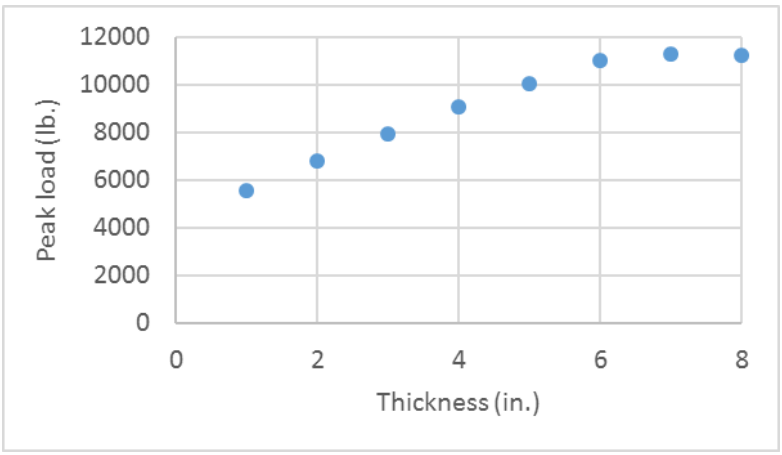

(a)

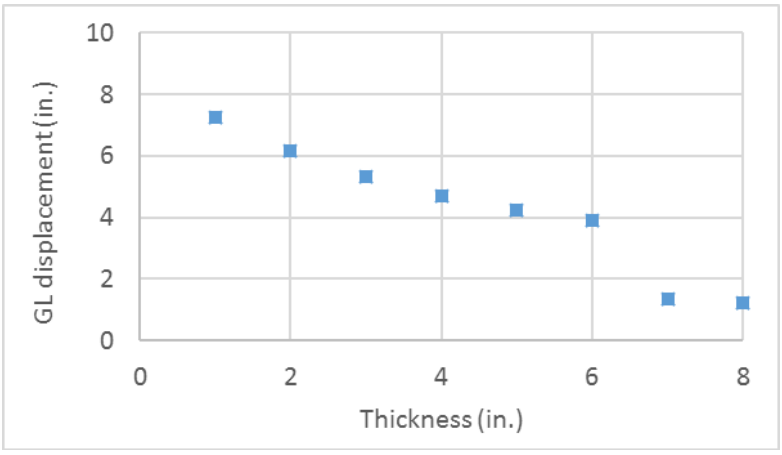

(b)

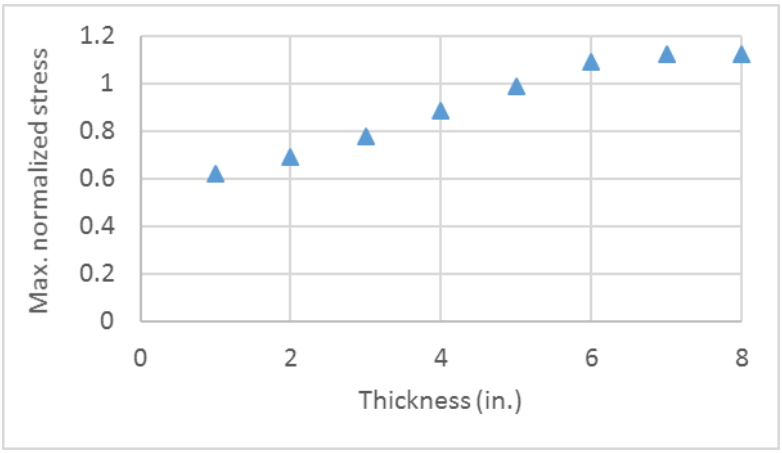

(c)

Figure 6.16 Effect of thickness on post restraint: (a) peak load, (b) GL displacement, and (c) maximum normalized stress

Figure 6.17 shows load-displacement curves for four representative rear distance cases (12, 24, 36, and 48 in.) with a default mow strip thickness of 4 in. Figure 6.18 shows the analysis results for various asphalt layer rear distances in terms of the three static performance criteria. The analysis results indicate the 48-in. wide mow strip design is likely to behave less satisfactorily compared to the other cases. Under the ground-level displacement criterion, the 42- and 48-in. wide rear distance mow strip cases demonstrate premature failure of the system due to plastic hinge formation in the post. Under the maximum strain/stress criterion, using a mow strip with 36-in. or wider rear distance may result in the excessive ground-level restraint and plastic deformation of the post.

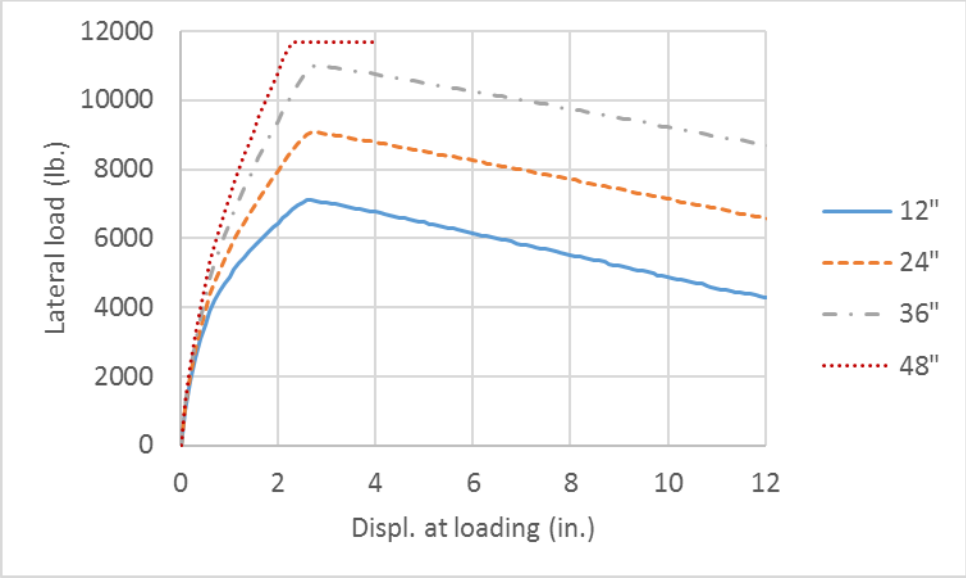

Figure 6.17 Effect of rear distance on post restraint shown via load-displacement

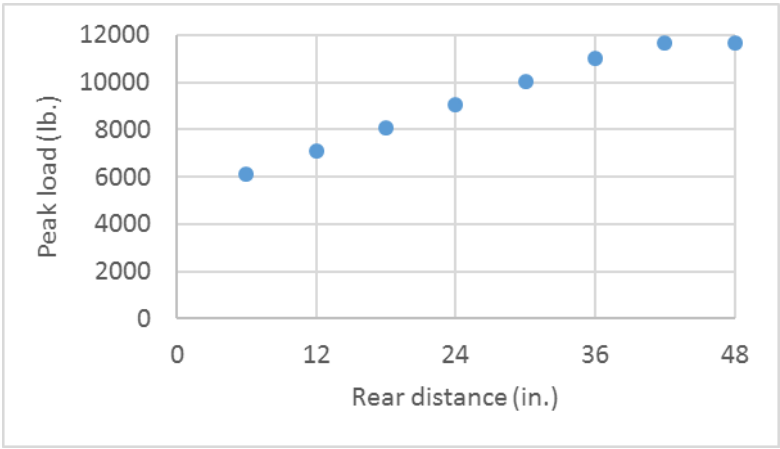

(a)

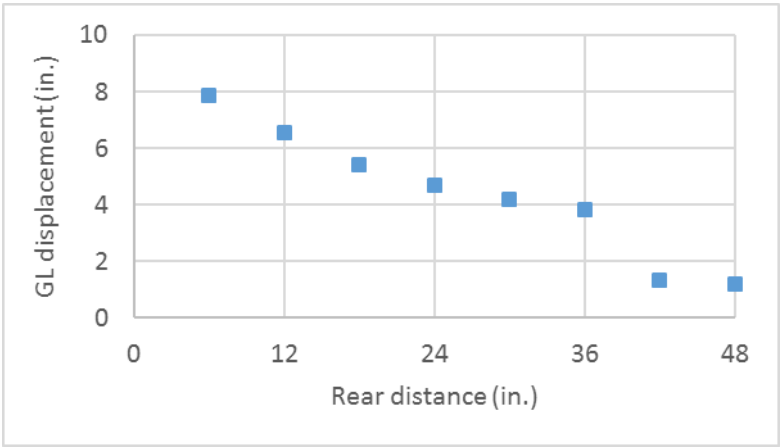

(b)

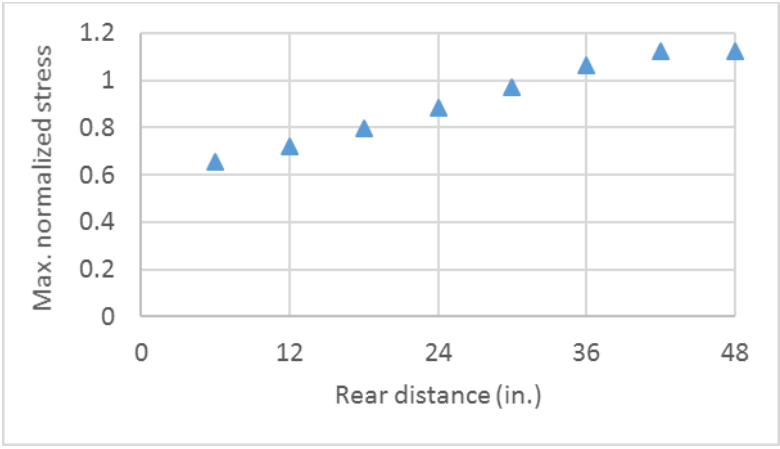

(c)

Figure 6.18 Effect of rear distance on post restraint: (a) peak load, (b) GL displacement, and (c) maximum normalized stress

Both thickness and rear distance effects can be visualized with a contour plot. This aids the user in determining whether a specific mow strip design satisfies the performance criteria. Figure 6.19 shows an example of peak applied load contour plot and Figure 6.20 shows an example of a ground-level displacement contour plot. The equivalent restraint level contour (green solid line) was determined from the static test results of the AASHTO leave-out configuration. These contour plots can be used to identify mow strip designs which are expected to have more ground-level restraint than the leave-out. However, it must be noted that these contour plots are valid only under the reference design variables given in Table 6.5.

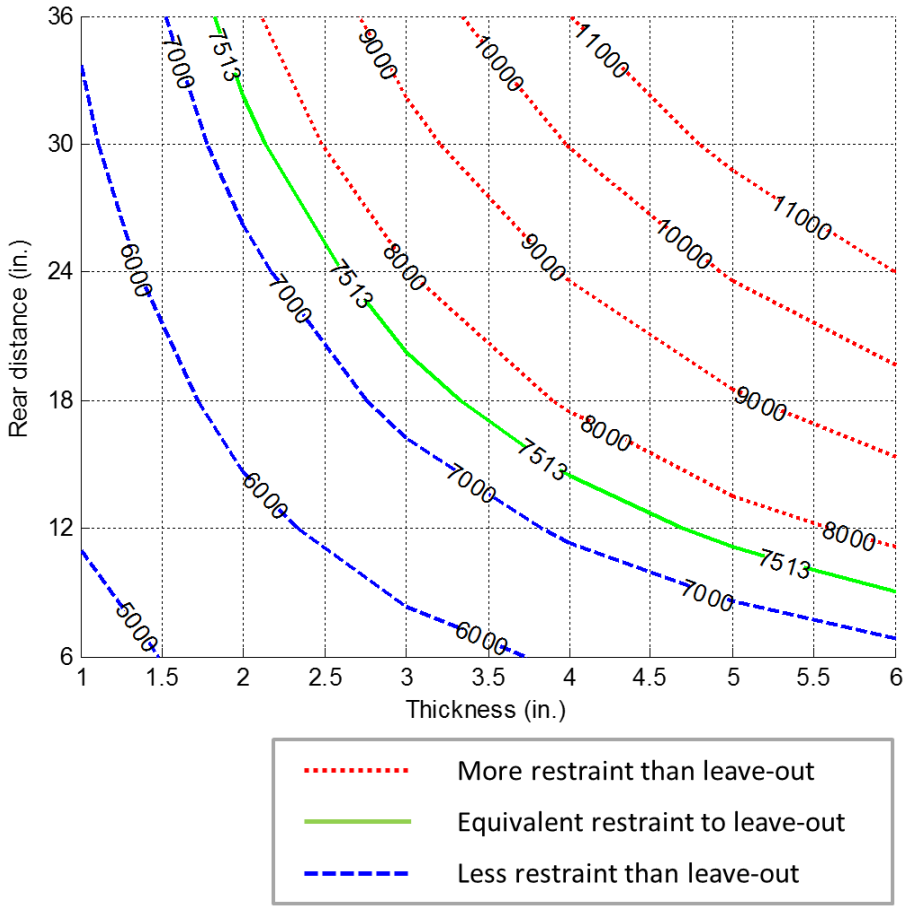

Figure 6.19 Performance criteria: peak load contour plot

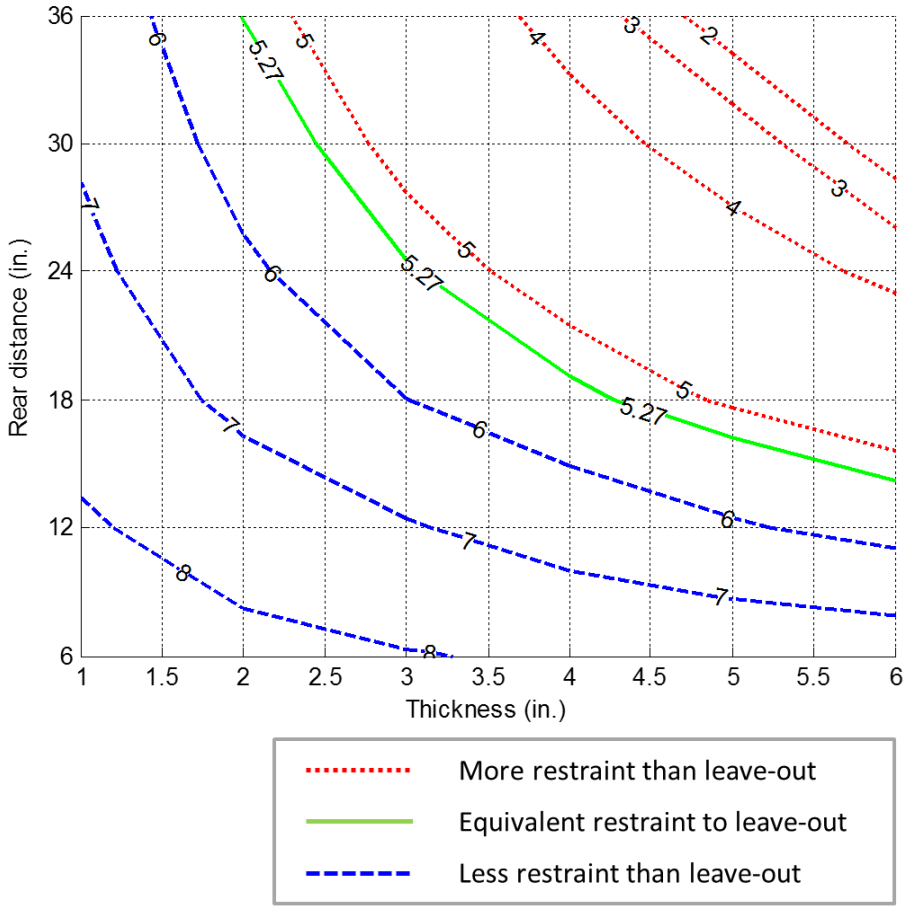

Figure 6.20 Performance criteria: ground-level displacement contour plot

6.4.2 Effects of temperature and age

From the specimen testing results, empirical temperature-cohesion and age-cohesion equations were developed as shown in Equation (4-8), (4-9), and (4-10). The asphalt lateral resistance model used in this study contains cohesion as a main parameter. The cohesion has a positive correlation with the asphalt lateral resistance and rupture capacity as shown in Equation (6-11). Hence, it can be expected that a given mow strip will behave differently under varying temperature and age conditions.

The effects of temperature and age on the model were investigated using the reference mow strip configuration (4-in. thick and 24-in. rear distance). Figure 6.21 shows load-displacement curves for four different temperature conditions (32, 50, 68, and 86 °F). Figure 6.22 shows the analysis results for various ambient temperatures in terms of the three static performance criteria. As expected, the overall performance of the asphalt mow strip is satisfactory in higher temperatures where the cohesion values are relatively small. Plastic hinging of the post is observed with relatively small ground-level displacement at the simulation of the lowest temperature condition (32 °F) where the cohesion value is the maximum among the cases considered.

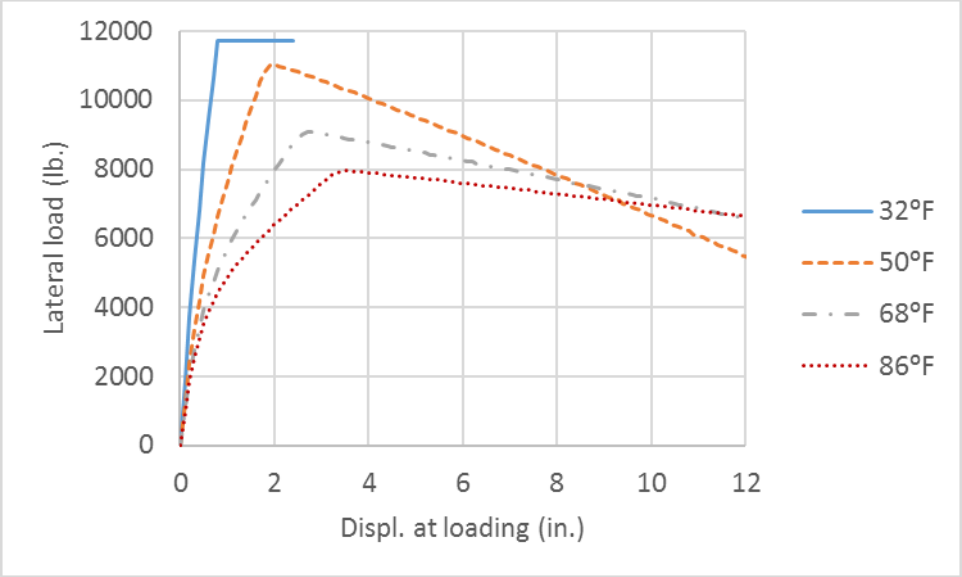

Figure 6.21 Effect of temperature on post restraint shown via load-displacement

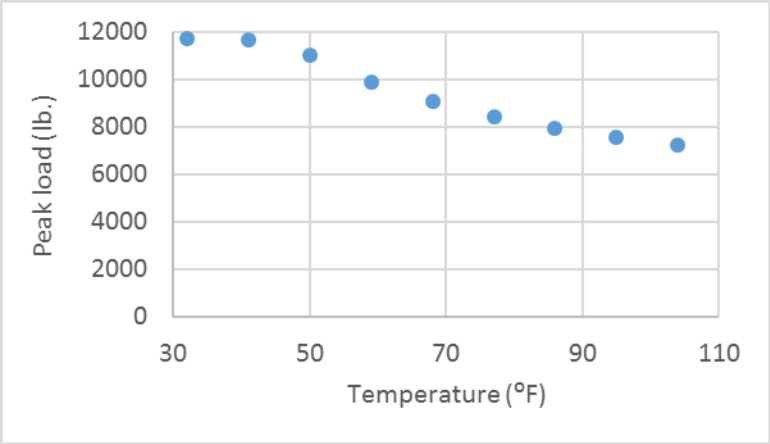

(a)

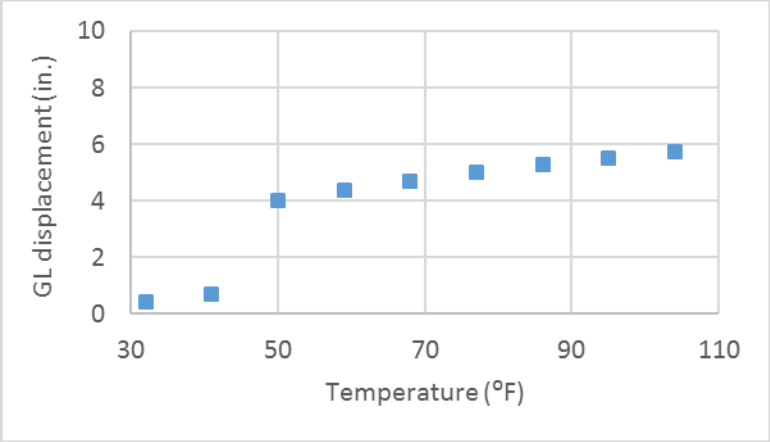

(b)

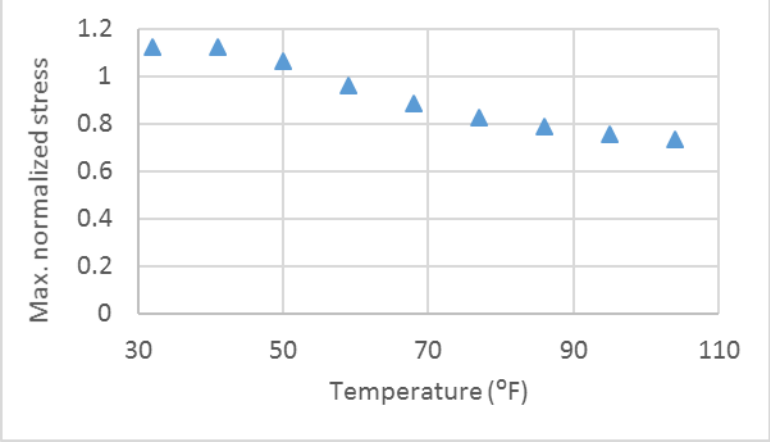

(c)

Figure 6.22 Effect of temperature on post restraint: (a) peak load, (b) GL displacement, and (c) maximum normalized stress

The effect of asphalt aging was investigated using the same analysis model and reference setting. Figure 6.23 shows load-displacement curves for various aging conditions. Figure 6.24 shows the analysis results for the various aging conditions in terms of the three static performance criteria. The performance change due to age effects seems not as significant as other design variables. This may be because of the empirical age-cohesion equation was constructed based on the specimen test results with a relatively short aging time. A new empirical age-cohesion model on various asphalt mix types would need to be developed to increase the accuracy of the analysis model in this study.

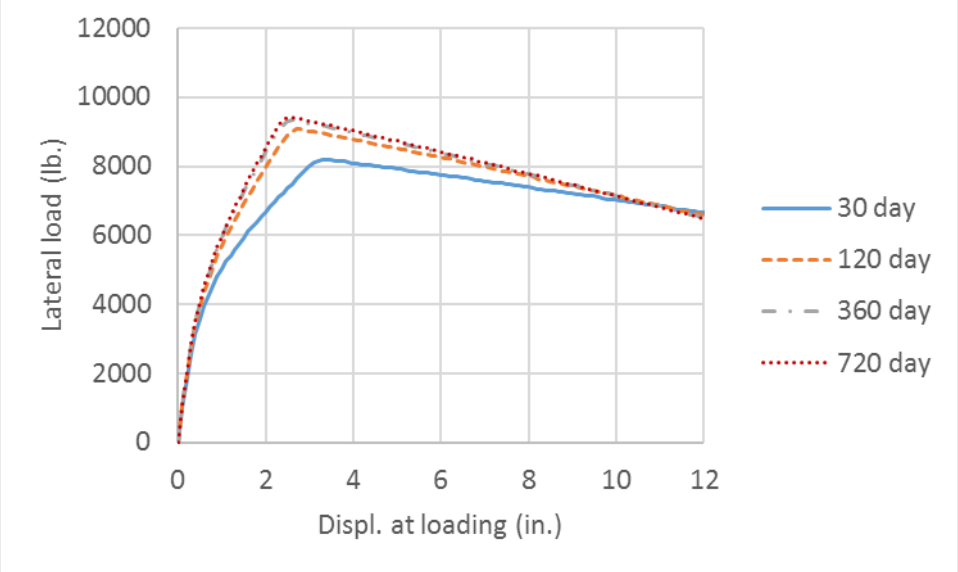

Figure 6.23 Effect of asphalt age on post restraint shown via load-displacement

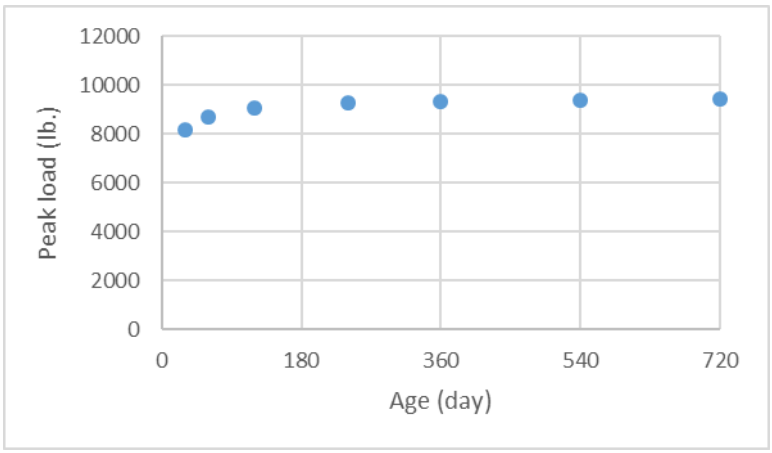

(a)

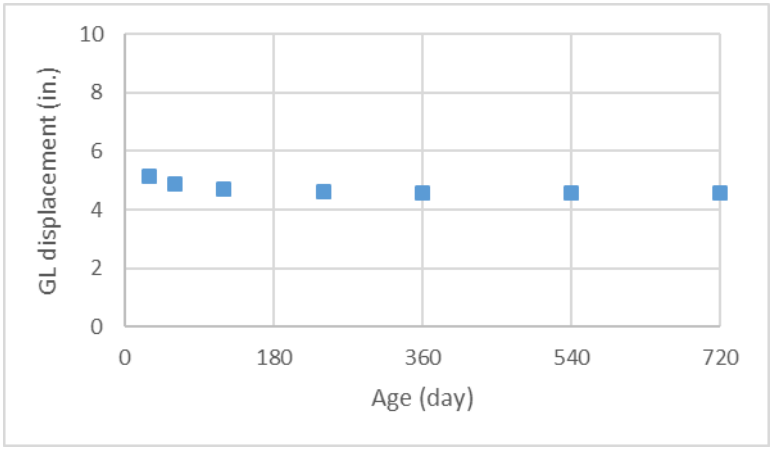

(b)

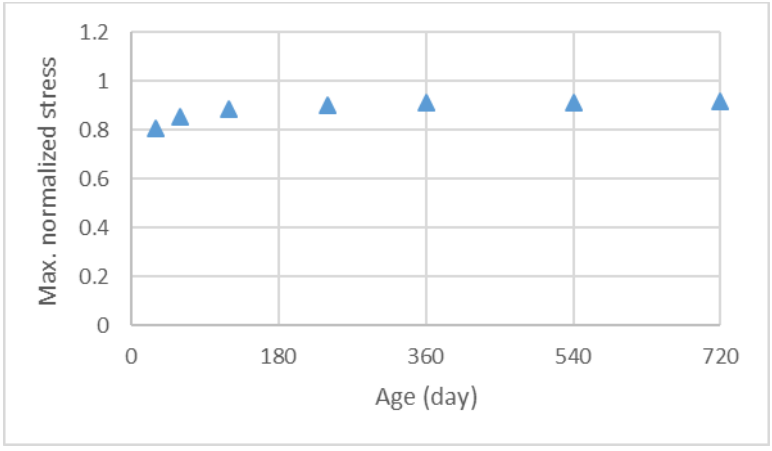

(c)

Figure 6.24 Effect of asphalt age on post restraint: (a) peak load, (b) GL displacement, and (c) maximum normalized stress

The effect of temperature and age can significantly impact the performance of the asphalt layer while the age of the asphalt mow strip is relatively less influential than the temperature once you move past the construction stage. Figure 6.25 shows two reference peak force contour lines (the reference value 7513-lb. from the average peak force of the static leave-out tests) drawn in different design conditions, A and B. The contour line under design condition A (temperature 43.1°F and age 2 years) is located below the contour line under design condition B (temperature 68°F and age 4 months). This indicates an asphalt mow strip of 2-in. thickness and 24-in. rear distance, marked as X in Figure 6.25, would behave satisfactorily under the B condition but not in the A condition.

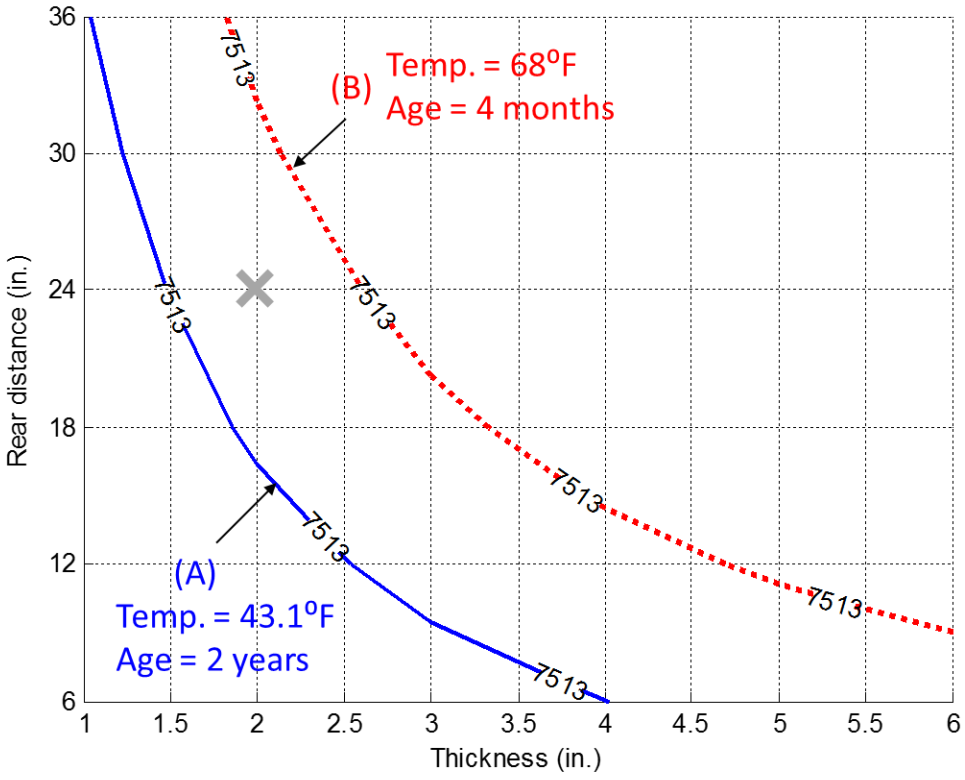

Figure 6.25 Peak force contour lines of two design conditions

6.5 Performance evaluation and design guidelines

6.5.1 Determination of critical design temperature

The sensitivity analysis showed that temperature is an influential factor which potentially changes the structural behavior of the post and the mow strip from a satisfactory to an unsatisfactory level. Specifically, excessive ground-level restraint by the mow strip is expected when ambient and resulting asphalt temperature drops below a given threshold. In conventional pavement design using the Performance Grading (PG) system, temperature is also a critical factor. The two numbers in the Performance Grade refer to design high and low temperatures where the asphalt binder is expected to perform satisfactorily. Calculation of design high and low pavement temperature at various reliability levels involves the compilation of a wide range of weather data and analysis. One of the most widely-used software tools developed for this purpose is LTPPBind [87]. This software contains a database of design high-low temperatures considering the reliability level for various sites throughout the United States. For instance, in Atlanta, GA, design high-low temperatures are 54.7 and -7.1 °C at a 65% reliability level and 59.1 and -11.7 °C at a 95% reliability level.

Roadway asphalt is designed where traffic loads are so frequent, a series of repeated loadings is applied on pavement every 3~4 seconds. Therefore, a roadway pavement should be designed for a high reliability level: an extremely low temperature condition to avoid thermal cracking. According to *NCHRP Report 673*, a reliability level of at least 90% is recommended for rural and residential roads and at least 95% is recommended for interstate highways and other major roads [88]. Selecting a proper reliability level is an

important step because the reliability level determines the design pavement temperatures. However, roadside asphalt which affects guardrail performance usually does not carry traffic loads, and more importantly, crashes on guardrail are a rare event. An average daily temperature lower than -12 °C (the low design pavement temperature in Atlanta at 95% reliability level is -11.7 °C) has been recorded less than 0.2% of the time in the last 100 years of daily temperature recordings in Atlanta [63]. Therefore, from a practical standpoint, the critical low design temperature of the asphalt mow strip can be defined with a lower reliability level than roadway asphalt.

MASH specifies one of its underlying design philosophies for crash test parameters as the "worst practical condition". The specified weight of the small passenger car test vehicle was chosen to represent the 98-th percentile of passenger-type vehicles. The combination of impact speed and angle stands for the 92.5 percentile of real-world crashes [13]. If a guardrail structure performs satisfactorily at the specified worst practical condition, the structure can be assumed as working as designed for most crash conditions.

Based on the *MASH* and roadway pavement design philosophy, a 5-th percentile of average daily temperature is proposed as the critical design temperature for asphalt in the present work. This implies only 5 percent of days are expected to have lower ambient temperatures than the specified design temperature. Table 6.6 shows a list of daily average percentiles for two U.S. cities calculated from the weather database [63]. Atlanta, GA, represents a city which typically experiences relatively warm winter weather, and Sioux Falls, SD, represents a city with relatively cold winter weather in the

United States. It is obvious that the asphalt mow strip configuration selected by the critical design temperature of Atlanta is less likely to perform satisfactorily in Sioux Falls most winter days.

Table 6.6 Daily average temperature percentiles in two U.S. cities

Percentile of daily average temperature	Atlanta, GA		Sioux Falls, SD	
	ºF	ºC	ºF	ºC
5	43.1	6.2	15.5	-9.2
25	49.1	9.5	25.7	-3.5
50	62.7	17.1	48.9	9.4
75	76.2	24.6	66.2	19.1
95	79.5	26.4	74.0	23.3

6.5.2 Mow strip design modification procedure

This section introduces an example of mow strip design modification based on the performance evaluation criteria. Because of the effect of temperature and age in asphalt mow strip performance, a mow strip design showing satisfactory performance in a specific region is not necessarily applicable to other regions. The critical design temperature and a reasonable assumption on the target asphalt age shall be designated in evaluating the mow strip performance. Table 6.7 gives a set of initial mow strip design variables for new guardrail construction in the target region, Atlanta, GA. The initial design of the guardrail system contains standard steel guardrail posts embedded in an asphalt mow strip of 4-in. thickness and 24-in. rear distance. The critical design

temperature of 43.1°F is determined from the 5-th percentile of average daily temperature in Atlanta, GA, and the target asphalt age is assumed to be 2 years in this example.

Table 6.7 Example of initial mow strip design variables for new guardrail construction

Design parameter	Value
Mow strip thickness	4 in.
Mow strip rear distance	24 in.
Embedment depth	40 in.
Post type	Standard steel: W6x9
Target region	Atlanta, GA
	Critical design temperature = 43.1 °F Target asphalt age = 2 years

To evaluate the initial design variables, a series of analysis runs are performed to generate contour plots. The design domain of the contour plot is set from 1 to 8 inches of thickness and from 6 to 48 inches of rear distance. Figure 6.26 and Figure 6.27 show contours of the peak force and the ground-level displacement based on the critical design temperature 43.1°F and the target asphalt age of 2 years. It can be seen in both performance criteria that the initial mow strip design has more restraint than the reference leave-out configuration.

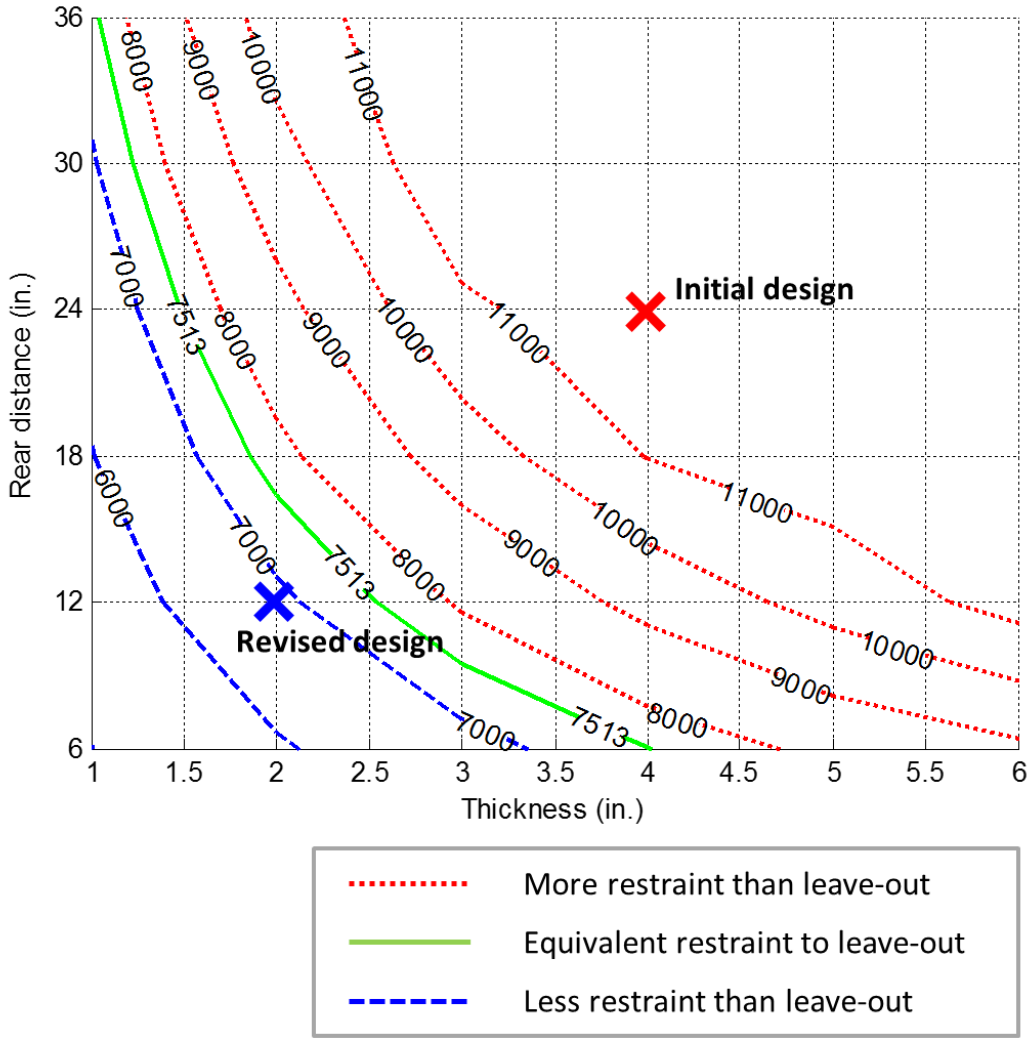

Figure 6.26 Peak force criterion contour plot in target region

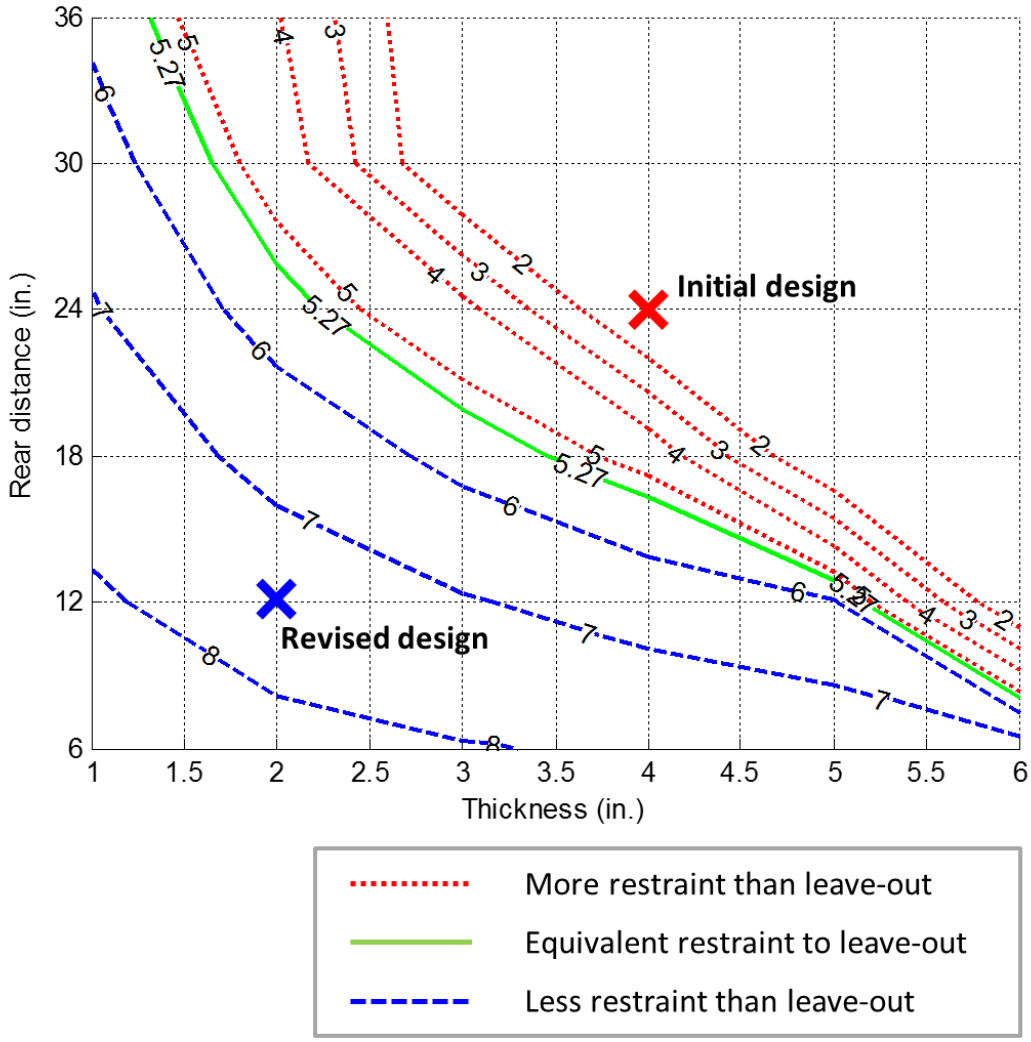

Figure 6.27 GL displacement criterion contour plot in target region

The simplest way to decrease the restraint on the post is to modify the mow strip geometry. For example, a revised design, reducing thickness to 2-in. and rear distance to 12-in., is expected to result in an acceptable level of ground-level restraint under both performance criteria. The load-displacement curves of the initial and revised mow strip designs are shown in Figure 6.28. It is expected that under a lateral load: (1) the post would exhibit plastic hinging with less translation in the initial design, and (2) the revised

mow strip design will allow the post to translate and dissipate more energy compared to the initial design.

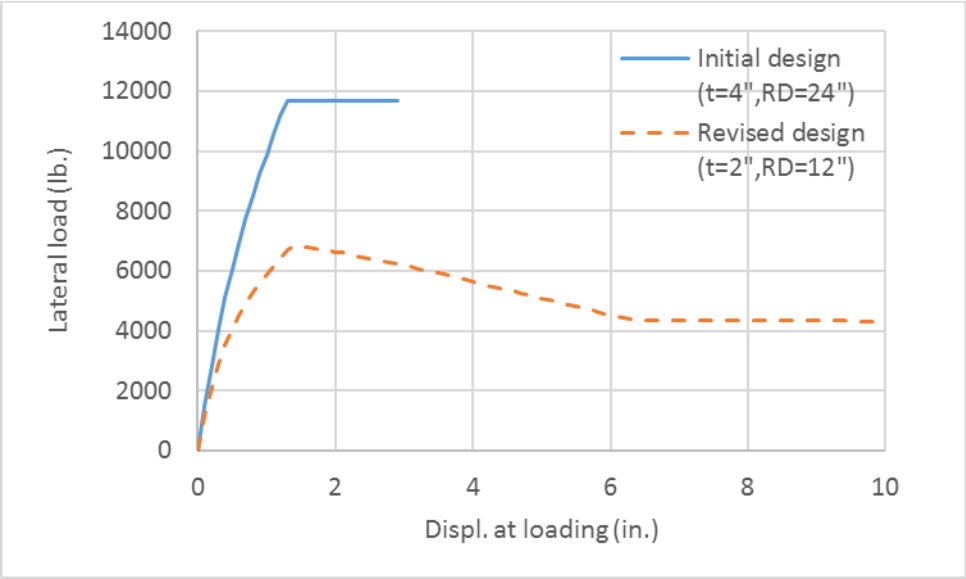

Figure 6.28 Reduced restraint by mow strip design revision (demonstrated via load-displacement curves)

6.5.3 Dynamic performance estimation using static analysis results

A static analysis model is generally not sufficient to predict dynamic performance. However, a static analysis model can be used to provide a general indication of expected dynamic structural response under an equivalent asphalt strength condition. Mow strip designs with a variation in dimension (Table 5.4 and Table 5.8) of the dynamic test program are selected and the test results are compared with the relevant static analysis results as shown in Table 6.8. Temperature and age of the asphalt mow strip in the analysis model are set to 68°F and 118 days to simulate the target strength used in the

dynamic test program (See Section 4.4 and 5.1.2 for details). The peak force and ground-level displacement criteria are used for this comparison.

Table 6.8 Comparison of static analysis and dynamic experimental results

Test configuration	Mow strip dimensions		Dynamic experiment		Static analysis	
	Thickness (in.)	Rear Distance (in.)	Peak force (lb.)	GL displ. at 137.9 k-in. (in.)	Peak force (in.)	GL displ. at 66.7 k-in. (in.)
Typical	3.5”	24”	12677	5.12	8492	5.01
Thin	1.5”	24”	7771	10.51	6178	6.67
Thick	5.5”	24”	15931	4.21	10507	4.08
Reduced RD	3.5”	12”	7922	11.73	6759	6.83
Thick and reduced RD	5.5”	12”	10030	8.23	7930	5.90

By using a linear regression method, two predictive equations which can be informative in estimating the dynamic performance are derived. Figure 6.29 shows a strong correlation between static and dynamic peak applied forces; the static-dynamic peak applied force equation can be written as follows:

$$P_{\max,dynamic} = 2.0144\, P_{\max,static} - 5194.8 \qquad (6\text{-}16)$$

where $P_{\max,dynamic}$ is the estimated dynamic peak applied force, and $P_{\max,static}$ is the peak applied force determined by static methods.

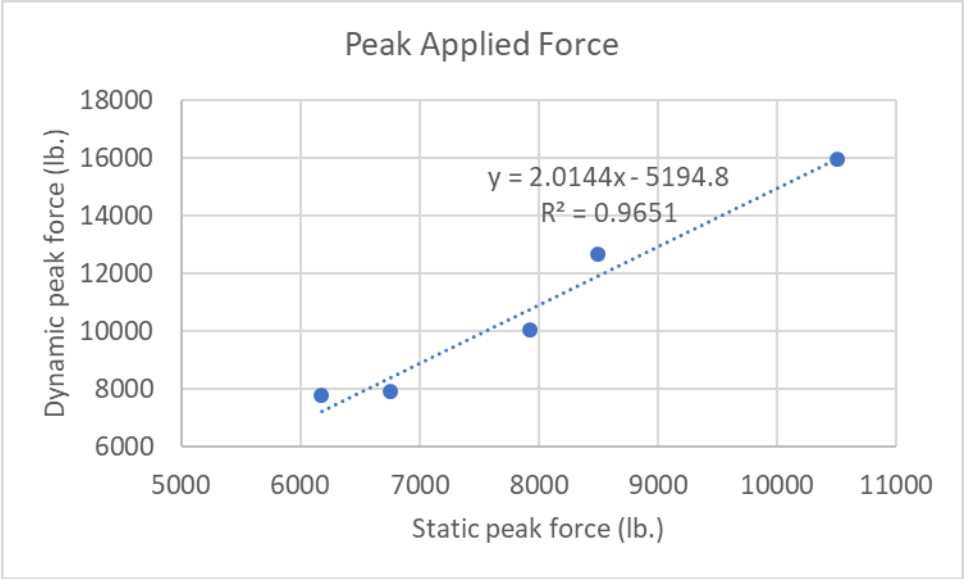

Figure 6.29 Peak applied force: static vs. dynamic results

For the ground-level displacement criterion, there is a strong correlation between static and dynamic results as illustrated in Figure 6.30. This static-dynamic relationship can be written as follows:

$$\Delta_{g,dynamic} = 2.7603\ \Delta_{g,static} - 7.7661 \qquad (6\text{-}17)$$

where $\Delta_{g,dynamic}$ is the ground-level displacement of the post from a kinetic energy input of 137.9 k-in., and $\Delta_{g,static}$ is the ground-level displacement of the post when 66.7 k-in. of work is done by a static load.

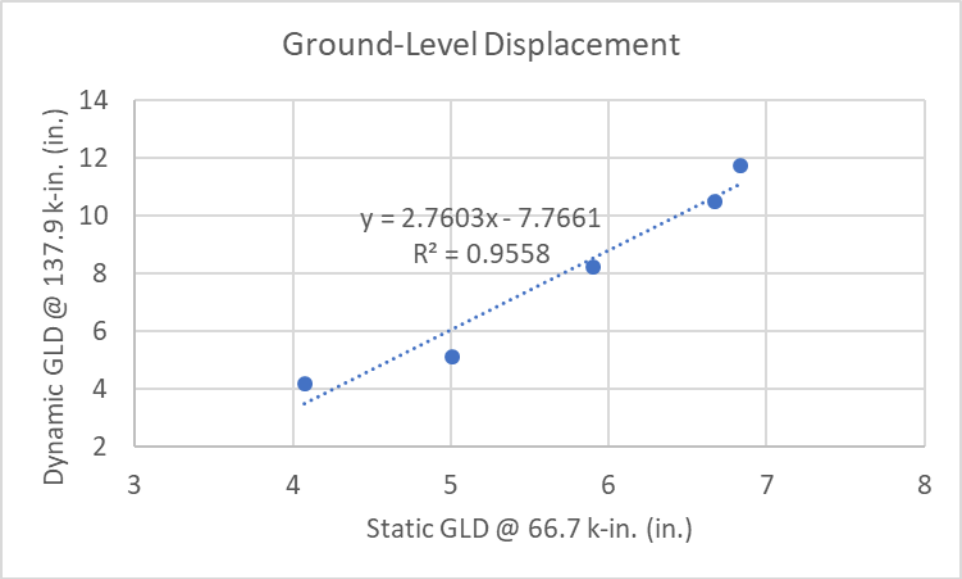

Figure 6.30 Ground-level displacement: static vs. dynamic results

6.6 Summary

Due to limitations in the experimental program, mow strip design variables affecting the performance of guardrail post were not able to be investigated in a collaborative manner. Hence, a simplified semi-empirical analysis model was developed to investigate not only few specific design cases but also broader range of design conditions. The analysis model addresses material and geometric properties of the subcomponent system as well as the variation in asphalt strength influenced by environmental factors. A guideline for mow strip design modification is presented as contour plots which provides multiple design alternatives with the potential for satisfactory structural performance.

CHAPTER 7
CONCLUSIONS

7.1 Summary and conclusions

This study presents the results of a comprehensive structural performance assessment on a guardrail subcomponent system including a standard steel post installed through an asphalt layer (mow strip). Specifically, this study addressed the deficiency of knowledge in the influence of asphalt mow strip design parameters on the structural behavior of guardrail posts in terms of the ground-level restraint caused by the mow strip. The major contributions of this study include the development of static/dynamic subcomponent test protocols, the characterization of structural properties of asphalt materials, the development of performance assessment criteria, and the use of a semi-empirical analysis model for guidance in the design of asphalt mow strips installed around guardrail posts.

Based on the results of the experimental and analytical investigation, the following conclusions can be made:

1. Static tests were designed and conducted to provide a general idea and a first-stage evaluation of design parameters related to the performance of posts encased in an asphalt mow strip. To determine the relative amount of ground-level restraint of the post, ground-level displacements and strains of the posts were measured in addition to the conventional *p-y* (load-deflection) measurement.
2. The effect of mow strip dimensions and asphalt properties on ground-level restraint of the post was evaluated using three quantitative performance criteria

based on static test measurements: (1) peak applied force, (2) ground-level displacement, and (3) maximum post strain. Under these performance criteria, static test results demonstrated the reduction of the width of the asphalt mow strip behind the post (rear distance), as well as the installation of pre-cuts, can lead to more satisfactory static performance of the post – less ground-level restraint – than a conventional leave-out application specified in the *AASHTO Roadside Design Guide*.

3. Testing on asphalt specimens provided an overview on the variability of asphalt strength with temperature and age and how that can affect the level of restraint imparted to a guardrail post by the asphalt layer. An empirical procedure based on the Mohr-Coulomb failure criterion was suggested and predictive compressive strength models were presented for asphalt material used in the static test program, accounting for the effects of temperature and age. Specifically, these models were used to select/determine an asphalt mix of equivalent strength for later experiments.
4. A novel dynamic test protocol using a high-speed hydraulic actuator and a movable test bed was developed as an alternative to existing dynamic test methods. The main purpose of dynamic tests was to provide a detailed observation on the dynamic performance of posts installed with various mow strip design alternatives, selected by the static test evaluation. Using shock-accelerometers and high-speed cameras, the dynamic structural behavior of the impacting object (flyer mass) and the post were precisely traced.

5. Four quantitative performance criteria were determined to assess the effect of mow strip design parameters on ground-level restraint of the post under a dynamic load: (1) peak dynamic force, (2) effective dynamic force, (3) ground-level displacement, and (4) impact-height displacement. The validation of the alternative mow strip designs was successfully made under these criteria: the effects of mow strip thickness, rear distance, and pre-cutting were significant. Specifically, the reduction of rear distance was determined to be the most efficient method for mitigating ground-level restraint, followed by reduction of thickness, and the application of pre-cuts or a leave-out.
6. A simplified semi-empirical analysis model was developed to predict the expected structural performance of guardrail posts with various mow strip design conditions. The model was calibrated with representative test results and used for the performance assessment with a broader range of mow strip design parameters compared to those in the static/dynamic experiments. Design guidance on the proper dimensioning of asphalt mow strips was suggested based on the analysis results and the design conditions including critical design temperature and asphalt age.

7.2 Recommendations

The following recommendations are presented for further research regarding to the scope and the limitation of the present study:

1. The relative structural efficiency of tested alternative designs to other mow strip designs currently in use can be determined after testing the combination of wood/steel posts with concrete/asphalt mow strips under the same test protocol.
2. Additional design parameters treated as constant in the experimental programs but considered in the literature review – such as post cross sections and embedment depth – can be investigated in follow-up experimental investigations.
3. The proposed dynamic test method could be extended to other roadside safety hardware such as concrete barriers, guardrail terminals, or traffic control devices.
4. A more detailed test setup including other guardrail elements such as w-beam and blockout would allow a user to assess localized damages by an impact.
5. Optimum pre-cut patterns and their detailed dimensions can be determined based on further experiments and/or more detailed finite element analyses.
6. A comprehensive dynamic material characterization investigation for various asphalt mix types can be performed. Empirical temperature- and age-strength models under different strain rates can be developed based on testing specimens with a broader range of temperature and a longer aging time, if applicable.
7. A more accurate analysis model to predict the dynamic behavior of impacted guardrail posts can be constructed from the characterization of material properties (e.g., internal friction angle of asphalt and soil) under various strain rates.

APPENDIX A
LABORATORY MATERIAL TESTING

A.1 Soil tests

Sieve tests

For soil material (GAB: Graded Aggregate Base) used in both static and dynamic test programs, sieve tests were conducted to determine the classification and qualification of the soil under AASHTO M147 requirement. As shown in sieve analysis results of both static and dynamic test programs, the test soil satisfied the AASHTO M147 Grade B requirement.

Table A.1 Summary of sieve analysis for static test soil

Sieve no.	Mass % passing	AASHTO M147 Grade B criteria		Pass/fail
		min.	Max.	
2 in.	100	100	100	Pass
1 in.	91.68	75	95	Pass
3/8 in.	59.84	40	75	Pass
No. 4	47.43	30	60	Pass
No. 10	36.67	20	45	Pass
No. 40	25.00	15	30	Pass
No. 200	7.728	5	20	Pass

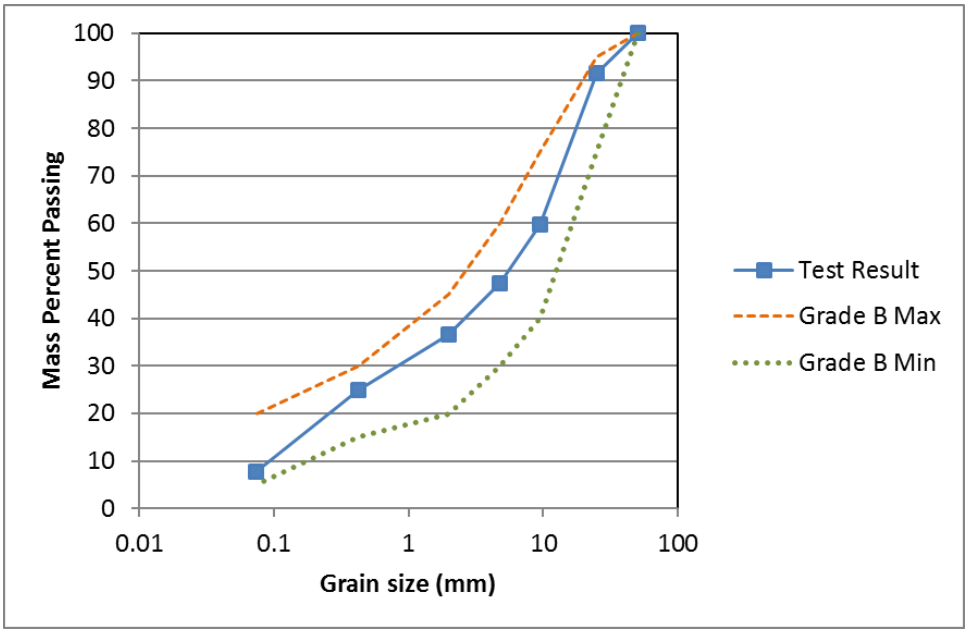

Figure A.1 Grain-size distribution curve of static test soil

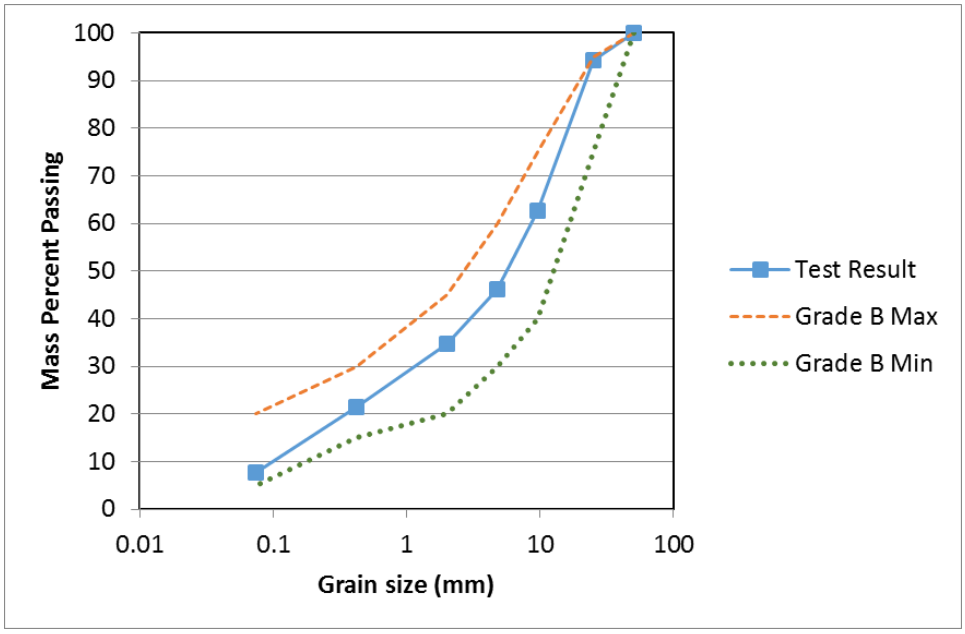

Figure A.2 Grain-size distribution curve of dynamic test soil

Table A.2 Summary of sieve analysis for dynamic test soil

Sieve no.	Mass % passing	AASHTO M147 Grade B criteria		Pass/fail
		min.	Max.	
2 in.	100	100	100	Pass
1 in.	94.3	75	95	Pass
3/8 in.	62.6	40	75	Pass
No. 4	46.2	30	60	Pass
No. 10	34.7	20	45	Pass
No. 40	21.5	15	30	Pass
No. 200	7.63	5	20	Pass

Proctor tests

A series of modified Proctor tests specified in AASHTO T 180 Method D was conducted. The maximum dry unit weight of test soil was determined to be 144.7 lb/ft3 at water content of 6.07%.

Table A.3 Summary of modified Proctor test results

Sample Name	Water Content	Wet Unit Weight		Dry Unit Weight	
	(%)	(kN/m³)	(lb/ft³)	(kN/m³)	(lb/ft³)
1	3.45	23.16	147.43	22.39	142.51
2	7.24	24.30	154.71	22.66	144.26
3	11.73	23.60	150.21	21.12	134.44

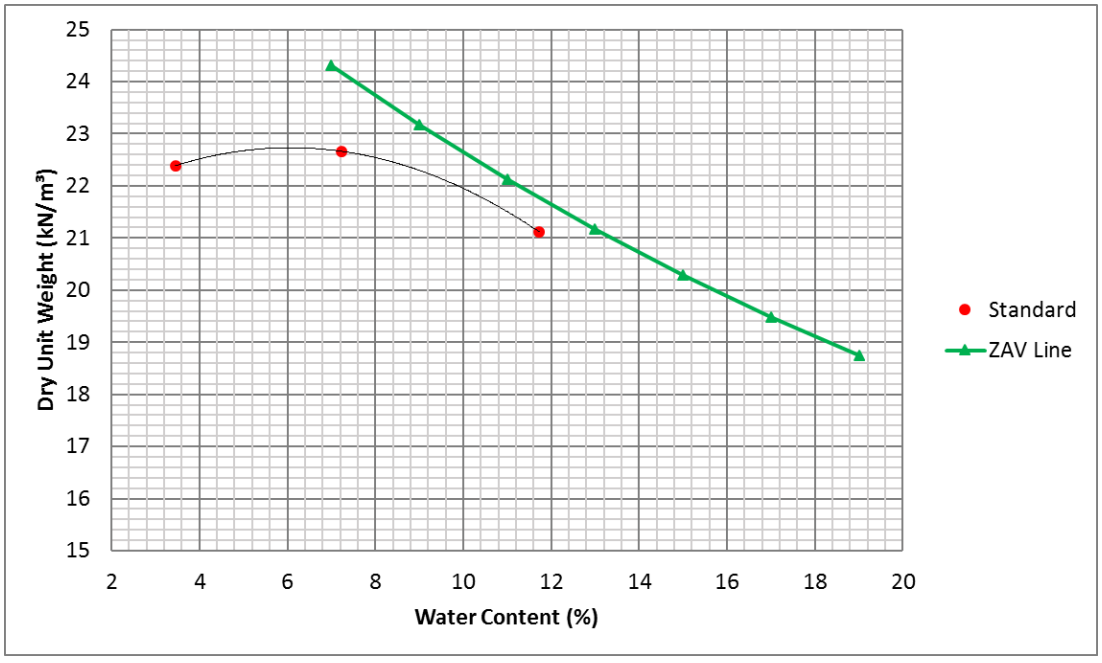

Figure A.3 Moisture-weight relationship for test soil

Sand cone tests

To check the in-place density of soil after the compaction using a plate compactor, a series of sand cone tests were conducted under the method specified in AASHTO T 191. The first and second sand cone tests were executed at approximately 47" depth (after compacting two soil layers), the third test at approximately 22" depth (after compacting few more layers), and the fourth test at the ground level. The average in-place dry unit weight of soil was determined to be 147 lb/ft^3 which exceeded 95% of the maximum dry unit weight (as specified in MASH). For the consistency of soil density, the level of compaction accompanied by the sand cone test was used in the rest of the test site construction.

Figure A.4 Sand cone test on compacted soil at static test site

A.2 Steel coupon tests

To determine tensile properties of steel guardrail post, steel coupons were cut from a representative steel guardrail post and tested under the method specified in ASTM A370. The tests were performed at the Georgia Institute of Technology Structural Engineering and Mechanics of Materials Laboratory.

Table A.4 Yield stress and tensile strength of steel coupons

Specimen designation	Yield stress		Tensile strength	
	(MPa)	(ksi)	(MPa)	(ksi)
F1	367.9	53.32	462.7	67.06
F2	340.3	49.32	452.2	65.54
W1	406.6	56.55	470.0	68.12
W2	390.2	67.59	466.4	67.59

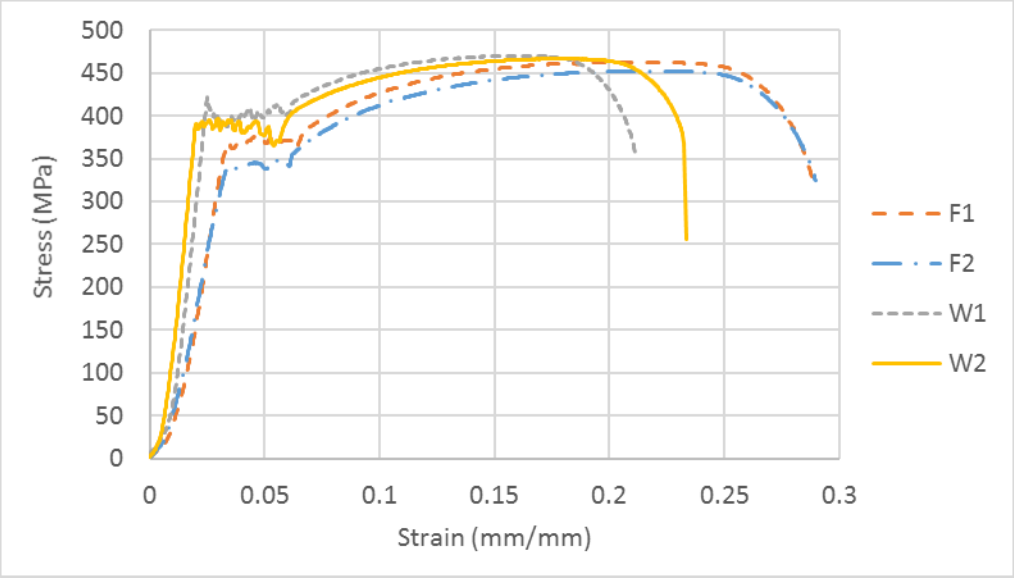

Figure A.5 Tensile stress-strain plots of steel coupons

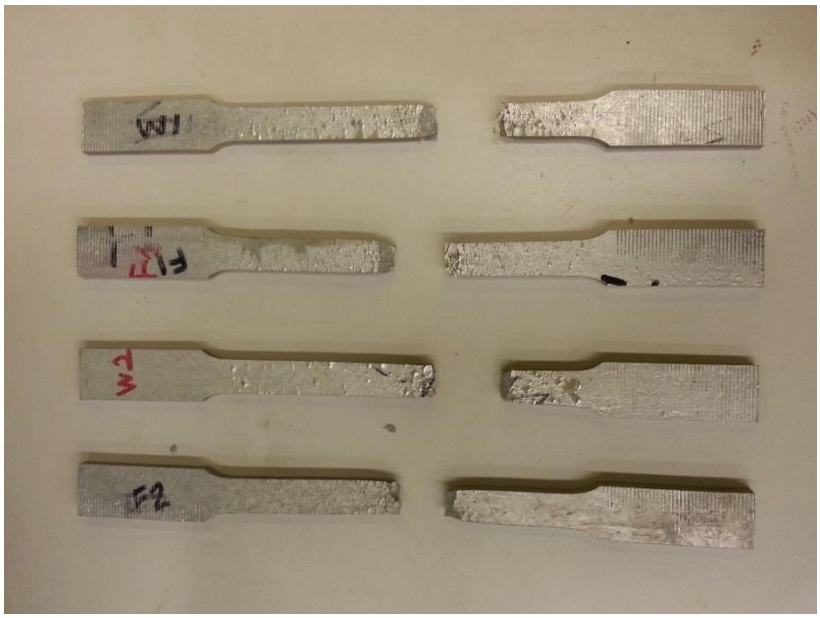

Figure A.6 Tested steel coupons

APPENDIX B

TEST INSTRUMENTATION SPECIFICATIONS

B.1 Static testing instrumentation

Strain gages

Table B.1 Strain gage specification

Manufacturer	Tokyo Sokki Kenkyujo
Model designation	FLA-5-11-3LT
Gage resistance	120 $\pm$ 0.5 ohm
Gage length	5 mm
Gage factor	2.13 ($\pm$1%)
Lead wire	Pre-wired, 3-wire system, 3-meter long
Coefficient of thermal expansion	11 ppm/^{o}C

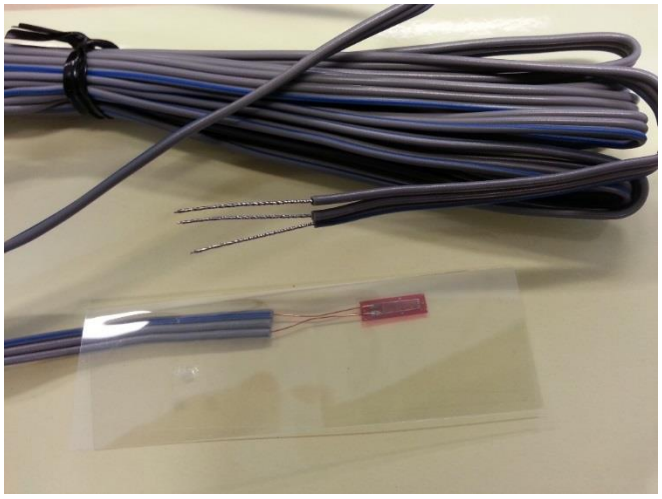

Figure B.1 Strain gage (FLA-5-11-3LT)

String potentiometers

Table B.2 String potentiometer specification

Manufacturer	Celesco
Model designation	PT1A-50-UP-500-M6-SG
Full stroke range	50 in.
Accuracy (% of F.S.)	0.1%
Cable tension (at 20% ext.)	5 oz.
Max. cable acceleration	3 g
Output signal	500 ohm
Weight	1 lb. max.
Dimensions	3.3 x 3.9 x 3.7 in.

Figure B.2 String potentiometer used in static tests

Load cell

Table B.3 Load cell specification

Model designation	STL-20K
Maximum capacity	20,000 lb. (both tension and compression)
Safe overload	150%
Ultimate overload	300%
Bridge resistance	350 ohm
Repeatability (% of F.S.)	0.02%
Linearity (% of F.S.)	0.03%

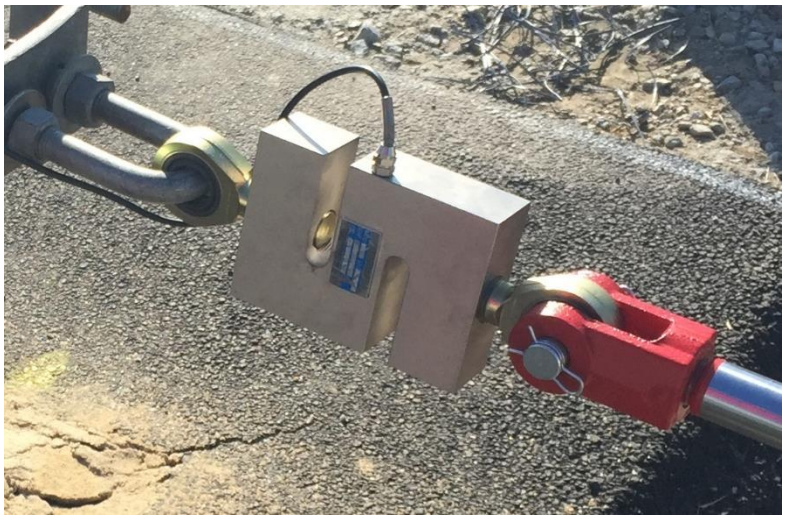

Figure B.3 Load cell used in static tests

B.2 Dynamic testing instrumentation

Accelerometers

Table B.4 Accelerometer specification

Manufacturer	PCB Piezotronics
Model designation	356B20
Sensitivity (±20%)	1.0 mV/g
Measurement range	±5000 g pk
Overload limit (shock)	±7000 g pk
Operating temperature range	-65 to +250°F
Frequency range (±5%)	2 to 7000 Hz (x axis) 2 to 10000 Hz (y or z axis)
Resonant frequency	≥ 55 kHz
Non-linearity	≤ 2.5%
Transverse sensitivity	≤ 5%
Weight	0.14 oz
Dimensions	0.4 x 0.4 x 0.4 in.

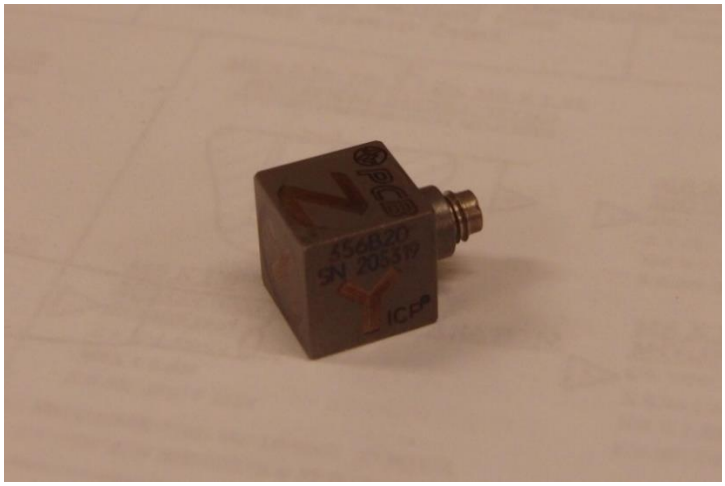

Figure B.4 Accelerometer (PCB 356B20)

Data acquisition system

Table B.5 Data acquisition system specification

Manufacturer	Hi-Techniques
Model designation	Synergy P
Number of input modules	4
Number of input channels	16
Maximum data rate	2 MS/s (for each channel)
Data streaming rate	500 kS/s (for all channels)
Maximum sampling rate with 16-bit resolution	100 MS/s (for each channel)

Figure B.5 Data acquisition system (Hi-Techniques Synergy P)

High-speed cameras

Table B.6 High-speed camera specification

Manufacturer	Vision Research	Vision Research
Model designation	Phantom Miro M310	Phantom Miro C110
Maximum resolution	1280 x 800	1280 x 1024
Pixel size	20 μm	5.6 μm
Maximum FPS at maximum resolution	3200 fps	915 fps
Maximum FPS at 720p HD resolution	3600 fps	1295 fps
Throughput	3.2 Gpx/s	1.2 Gpx/s
Minimum exposure	1 μs	5 μs

(a) Phantom Miro M310

(b) Phantom Miro C110

Figure B.6 High-speed cameras used in dynamic tests

B.3 Universal testing machine

For testing steel coupons and asphalt specimens, the INSTRON-SATEC Model No.5591 Universal Testing System was used. The testing machine is located at the Georgia Institute of Technology Structural Engineering and Mechanics of Materials Laboratory.

Figure B.7 Universal testing system (INSTRON-SATEC Model No.5591)

Table B.7 Testing frame specifications

Maximum frame capacity		67,000 lb.
Standard dimensions	Between column width	30 in.
	Tension opening	0 – 48 in.
	Compression opening	1 – 49 in.
	Column diameter (notch)	3.5 in.
	Table size (W x D)	30 x 30 in.
Maximum speed	Testing	3 in./min
	Adjusting	10 in./min
Max. specimen size (with crosshead grips)	Flat	1.375 x 2.5 in.
	Round	1.5 in.

(a) (b)

Figure B.8 Upper crosshead: tension testing of steel coupon (a); and lower crosshead: compression testing of asphalt cylinder (b)

APPENDIX C

TEST RECORD SHEETS

C.1 Static test record sheets

Test 1-1 **B1**

* Baseline configuration
* No mow strip
* Temperature recording not needed

Mow strip configuration	Thickness	**0** inch
	Rear Distance	**0** inch
	Modification	**N.A.**

Location	**SEMM Lab, Georgia Tech, Atlanta, GA**
Test date	**6/3/2014**
Temperature	**80** °F
Asphalt age	**N.A.** days from placement

Test drawings

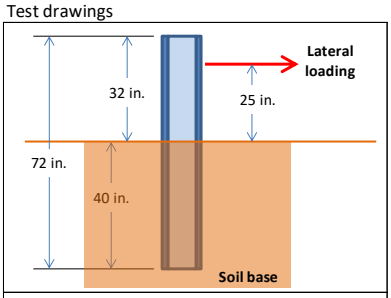

Test pictures

Start

End

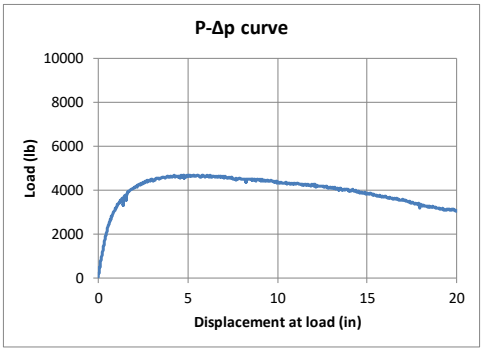

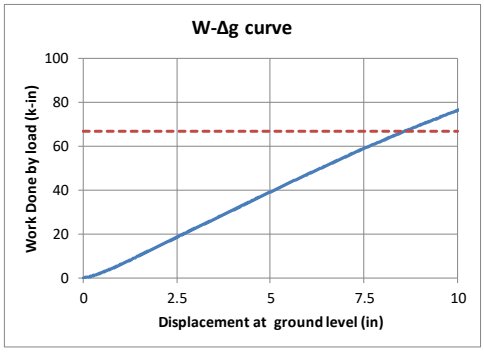

Peak load (lb)	**4673.3**
Δp at peak load (in)	5.5176

Δg at 66.7 k-in work (in)	**8.5762**

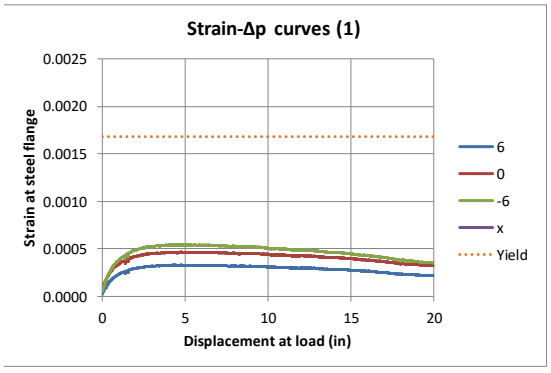

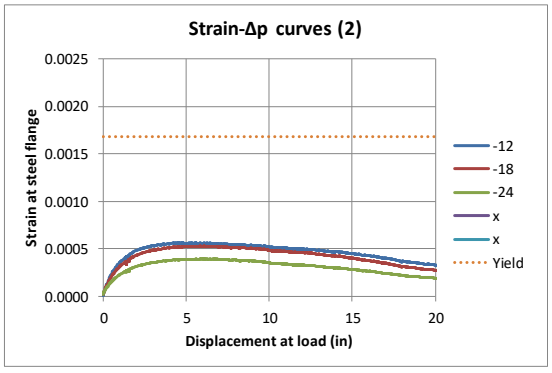

Gage location (in)	6	0	-6	x	-12	-18	-24	x	x
Maximum strain	**0.0003**	**0.0005**	**0.0005**	**0**	**0.0006**	**0.0005**	**0.0004**	**0**	**0**
Yield %	19.608	27.769	32.43	0	33.629	31.547	23.571	0	0

Figure C.1 Summary of static test results: B1

Test 1-2 **B2**

* Baseline configuration
* No mow strip
* Temperature recording not needed

Mow strip configuration	Thickness	**0** inch
	Rear Distance	**0** inch
	Modification	**N.A.**

Location	**SEMM Lab, Georgia Tech, Atlanta, GA**
Test date	**6/3/2014**
Temperature	**80** °F
Asphalt age	**N.A.** days from placement

Test drawings

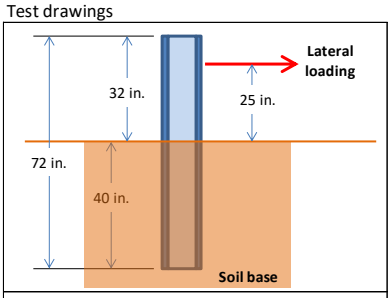

Test pictures

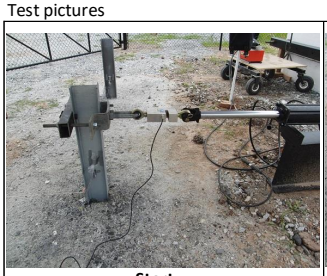
Start


End

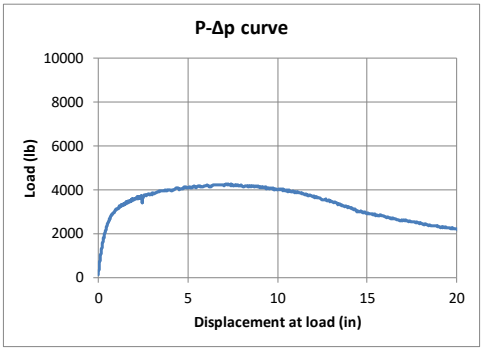

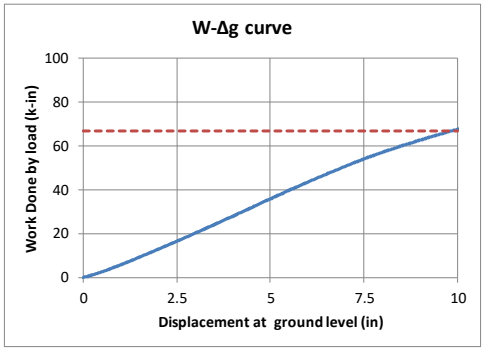

Peak load (lb)	**4247.3**
Δp at peak load (in)	7.1104

Δg at 66.7 k-in work (in)	**9.8343**

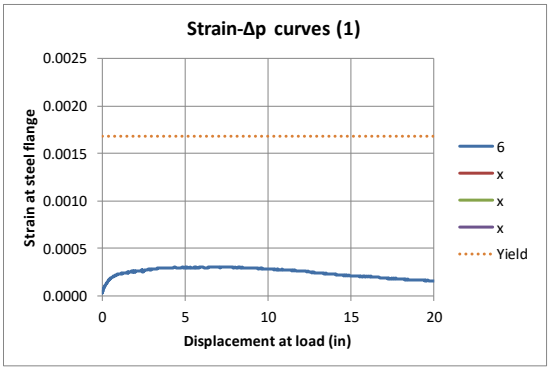

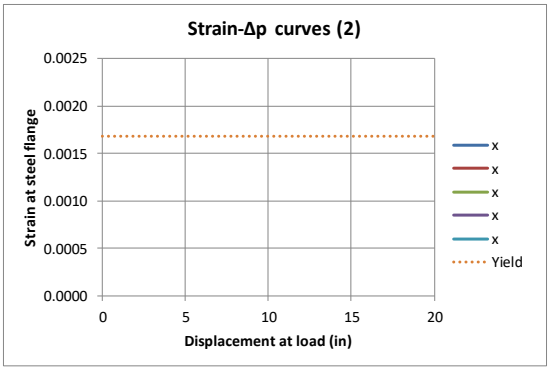

Gage location (in)	6	x	x	x	x	x	x	x	x
Maximum strain	**0.0003**	**0**	**0**	**0**	**0**	**0**	**0**	**0**	**0**
Yield %	18.201	0	0	0	0	0	0	0	0

Figure C.2 Summary of static test results: B2

Test 1-3 **B3**

* Baseline configuration
* No mow strip
* Temperature recording not required

Mow strip configuration	Thickness	**0** inch
	Rear Distance	**0** inch
	Modification	**N.A.**

Location	**SEMM Lab, Georgia Tech, Atlanta, GA**
Test date	**6/3/2014**
Temperature	**80** °F
Asphalt age	**N.A.** days from placement

Test drawings

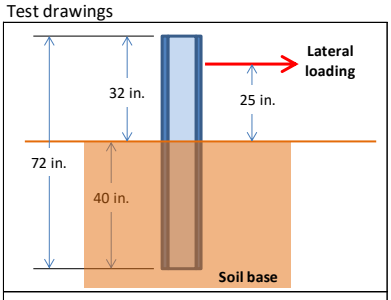

Test pictures

Start

End

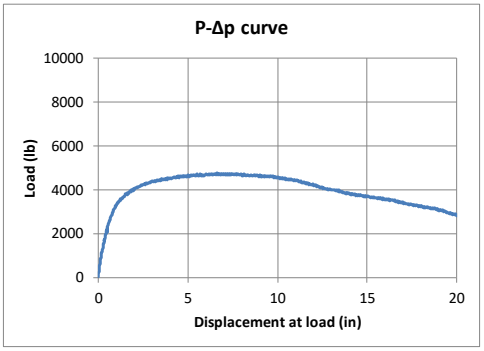

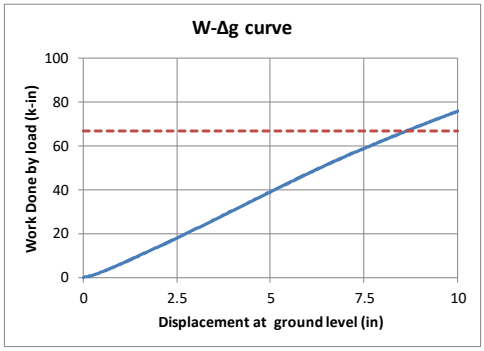

Peak load (lb)	**4743.7**
Δp at peak load (in)	6.5931

Δg at 66.7 k-in work (in)	**8.6243**

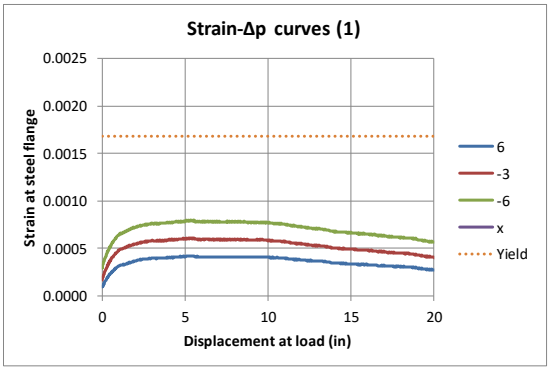

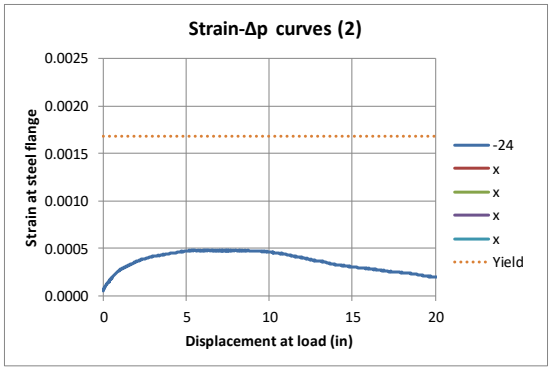

Gage location (in)	6	-3	-6	x	-24	x	x	x	x
Maximum strain	**0.0004**	**0.0006**	**0.0008**	**0**	**0.0005**	**0**	**0**	**0**	**0**
Yield %	24.548	35.687	46.781	0	28.618	0	0	0	0

Figure C.3 Summary of static test results: B3

Test 2-1	**T1**	
* Typical mow strip practice in U.S.		
* 2" thickness and 24" rear distance behind the post		
*		
Mow strip configuration	Thickness	**2** inch
	Rear Distance	**24** inch
	Modification	**N.A.**

Location	**SEMM Lab, Georgia Tech, Atlanta, GA**
Test date	**7/8/2014**
Temperature	**90** °F
Asphalt age	**18** days from placement

Test drawings

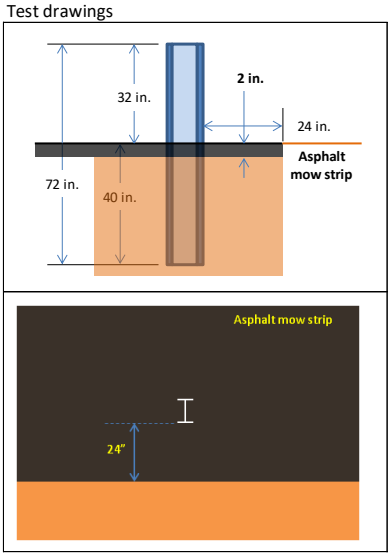

Test pictures

Start

End

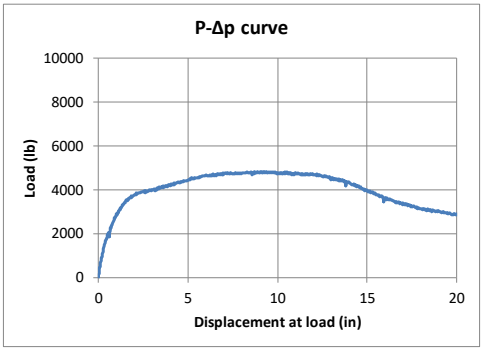

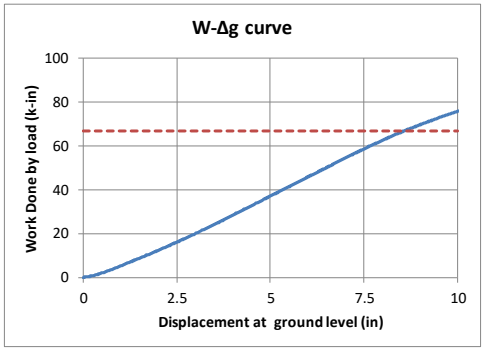

Peak load (lb)	**4827.3**
Δp at peak load (in)	9.4226

Δg at 66.7 k-in work (in)	**8.5604**

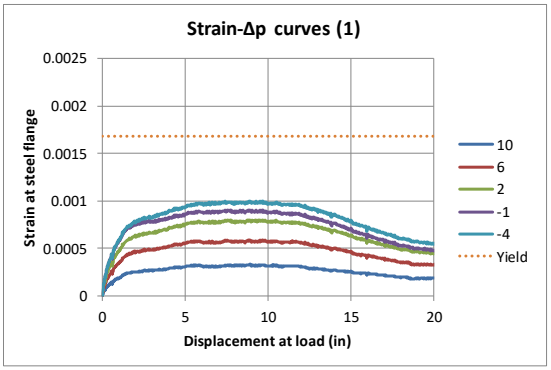

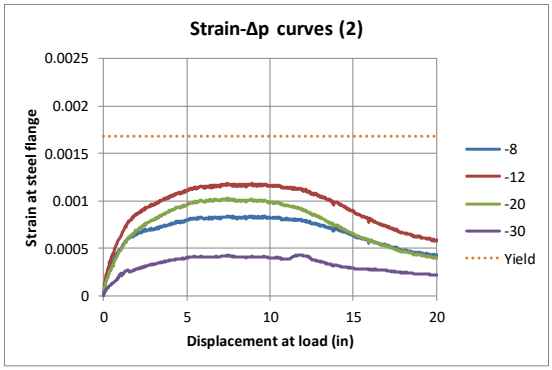

Gage location (in)	10	6	2	-1	-4	-8	-12	-20	-30
Maximum strain	**0.0003**	**0.0006**	**0.0008**	**0.0009**	**0.001**	**0.0008**	**0.0012**	**0.001**	**0.0004**
Yield %	19.67	35.092	47.768	53.76	59.334	50.02	70.335	60.045	24.764

Figure C.4 Summary of static test results: T1

Test 2-2 **T2**

* Typical mow strip practice in U.S.
* 2" thickness and 24" rear distance behind the post
*

Mow strip configuration	Thickness	**2** inch
	Rear Distance	**24** inch
	Modification	**N.A.**

Location	**SEMM Lab, Georgia Tech, Atlanta, GA**
Test date	**7/8/2014**
Temperature	**90** °F
Asphalt age	**18** days from placement

Test drawings

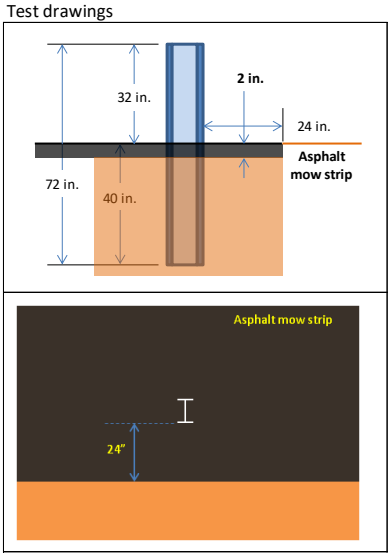

Test pictures

Start

End

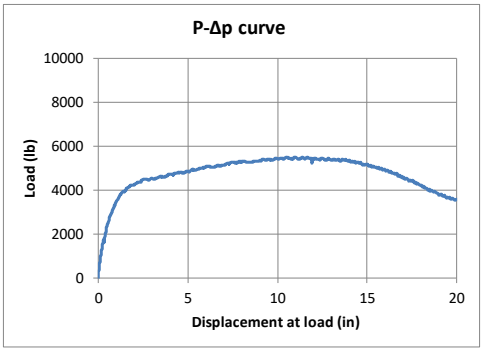

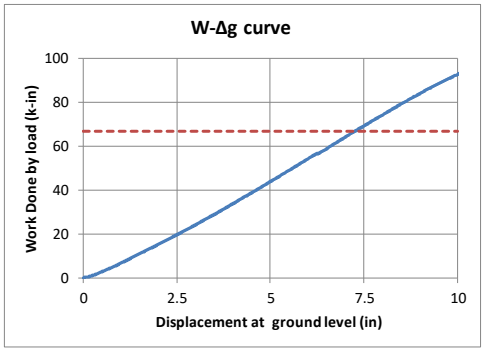

Peak load (lb)	**5490.6**
Δp at peak load (in)	10.958

Δg at 66.7 k-in work (in)	**7.2572**

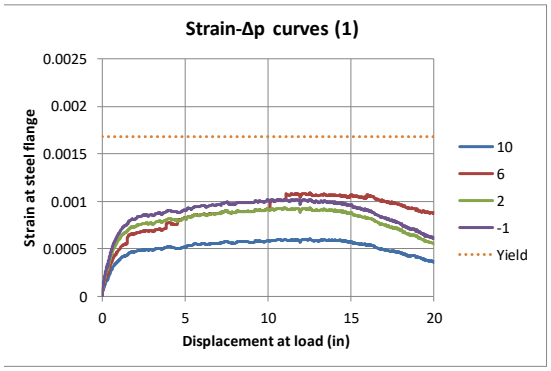

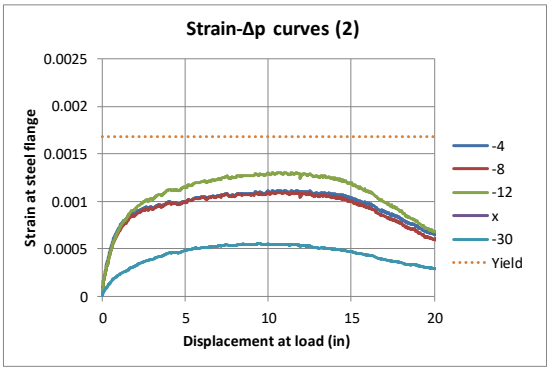

Gage location (in)	10	6	2	-1	-4	-8	-12	x	-30
Maximum strain	**0.0006**	**0.0011**	**0.0009**	**0.001**	**0.0011**	**0.0011**	**0.0013**	**0**	**0.0005**
Yield %	35.701	64.228	55.41	60.864	66.362	65.316	77.567	0	32.646

Figure C.5 Summary of static test results: T2

Test 3-4	**T3**
*	Typical mow strip practice in U.S.
*	2" thickness and 24" rear distance behind the post
*	

Mow strip configuration	Thickness	**2** inch
	Rear Distance	**24** inch
	Modification	**N.A.**

Location	**SEMM Lab, Georgia Tech, Atlanta, GA**
Test date	**2/12/2015**
Temperature	**50** °F
Asphalt age	**118** days from placement

Test drawings

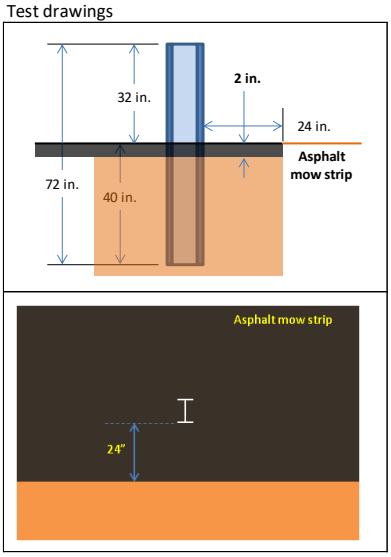

Test pictures

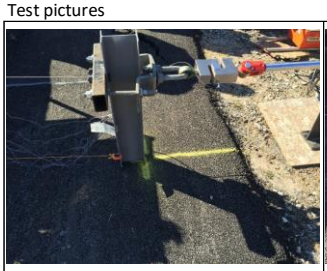

Start

End

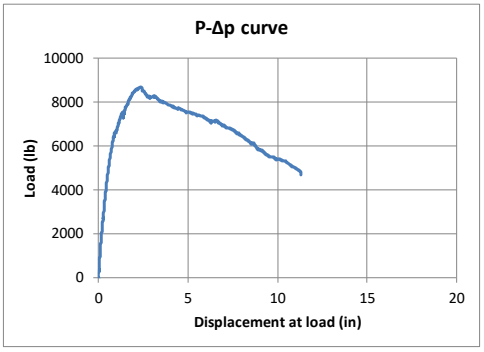

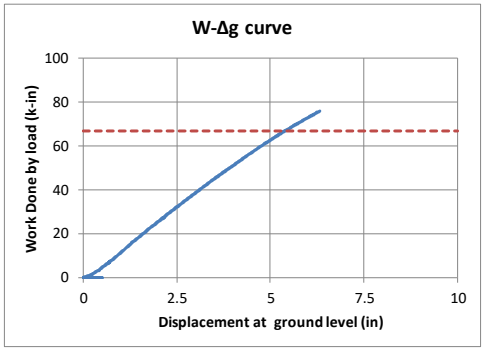

Peak load (lb)	**8671.7**
Δp at peak load (in)	2.307

Δg at 66.7 k-in work (in)	**5.3739**

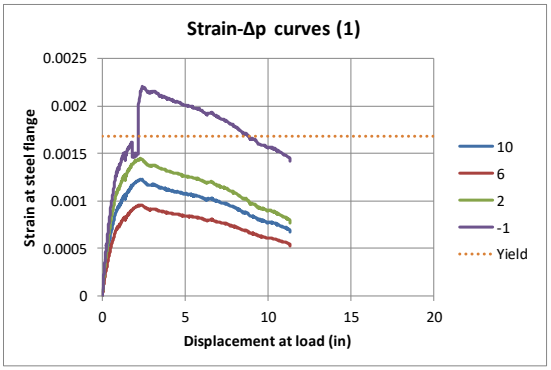

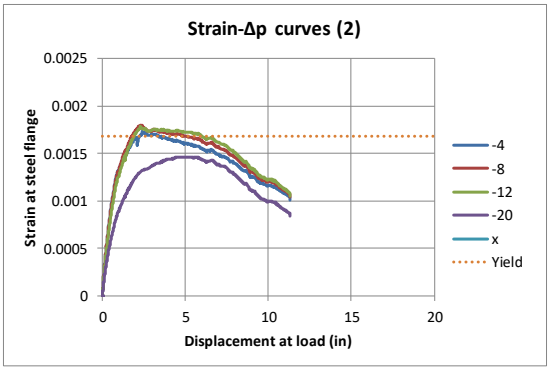

Gage location (in)	10	6	2	-1	-4	-8	-12	-20	x
Maximum strain	**0.0012**	**0.001**	**0.0014**	**0.0022**	**0.0017**	**0.0018**	**0.0018**	**0.0013**	**0**
Yield %	73.087	57.15	86.289	131.6	103.22	106.79	105.91	79.244	0

Figure C.6 Summary of static test results: T3

Test 4-3 **T4**

* Typical mow strip practice in U.S.
* 2" thickness and 24" rear distance behind the post
*

Mow strip configuration	Thickness	**2** inch
	Rear Distance	**24** inch
	Modification	**N.A.**

Location	**SEMM Lab, Georgia Tech, Atlanta, GA**
Test date	**5/5/2015**
Temperature	**75** °F
Asphalt age	**40** days from placement

Test drawings

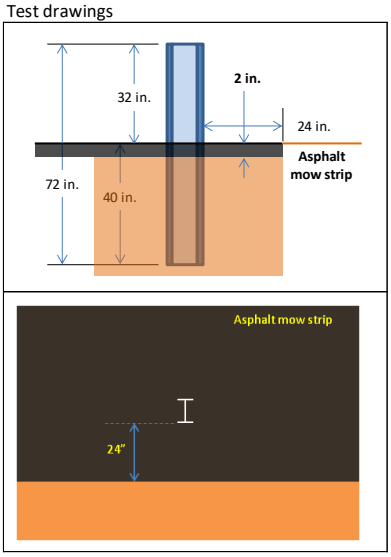

Test pictures

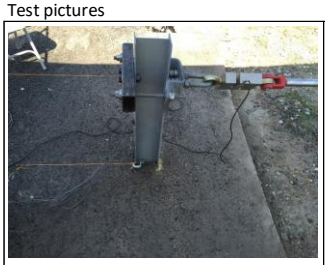

Start

End

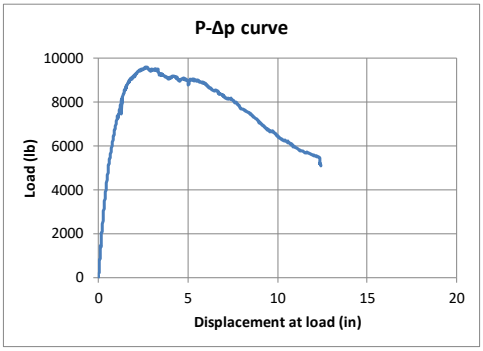

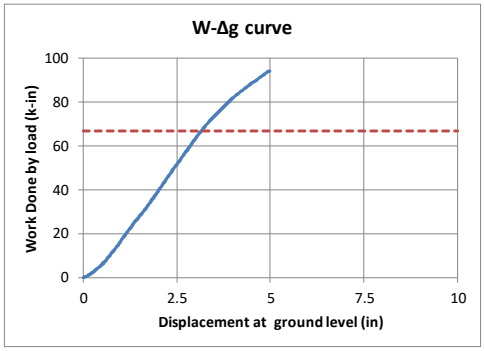

Peak load (lb)	**9597.5**
Δp at peak load (in)	2.6498

Δg at 66.7 k-in work (in)	**3.153**

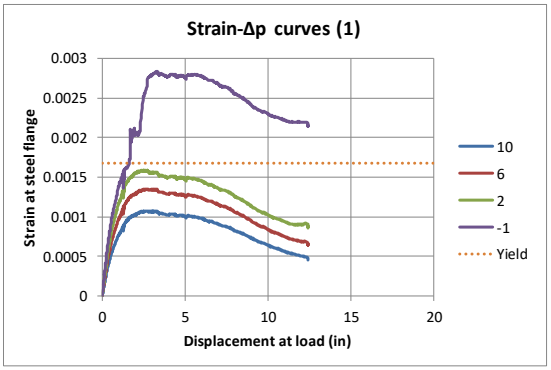

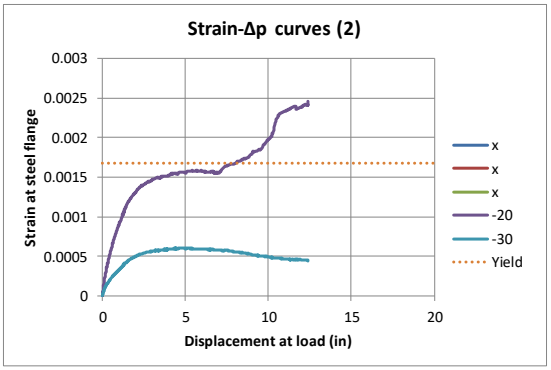

Gage location (in)	10	6	2	-1	x	x	x	-20	-30
Maximum strain	**0.0011**	**0.0014**	**0.0016**	**0.0028**	**0**	**0**	**0**	**0.0014**	**0.0006**
Yield %	64.144	80.633	94.289	164.95	0	0	0	86.166	33.177

Figure C.7 Summary of static test results: T4

Test 2-3 **T5**

* Typical mow strip practice in U.S.
* 3.5" thickness and 24" rear distance behind the post
*

Mow strip configuration	Thickness	**3.5** inch
	Rear Distance	**24** inch
	Modification	**N.A.**

Location	**SEMM Lab, Georgia Tech, Atlanta, GA**
Test date	**7/8/2014**
Temperature	**90** °F
Asphalt age	**18** days from placement

Test drawings

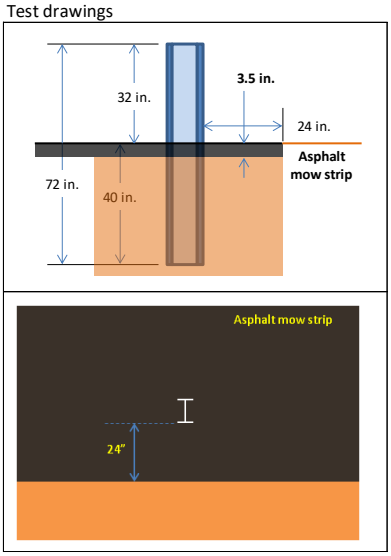

Test pictures

Start

End

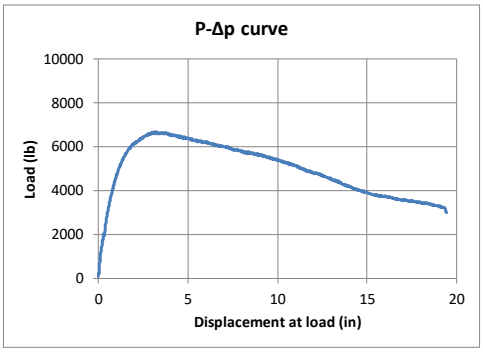

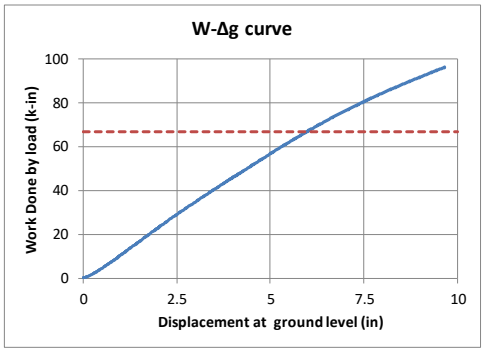

Peak load (lb)	**6662.8**
Δp at peak load (in)	3.1083

Δg at 66.7 k-in work (in)	**5.9724**

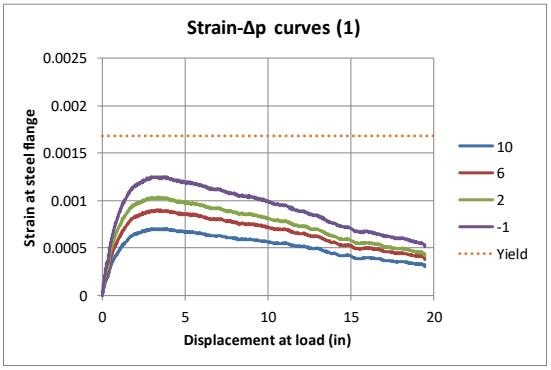

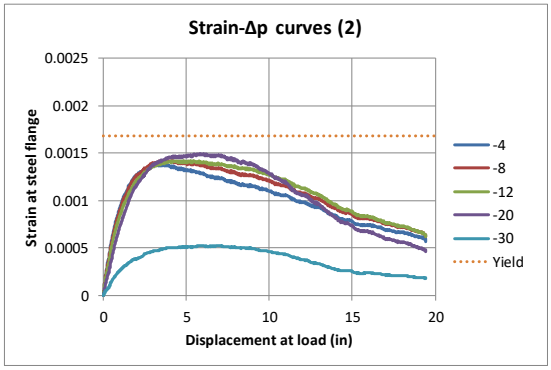

Gage location (in)	10	6	2	-1	-4	-8	-12	-20	-30
Maximum strain	**0.0007**	**0.0009**	**0.001**	**0.0013**	**0.0014**	**0.0014**	**0.0014**	**0.0014**	**0.0005**
Yield %	41.952	53.66	61.673	74.697	82.398	84.249	82.915	84.586	28.64

Figure C.8 Summary of static test results: T5

Test 2-4 **T6**

* Typical mow strip practice in U.S.
* 3.5" thickness and 24" rear distance behind the post
*

Mow strip configuration	Thickness	**3.5** inch
	Rear Distance	**24** inch
	Modification	**N.A.**

Location	**SEMM Lab, Georgia Tech, Atlanta, GA**
Test date	**7/8/2014**
Temperature	**90** °F
Asphalt age	**18** days from placement

Test drawings

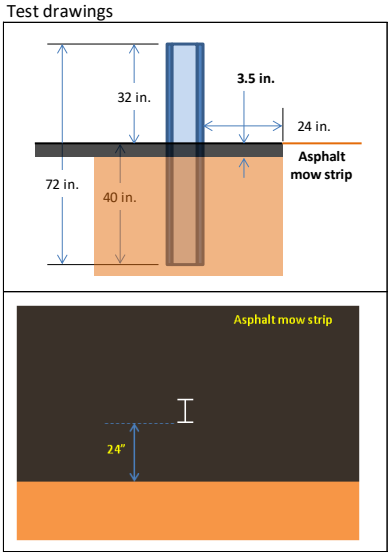

Test pictures

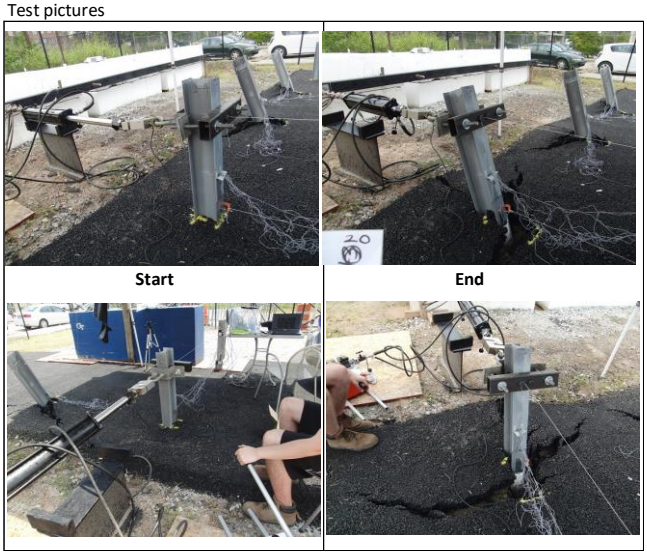

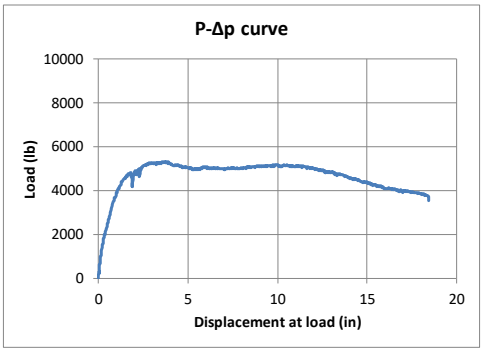

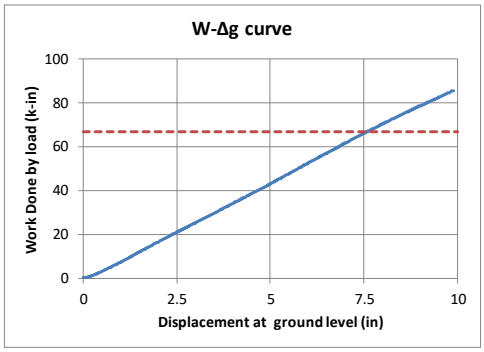

Peak load (lb)	**5317.5**
Δp at peak load (in)	3.5497

Δg at 66.7 k-in work (in)	**7.5782**

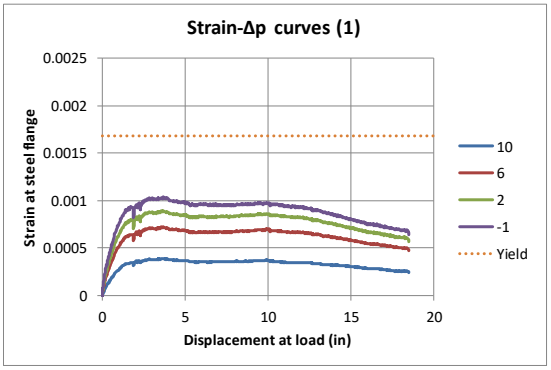

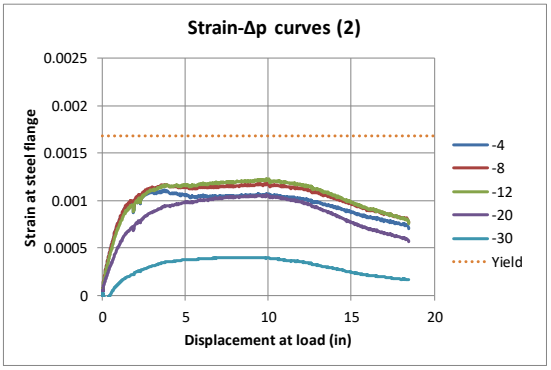

Gage location (in)	10	6	2	-1	-4	-8	-12	-20	-30
Maximum strain	**0.0004**	**0.0007**	**0.0009**	**0.001**	**0.0011**	**0.0012**	**0.0012**	**0.0009**	**0.0004**
Yield %	23.19	43.044	53.186	61.736	65.965	69.619	69.18	56.31	21.144

Figure C.9 Summary of static test results: T6

Test 3-3 **T7**

* Typical mow strip practice in U.S.
* 3.5" thickness and 24" rear distance behind the post
*

Mow strip configuration	Thickness	**3.5** inch
	Rear Distance	**24** inch
	Modification	**N.A.**

Location	**SEMM Lab, Georgia Tech, Atlanta, GA**
Test date	**2/12/2015**
Temperature	**50** °F
Asphalt age	**118** days from placement

Test drawings

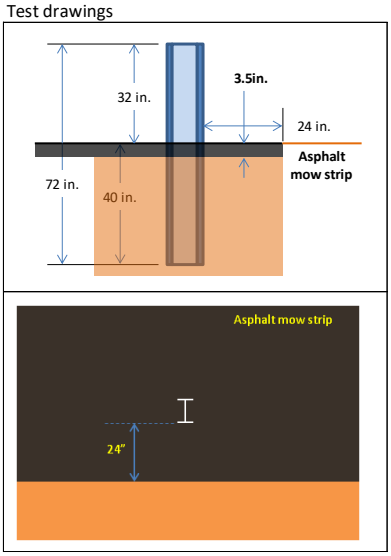

Test pictures

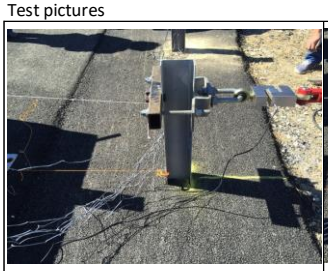

Start

End

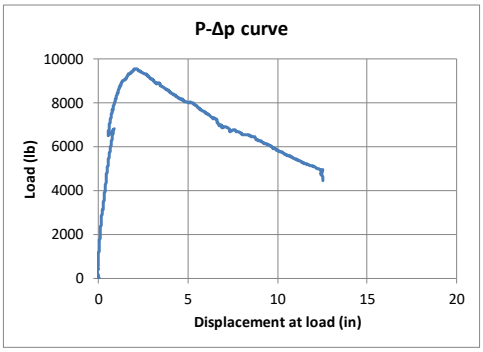

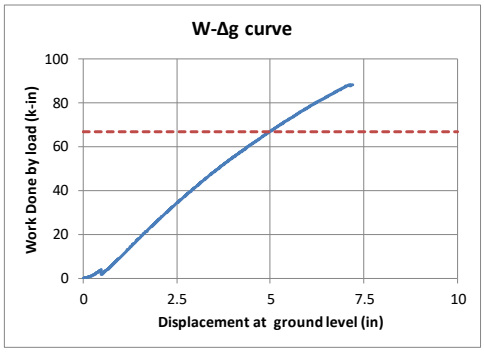

Peak load (lb)	**9553**
Δp at peak load (in)	2.0505

Δg at 66.7 k-in work (in)	**4.9816**

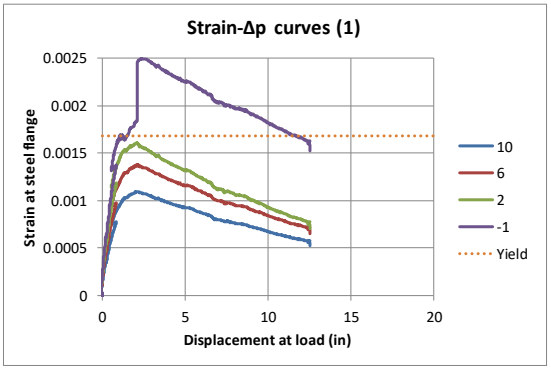

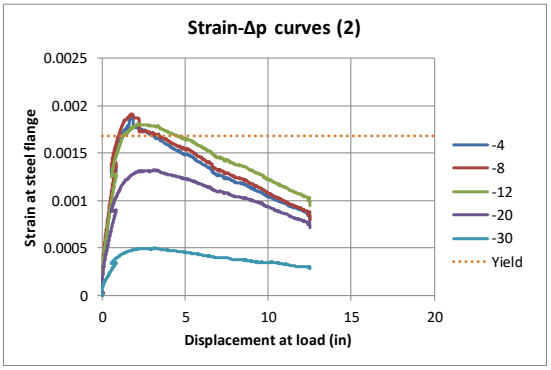

Gage location (in)	10	6	2	-1	-4	-8	-12	-20	-30
Maximum strain	**0.0011**	**0.0014**	**0.0016**	**0.0025**	**0.0018**	**0.0019**	**0.0018**	**0.0013**	**0.0005**
Yield %	65.143	81.827	95.849	147.81	105.99	111.5	107.49	77.869	29.284

Figure C.10 Summary of static test results: T7

Test 3-1 **L1**

* Typical leave-out application
* 18"x18" low strength grout as leave-out material
* Recommended by the AASHTO Roadside Design Guide

Mow strip configuration	Thickness	**3.5** inch
	Rear Distance	**24** inch
	Modification	**Typical grout leave-out**

Location	**SEMM Lab, Georgia Tech, Atlanta, GA**
Test date	**2/12/2015**
Temperature	**50** °F
Asphalt age	**118** days from placement
Grout strength	**105.6** psi (28-day comp. strength less than 120 psi)

Test drawings

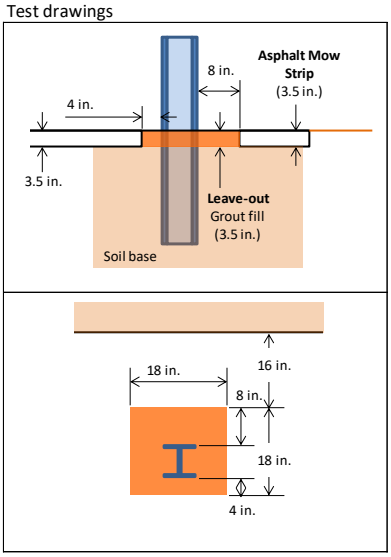

Test pictures

Start

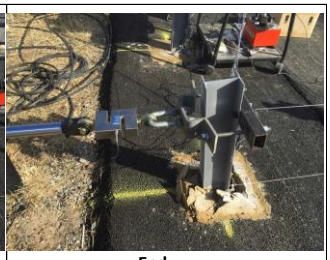

End

The 3-1 test was terminated earlier than expected due to the malfunction of hydraulic cylinder.

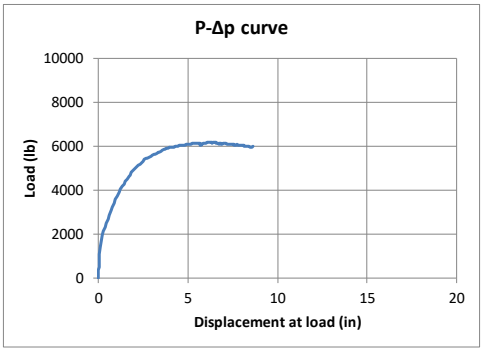

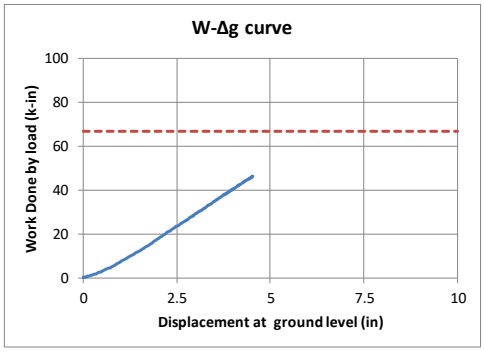

Peak load (lb)	**6181.3**
Δp at peak load (in)	6.1802

Δg at 66.7 k-in work (in)	**6.353**	* expected value

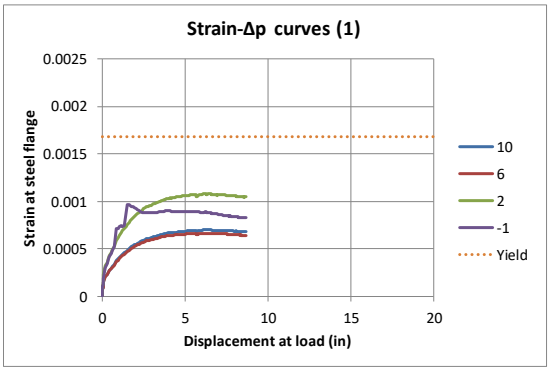

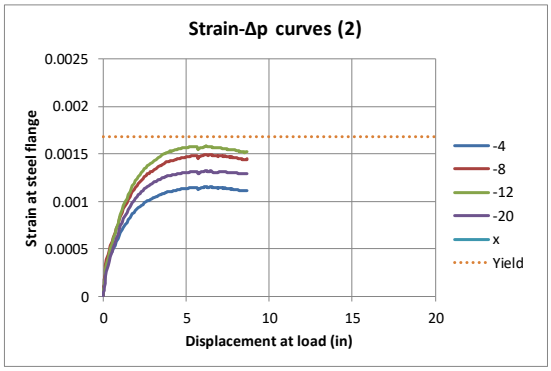

Gage location (in)	10	6	2	-1	-4	-8	-12	-20	x
Maximum strain	**0.0007**	**0.0007**	**0.0011**	**0.0009**	**0.0012**	**0.0015**	**0.0016**	**0.0013**	**0**
Yield %	41.843	39.695	64.4	52.882	68.733	89.025	94.111	78.688	0

Figure C.11 Summary of static test results: L1

Test 3-2 **L2**

* Typical leave-out application
* 18"x18" low strength grout as leave-out material
* Recommended by the AASHTO Roadside Design Guide

Mow strip configuration	Thickness	**3.5** inch
	Rear Distance	**24** inch
	Modification	**Typical grout leave-out**

Location	**SEMM Lab, Georgia Tech, Atlanta, GA**
Test date	**2/12/2015**
Temperature	**50** °F
Asphalt age	**118** days from placement
Grout strength	**105.6** psi (28-day comp. strength less than 120 psi)

Test drawings

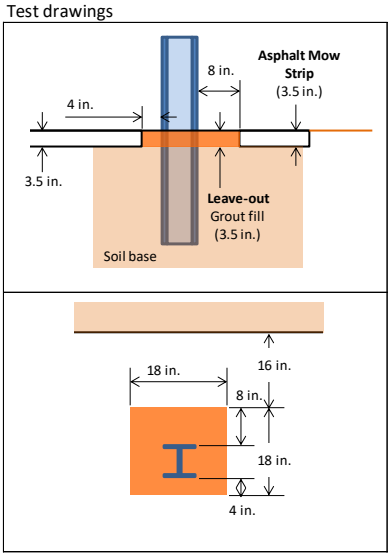

Test pictures

Start

End

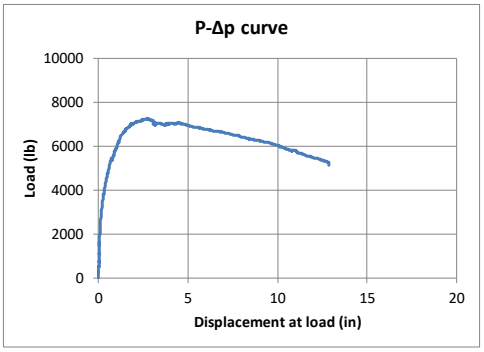

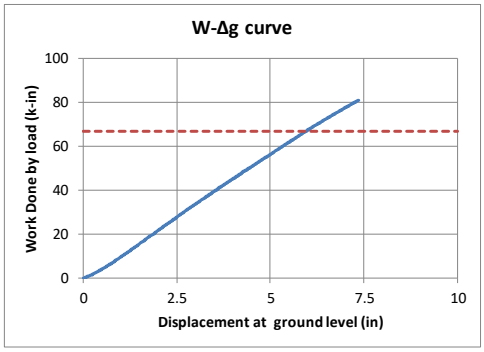

Peak load (lb)	**7261.6**
Δp at peak load (in)	2.7534

Δg at 66.7 k-in work (in)	**5.9496**

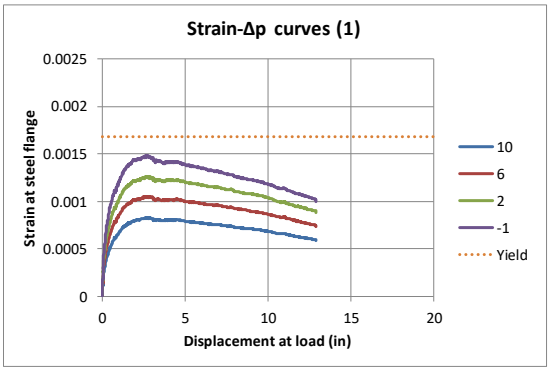

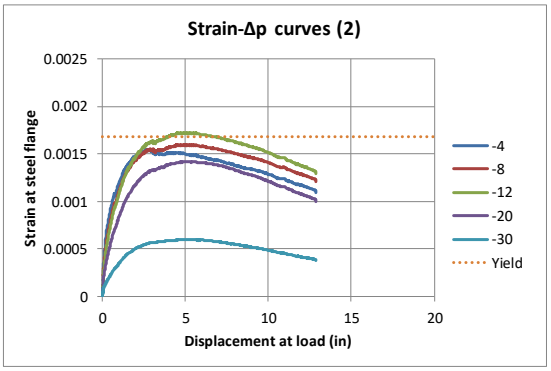

Gage location (in)	10	6	2	-1	-4	-8	-12	-20	-30
Maximum strain	**0.0008**	**0.0011**	**0.0013**	**0.0015**	**0.0015**	**0.0016**	**0.0016**	**0.0013**	**0.0006**
Yield %	49.478	62.643	75.158	88.106	92.142	92.349	97.574	79.691	34.048

Figure C.12 Summary of static test results: L2

Test 5-3 **L3**

* Typical leave-out application
* 18"x18" low strength grout as leave-out material
* Recommended by the AASHTO Roadside Design Guide

Mow strip configuration	Thickness	**3.5** inch
	Rear Distance	**24** inch
	Modification	**Typical grout leave-out**

Location	**SEMM Lab, Georgia Tech, Atlanta, GA**
Test date	**7/14/2015**
Temperature	**70** °F
Asphalt age	**32** days from placement
Grout strength	**55.23** psi (28-day comp. strength less than 120 psi)

Test drawings

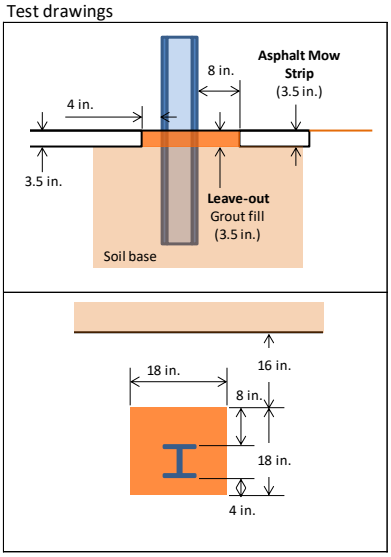

Test pictures

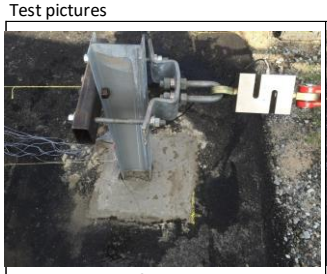

Start

End

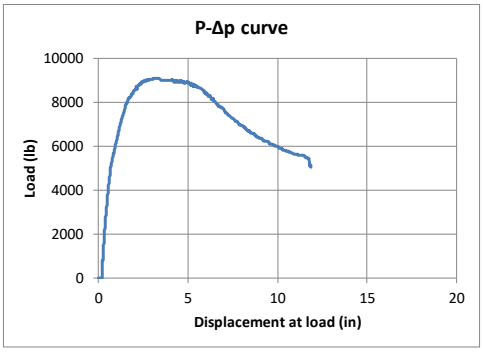

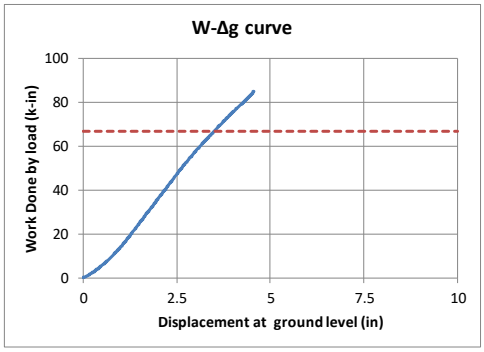

Peak load (lb)	**9096.2**
Δp at peak load (in)	3.1116

Δg at 66.7 k-in work (in)	**3.4974**

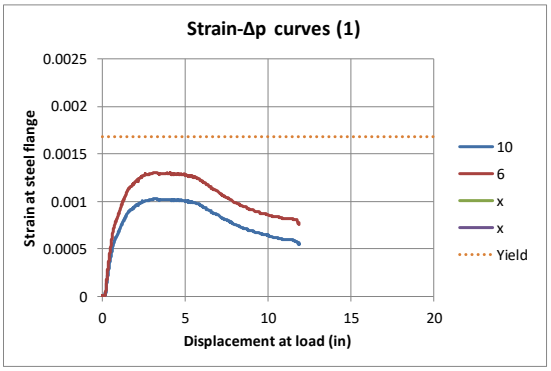

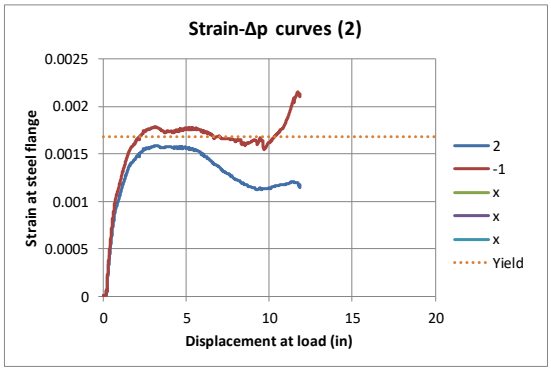

Gage location (in)	10	6	x	x	2	-1	x	x	x
Maximum strain	**0.001**	**0.0013**	**0**	**0**	**0.0016**	**0.0018**	**0**	**0**	**0**
Yield %	61.11	77.549	0	0	94.367	106.36	0	0	0

Figure C.13 Summary of static test results: L3

Test 4-4 **R1**

* Reduced rear distance design
* 2" thickness and 6" rear distance behind the post
*

Mow strip configuration	Thickness	**2** inch
	Rear Distance	**6** inch
	Modification	**N.A.**

Location	**SEMM Lab, Georgia Tech, Atlanta, GA**
Test date	**5/5/2015**
Temperature	**75** °F
Asphalt age	**40** days from placement

Test drawings

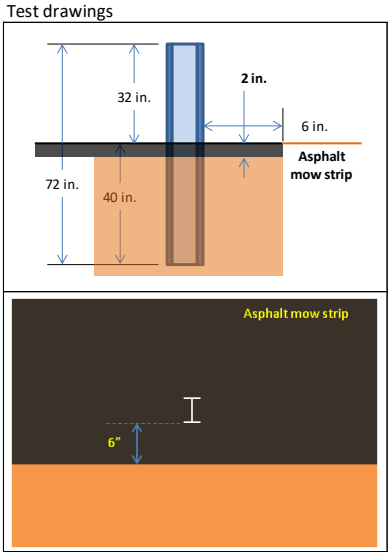

Test pictures

Start

End

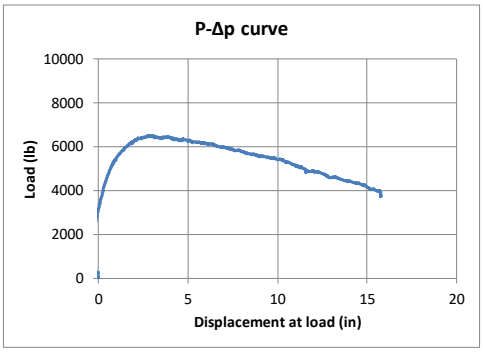

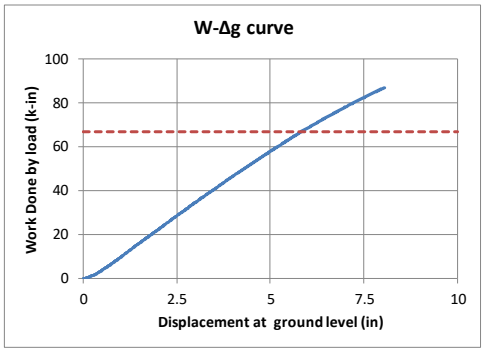

Peak load (lb)	**6492.3**
Δp at peak load (in)	2.9432

Δg at 66.7 k-in work (in)	**5.8172**

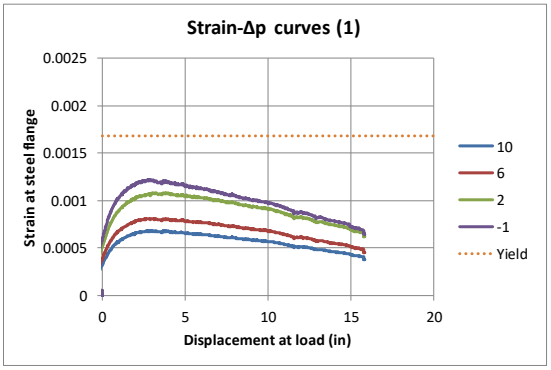

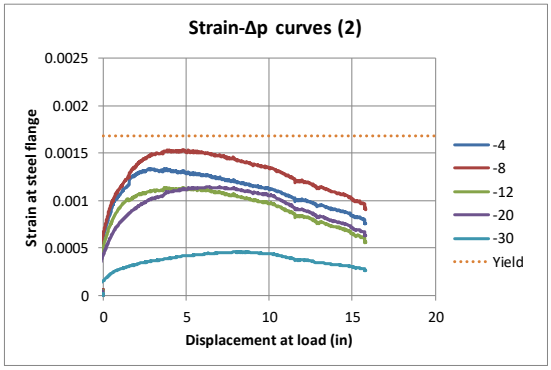

Gage location (in)	10	6	2	-1	-4	-8	-12	-20	-30
Maximum strain	**0.0007**	**0.0008**	**0.0011**	**0.0012**	**0.0013**	**0.0015**	**0.0011**	**0.001**	**0.0004**
Yield %	40.628	48.393	64.587	72.555	79.703	89.104	66.013	61.609	22.13

Figure C.14 Summary of static test results: R1

Test 4-1 **R2**

* Reduced rear distance design
* 2" thickness and 12" rear distance behind the post
*

Mow strip configuration	Thickness	**2** inch
	Rear Distance	**12** inch
	Modification	**N.A.**

Location	**SEMM Lab, Georgia Tech, Atlanta, GA**
Test date	**5/5/2015**
Temperature	**75** °F
Asphalt age	**40** days from placement

Test drawings

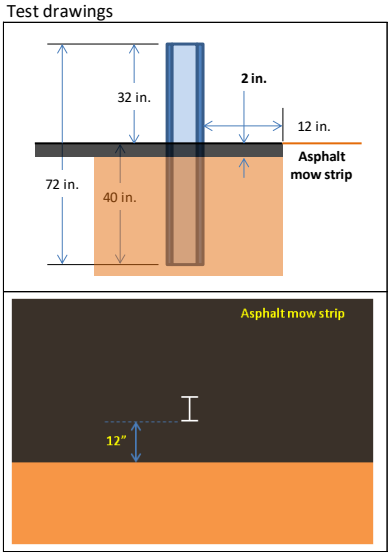

Test pictures

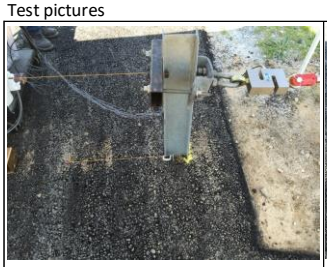

Start

End

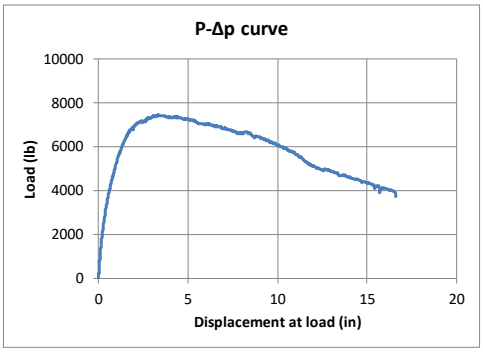

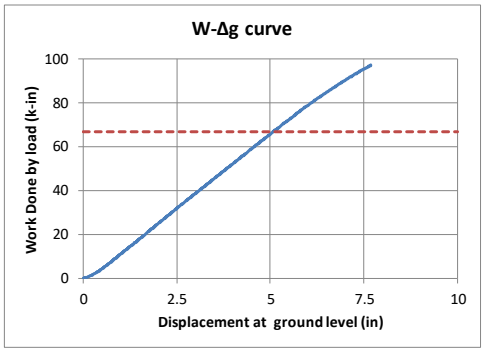

Peak load (lb)	**7429.3**
Δp at peak load (in)	3.329

Δg at 66.7 k-in work (in)	**5.0702**

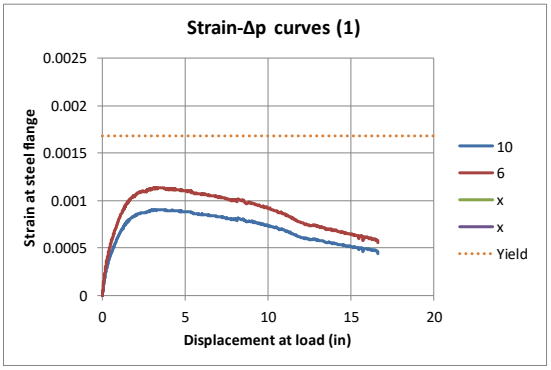

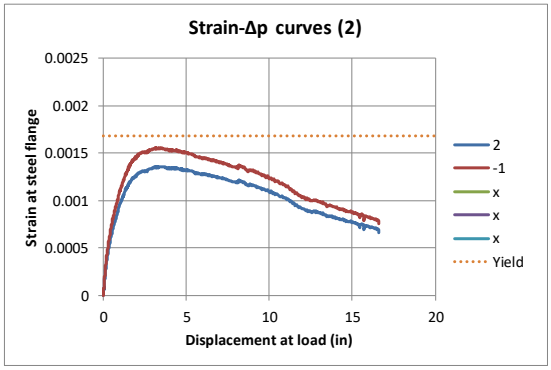

Gage location (in)	10	6	x	x	2	-1	x	x	x
Maximum strain	**0.0009**	**0.0011**	**0**	**0**	**0.0014**	**0.0016**	**0**	**0**	**0**
Yield %	53.97	67.591	0	0	80.772	92.432	0	0	0

Figure C.15 Summary of static test results: R2

Test 5-2 **R3**

* Reduced rear distance design
* 3.5" thickness and 12" rear distance behind the post
*

Mow strip configuration	Thickness	**3.5** inch
	Rear Distance	**12** inch
	Modification	**N.A.**

Location	**SEMM Lab, Georgia Tech, Atlanta, GA**
Test date	**7/14/2015**
Temperature	**70** °F
Asphalt age	**32** days from placement

Test drawings

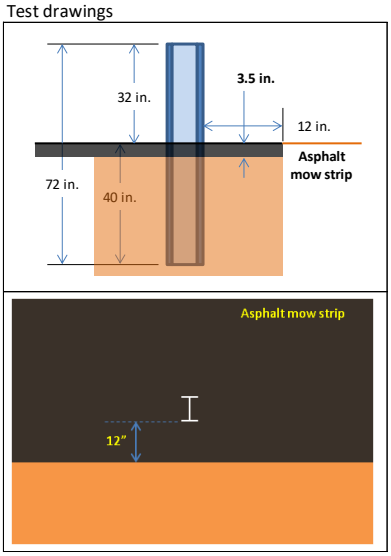

Test pictures

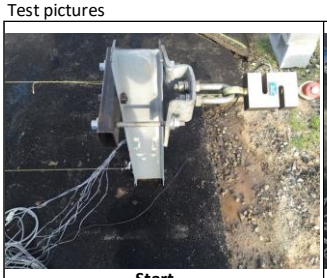

Start

End

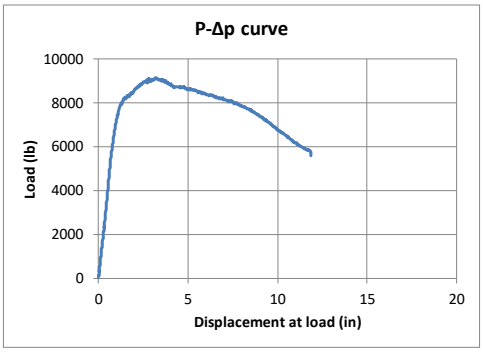

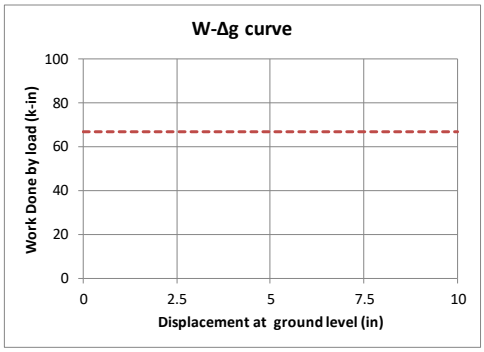

Peak load (lb)	**9135.5**
Δp at peak load (in)	3.1831

Δg at 66.7 k-in work (in)	**Dg record not available**

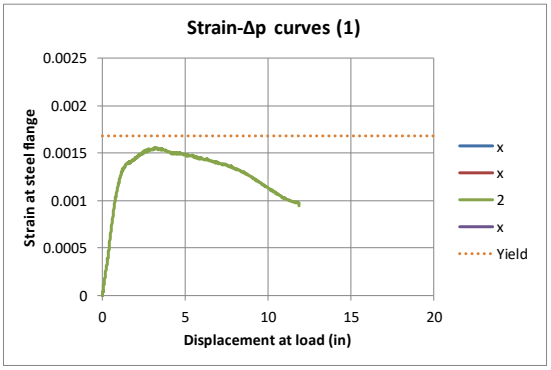

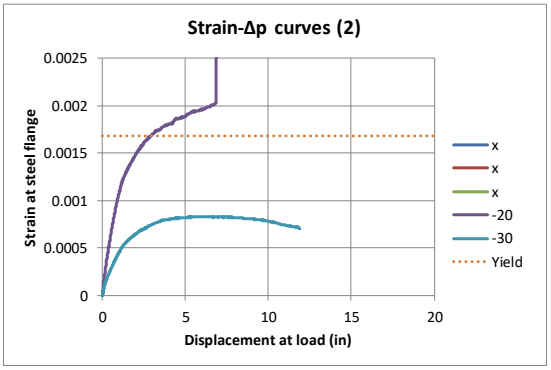

Gage location (in)	x	x	2	x	x	x	x	-20	-30
Maximum strain	**0**	**0**	**0.0016**	**0**	**0**	**0**	**0**	**0.0017**	**0.0008**
Yield %	0	0	92.831	0	0	0	0	102.94	45.553

Figure C.16 Summary of static test results: R3

Test 4-2 **P1**

* Pre-cut mow strip design
* 2" thickness and 24" rear distance behind the post
* Parallel pre-cut pattern

Mow strip configuration	Thickness	**2** inch
	Rear Distance	**24** inch
	Modification	**Pre-cutting**

Location	**SEMM Lab, Georgia Tech, Atlanta, GA**
Test date	**5/5/2015**
Temperature	**75** °F
Asphalt age	**40** days from placement

Test drawings

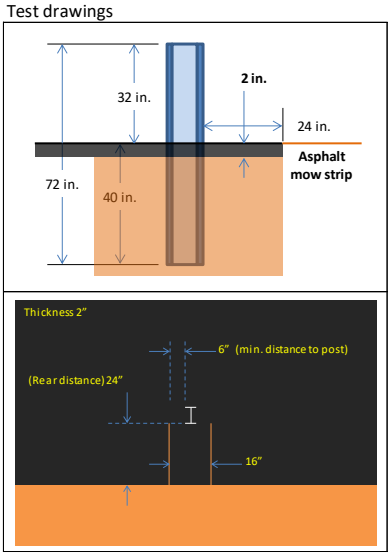

Test pictures

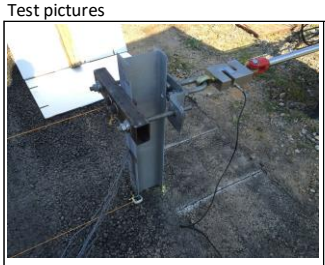

Start

End

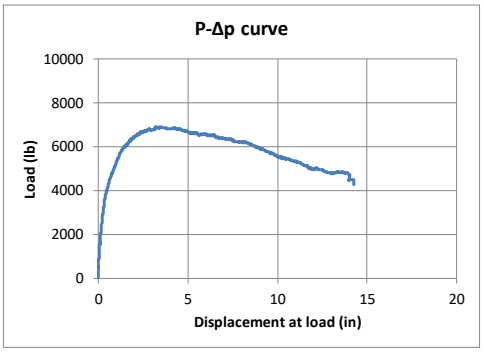

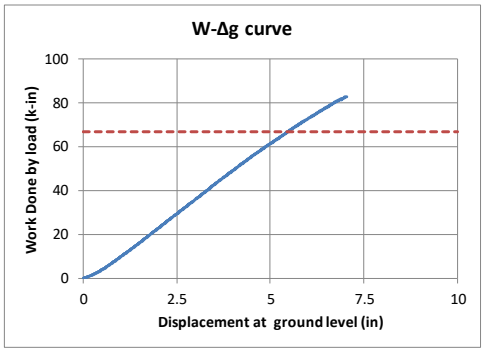

Peak load (lb)	**6912.2**
Δp at peak load (in)	3.2207

Δg at 66.7 k-in work (in)	**5.4621**

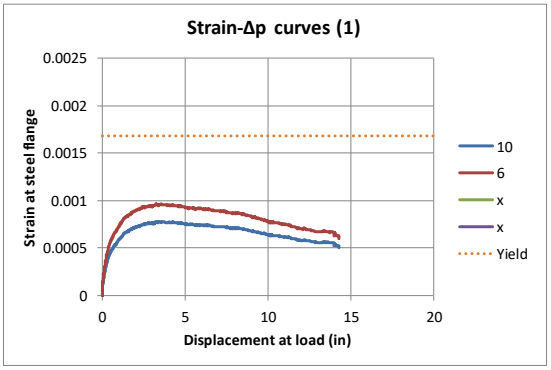

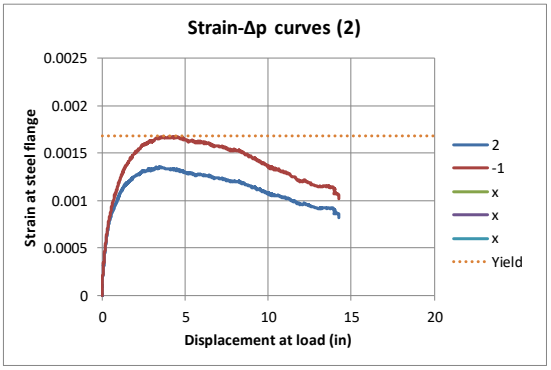

Gage location (in)	10	6	x	x	2	-1	x	x	x
Maximum strain	**0.0008**	**0.001**	**0**	**0**	**0.0014**	**0.0017**	**0**	**0**	**0**
Yield %	46.257	57.211	0	0	80.514	98.841	0	0	0

Figure C.17 Summary of static test results: P1

Test 5-1 **P2**

* Pre-cut mow strip design
* 3.5" thickness and 24" rear distance behind the post
* Diagonal pre-cut pattern

Mow strip configuration	Thickness	**3.5** inch
	Rear Distance	**24** inch
	Modification	**Pre-cutting**

Location	**SEMM Lab, Georgia Tech, Atlanta, GA**
Test date	**7/14/2015**
Temperature	**70** °F
Asphalt age	**32** days from placement

Test drawings

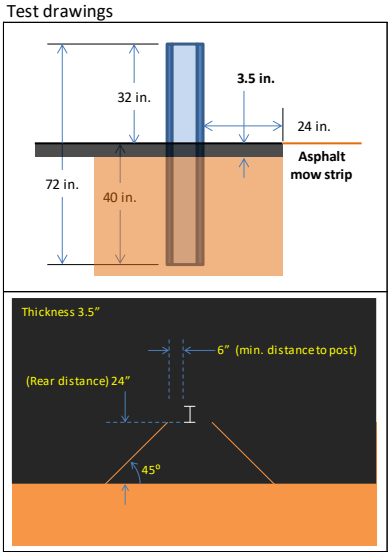

Test pictures

Start

End

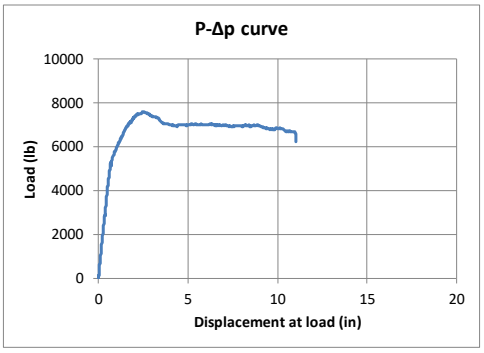

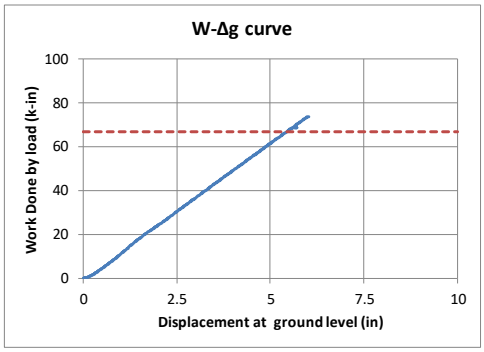

Peak load (lb)	**7577.1**
Δp at peak load (in)	2.4996

Δg at 66.7 k-in work (in)	**5.4293**

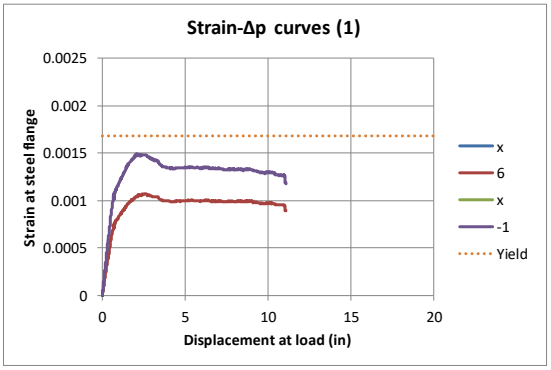

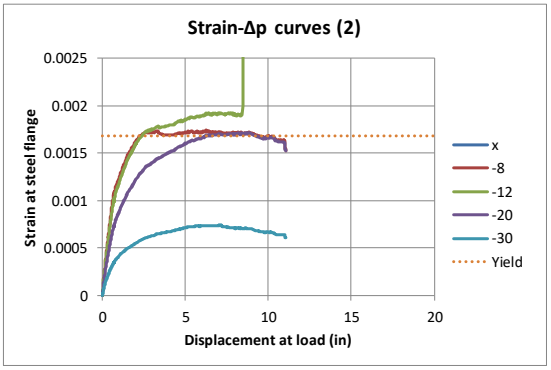

Gage location (in)	x	6	x	-1	x	-8	-12	-20	-30
Maximum strain	**0**	**0.0011**	**0**	**0.0015**	**0**	**0.0017**	**0.0017**	**0.0014**	**0.0006**
Yield %	0	63.687	0	88.291	0	102.81	103.85	82.141	36.86

Figure C.18 Summary of static test results: P2

Test 5-4 **P3**

* Pre-cut mow strip design
* 3.5" thickness and 24" rear distance behind the post
* Diagonal pre-cut pattern with asphalt sealer application

Mow strip configuration	Thickness	**3.5** inch
	Rear Distance	**24** inch
	Modification	**Pre-cutting and sealing**

Location	**SEMM Lab, Georgia Tech, Atlanta, GA**
Test date	**7/14/2015**
Temperature	**70** °F
Asphalt age	**32** days from placement

Test drawings

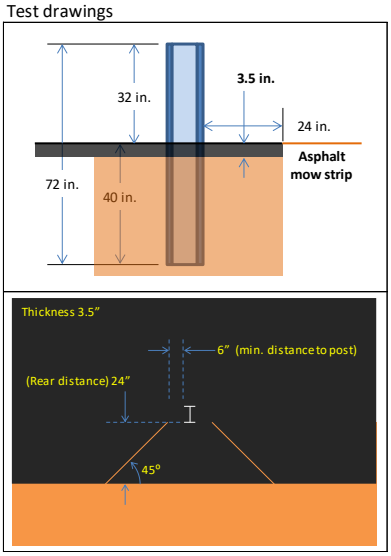

Test pictures

Start

End

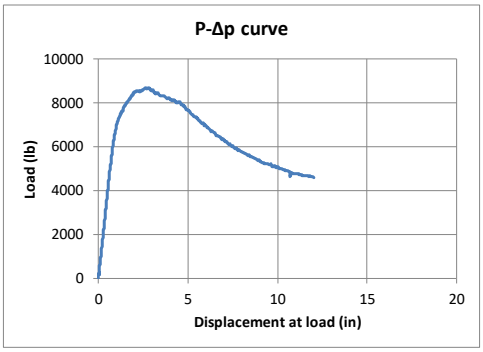

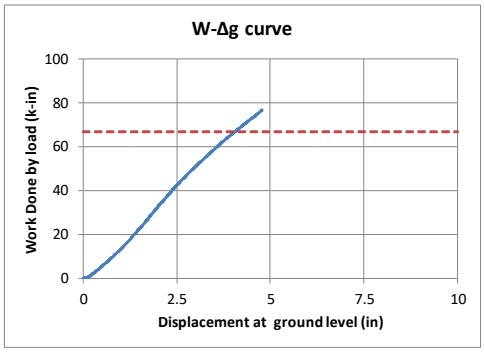

Peak load (lb)	**8688.9**
Δp at peak load (in)	2.6309

Δg at 66.7 k-in work (in)	**4.0483**

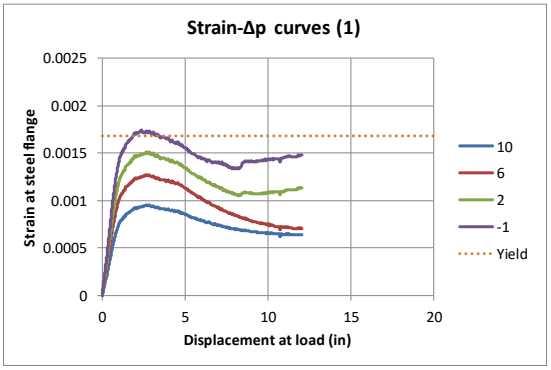

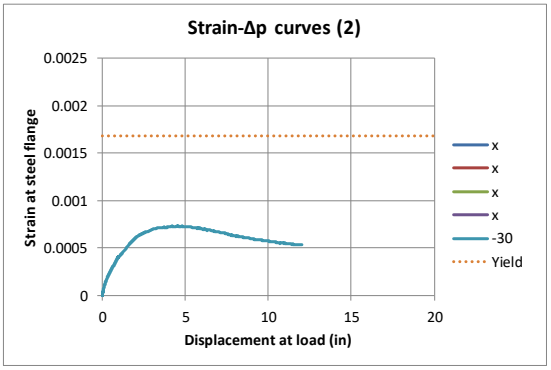

Gage location (in)	10	6	2	-1	x	x	x	x	-30
Maximum strain	**0.001**	**0.0013**	**0.0015**	**0.0017**	**0**	**0**	**0**	**0**	**0.0007**
Yield %	56.903	75.869	90.121	103.35	0	0	0	0	40.957

Figure C.19 Summary of static test results: P3

C.2 Dynamic test record sheets

Dynamic Test #13 **Baseline**

* Baseline configuration
* No mow strip
*

Mow strip configuration	Thickness	0 in.
	Rear Distance	0 in.
	Modification	N.A.

Impact conditions		
Speed	**15.0** m/s	32.4 mph
Mass	**139** kg	305.8 lb.
KE	15638 J	137.65 kip-in.

Test location	**SEMM Lab, Georgia Tech, Atlanta, GA**
Test date	**1/26/2017**
Temperature	**71** °F 21.7 °C
Asphalt age	N.A.

Test configuration drawings

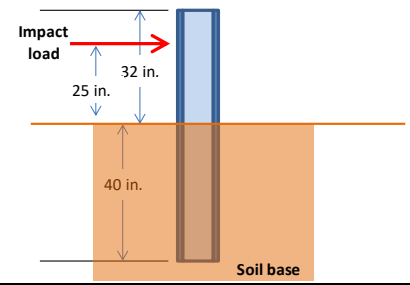

Sequential test pictures

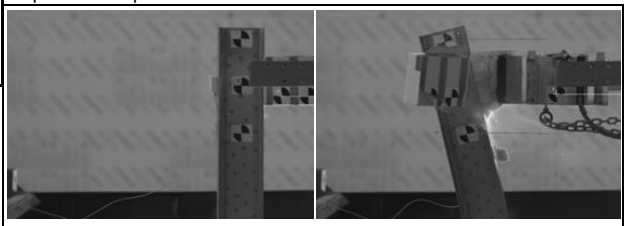

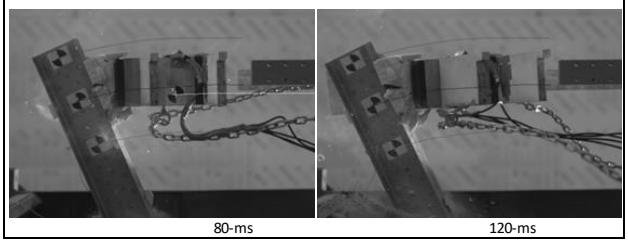

End of test pictures

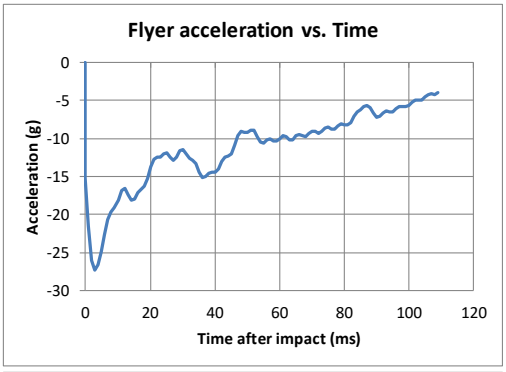

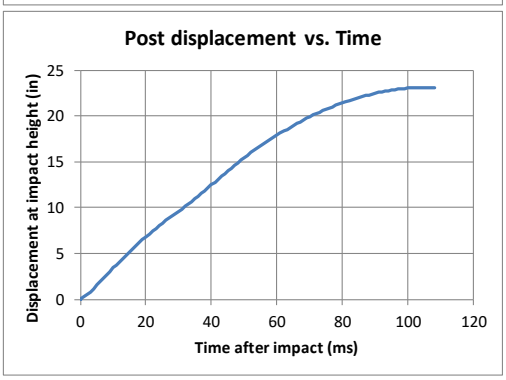

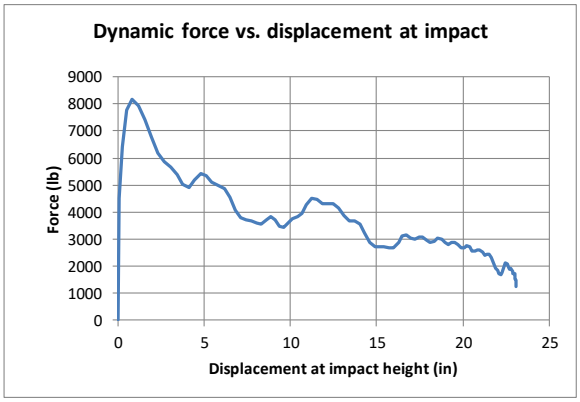

Peak flyer acceleration (g)	-27.36
Impact duration (ms)	109
time at peak acceleration (ms)	3
Max. displacement at impact (in)	23.11
Peak dynamic force (lb)	8154

Figure C.20 Summary of dynamic test results: baseline

Dynamic Test #6 **Typical mow strip**

* 3.5" thickness and 24" rear distance behind the post
*
*

Mow strip configuration	Thickness	3.5	in.
	Rear Distance	24	in.
	Modification	N.A.	

Impact conditions			
Speed	**15.0** m/s	32.4	mph
Mass	**139** kg	305.8	lb.
KE	15638 J	137.65	kip-in.

Test location	**SEMM Lab, Georgia Tech, Atlanta, GA**
Test date	**12/19/2016**
Temperature	**66** °F 18.9 °C
Asphalt age	**14** days from placement

Test configuration drawings

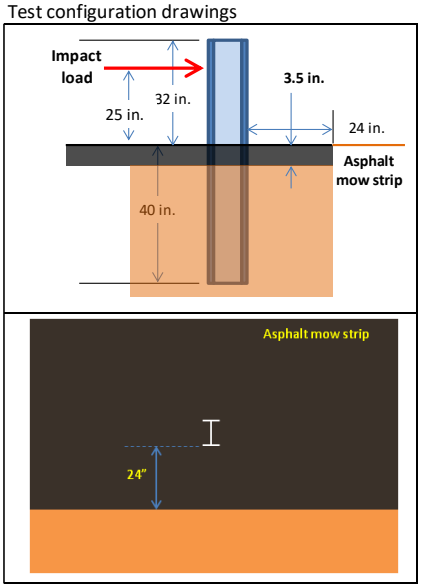

Sequential test pictures

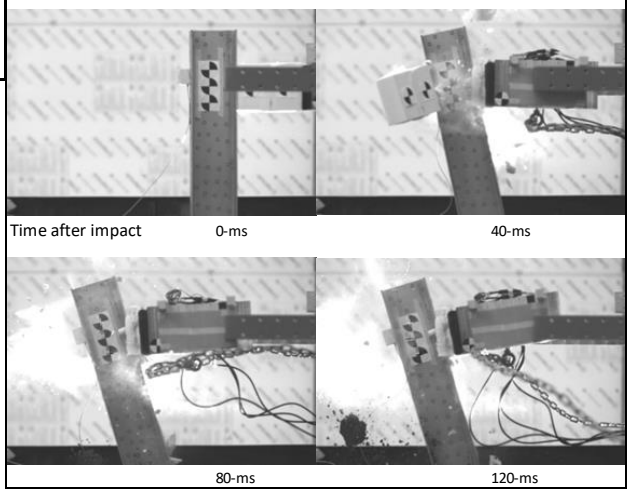

End of test pictures

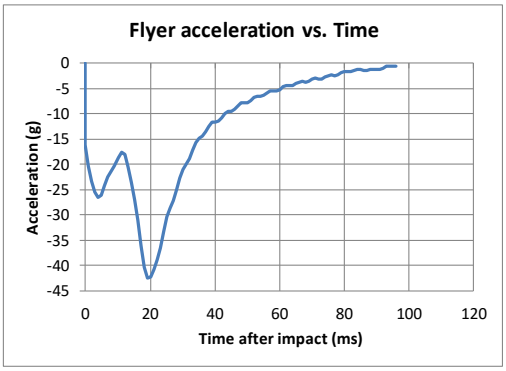

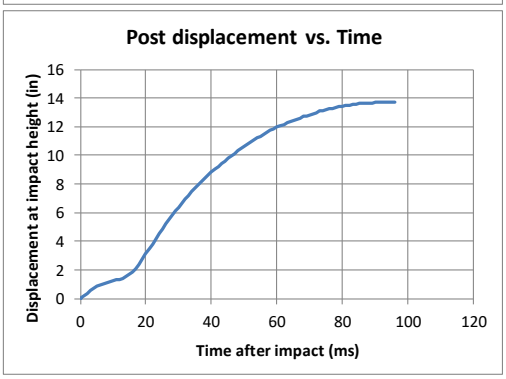

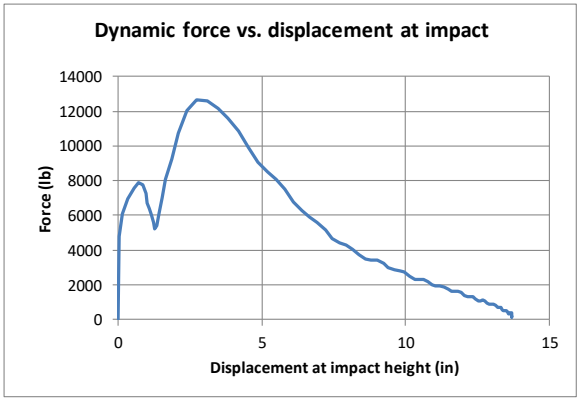

Peak flyer acceleration (g)	-42.53
Impact duration (ms)	96
time at peak acceleration (ms)	19
Max. displacement at impact (in)	13.71
Peak dynamic force (lb)	12677

Figure C.21 Summary of dynamic test results: typical mow strip

Dynamic Test #12 **Leave-out**

* Typical leave-out application
* 18"x18" low strength grout as leave-out material
* Recommended by the AASHTO Roadside Design Guide

Mow strip configuration	Thickness	3.5 in.
	Rear Distance	24 in.
	Modification	Typical grout leave-out

Impact conditions		
Speed	**15.0** m/s	32.4 mph
Mass	**139** kg	305.8 lb.
KE	15638 J	137.65 kip-in.

Test location	**SEMM Lab, Georgia Tech, Atlanta, GA**
Test date	**1/26/2017**
Temperature	**71** °F 21.7 °C
Asphalt age	**13** days from placement

Test configuration drawings

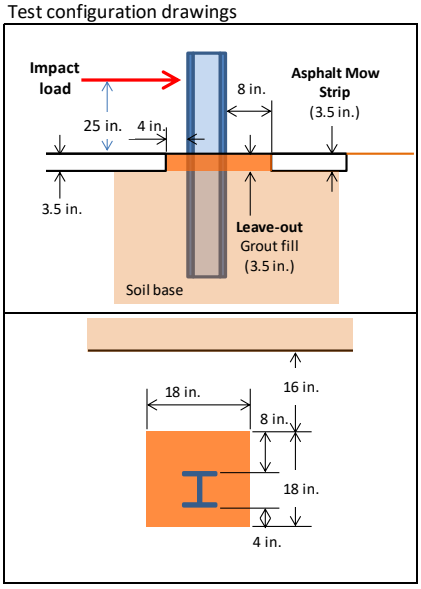

Sequential test pictures

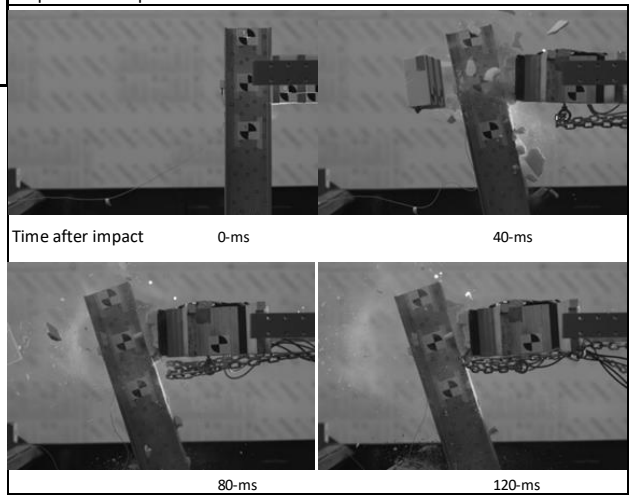

End of test pictures

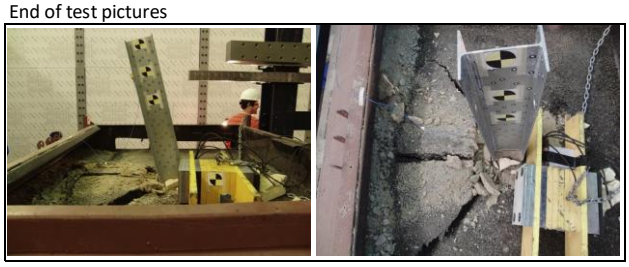

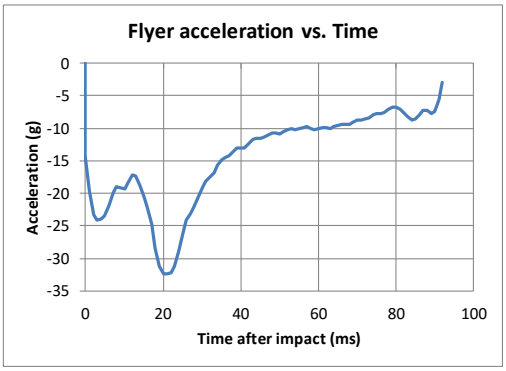

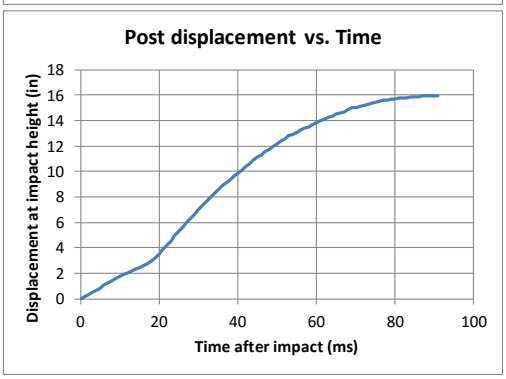

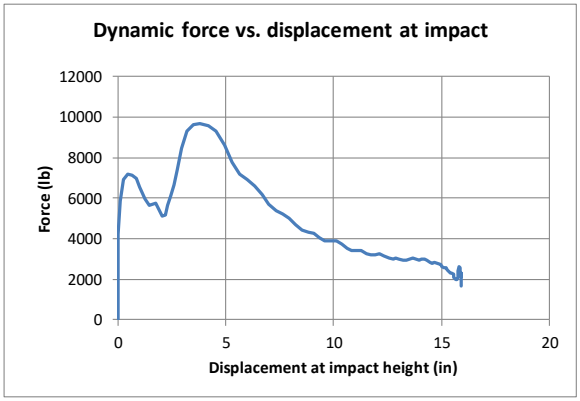

Peak flyer acceleration (g)	-32.38
Impact duration (ms)	92
Time at peak acceleration (ms)	21
Max. displacement at impact (in)	15.91
Peak dynamic force (lb)	9650

Figure C.22 Summary of dynamic test results: leave-out installation

Dynamic Test #8 **Pre-cut (parallel)**

* Pre-cut mow strip design
* 3.5" thickness and 24" rear distance behind the post
* Parallel pre-cut pattern

Mow strip configuration	Thickness	3.5 in.
	Rear Distance	24 in.
	Modification	Pre-cut application (parallel)

Impact conditions		
Speed	**15.0** m/s	32.4 mph
Mass	**139** kg	305.8 lb.
KE	15638 J	137.65 kip-in.

Test location	**SEMM Lab, Georgia Tech, Atlanta, GA**
Test date	**12/20/2016**
Temperature	**68** °F 20 °C
Asphalt age	**13** days from placement

Sequential test pictures

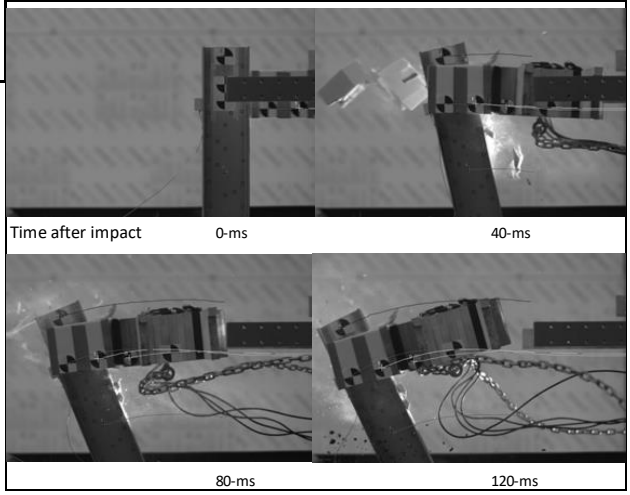

Test configuration drawings

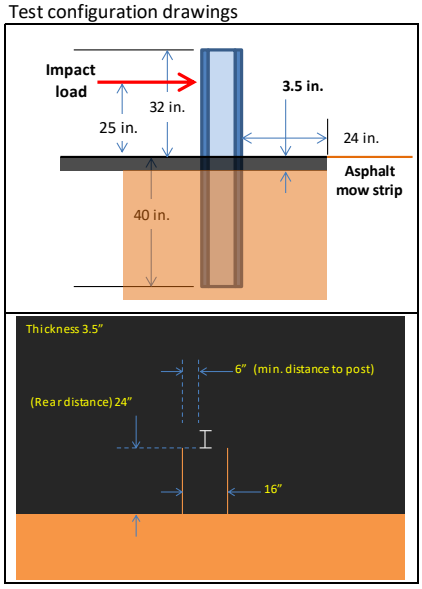

End of test pictures

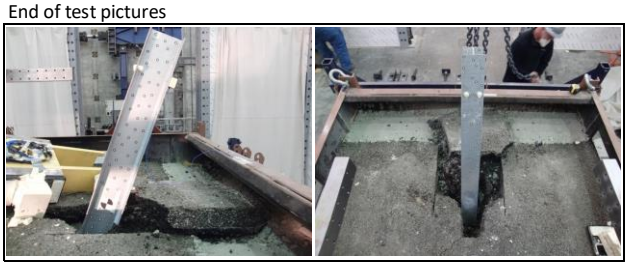

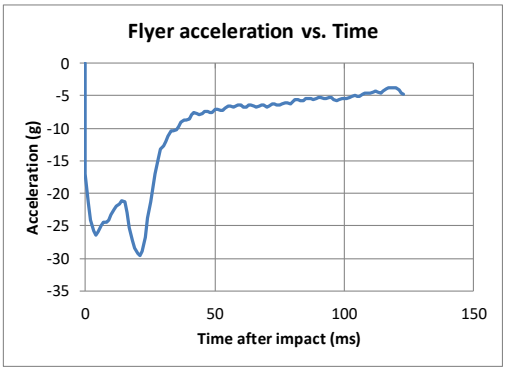

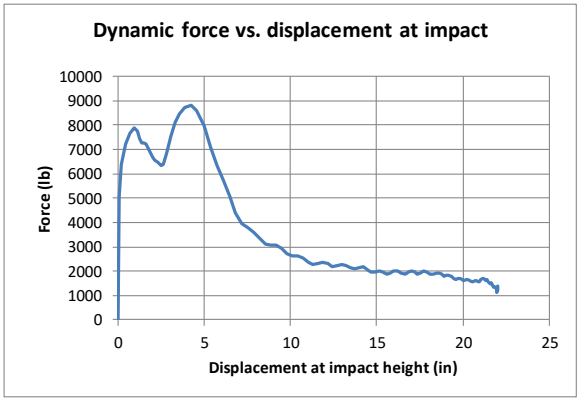

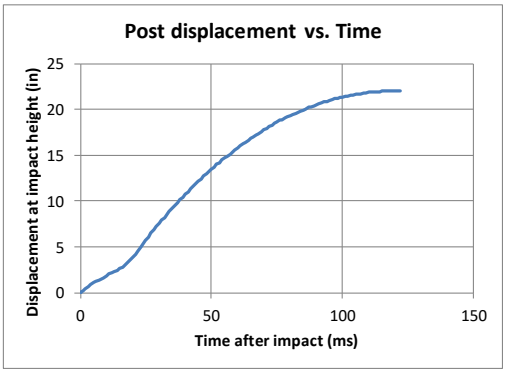

Peak flyer acceleration (g)	-29.60
Impact duration (ms)	123
time at peak acceleration (ms)	21
Max. displacement at impact (in)	22.00
Peak dynamic force (lb)	8821

Figure C.23 Summary of dynamic test results: parallel pre-cut

Dynamic Test #10 **Pre-cut (diagonal)**

* Pre-cut mow strip design
* 3.5" thickness and 24" rear distance behind the post
* Diagonal pre-cut pattern

Mow strip configuration	Thickness	3.5 in.
	Rear Distance	24 in.
	Modification	N.A.

Impact conditions		
Speed	**15.0** m/s	32.4 mph
Mass	**139** kg	305.8 lb.
KE	15638 J	137.65 kip-in.

Test location	**SEMM Lab, Georgia Tech, Atlanta, GA**
Test date	**1/5/2017**
Temperature	**71** °F 21.7 °C
Asphalt age	**16** days from placement

Test configuration drawings

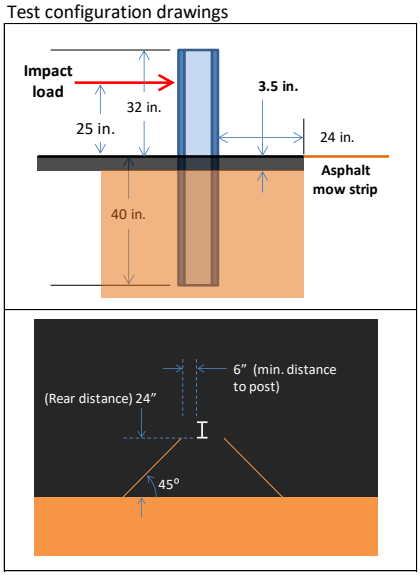

Sequential test pictures

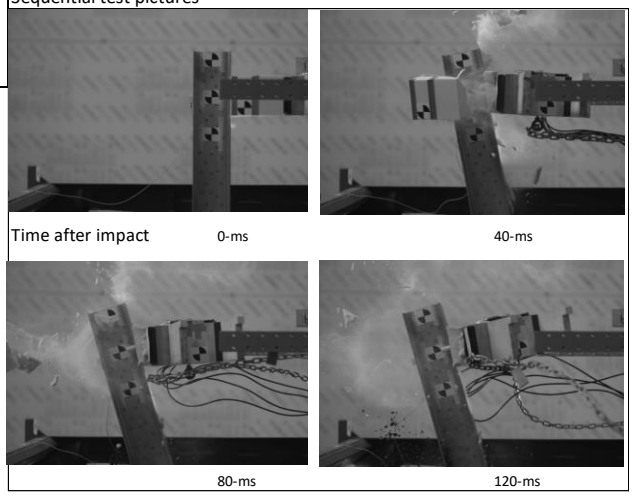

End of test pictures

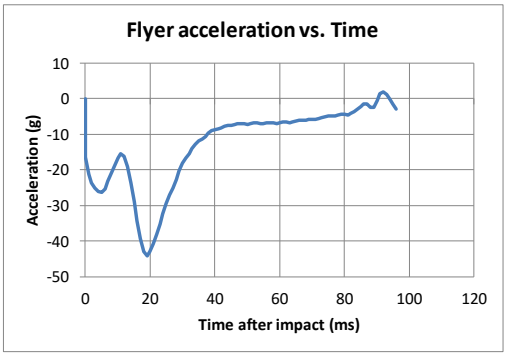

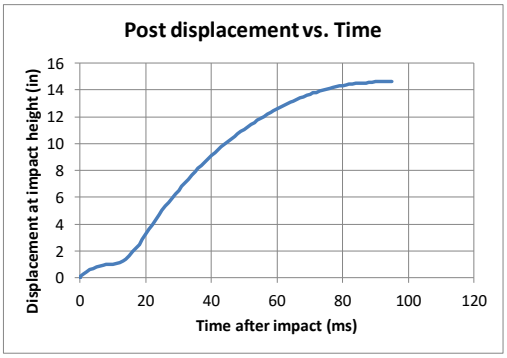

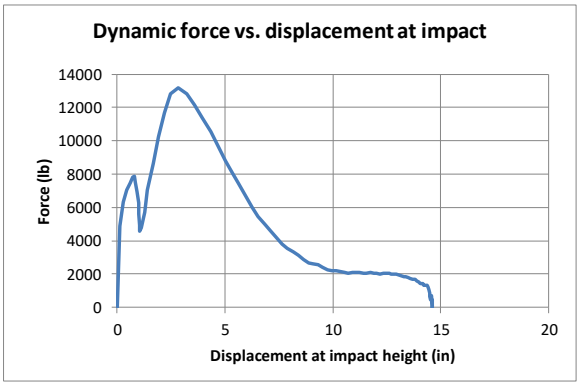

Peak flyer acceleration (g)	-44.22
Impact duration (ms)	96
time at peak acceleration (ms)	19
Max. displacement at impact (in)	14.61
Peak dynamic force (lb)	13180

Figure C.24 Summary of dynamic test results: diagonal pre-cut

Dynamic Test #9 **Thin mow strip**

* 1.5" thickness and 24" rear distance behind the post
*
*

Mow strip configuration	Thickness	1.5 in.
	Rear Distance	24 in.
	Modification	N.A.

Impact conditions		
Speed	**15.0** m/s	32.4 mph
Mass	**139** kg	305.8 lb.
KE	15638 J	137.65 kip-in.

Test location	**SEMM Lab, Georgia Tech, Atlanta, GA**
Test date	**1/5/2017**
Temperature	**71** °F 21.7 °C
Asphalt age	**16** days from placement

Test configuration drawings

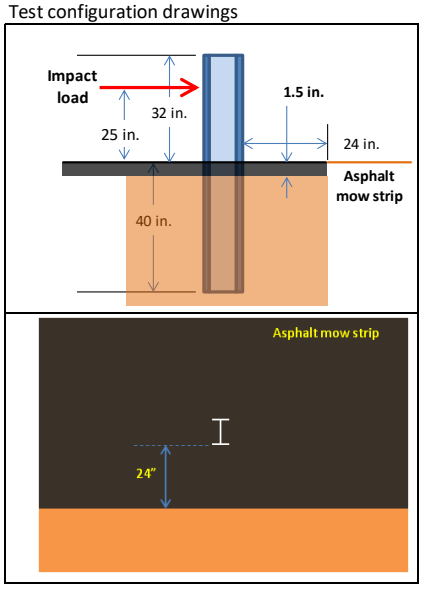

Sequential test pictures

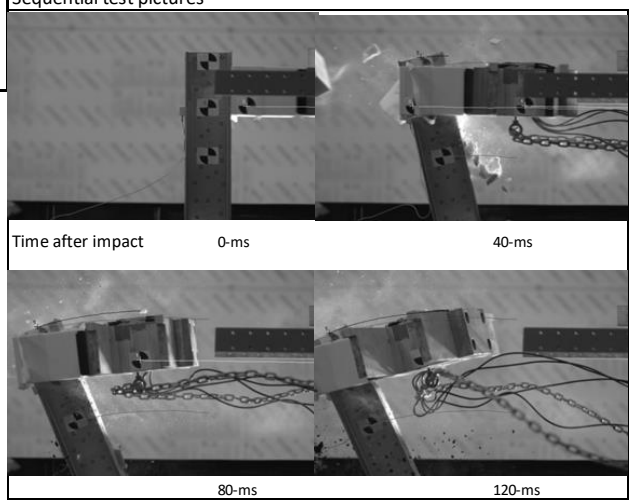

End of test pictures

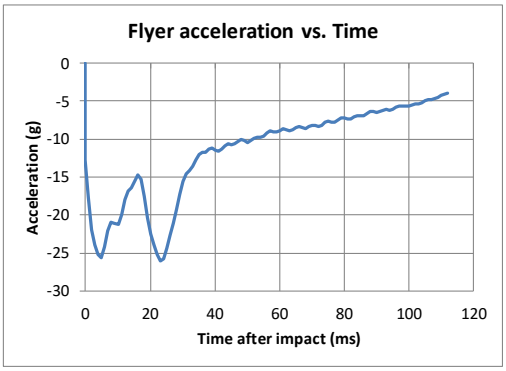

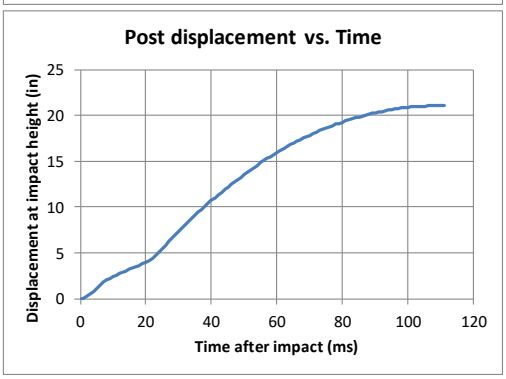

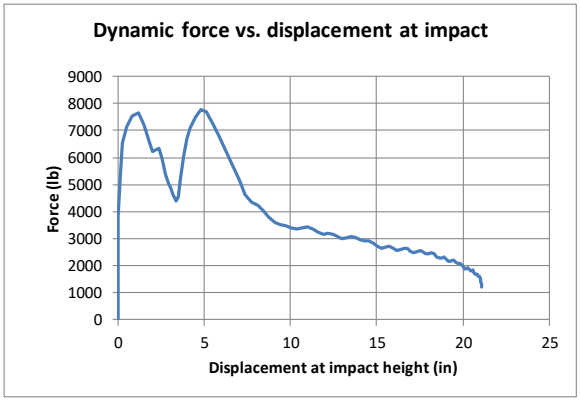

Peak flyer acceleration (g)	-26.07
Impact duration (ms)	112
time at peak acceleration (ms)	23
Max. displacement at impact (in)	21.08
Peak dynamic force (lb)	7771

Figure C.25 Summary of dynamic test results: thin mow strip

Dynamic Test #11 **Thick mow strip**

* 5.5" thickness and 24" rear distance behind the post
*
*

Mow strip configuration	Thickness	5.5	in.
	Rear Distance	24	in.
	Modification	N.A.	

Impact conditions			
Speed	**15.0** m/s	32.4	mph
Mass	**139** kg	305.8	lb.
KE	15638 J	137.65	kip-in.

Test location	**SEMM Lab, Georgia Tech, Atlanta, GA**
Test date	**1/6/2017**
Temperature	**71** °F 21.7 °C
Asphalt age	**16** days from placement

Test configuration drawings

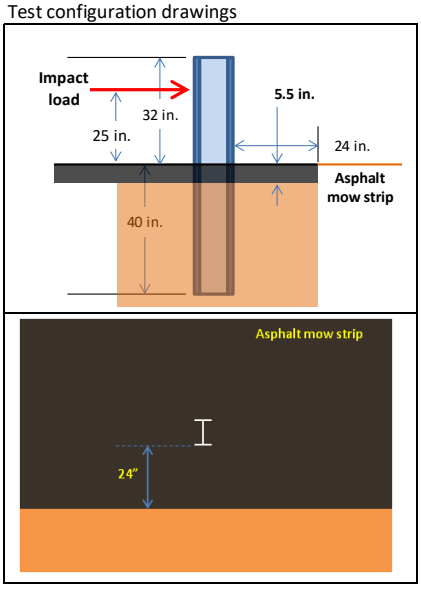

Sequential test pictures

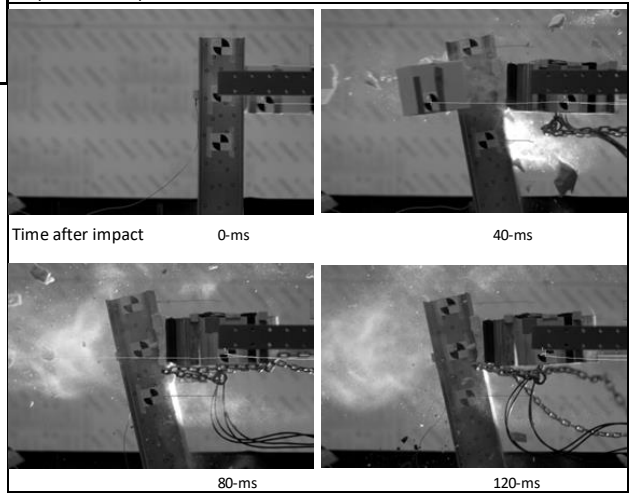

End of test pictures

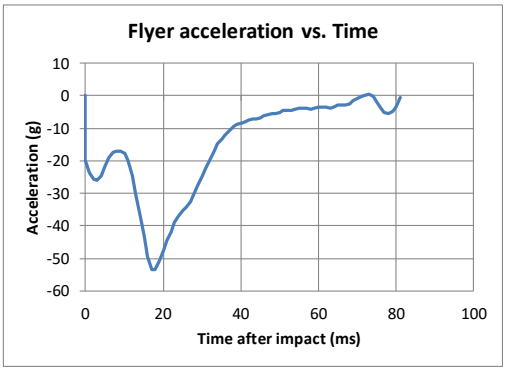

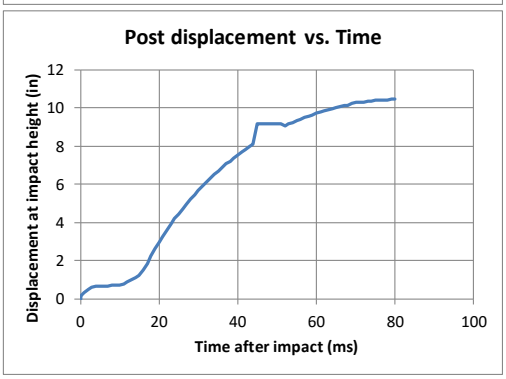

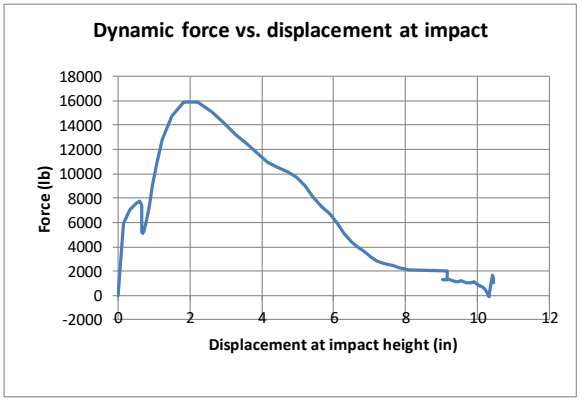

Peak flyer acceleration (g)	-53.45
Impact duration (ms)	81
time at peak acceleration (ms)	18
Max. displacement at impact (in)	10.45
Peak dynamic force (lb)	15931

Figure C.26 Summary of dynamic test results: thick mow strip

Dynamic Test #7 **Reduced RD**

* 3.5" thickness and 12" rear distance behind the post
*
*

Mow strip configuration	Thickness	3.5	in.
	Rear Distance	12	in.
	Modification	N.A.	

Impact conditions			
Speed	**15.0** m/s	32.4	mph
Mass	**139** kg	305.8	lb.
KE	15638 J	137.65	kip-in.

Test location	**SEMM Lab, Georgia Tech, Atlanta, GA**
Test date	**12/19/2016**
Temperature	**68** °F 20 °C
Asphalt age	**13** days from placement

Test configuration drawings

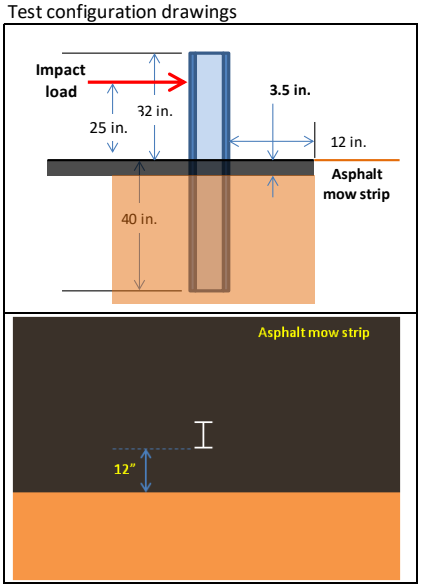

Sequential test pictures

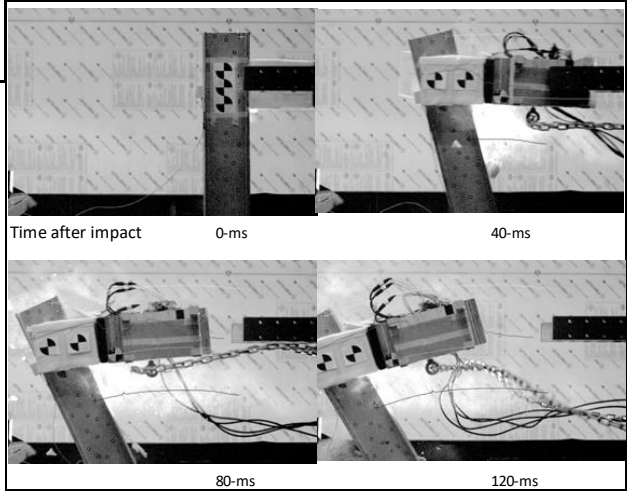

End of test pictures

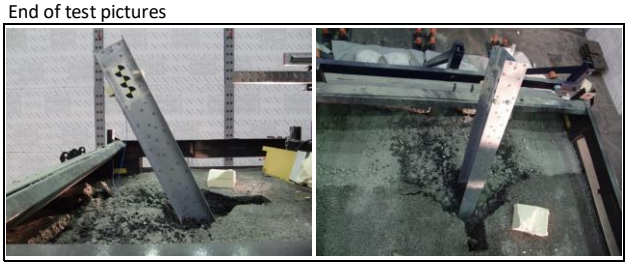

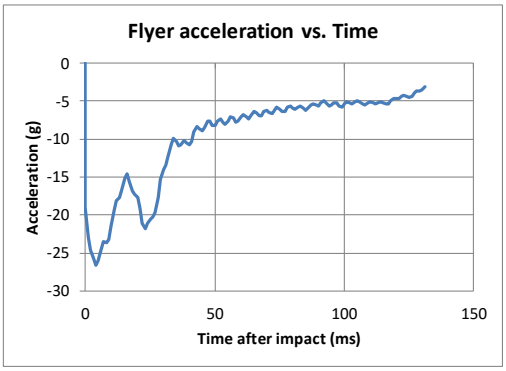

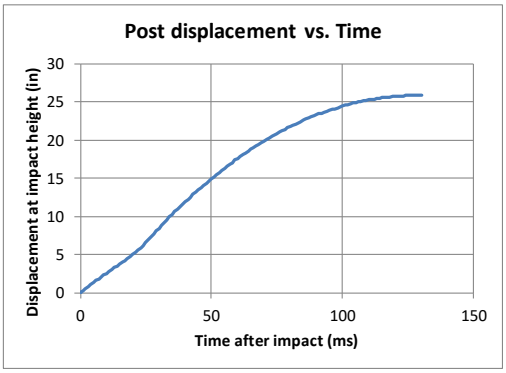

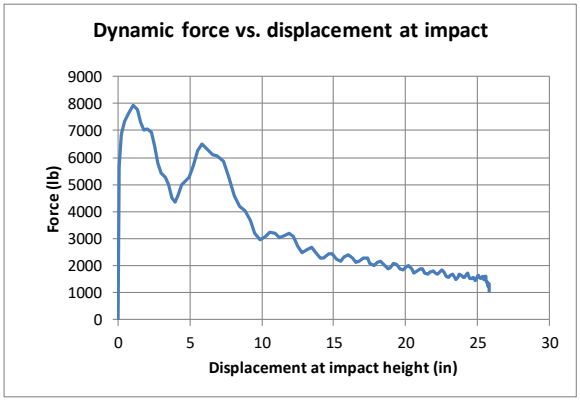

Peak flyer acceleration (g)	-26.58
Impact duration (ms)	131
time at peak acceleration (ms)	4
Max. displacement at impact (in)	25.81
Peak dynamic force (lb)	7922

Figure C.27 Summary of dynamic test results: reduced RD

Dynamic Test #14 **Thick & Reduced RD**

* 5.5" thickness and 12" rear distance behind the post
*
*

Mow strip configuration	Thickness	5.5	in.
	Rear Distance	12	in.
	Modification	N.A.	

Impact conditions			
Speed	**15.0** m/s	32.4	mph
Mass	**139** kg	305.8	lb.
KE	15638 J	137.65	kip-in.

Test location	**SEMM Lab, Georgia Tech, Atlanta, GA**
Test date	**1/27/2017**
Temperature	**69** °F 20.6 °C
Asphalt age	**11** days from placement

Test configuration drawings

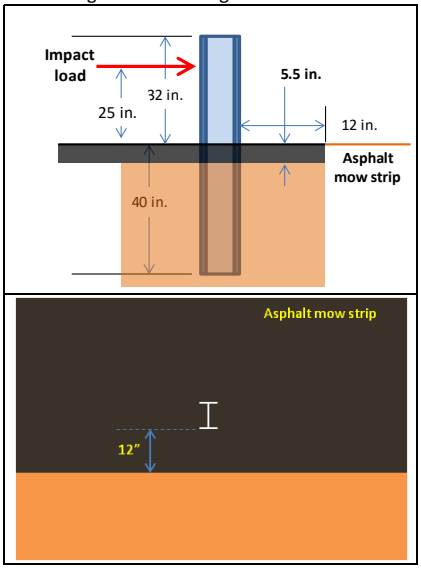

Sequential test pictures

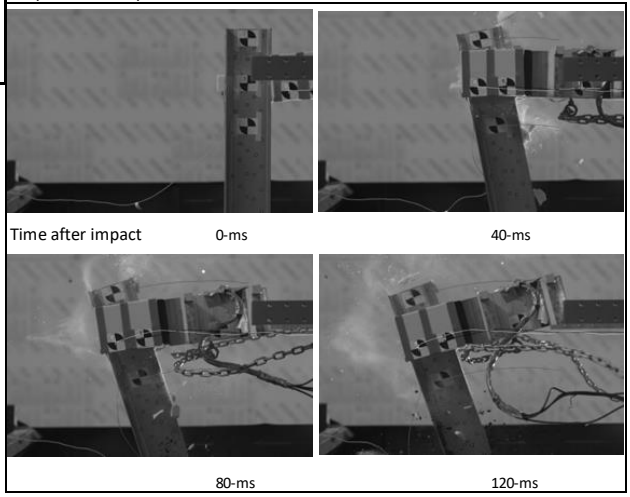

End of test pictures

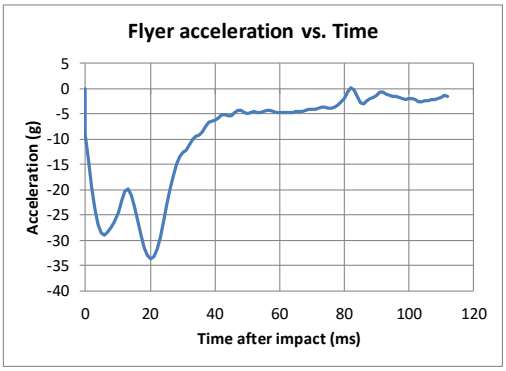

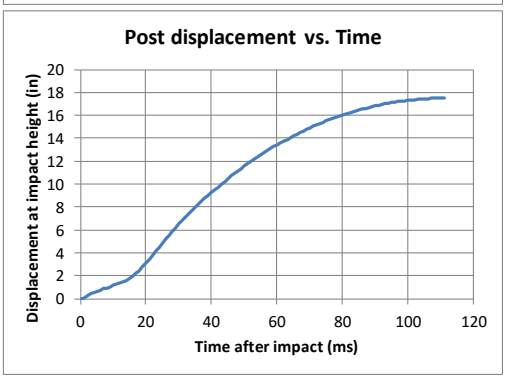

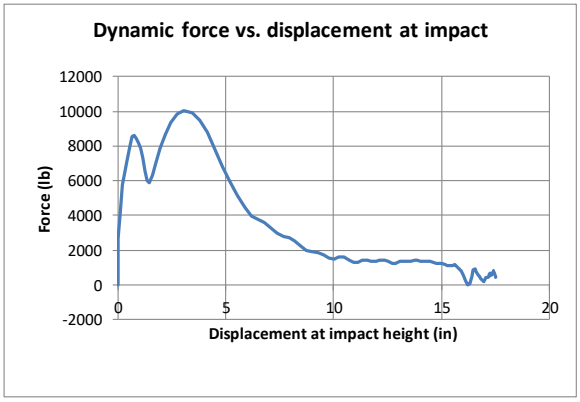

Peak flyer acceleration (g)	-33.65
Impact duration (ms)	112
time at peak acceleration (ms)	20
Max. displacement at impact (in)	17.52
Peak dynamic force (lb)	10030

Figure C.28 Summary of dynamic test results: thick and reduced RD

APPENDIX D

DETAILED DRAWINGS OF FLYER MASS COMPONENTS

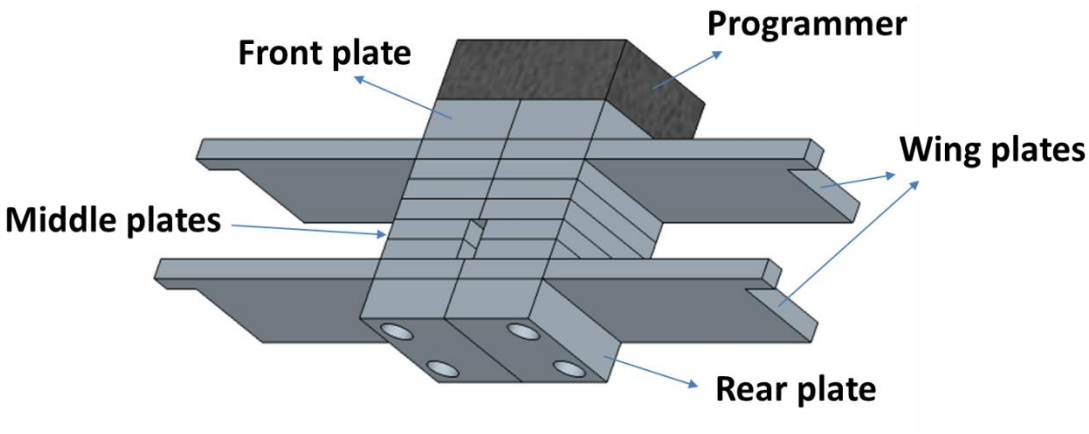

Figure D.1 Description of flyer mass components

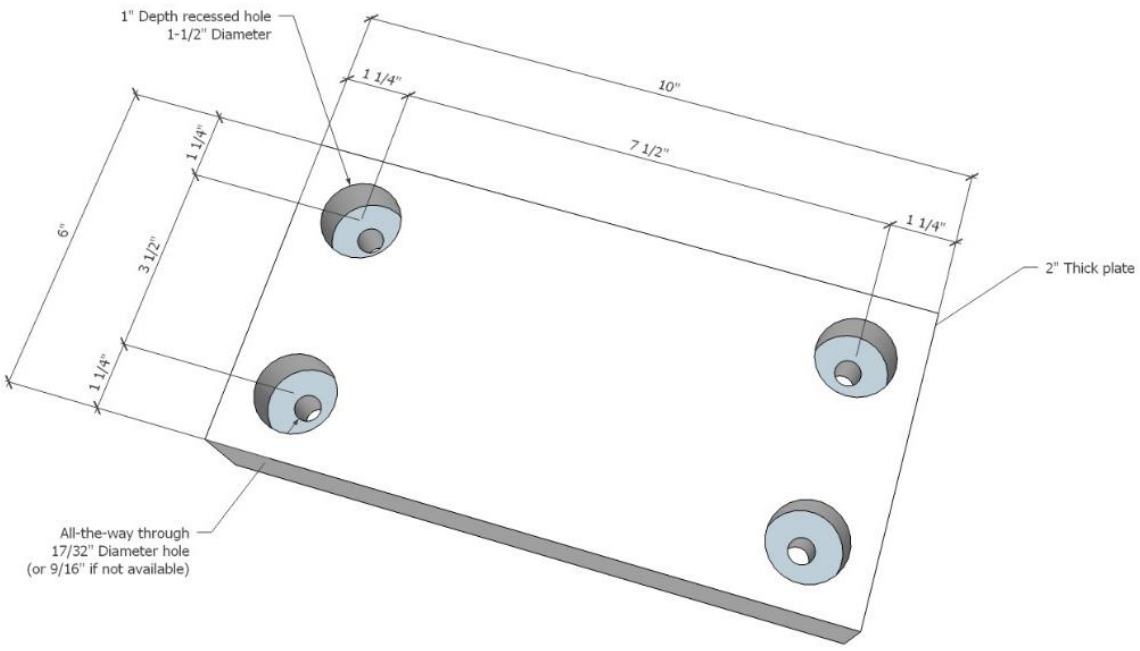

(a): 6 x 10 x 2” front plate

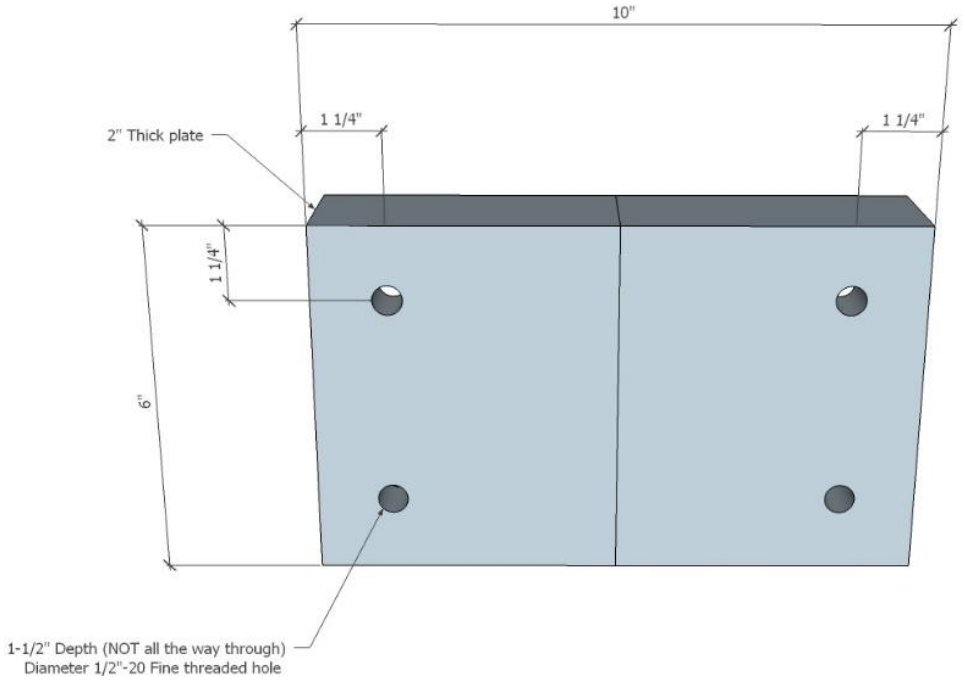

(b): 6 x 10 x 2” rear plate

Figure D.2 Detailed dimensions of flyer mass components

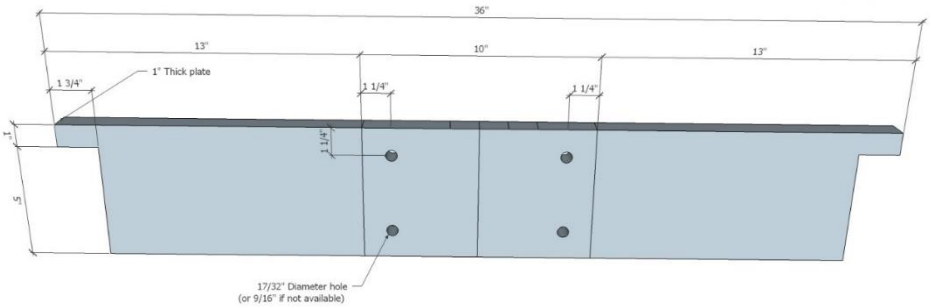

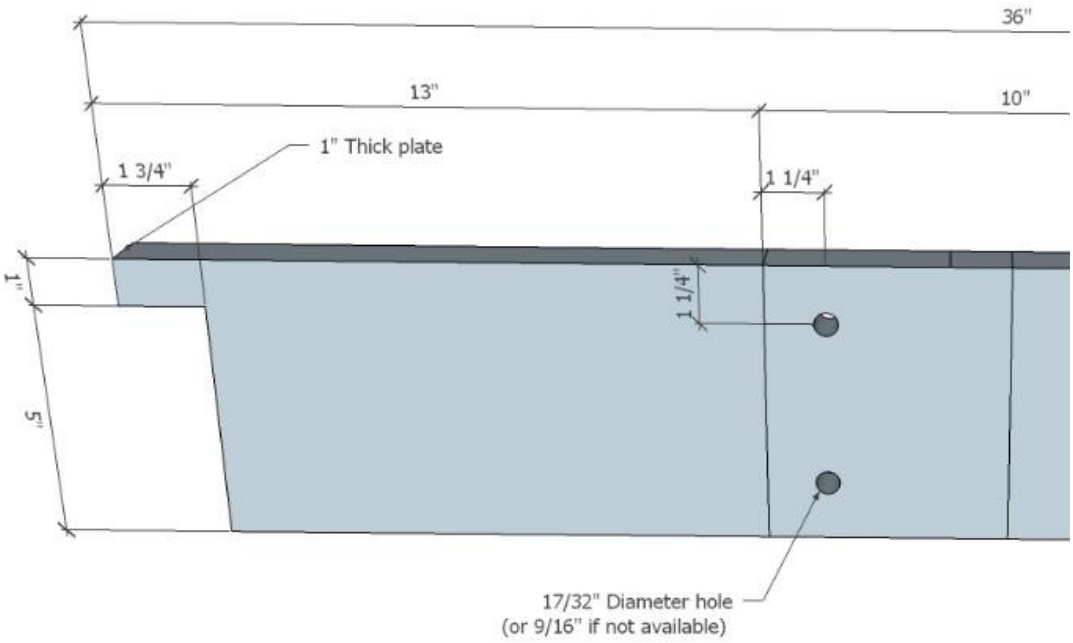

(c): 6 x 36 x 1” wing plates

Figure D.2 (continued).

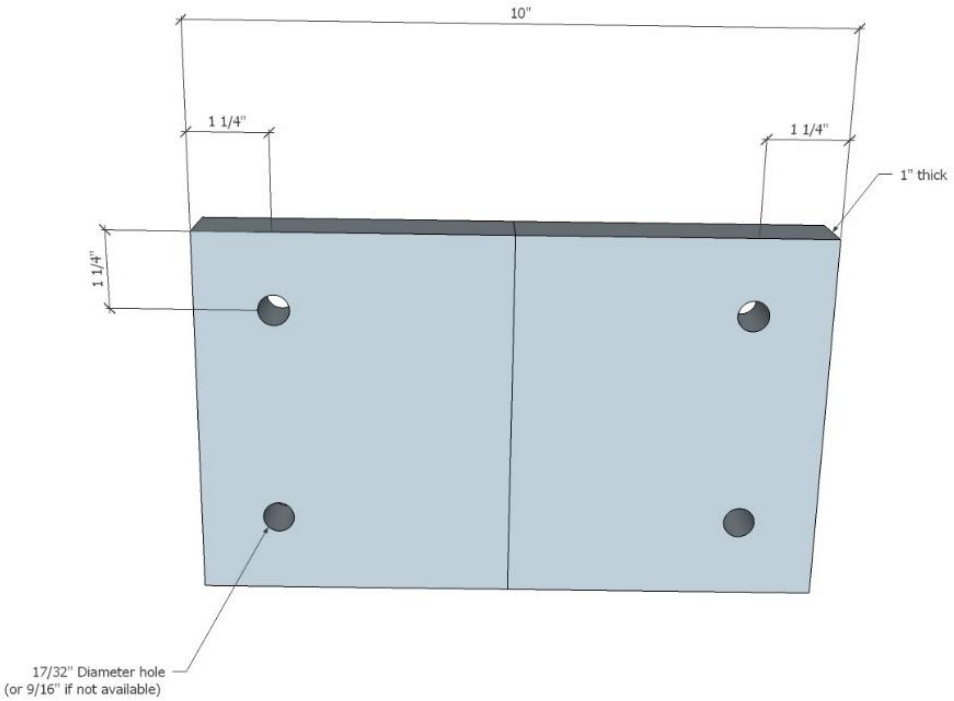

(d) 6 x 10 x 1” middle plate

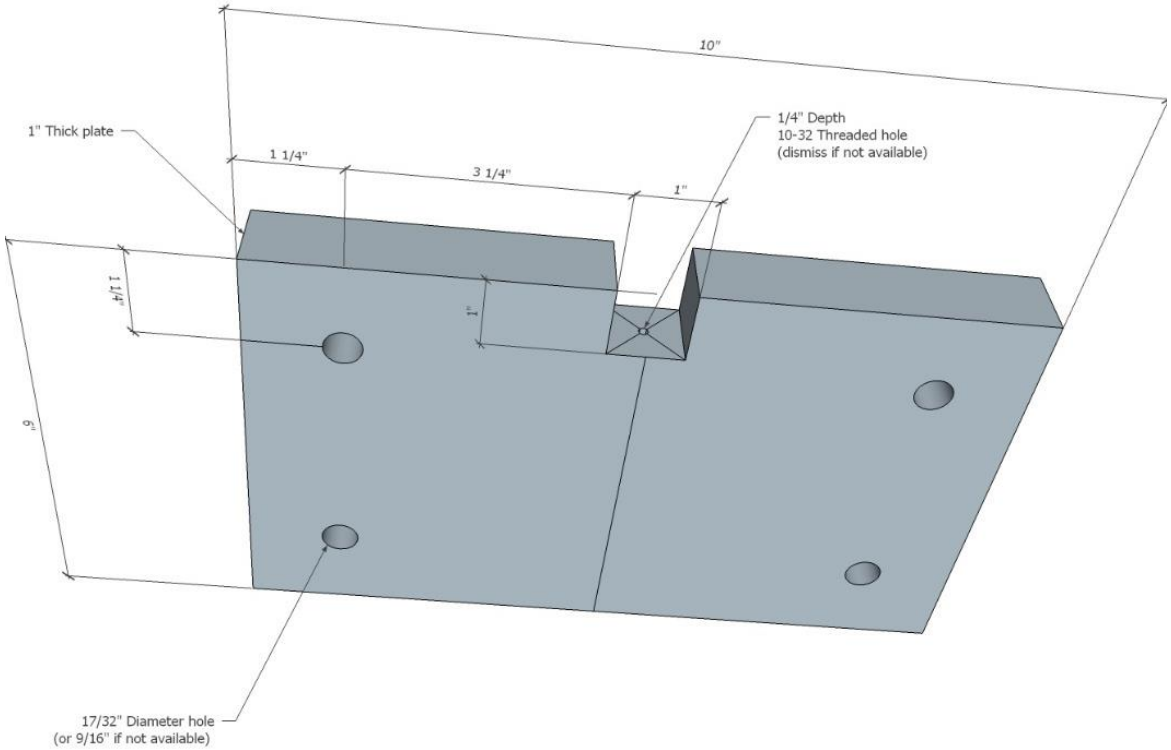

(c) 6 x 10 x 1” middle plate with accelerometer

Figure D.2 (continued).

REFERENCES

1. AASHTO, *Roadside Design Guide, Fourth Edition*. 2011, Washington, DC: American Association of State Highway and Transportation Officials (AASHTO).

2. RAY, M. H., AND MCGINNIS, R. G., *NCHRP Synthesis of Highway Practice 244: Guardrail and Median Barrier Crashworthiness*. 1997, Washington, DC: TRB National Research Council.

3. ABU-ODEH, A. Y., KIM, K-.M.. AND BLIGH, R. P., *Guardrail deflection analysis: phase I: (2010-11).* Report No. 405160-24, 2011.

4. BLIGH, R. P., SECKINGER, N. R., ABU-ODEH, A., ROSCHKE, P. N., MENGES, W. L., AND HAUG, R. R., *Dynamic Response of Guardrail Systems Encased in Pavement Mow Strips.* Research Report FHWA/TX-04/0-4162-2, 2004.

5. ROSENBAUGH, S. K., SCHMIDT, T. L., FALLER, R. K., AND REID, J. D., *Development of Socked Foundations for S3x5.7 Posts.* Research Report TRP-03-293-15, 2015.

6. MAK, K. K., BLIGH, R. P., AND MENGES, W. L., *Testing of State Roadside Safety Systems—Volume XI: Appendix J—Crash Testing and Evaluation of Existing Guardrail Systems.* Report FHWA-RD-98-046, 1998.

7. WU, W., AND THOMSON, R., *A study of the interaction between a guardrail post and soil during quasi-static and dynamic loading.* International Journal of Impact Engineering 2007. **34**: p. 883-898.

8. BELL, C. A., *Summary Report on Aging of Asphalt-Aggregate Systems.* SHRP Report SR-OSU-A-003A-89-2, 1989.

9. FARRAR, M. J., TURNER, T. F., PLANCHE, J-P., SCHABRON, J. F., AND HARNSBERGER, P. M., *Evolution of the Crossover Modulus with Oxidative Aging.* Transportation Research Record, 2013. **2370**: p. 76-83.

10. FWA, T., TAN, S., AND ZHU, L., *Rutting Prediction of Asphalt Pavement Layer Using C-ϕ Model.* J. Transp. Eng., 2004. **130**(5): p. 675-683.

11. ZHANG, Y., LUO, R. AND LYTTON, R. L., *Characterization of Viscoplastic Yielding of Asphalt Concrete.* Constr.Build. Mater., 2013. **47**: p. 671-679.

12. BAKHTIARY, E., *Assessment of Guardrail Systems in Stiff Ground Layers via Continuum and Discrete Simulation Approaches*. 2017, Georgia Institute of Technology: Atlanta, GA.

13. AASHTO, *Manual for Assessing Safety Hardware (MASH), First Edition*. 2009, Washington, DC: American Association of State Highway and Transportation Officials (AASHTO).

14. ROSS, H. E., SICKING, D. L., ZIMMER, R. A., AND MICHIE, J. D., *Recommended procedures for the safety performance evaluation of highway features*. National Cooperative Highway Research Program (NCHRP) Report 350. 1993, Washington, DC: Transportation Research Board.

15. BULLARD, D. L., MENGES, W. L., AND ALBERSON, D. C., *NCHRP Report 350 Compliance Test 3-11 of the Modified G4(1S) Guardrail with Timber Blockouts.* FHWA-RD-96-175, 1996.

16. BLIGH, R. P., MENGES, W. L., AND BUTLER, B. G., *Evaluation of a Modified Steel Post W-Beam Guardrail System.* Report No. 439637-1, 1997.

17. BLIGH, R. P., AND MENGES, W. L., *Testing and Evaluation of Modified Steel Post W-Beam Guardrail with Recycled Polyethylene Blockouts.* TTI Project 400001-MPT, 1997.

18. ROHDE, J. R., AND HERR, J., *Development of Guidelines for Placement of Guardrail Posts in Rock.* Transportation Research Record, 2004. **1890**: p. 42-48.

19. ALBERSON, D. C., MENGES, W. L., AND SCHOENEMAN, S. K., *NCHRP Report 350 Test 3-11 of the G4 W-Beam Guardrail System with Central Fabricators, Inc. Steel Post and Plastic Blockout.* Report No. 400001-CFI1, 2001.

20. KENNEDY, J. C., PLAXICO, C.A., AND MIELE, C.R., *Design, Development, and Qualification of New Guardrail Post.* Transportation Research Record, 2006. **1984**: p. 69-81.

21. FALLER, R., REID, J., KRETSCHMANN, D., HASCALL, J. AND SICKING, D., *Midwest Guardrail System with round timber posts.* Transportation Research Record: Journal of the Transportation Research Board, 2009(2120): p. 47-59.

22. BLIGH, R. P., AND BULLARD, D. L., *Crash Testing and Evaluation of Round, Wood Post, W-Beam Guardrail System.* Report No. 405391, 1995.

23. ALBERSON, D. C., MENGES, W. L., AND SCHOENEMAN, S. K., *NCHRP Report 350 Test 3-11 on the G4 Guardrail with Amity Recycled Plastic Posts and Wood Blockouts.* Report No. 400001-APL1, 2000.

24. ALBERSON, D. C., BLIGH, P. R., MENGES, W. L., AND HAUG, R. R., *NCHRP Report 350 Test 3-11 on W-Beam Guardrail with Imperial 5-Lam Glu-Laminated Posts and Blockouts.* Report No. 400001-ILP2, 2001.

25. SICKING, D. L., REID, J. D., AND ROHDE, J. R., *Development of the Midwest Guardrail System.* Transportation Research Record, 2002. **1797**.

26. POLIVKA, K. A., FALLER, R.K., SICKING, D.L., ROHDE, J.R., BIELENBERG, R.W., AND REID, J.D., *Performance Evaluation of the Midwest Guardrail System - Update to NCHRP Report 350 Test No. 3-11 (2214MG-1).* Report No. TRP-03-170-06, 2006.

27. POLIVKA, K. A., FALLER, R.K., SICKING, D.L., REID, J.D., ROHDE, J.R., HOLLOWAY, J.C., BIELENBERG, R.W., AND KUIPERS, B.D., *Performance Evaluation of the Midwest Guardrail System - Update to NCHRP Report 350 Test No. 3-11 with 28" C.G. Height (2214MG-2).* Report No. TRP-03-171-06, 2006.

28. FALLER, R. K., SICKING, D.L., BIELENBERG, R.W., ROHDE, J.R., POLIVKA, K.A., AND REID, J.D., *Performance of Steel-Post, W-Beam Guardrail Systems.* Transportation Research Record, 2007. **2025**: p. 18-33.

29. POLIVKA, K. A., FALLER, R.K., SICKING, D.L., REID, J.D., ROHDE, J.R., HOLLOWAY, J.C., BIELENBERG, R.W., AND KUIPERS, B.D., *Development of the Midwest Guardrail System (MGS) for Standard and Reduced Post Spacing and in Combination with Curbs.* Report No. TRP-03-139-04, 2004.

30. HASCALL, J. A., FALLER, R.K., REID, J.D., AND SICKING, D.L., *Investigating the Use of Small Diameter Softwood as Guardrail Posts (Dynamic Test Results).* Report No. TRP-03-179-07, 2007.

31. LECHTENBERG, K. A., REID, J.D., SICKING, D.L., FALLER, R.K., BIELENBERG, R.W., AND ROHDE, J.R., *Approach Slope for Midwest Guardrail System.* Report No. TRP-03-188-08, 2008.

32. POLIVKA, K. A., SICKING, D.L., FALLER, R.K., AND BIELENBERG, R.W., *Midwest Guardrail System Adjacent to a 2:1 Slope.* Transportation Research Record, 2008. **2060**: p. 74-83.

33. BIELENBERG, R. W., FALLER, R.K., ROHDE, J.R., REID, J.D., SICKING, D.L., HOLLOWAY, J.C., ALLISON, E.M., AND POLIVKA, K.A., *Midwest Guardrail System for Long-Span Culvert Applications.* Report No. TRP-03-187-07, 2007.

34. FHWA. *Roadside Hardware Policy and Guidance on the AASHTO MASH*. 2009 September 30, 2015 October 9, 2015]; Available from: http://safety.fhwa.dot.gov/roadway_dept/policy_guide/road_hardware/ctrmeasures/mash/.

35. WIEBELHAUS, M. J., LECHTENBERG, K.A., FALLER, R.K., SICKING, D.L., BIELENBERG, R.W., REID, J.D., AND ROHDE, J.R., *Development and Evaluation of the Midwest Guardrail System (MGS) Placed Adjacent to a 2:1 Fill Slope.* Report No. TRP-03-185-10, 2010.

36. BLIGH, R. P., ABU-ODEH, A., AND MENGES, W. L., *Mash Test 3-10 on 31-Inch W-Beam Guardrail with Standard Offset Blocks.* Report 9-1002-4 2011.

37. WILLIAMS, W. F., AND MENGES, W. L., *MASH Test 3-11 of the W-Beam Guardrail on Low-Fill Box Culvert.* Report No. 405160-23-2, 2011.

38. STOLLE, C. J., LECHTENBERG, K.A., FALLER, R.K., ROSENBAUGH, S.K., SICKING, D.L., AND REID, J.D. , *Evaluation of the Midwest Guardrail System (MGS) with White Pine Wood Posts.* Report No. TRP-03-241-11, 2011.

39. STOLLE, C. J., LECHTENBERG, K.A., REID, J.D., FALLER, R.K., BIELENBERG, R.W., ROSENBAUGH, S.K., SICKING, D.L., JOHNSON, E.A., *Determination of the Maximum MGS Mounting Height – Phase I Crash Testing.* Report No. TRP-03-255-12, 2012.

40. SCHRUM, K. D., LECHTENBERG, K.A., BIELENBERG, R.W., ROSENBAUGH, S.K., FALLER, R.K., REID, J.D., SICKING, D.L., *Safety*

Performance Evaluation of the Non-Blocked Midwest Guardrail System (MGS). Report No. TRP-03-262-12, 2013.

41. WEILAND, N. A., REID, J.D., FALLER, R.K., SICKING, D.L., BIELENBERG, R.W., AND LECHTENBERG, K.A., *Minimum Effective Guardrail Length For The MGS.* Report No. TRP-03-276-13, 2013.

42. CALCOTE, L. R., AND KIMBALL, C.E., *Properties of Guardrail Posts for Various Soil Types*. Transportation Research Record. Vol. 679. 1978, Washington, DC: TRB. 22-25.

43. MICHIE, J. D., *Response of guardrail posts during impact.* Research Report No. 03-9051, 1970.

44. DEWEY, J. F., JEYAPALAN, J. K., HIRSCH, T. J., & ROSS, H. E., *A study of the soil structure interaction behavior of highway guardrail posts.* Research Report 343-1, 1983.

45. BEDEWI, N. E., *Response of Guardrail Posts in Soil*. Report No. FHW AIRD-861147. 1985: University of Maryland.

46. EGGERS, W., AND HIRSCH, T. I., *The Effects of Embedment Depth, Soil Properties, and Post Type on the Performance of Highway Guardrail Post*. Report No. FHWAlTX-86/64+405-1. 1986, College Station, TX: TTI.

47. COON, B. A., REID, J.D., AND ROHDE, JR. , *Dynamic Impact Testing of Guardrail Posts Embedded in Soil.* Research Report TRP-03-77-98, 1999.

48. DEY, G., FALLER, R., HASCALL, J., BIELENBERG, R., LECHTENBERG, K., AND MOLACEK, K., *Dynamic Impact Testing of W152x13.4 (W6x9) Steel Posts on a 2:1 Slope.* Report No. TRP-03-165-07, 2007.

49. GABAUER, D. J., KUSANO, K. D., MARZOUGUI, D., OPIELA, K., HARGRAVE, M., AND GABLER, H. C., *Pendulum Testing as a Means of Assessing the Crash Performance of Longitudinal Barrier With Minor Damage.* International Journal of Impact Engineering, 2010. **37**(11): p. 1121-1137.

50. HAMPTON, C. E., AND GABLER, H. C., *Crash Performance of Strong-Post W-Beam Guardrail with Missing Blockouts.* International Journal of Crashworthiness, 2012. **17**(1): p. 93-103.

51. SCHMIDT, T., MONGIARDINI, M., BIELENBERG, R., LECHTENBERG, K., REID, J., AND FALLER, R., *Dynamic Testing of MGS W6x8.5 Posts at Decreased Embedment.* Report No. TRP-03-271-12, 2012.

52. ARRINGTON, D. R., BLIGH, R. P., AND MENGES, W. L., *Alternative Design of Guardrail Posts in Asphalt or Concrete Mowing Pads.* Research Report 405160-14-1, 2009.

53. JOWZA, E. R., FALLER, R.K., ROSENBAUGH, S.K., SICKING, D.L., AND REID, J.D., *Safety Investigation and Guidance for Retrofitting Existing Approach Guardrail Transitions.* MwRSF Research Report No. TRP-03-266-12, 2012.

54. WHITESEL, D., JEWELL, J., AND MELINE, R., *Development of weed control barrier beneath metal beam guardrail.* Technical Report FHWA/CA10-0515, 2011.

55. HERBST, B. R., MEYER, S.E., OLIVER, A.A., FORREST, S.M. *Rear Impact Test Methodologies: Quasistatic and Dynamic*. in *21st International Technical Conference on the Enhanced Safety of Vehicles*. 2009. Stuttgart, Germany.

56. VIANO, D. C., *Role of the Seat in Rear Crash Safety*. Vol. R-317. 2002: SAE International.

57. FALLER, R. K., POLIVKA, K.A., KUIPERS, B.D., BIELENBERG, R.W., REID, J.D., ROHDE, J.R., SICKING, D.L., *Midwest Guardrail System for Standard and Special Application.* Transportation Research Board, 2004(1890): p. pp. 19-33.

58. AASHTO, *Standard Specification for Materials for Aggregate and Soil-Aggregate Subbase, Base and Surface Courses (AASHTO M147)*. 1990, American Association of State Highway and Transportation Officials (AASHTO).

59. AASHTO, *Construction Manual for Highway Construction (AASHTO CM4) - Sections 304.05*. 1990, American Association of State Highway and Transportation Officials (AASHTO).

60. AASHTO, *Standard Method of Test for Density of Soil In-Place by the Sand-Cone Method (AASHTO T191)*. 2014, American Association of State Highway and Transportation Officials (AASHTO).

61. AASHTO, *Standard Method of Test for Moisture-Density Relations of Soils Using a 4.54-kg (10-lb) Rammer and a 457-mm (18-in.) Drop (AASHTO T 180)*. 2010, American Association of State Highway and Transportation Officials (AASHTO).

62. SCOTT, D. W., WHITE, D. W., STEWART, L. K., BAKHTIARY, E., AND LEE, S.-H., , *Evaluating the Performance of Guardrail Posts Installed by Driving Through Asphalt Layers.* Report 13-21, 2015.

63. NOAA. *NOAA Online Weather Data*. [cited 2017; Available from: http://w2.weather.gov/climate/xmacis.php?wfo=ffc.

64. ASTM, *Standard Test Methods and Definitions for Mechanical Testing of Steel Products (ASTM A370)*. 2015, ASTM International.

65. AASHTO, *AASHTO Guide for Design of Pavement Structures*. 1993, Washington, D.C.: American Association of State Highway and Transportation Officials (AASHTO).

66. MCLEOD, N. W. *A Rational Approach to the Design of Bituminous Paving Mixtures*. in *Association of Asphalt Paving Technologists*. 1950. St. Paul, MN.

67. SMITH, V. R., *Application of the Triaxial Test to Bituminous Mixtures.* ASTM Special Techical Publication, 1951(106): p. 55-78.

68. FWA, T., TAN, S., AND ZHU, L., *Reexamining C-ϕ Concept for Asphalt Paving Mix Design.* Journal of Transportation Engineering, 2001. **127**(1): p. 67-73.

69. PELLINEN, T. K., XIAO, S., *Stiffness of Hot-Mix Asphalt.* Report No. FHWA/IN/JTRP-2005/20.2006, 2006.

70. AASHTO, *Standard Specification for Performance-Graded Asphalt Binder (AASHTO T320)*. 2007, American Association of State Highway and Transportation Officials (AASHTO).

71. WU, C. F. J., HAMADA, M. S., *Experiments: Planning, Analysis, and Optimization*. 2nd ed. 2009, Hoboken, NJ: John Wiley & Sons, Inc.

72. ASTM, *Standard Test Method for Compressive Strength of Asphalt Mixtures (ASTM D1074)*. 2009, ASTM International.

73. ASTM, *Test Method for Effect of Water on Compressive Strength of Compacted Bituminous Mixtures (ASTM D1075)*. 2011, ASTM International.

74. NIAZI, Y., JALILI, M., *Effect of Portland cement and lime additives on properties of cold in-place recycled mixtures with asphalt emulsion.* Construction and Building Materials, 2009. **23**: p. 1338-1343.

75. XU, J., HUANG, S., QIN, Y., LI, F., *The Impact of Cement Contents on the Properties of Asphalt Emulsion Stabilized Cold Recycling Mixtures.* Int. J. Pavement Res. Technol., 2011. **4**(1): p. 48-55.

76. STEWART, L. K., GAO, N., PEZZOLA, G., SANBORN, M., SANBORN, K., NAIL, A., LORETO, G. *Georgia Institute of Technology Laboratory for Blast, Shock, and Impact*. in *7th International Conference on Advances in Experimental Structural Engineering (7AESE)*. 2017. Pavia, Italy.

77. GRAM, M. M., CLARK, A.J., HEGEMIER, G.A., SIEBLE, F., *Laboratory Simulation of Blast Loading on Building and Bridge Structures.* WIT Transactions on The Built Environment, 2006. **87**(Structures Under Shock and Impact IX): p. 33-44.

78. STEWART, L. K., FREIDENBERG, A., RODRIGUEZ-NIKL, T., OESTERLE, M., WOLFSON, J., DURANT, B., ARNETT, K., ASARO, R.J., HEGEMIER, G.A., *Methodology and validation for blast and shock testing of structures using high-speed hydraulic actuators.* Engineering Structures, 2014. **70**: p. 168-180.

79. SAE, *Instrumentation for Impact Test, Part 1, Electronic Instrumentation (SAE J211-1)*. 1995, Warrendale, PA: SAE International.

80. RESEARCH, V., *PCC (Phantom Camera Control)*. 2016.

81. HUANG, M., *Vehicle Crash Mechanics*. 2002, Boca Raton, FL: CRC Press.

82. FEMA, *Prestandard and Commentary for the Seismic Rehabilitation of Buildings (FEMA 356)*. 2000, Washington, DC: Federal Emergency Management Agency (FEMA).

83. API, *Recommended Practice for Planning, Designing and Constructing Fixed Offshore Platforms-Working Stress Design, Twenty-first edition*. 2005, Washington, DC: American Petroleum Institute (API).

84. PRASAD, Y., AND CHARI, T, *Lateral Capacity of Model Rigid Piles in Cohesionless Soils.* Soils and Foundations, 1999. **39**(2): p. 21-29.

85. MURCHISON, J. M., AND O'NEILL, M. W. *Evaluation of p–y relationships in cohesionless soils.* in *Analysis and design of pile foundations: proceedings of a symposium sponsored by the ASCE geotechnical engineering division and a session sponsored by the ASCE technical council on codes and standards in conjunction with the ASCE national convention*. 1984. San Francisco, CA.

86. LEE, S.-H., BAKHTIARY, E., SCOTT, D. W., STEWART, L. K., WHITE, D. W., *Influence of geometric parameters on the restraint of guardrail posts by asphalt mow strips.* Sustainable and Resilient Infrastructure, 2017. **2**(1): p. 22-36.

87. FHWA. *LTPPBind (Version 3.1)*. [cited 2017; Available from: https://www.fhwa.dot.gov/research/tfhrc/programs/infrastructure/pavements/ltpp/.

88. ADVANCED ASPHALT TECHNOLOGIES, L., *A Manual for Design of Hot-Mix Asphalt with Commentary*. National Cooperative Highway Research Program (NCHRP) Report 673. 2011, Washington, D.C.: Transportation Research Board of the National Academies.